Improved characterisation and modelling of heterolithic tidal sandstone reservoirs

Benoît Yves Ghislain Massart

Imperial College London
Department of Earth Science and Engineering

A dissertation submitted in fulfilment of the requirements for the degree of
Doctor of Philosophy in Geology of Imperial College London

June, 2014

This thesis is dedicated to my grandfathers:
they paved the way that brought me to London

Cette thèse est dédiée à mes grands-pères :
ils ont pavé la voie qui m'a mené à Londres

Declaration of originality

I hereby declare that this thesis, “Improved characterisation and modelling of heterolithic tidal sandstone reservoirs”, is entirely my own work under the supervision of Prof. Matthew D. Jackson, Dr. Gary J. Hampson, Prof Howard D. Johnson, Dr. Christopher A.-L. Jackson and Dr. Berit Legler, and performed in the Department of Earth Science and Engineering at Imperial College London. All other material in this thesis has been given full acknowledgement where appropriate. This work has not been previously submitted, in whole or in part, to any other academic institution for a degree, diploma, or any other qualification.

Benoît Yves Ghislain MASSART

Department of Earth Science and Engineering

Imperial College London

Copyright declaration

“The copyright of this thesis rests with the author and is made available under a Creative Commons Attribution Non-Commercial No Derivates license. Researchers are free to copy, distribute or transmit the thesis on the condition that they attribute it, that they do not use it for commercial purposes and that they do not alter, transform or build upon it. For any reuse or redistribution, researchers must make clear to others the license terms of this work.”

Abstract

Tidal heterolithic sandstone reservoirs comprise millimetre- to centimetre-scale intercalations of mudstone and sandstone. Their effective flow properties are poorly predicted by data that do not sample a representative elementary volume (REV), or models that fail to capture the complex 3D architecture of sandstone and mudstone layers. The aim of this dissertation is to develop improved predictions of effective single and multiphase permeabilities in heterolithic tidal sandstones.

A surface-based modelling approach has been developed, which honours the geometry of geologic heterogeneity surfaces, integrating easily measurable outcrop derived dataset as input parameters. The workflow uses template surfaces to represent heterogeneities classified by geometry rather than length-scale. The surface-based methodology has been applied to generate generic, 3D mini-models of trough and planar cross-bedded tidal sandstones with differing proportions of sandstone and mudstone. The models closely capture the bedform architectures observed at outcrop and are suitable for flow simulation. Quantitative geometrical input data to construct the models was extracted from an outcrop analogue which records deposition in a tide-dominated deltaic and estuarine setting.

The model results demonstrate that effective single-phase permeability of tidal cross-bedded sandstones varies with sample volume. A REV of 1 m^3 was identified, confirming that the model volume of 9 m^3 (> REV) yields representative values. The impact on effective permeability of seven geometric parameters controlling the density of mudstone drapes was determined: mudstone drape coverage, foreset thickness, toeset dip angle, dune climb angle, foreset to toeset ratio, style of cross-bedding (trough or tabular), size of the mudstone drape patches. The impact of seven geometric parameters on effective permeability was determined. Effective permeability decreases as the mudstone fraction increases, and is highly anisotropic. Each parameter investigated can significantly impact on effective permeability, depending upon the flow direction and sandstone fraction, causing considerable spread of the values. During oil/water flow, relative permeabilities are not affected by mudstone drapes, but the irreducible oil saturation varies depending on flow direction and mudstone content. The workflow presented here can be used with subsurface data, supplemented by outcrop analog observations, to generate effective single and multi-phase permeability values to be derived for use in larger-scale reservoir models.

Acknowledgements

All my gratitude goes to my numerous PhD supervisors, who were so supportive during the whole four years of the PhD, who pushed me forward, offered me the best opportunities, and taught me so much with infinite patience. In particular, I want to thank Prof. Matthew Jackson for continuously shedding light on the pathway leading to success in the shadows of my mind, and here I am talking about the exploit of bringing a geologist to reservoir engineering. I want to thank Dr. Gary Hampson for showing me how to be organized and meticulous in my work: not sure I changed that much through contact with him, but for sure he tried his best, being an amazing example of dedication to a job. I want to thank Prof. Howard Johnson for his unfailing enthusiasm and support, when the motivation was high, but especially when it was low. I want to thank Dr. Berit Legler for being my guide through the four years of my PhD, an organized and meticulous colleague at work, a great companion during field campaigns, and a very close friend for life. I want to thank Dr. Christopher Jackson for his communicative energy on a day-to-day basis, for thoughtful comments on my work, and legendary Christmas parties. It is really not a lie or an exaggeration, but as it is already good fortune for a PhD student to find one supportive and competent supervisor, saying I feel extremely lucky to have worked closely with five of them during four years is an understatement, I feel blessed. Thank you so much.

Funding for this work is gratefully acknowledged from Norske Shell and the partners of the Linnorm license: Petoro, Statoil and Total. Extra funding was provided by Prof. Howard Johnson and Prof. Matthew Jackson for the completion of the thesis: I will have to find a way to pay this back. I would like to thank Roxar for providing the academic use of RMS software, and Schlumberger for providing the academic use of Petrel and Eclipse 100 software packages. I want to deeply thank Shell Americas and Statoil for giving me the opportunity to join their research team during two internships, which gave me great insight in the oil industry, about the future problems I would face in my future career.

I need to take the time to thank my fellow PhD comrades, and beforehand Dr. Gavin Graham. Not many PhD students can talk about their PhD research as a team work, but it was the case for the two of us, thanks to a common methodology in our respective projects, and thanks to a deep friendship, the kind of one built in ordeals and adversity. And flies. The others will hate me for not developing more, but each of them knows how much I am grateful for their friendship during my life in London: Fahad, Pete, Jorge, Obi, Akela, Thilo, Aruna, Matt, Nick, Stefano, David, Masoud, Claire, Liz, Andreas, Tenice, David, Olga, Marion, Queenie, Wim, Claire, Ian, Yvette, Sarah, Matt, Anne-Lise, Irina, Munira, Bisma, Tony, Amandine, Renato, Riki, Phoebe, Boeke, Clara, Hugo, Evelina, Anna, Abdulaziz, Ahmed, Frédéric, Olivier, James, Piotr, Vikram ... the Lagrange team, my ENSG friends in France, Amélie and Valérie.

I want to thank the teachers that made my interest in geology grow over the years at university: Mr. Fogelgesang at Sainte-Geneviève, a passionate geologist, who convinced me that I was also “born this way”; Dr. Mary Ford, who brought this thesis project to my attention when I needed it the most; the sedimentologist team of ENSG Nancy, Dr. Fabrice Malartre and Dr. Antoine LeSolleuz, for their continuous support over the years, first with their patience for shaping a stupid student into a successful geologist, and then for making my confidence grow in my PhD work.

And finally, let me acknowledge my family. I miss the dear ones I lost during these four years, it is always too soon. My thesis is dedicated to them. For the ones who stay, I say thank you, I love you dearly. I want you to take credit for my achievements, you deserve it as much as I do. You always wanted the best for me in my education, and provided the means for it so I could reach success and pride in my work. But there is much more to me you have to be proud about, I hope you will see it eventually someday. I am also grateful for the new family I found in Camille, Michèle and Yves. And before all I am grateful for Romain without whom I would not have made it through these last four years: I love you so much.

Contents

Declaration of originality 5
Copyright declaration 5
Abstract 7
Acknowledgements 8

Chapter 1: Introduction 17

1.1. Reservoir potential of tidally-influenced heterolithic sandstones 17
1.2. Aims and objectives 18
1.3. Thesis structure 19
1.4. Publications 21

Chapter 2: Literature review 25

2.1. Heterogeneities in tidally-influenced heterolithic sandstone reservoirs 25
2.2. Reservoir modelling techniques for the representation of tidally-influenced heterolithic sandstones 29
2.3. Estimation of the effects of small-scale heterogeneities on reservoir properties 35

Chapter 3: Effective flow properties of heterolithic, cross-bedded tidal sandstones: part 1. Surface-based modelling 39

3.1. Introduction 40
3.2. Methodology 43
3.2.1. Model-construction methodology 43
3.2.2. Application to heterolithic, cross-bedded tidal sandstones 45
3.2.3. Modelling of elemental volumes 46
3.2.4. Modelling template surfaces within elemental volumes 47
3.2.5. Modelling of mudstone drapes along foreset-toeset surfaces 55
3.2.6. Outcrop analogue data analysis to define model input parameters 57
3.3. Results 65
3.3.1. Models constructed from outcrop analogue data 65
3.3.2. Calculation of effective permeability 69
3.4. Conclusions 73

Chapter 4: Effective flow properties of heterolithic, cross-bedded tidal sandstones: part 2. Single-phase flow simulation 77

4.1. Introduction 78
4.2. Methodology 80
4.2.1. Surface-based model construction 80
4.2.2. Identification of the REV for heterolithic, cross-bedded tidal sandstones 82
4.2.3. Impact of mudstone drape coverage on effective permeability 83
4.2.4. Range of effective permeability from trough and tabular cross-bedded end-member models 86
4.2.5. Sensitivity analysis of geometric parameters 86
4.2.6. Calculation of effective permeability 87

4.3. Results 92
4.3.1. Visualization and qualitative analysis of cross-bedded heterolithic tidal sandstone models 92
4.3.2. Impact of sample volume on effective permeability 93
4.3.3. Impact of sandstone fraction on effective permeability 95
4.3.4. Range of effective permeability across end-member models of tabular and trough cross-bedding 97
4.3.5. Influence of toeset bedding style on flow and effective permeability 99
4.3.6. Sensitivity analysis of effective permeability to various cross-bedding geometric parameters 102
4.4. Discussion 103
4.5. Conclusions 107

Chapter 5: Effective relative permeabilities and residual oil saturation for oil/water flow in heterolithic cross-bedded tidal sandstones 111

5.1. Introduction 112
5.2. Methodology 113
5.2.1. Two-phase flow simulation 113
5.2.2. Experimental programme 118
5.2.3. Calculation artefacts introduced by corner-point grid architecture 118
5.3. Results 120
5.3.1. Typical flow simulation results 120
5.3.2. Impact of orientation of flow 120
5.3.3. Impact of mudstone drape coverage 125
5.3.4. Impact of input curves of sandstone relative permeability 128
5.4. Discussion 128
5.5. Recommendations for future work 131
5.6. Conclusions 131

Chapter 6: General discussion and conclusions 135

6.1. Applications of outcrop-analogue based studies for reservoir modelling 135
6.2. Advances in the potential for geological realism of reservoir models: surface-based reservoir models and gridding 137
6.3. Upscaling methodologies for heterolithic sandstones 141
6.4. Recommendations for future work 145
6.5. Conclusions 146

Chapter 7: References 151

Appendix: Program description 163

Table of figures

Figure 2.1: Schematic drawing of dune migration during a single flood-ebb cycle A. with weak subordinate currents; B. with strong subordinate currents (Nio and Yang, 1991). 26

Figure 2.2: Schematic drawing of a neap-spring tidal bundle sequence (Visser, 1980; Nio and Yang, 1991). 28

Figure 2.3: 3D-diagrams representing the organisation, distribution and connectivity of sandstone layers in tidal deposits: flaser bedding, wavy bedding, lenticular bedding (Reineck and Singh, 1980; modified after Reineck and Wunderlich, 1968). 28

Figure 2.4: Surface-based modelling workflow for models of flaser bedded and wavy bedded rock specimens (Jackson *et al.*, 2005). 31

Figure 2.5: Surface-based model of wavy-bedded deposits generated by the software SBED (Ringrose *et al.*, 2005). 34

Figure 3.1: Three-step methodology for constructing models of heterolithic, cross-bedded tidal sandstones. 44

Figure 3.2: Modern 3D dune in an inter-tidal flat environment, the Wash Estuary, United Kingdom, and interpretation of the erosion surface resulting from migration of a dune and associated scour pool. 48

Figure 3.3: Ancient trough cross-bed set viewed in cross-section oriented approximately along depositional dip, Dir Abu Lifa Member, Gecko Nose location, Western Desert, Egypt, and interpretation of the cross-bed set as the lower part of an ellipsoidal elemental volume with corresponding 3D best fit ellipsoidal elemental volume. 49

Figure 3.4: Ancient trough cross-bed set viewed in cross-section oriented approximately along depositional strike, Dir Abu Lifa Member, Gecko Nose location, Western Desert, Egypt; interpretation of the cross-bed set as the lower part of an ellipsoidal elemental volume; extraction of the erosive base of the cross-bed set from the photomontage. 52

Figure 3.5: Detail of transition between foreset and toeset along template surfaces within an elemental volume. Input parameters required to describe the geometry of the foreset-toeset surfaces. 55

Figure 3.6: Map of Egypt highlighting the position of the Eocene Dir Abu Lifa outcrop belt; map of the main outcrop belt of the Dir Abu Lifa Member, highlighting the Gecko Nose and Butterfly Canyon localities; close-up of the Gecko Nose outcrop. 59

Figure 3.7: Photograph of the two nearly perpendicular cliff faces at Gecko Nose. 59

Figure 3.8: Photomontage and interpretation of the WNW-ESE-oriented face of Gecko Nose, oblique to depositional strike.
61

Figure 3.9: Distribution of the preserved height H_A and the preserved apparent width W_A of 49 trough cross-bed sets exposed on the WNW-ESE-oriented face of Gecko Nose.
62

Figure 3.10: Point clouds defining 90 foreset-toeset surfaces and best-fit line definition for a foreset-toeset template surface.
63

Figure 3.11: Log-normal distribution of foreset thickness F_T for 544 foreset-toeset surfaces of 12 cross-bed sets.
64

Figure 3.12: Point cloud defining the coverage of mudstone drapes along 90 foreset-toeset surfaces from 3 cross-bed sets and best-fit line definition for mudstone drape coverage.
64

Figure 3.13 : 3D view and cross-sections of the generic trough cross-bedding model, generated with input parameters extracted from the Gecko Nose outcrop.
66

Figure 3.14 : 3D view and cross-sections of the generic tabular cross-bedding model, generated with input parameters extracted from the Butterfly canyon outcrop.
67

Figure 3.15: Comparison between outcrop photographs and corresponding cross-sections of surface-based models showing foreset-toeset surfaces and mudstone drapes along these surfaces.
68

Figure 3.16: Determination of effective permeability of two outcrop models.
71

Figure 4.1: Variation in a measured reservoir property for different sample volumes and definition of the Representative Element Volume (REV) (Bear, 1972).
79

Figure 4.2: Four mudstone drape coverage scenarios of the intermediate model.
85

Figure 4.3: Intermediate surface-based model of trough cross-bedded tidal sandstone, generated using input parameters extracted from the Gecko Nose outcrop analogue, with the conditions of a flow simulation experiment in the dip orientation.
85

Figure 4.4: Outcrop photograph of one cross-bed set featuring trough cross-bedding lined up with mudstone drapes, and corresponding 3D view and cross-sections of the trough cross-bedded end-member model.
88

Figure 4.5: Outcrop photograph of tabular cross-bed sets, and corresponding 3D view and cross-sections of the tabular cross-bedded end-member model.
89

Figure 4.6: Single-phase flow simulation of the surface-based intermediate model with 25% mudstone drape coverage.
94

Figure 4.7: Normalized effective horizontal permeability versus sample volume.
94

Figure 4.8: Normalized effective permeability in three orthogonal directions for the intermediate model of heterolithic, cross-bedded tidal sandstones for varying sandstone content.
96

Figure 4.9: Normalized effective permeability of the intermediate, trough cross-bedded end-member, and tabular cross-bedded end-member models, for models with wavy-bedded toesets or for models with lenticular-bedded toesets.
98

Figure 4.10: Dip-oriented cross-sections through the trough cross-bedded end-member, intermediate and tabular cross-bedded end-member models, showing the water potential at steady-state.
100

Figure 4.11: Tornado charts summarising the impact on effective permeability of variations in six geometric input parameters in the dip- and strike-oriented directions.
103

Figure 5.1: Intermediate surface-based model of trough cross-bedded tidal sandstone, generated using input parameters extracted from the Gecko Nose outcrop analogue, with the conditions of a flow simulation experiment in the (down) dip orientation.
115

Figure 5.2: Oil/water flow simulation in the horizontal dip and vertical orientations in the intermediate tidal cross-bedding model with only sandstone and difference between effective and fine-scale curves corresponding to the simulation error.
119

Figure 5.3: Evolution of pressures and flow rates through time in the intermediate model with 25% mudstone drape coverage for a horizontal dip oriented flow of 90% oil/10% water.
121

Figure 5.4: Variations in relative permeabilities for flow simulation in two perpendicular orientations of the 25% mudstone drape coverage intermediate model.
122

Figure 5.5: Variations in relative permeabilities for flow simulation in two opposite directions of the 25% mudstone drape coverage intermediate model.
123

Figure 5.6: Oil saturation profiles at steady state for oil/water flow simulation in three orthogonal flow orientations with 100% water injected fluid.
124

Figure 5.7: Variations in relative permeabilities for flow simulation in two opposite directions of the 70% mudstone drape coverage intermediate model.
126

Figure 5.8: Results of relative permeabilities depending on water saturation for two different input saturation curves, the Corey relationships and linear relationships in the 25% mudstone drape coverage intermediate model.
127

Figure 5.9: Comparison of residual oil saturation S_{or} for the different simulations presented in Figures 5.4, 5.5 and 5.7.
129

Figure 5.10: Oil saturation profile at different time steps of a simulated waterflood along depositional strike of a fully oil-saturated, tidal cross-bedded sandstone with 25% mudstone drape coverage.
130

Figure 5.11: Oil saturation profile for the same water injection experiment as shown in Figure 5.10 after 30 months, when steady-state has been reached.
131

Figure 6.1: Three-dimensional models of channels created with different modelling techniques (Jackson *et al.*, in press).
138

Figure 6.2: Alternative gridding for an idealized (elliptical) uneroded cross-bed set containing foreset-toeset surfaces using an unstructured tetrahedral mesh (Jackson *et al.*, in press; after work by A. El-Sheikh and B. Y. G. Massart).
140

Figure 6.3: Snapshots through time of a two-layer high and low permeability model during injection of a tracer across the lower boundary of the model, moving upwards (Jackson *et al.*, in press).
141

Figure 6.4: Cartoons illustrating three alternative template surfaces to capture the different bedding styles in surface-based models of tidally-influenced heterolithic sandstones: parallel-bedding template, wavy-bedding template, and sigmoidal-bedding template.
142

Table of tables

Table 3.1: Input parameters for the Gecko Nose and Butterfly Canyon models.
51

Table 3.2: Results for the Gecko Nose and Butterfly Canyon models after single phase flow simulation.
68

Table 4.1: Input parameters for the intermediate model and for the two end-member settings.
84

Table 5.1: Fluid and rock properties for the oil/water flow simulation of the intermediate tidal cross-bedded sandstone model.
115

Table 5.2: List of water-oil flow simulations conducted for the study.
117

Chapter 1
Introduction

1.1. Reservoir potential of tidally-influenced heterolithic sandstones

Shallow-marine clastic reservoirs continue to be economically important for the oil industry, in line with the diversification of hydrocarbon plays over the past twenty years, in terms of hydrocarbon type (liquefied gas, gas condensates, bitumen) and reservoir nature (tight and heterolithic sandstones, shales). The status of hydrocarbon-bearing heterolithic sandstones has shifted from non-reservoir to reservoir in many plays, as production data has demonstrated their contribution to hydrocarbon recovery. In parallel, recovery techniques have improved over the same period, making heterolithic sandstones more economically viable. However, and despite considerable effort dedicated to their characterisation, the reservoir performance of heterolithic sandstones remains unpredictable due to their highly variable and complex internal architecture, both laterally and vertically.

In shallow-marine reservoirs, heterolithic sandstones constitute a large part of the sedimentary record. Tidally-influenced heterolithic sandstones result from successions of mudstone and sandstone layers as a consequence of periodic variations in the strength of the tidal currents. Tidally-influenced heterolithic sandstone reservoirs are found extensively worldwide, and are being produced in Alaska, Canada, Venezuela and Russia (Martinius *et al.*, 2005). These reservoirs are of particular importance in the Halten Terrace province of the North Sea, which constitutes the most prolific hydrocarbon province offshore mid-Norway with 2.5 billion barrels of recoverable oil and 7.8 trillion cubic feet of recoverable gas. High-profile fields include the Norne, Heidrun and Smørbukk oil fields, and the Midgard, Mikkel and Kristin gas fields (Martinius *et al.*, 2005; NPD, Norwegian Petroleum Directorate). Tidally-influenced heterolithic intervals consist of Early and Middle Jurassic formations: the Åre, Tilje, Tofte, Ile and Garn Formations (Dalland *et al.*, 1988; Martinius *et al.*, 2005). The Tilje Formation has been extensively studied during the past two decades for both sedimentological

(Karlsson, 1984; Gjelberg *et al.*, 1987; Pedersen *et al.*, 1989; Ekern, 1990; Dreyer, 1992, 1993; Taylor and Gawthorpe, 1993; van de Weerd, 1996; Martinius *et al.*, 2001, 2005) and geomodelling purposes (Henriquez and Jourdan, 1996; Wen *et al.*, 1998; Brandsæter *et al.*, 2001, 2005; Nordahl *et al.*, 2005, 2006; Ringrose *et al.*, 2003, 2005).

In particular, the presence of small-scale heterogeneities in the heterolithic sandstones, acting as baffles or barriers to flow, has a significant impact on effective reservoir properties, fluid displacements, and hydrocarbon recovery (Begg and King, 1985; Brandsaeter *et al.*, 2001, 2005; Haldorsen and Lake, 1984; Jackson and Muggeridge, 2000; Jackson *et al.*, 2003, in press; Lasseter *et al.*, 1986; Nordahl *et al.*, 2005; Richardson *et al.*, 1978; Ringrose *et al.*, 2003, 2005; Warren and Price, 1961; Weber, 1982, 1986; White *et al.*, 2004). The permeabilities of tidally-influenced heterolithic sandstone intervals are typically low and highly variable, ranging from 0.1 mD to 3000 mD in the case of the Tilje Formation of the Heidrun field (Nordahl *et al.*, 2005). The work presented in this thesis has been applied in part by Shell Norway to appraisal of the Tilje Formation reservoir in the Linnorm field. Characterisation of upscaled effective reservoir properties of the tidally-influenced heterolithic sandstone intervals is of key importance for determining the producibility of the hydrocarbons that they contain, not only for the Linnorm case, but for any similar reservoir.

1.2. Aims and objectives

The aim of this study is to characterize the influence of small-scale heterogeneities in tidally-influenced heterolithic sandstones on effective flow properties. Several objectives have been identified to meet this aim:

(1) To develop a surface-based modelling method for the building of generic models of tidally-influenced heterolithic sandstones which reproduce the heterogeneities observed at outcrop. The surface-based modelling method should be sufficiently flexible to ensure the incorporation of surface dimensions and geometries measured at outcrop as input parameters.

(2) To quantify the impact on effective permeability of small-scale heterogeneities depending on the mudstone content of cross-bedded heterolithic tidal sandstones on the 3D geometry of the surfaces and associated heterogeneity, and on the distribution of this heterogeneity in the sandstone.

(3) To estimate the relative impact on effective permeability of the different model input parameters, in order to identify which are necessary and sufficient to predict effective permeability, and how effective permeability can be predicted using available subsurface measurements.

(4) To quantify the impact of small-scale heterogeneities on fluid effective relative permeabilities and recovery in the case of oil and water multi-phase flow.

1.3. Thesis structure

In Chapter 2, the key elements of previous studies dedicated to the description of heterogeneities in heterolithic sandstones, the present ways of incorporating the heterogeneities in reservoir simulation models, and their impact on flow are presented to give context to this present study.

In Chapter 3, a novel surface-based modelling workflow is presented for the building of generic models of tidally influenced cross-bedded sandstones. The input parameters for the modelling workflow are listed. These input parameters are required for reproducing the 3D geometry and positioning of foreset-toeset surfaces in cross-bed sets. The results of a statistical analysis performed on the dataset extracted from the Dir Abu Lifa Member are presented. Required input parameters are calculated and generic cross-bedded heterolithic models of two facies observed at outcrop localities are built. The models are visually compared with outcrop exposures to validate the consistency of the surface-based modelling workflow.

In Chapter 4, single phase flow simulation is performed in a set of generic models of tidally influenced cross-bedded sandstone to calculate the effective permeability of this facies. The variation of effective permeability as a function of the sample volume is studied, and a Representative Elementary Volume (REV) for the facies is defined. Flow simulation is performed in three perpendicular orientations for one generic model, and effective permeability is calculated depending on the mudstone drape coverage of foreset-toeset surfaces in cross-bed sets. A sensitivity analysis is performed on the different geometrical input parameters required for the surface-based modelling workflow, in order to determine their relative impact on effective permeability. The spread of plausible values of each parameter is defined by statistical analysis of the outcrop analogue presented in Chapter 3. Applications of the flow-simulation technique for reservoir property modelling of tidally-influenced heterolithic sandstones to hydrocarbon reservoir characterisation are discussed.

In Chapter 5, oil and water multi-phase flow simulation is conducted in one generic model of tidally-influenced cross-bedded heterolithic sandstone, in order to study the impact of mudstone drapes on the effective relative permeabilities of oil and water and on irreducible oil saturation. The impact of mudstone drape coverage and flow orientation are studied. The extra oil trapped in the model due to the introduction of mudstone drapes is tracked, and the mechanisms of oil trapping are discussed.

In Chapter 6, the results of the thesis are put into the perspective of their application in the oil industry. The growing interest in outcrop-based geological modelling is discussed. The benefits of the surface-based methodology are reviewed for different facies and length-scales. Advances in geological and reservoir model gridding are presented, with implications for a new generation of flow simulator software. Finally, the conclusions of the thesis are summarized, followed by recommendations for future work.

1.4. Publications

My PhD supervisors, Matthew D. Jackson, Gary H. Hampson, Howard D. Johnson, Christopher A.-L. Jackson (Imperial College London) and Berit Legler (Wintershall, Germany) provided guidance and feedback during my doctoral research, and during the writing of the thesis and the articles listed below.

Two publications from the thesis are planned for journal submission, corresponding respectively to Chapters 3 and 4:

Massart, B. Y. G., M. D. Jackson, G. J. Hampson, B. Legler, H. D. Johnson, C. A.-L. Jackson, R. Ravnås and M. Sarginson, in preparation, Effective flow properties of heterolithic, cross-bedded tidal sandstones: part 1. Surface-based modelling, to be submitted to *AAPG Bulletin*.

Massart, B. Y. G., M. D. Jackson, G. J. Hampson, B. Legler, H. D. Johnson, C. A.-L. Jackson, R. Ravnås and M. Sarginson, in preparation, Effective flow properties of heterolithic, cross-bedded tidal sandstones: part 2. Flow simulation, to be submitted to *AAPG Bulletin*.

During the course of my PhD, I contributed to three other publications:

Legler B., H. D. Johnson, G. J. Hampson, **B. Y. G. Massart**, C. A.-L. Jackson, M. D. Jackson, A. El-Barkooky and R. Ravnås, 2013, Facies model of a fine-grained, tide-dominated delta: Lower Dir Abu Lifa Member (Eocene), Western Desert, Egypt, *Sedimentology*, **60**, 1313-1356.

Jackson, M. D., G. J. Hampson, A. El Sheikh, J. H. Saunders, G. H. Graham and **B. Y. G. Massart**, in press, Surface-based reservoir modelling, Sediment body geometry and heterogeneity: analogue studies for modelling the subsurface, *Geological Society (London) Special Publication*, **387**.

Legler B., G. J. Hampson, C. A.-L. Jackson, H. D. Johnson, **B. Y. G. Massart**, M. Sarginson and R. Ravnås, in review, Facies relationships and stratigraphic architecture of a distal, mixed tide-and-wave-influenced delta: Lower Sego sandstone, Western Colorado, USA, submitted to *Journal of Sedimentary Research*.

Six presentations based on this thesis research were given as talks (*) or posters at international conferences:

Legler B., **B. Y. G. Massart**, H. D. Johnson, G. J. Hampson, M. D. Jackson, C. A.-L. Jackson, A. El-Barkooky, R. Ravnås, D. Alsop and X. Le Varlet, 2010, Characterisation of a tide-dominated heterolithic reservoir analog; the Eocene Dir Abu Lifa Member (Western Desert, Egypt): AAPG annual convention and exhibition, April 11-14, New Orleans, USA.

***Massart, B. Y. G.**, M. D. Jackson, G. J. Hampson, B. Legler, H. D. Johnson, C. A.-L. Jackson, A. Bréhéret, J. Daboer, R. Ravnås and M. Sarginson, 2010, Improved characterisation and modelling of low permeability heterolithic deltaic sandstone reservoirs: Petroleum Geoscience Research Collaboration Showcase, November 23-25, London, UK.

***Massart, B. Y. G.**, M. D. Jackson, G. J. Hampson, B. Legler, H. D. Johnson, C. A.-L. Jackson, R. Ravnås and M. Sarginson, 2011, Three-dimensional characterisation and surface-based modeling of tide-dominated heterolithic sandstones: 73rd EAGE conference and exhibition, May 23-26, Vienna, Austria.

Massart, B. Y. G., M. D. Jackson, G. J. Hampson, B. Legler, H. D. Johnson, C. A.-L. Jackson, R. Ravnås and M. Sarginson, 2011, Characterisation and surface-based modelling of heterolithic tidal sandstone reservoirs: BSRG annual meeting, December 18-21, London, UK.

***Massart, B. Y. G.**, M. D. Jackson, G. J. Hampson, B. Legler, H. D. Johnson, C. A.-L. Jackson, R. Ravnås and M. Sarginson, 2012, Three-dimensional surface-based modeling and flow simulation of heterolithic tidal sandstone reservoirs; examples from the Eocene Dir Abu Lifa Formation reservoir analogue, Western Desert, Egypt: AAPG annual convention and exhibition, April 22-25, Long Beach, USA.

***Massart, B. Y. G.**, M. D. Jackson, G. J. Hampson, B. Legler, H. D. Johnson, C. A.-L. Jackson, R. Ravnås and M. Sarginson, 2013, Effective permeability in tidal heterolithic cross-bedded sandstones: AAPG annual convention and exhibition, May 19-22, Pittsburgh, USA.

Chapter 2
Literature review

2.1. Heterogeneities in tidally-influenced heterolithic sandstone reservoirs

The main characteristic of tidal deposits is horizontal (lateral) and vertical cyclicity. Tidal cyclicity is related to lunar cycles, with typical diurnal successions of oppositely directed flood and ebb tidal currents, separated by slack water periods. During these slack-water periods, mud particles and clay flocculate due to electronic interactions as flocs of higher density that are deposited from suspension in structureless mudstone layers up to several meters in the form of fluidized muds (or fluid muds) in the maximum turbidity areas of estuaries and deltas (Wright *et al.*, 1988; Uncles *et al.*, 2006; Ichaso and Dalrymple, 2009; Legler *et al.*, 2013). Fluid muds correspond to mobile near-bed body of flocculated fine-grained sediment with a solid concentration superior to 10 $g.L^{-1}$. Fluid muds may form continuous mudstone drapes over underlying sandy bedforms (Allen, 1981; Dalrymple *et al.*, 2003). Lithological boundaries between sandstone laminae and mudstone drapes constitute centimetre- to metre-scale heterogeneities in tidally-influenced heterolithic sandstones, and are referred as small-scale heterogeneities in this study (*sensu* Martinius *et al.*, 2005). Mudstone drapes are preferentially formed and preserved in the transition zone of estuaries and deltas, where mixing of fresh riverine water and saline marine water into brackish water occurs (Dalrymple and Choi, 2007). The variation of salinity in this transition zone leads to the flocculation of clay particles, which are deposited as cohesive mudstone drapes. In fact, due to the electronic interactions of the clay elements, mudstone drapes require a high energy to be eroded, most of the time only partially (Nio and Yang, 1991 ; Dalrymple *et al.*, 2003).

In tide-influenced coastal depositional environments, cross-strata are resulting from the migration of dunes and bars that are composed of sandstone and intercalated mudstone. The mudstone is distributed according to periodic cycles in tidal current velocity. Different orders of tidal cyclicity are recorded in the resulting successions (e.g. Nio and Yang, 1991). The shortest

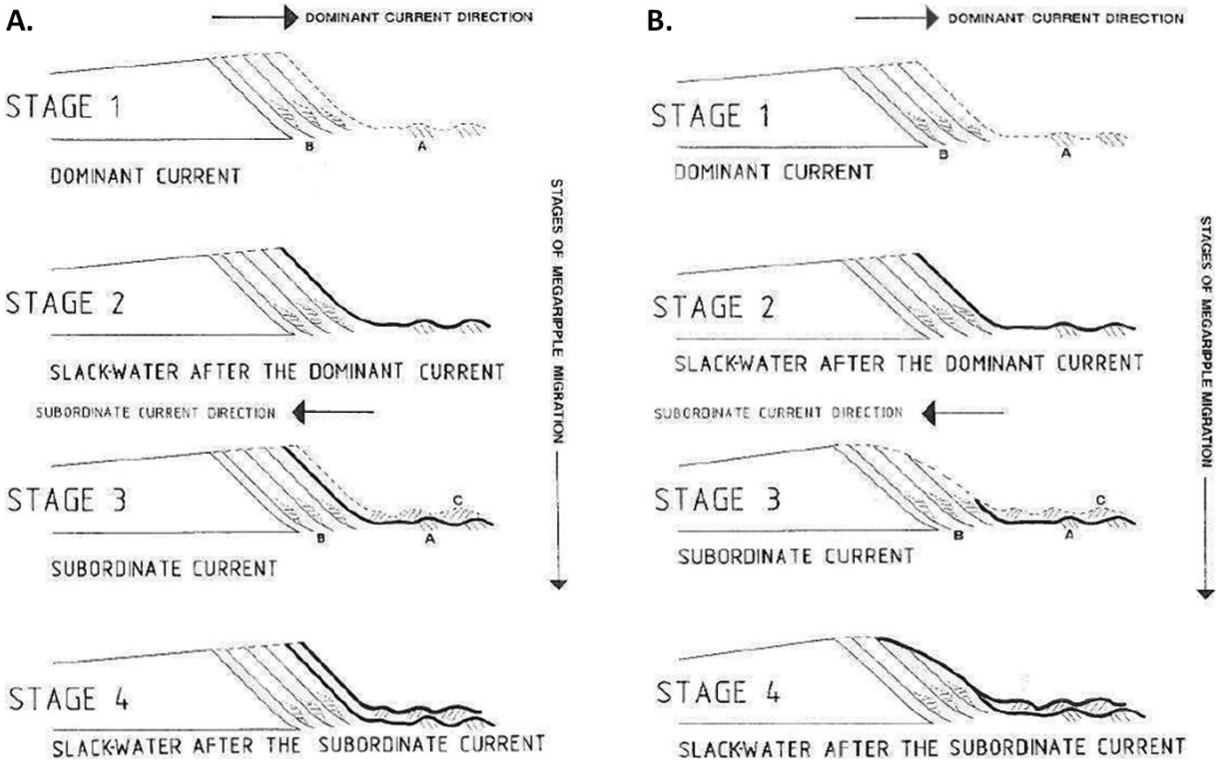


Figure 2.1: Schematic drawing of dune migration during a single flood-ebb cycle A. with weak subordinate currents; B. with strong subordinate currents. Stage 1: co-flow ripple cross-lamination is formed during dominant current stage; Stage 2: mudstone drape is deposited during slack water; Stage 3: small ripple cross-lamination set is produced by subordinate current; Stage 4: mudstone drape is deposited during slack water (Nio and Yang, 1991).

tidal cycle is semi-diurnal (c. 12 hour periodicity), and is characterized by the alternation of the flood and ebb tidal current stages, separated by slack-water periods. In an idealized semi-diurnal tidal cycle, both the ebb and flood tides are recorded by deposition of a sand lamina on the lee face (foreset) of a dune (Visser, 1980) (Figure 2.1). In the dune toesets, sand ripples of opposed orientation are deposited during ebb and flood tides (Klein, 1970; Boersma and Terwindt, 1981). The slack-water periods are recorded by mudstone drapes that separate foreset-toeset sand laminae of the ebb-tidal and flood-tidal currents. The tide is typically asymmetric, such that either the ebb-tidal or flood-tidal currents are dominant (Visser, 1980). The dominant tide is represented by a thicker foreset-toeset sand lamina and the subordinate tide by a thinner lamina. A single, fully preserved semi-diurnal tidal cycle is thus represented by two sand laminae and two mudstone drapes (“paired mudstone drapes” of Nio and Yang, 1991, or “mud couplet” of Visser, 1980), and represents one tidal bundle (Boersma, 1969). Mudstone drapes can be partially or entirely eroded by the succeeding tidal current if this current is sufficiently strong

as indicated above, such that only one mudstone drape and one reactivation surface may be preserved (e.g. de Mowbray and Visser, 1984). As a result, the mud couplet is preferentially preserved in the dune toeset. Due to the cohesive nature of the mudstone drapes, patchy mudstone drapes occur, where the mudstone is torn away in patches instead of being eroded particle after particle, resulting in a continuous mudstone drape but with "holes" of varying size, up to 20 cm wide (Martinius and Van den Berg, 2011).

The second tidal cycle is diurnal in period (c. 24 hours). A thick-thin alternation of successive semi-diurnal tidal bundles is observed in diurnal tidal systems due to the unequal velocities reached by successive ebb or flood tides (Figure 2.2). A third tidal cycle records variations in peak tidal current velocities over a lunar cycle (spring-neap cycle) of c. 14 days. Close to the full moon, the tide is more energetic (spring tide) with the result that semi-diurnal tidal bundles are thicker and more sand-rich, reflecting stronger and more sustained tidal currents. During the new moon, the tide is less energetic (neap tide) and the semi-diurnal bundles are thinner and more mud-rich. An idealized neap-spring cycle contains a systematic variation in the thickness and sand content of 28 semi-diurnal tidal bundles. Longer period tidal cycles are noted in the sedimentary record (Kvale *et al.*, 1989), but they are exceptionally rare.

Superposition of the different tidal cycles, combined with other sediment transport processes (i.e. erosion pattern, aggradation of the structures, marine and fluvial current relative strengths compared to tidal current strength), leads to preservation of sandy foresets and muddy toesets. A vertical profile through dune toeset deposits typically exhibits rhythmical alternation of millimetre- to centimetre-thick, wavy bedded mudstone and sandstone layers (Reineck and Singh, 1969). Depending on the strength of the subordinate tidal current, mudstone drapes are more or less preserved in the toesets, generating lenticular or flaser bedding, respectively. The transition between foresets and toesets of laminae in a cross-bed set is marked by a gradual downcurrent curvature. The resulting foreset-toeset geometry may be referred as "shovel" shaped (van den Berg *et al.*, 2007). In rhythmites the same tidal cycles can be recognized, accreting vertically. Rhythmites have the same aspect as the toesets of cross-bed sets, featuring planar- or wavy-bedding depending on the current strength. Wavy-bedded layers display a range of sandstone contents due to differences in mud preservation

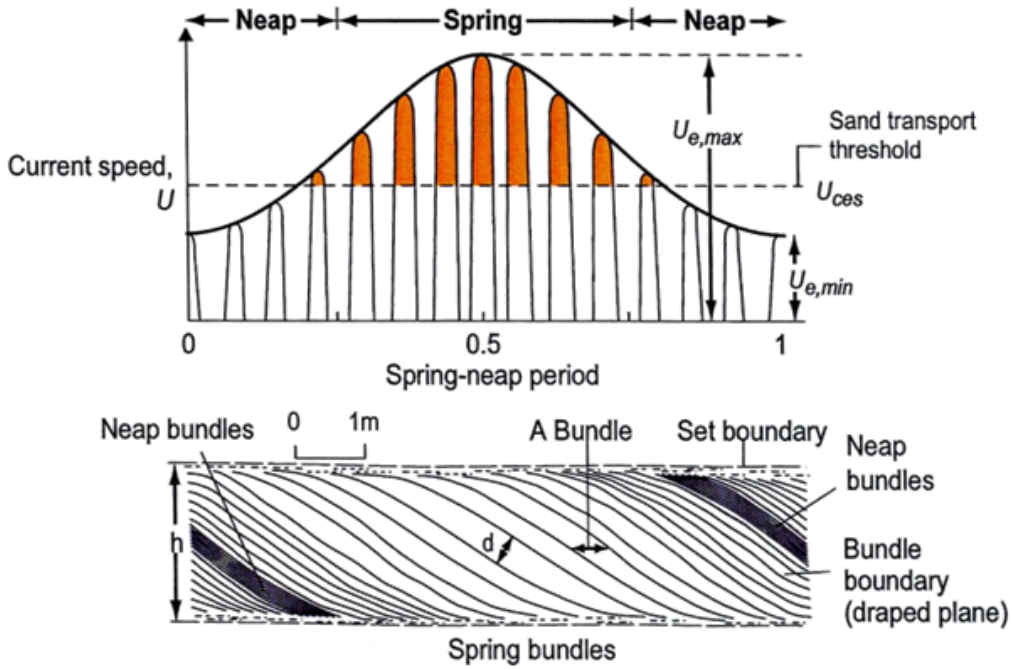
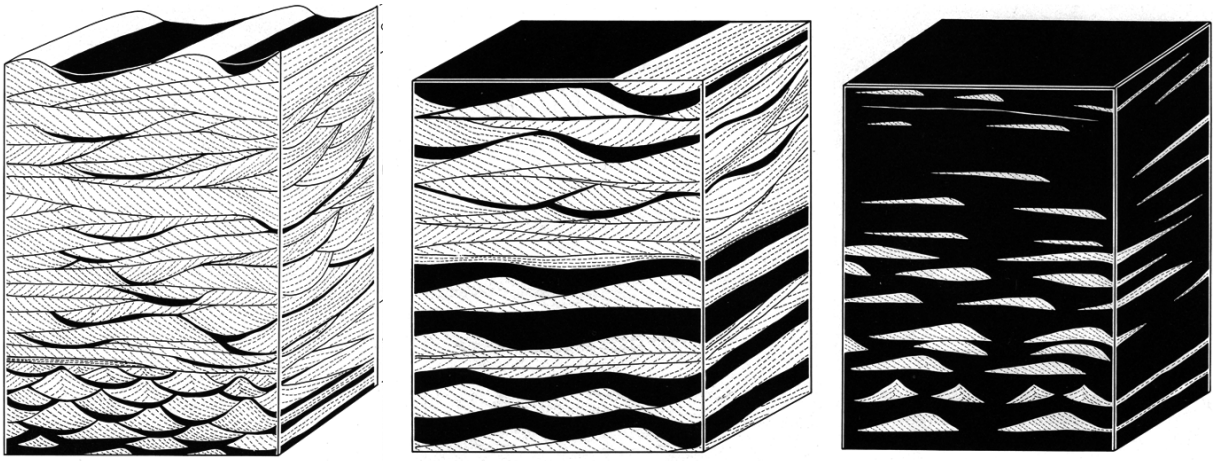


Figure 2.2: Schematic drawing of a neap-spring tidal bundle sequence. The bundle boundaries have thin mudstone drapes and/or erosional reactivation surfaces. During the spring tides, the tidal current is strong enough to transport sand ($U_e > U_{ces}$, sand transport threshold) so the bundles are thick. Thin bundles occur during neap tides (Visser, 1980; Nio and Yang, 1991)



A. Flaser bedding B. Wavy bedding C. Lenticular bedding

Figure 2.3: 3D-diagrams representing the organisation, distribution and connectivity of sandstone layers in tidal deposits: A. flaser bedding; B. wavy bedding ; C. lenticular bedding (Reineck and Singh, 1980 ; modified after Reineck and Wunderlich, 1968)

depending on current strength (Figure 2.3 B). Flaser bedding corresponds to higher energy domains where the mudstone layers are poorly preserved, leading to high connectivity of the sandstone layers both laterally and vertically (Figure 2.3 A). Lenticular bedding consists of sandstone lenses which are enclosed by adjacent mudstone layers. The connectivity of sandstone layers is limited or absent (Figure 2.3 C). Lenticular bedding is characteristic of low current domains.

2.2. Reservoir modelling techniques for the representation of tidally-influenced heterolithic sandstones

Traditional modelling techniques use stochastic methods to generate the distribution of petrophysical properties in reservoir models. These methods can be divided into three main groups: (1) sequential simulations (sequential Gaussian simulation or SGSIM) or indicator kriging (sequential indicator simulation or SISIM) (e.g. Journel and Huijbregts, 1978), (2) object based modelling (OBM) (e.g. Haldorsen and Damsleth, 1990) and (3) hybrid techniques (as multiple point statistics, MPS) (as multiple point statistics, MPS, e.g. Strebelle, 2002). Despite their range of application, these methods fail to adequately reproduce petrophysical property distributions in heterolithic sandstones because lithology distributions vary locally over very small distances, so the predictability of the lithology distribution is highly uncertain and cannot be approached using standard stochastic methods (Sech *et al.*, 2005; Jackson *et al.*, 2003, 2005, 2013) (note: all these techniques are variogram-based).

Outcrop modelling methods

Outcrop analogues have been used in previous studies to gain qualitative and quantitative understanding of depositional processes, lithology distributions and petrophysical property trends in heterolithic sandstone reservoirs. In particular, high-resolution flow models have been constructed using outcrop analogues to demonstrate the influence of geological heterogeneities on recovery. These high-resolution flow models capture a very exhaustive heterogeneity hierarchy at multiple scales by physically representing the heterogeneities as volumes of cells in a grid as opposed to interface transmissibility mutlipliers (sensu Kjønsvik *et al.*, 1994; Sech *et al.*, 2005). In order to introduce the hierarchy of heterogeneities with realistic geometries, reservoir models with a high number of cells are required. For example, the influence of clinoforms in shoreface parasequences has been studied using outcrop analogues of the Cretaceous Blackhawk Formation in the Book Cliffs, Utah (Sech *et al.*, 2009); and the impact of boundaries between large sedimentary objects (e.g. bars and channels) in the tidal deltaic environment of the Tilje Formation (Brandsæter *et al.*, 2005). Most analogues are exposed

in 2-D cliff faces, which have been reconstructed as 2-D models (White and Barton, 1999; Willis and White, 2000; White *et al.*, 2004). Deterministic surface-based modelling techniques were used in generating these models because they suit the complexity and tight constraints of datasets extracted from outcrop analogues. Surfaces representing stratigraphic surfaces, facies and lithology boundaries, mudstone drapes and cements are traced from distortion-corrected photomontages (White *et al.*, 2004). These surfaces are then used to constrain a cornerpoint grid in which the architecture of the grid layers is governed by the architecture of the modelled surfaces. As the grid is specifically designed to capture heterogeneities, a minimum number of active grid cells is required.

3D-outcrop analogue modelling studies are very limited. However outcrop modelling techniques were already used to build deterministic models of tidally-influenced sandstone rock specimens, using 3D-reconstruction of serial sections (e.g. Figure 2.4) (Jackson *et al.*, 2005). The dimensions of the models of Jackson *et al.*, and the small scale heterogeneities described at the outcrop and introduced in the models are similar to the scale of models described in this thesis afterwards. As discussed in the previous sections, small-scale heterogeneities introduced by tidal processes vary laterally. Lateral and vertical continuity and connectivity of sandstone layers and mudstone drapes in heterolithic facies are the key parameters to reproduce for building accurate models. A surface-based modelling workflow was developed to capture the complex geometry of small-scale heterogeneities in tidally-influenced sandstones, and their complex 3D connectivity (Jackson *et al.*, 2005).

Surface-based modelling methods

Predictive reservoir models for heterolithic tidal sandstones should incorporate heterogeneities with realistic geometries, reproducing the complex connectivity of mudstone and sandstone layers as observed in outcrop analogues (Jackson and Muggeridge, 2000). However, most modelling processes are grid-based, with facies and lithologies being distributed on a pre-defined grid that only honours the geometry of the main horizons of a structural model. Intermediate horizons are typically subordinate to the grid architecture, such that

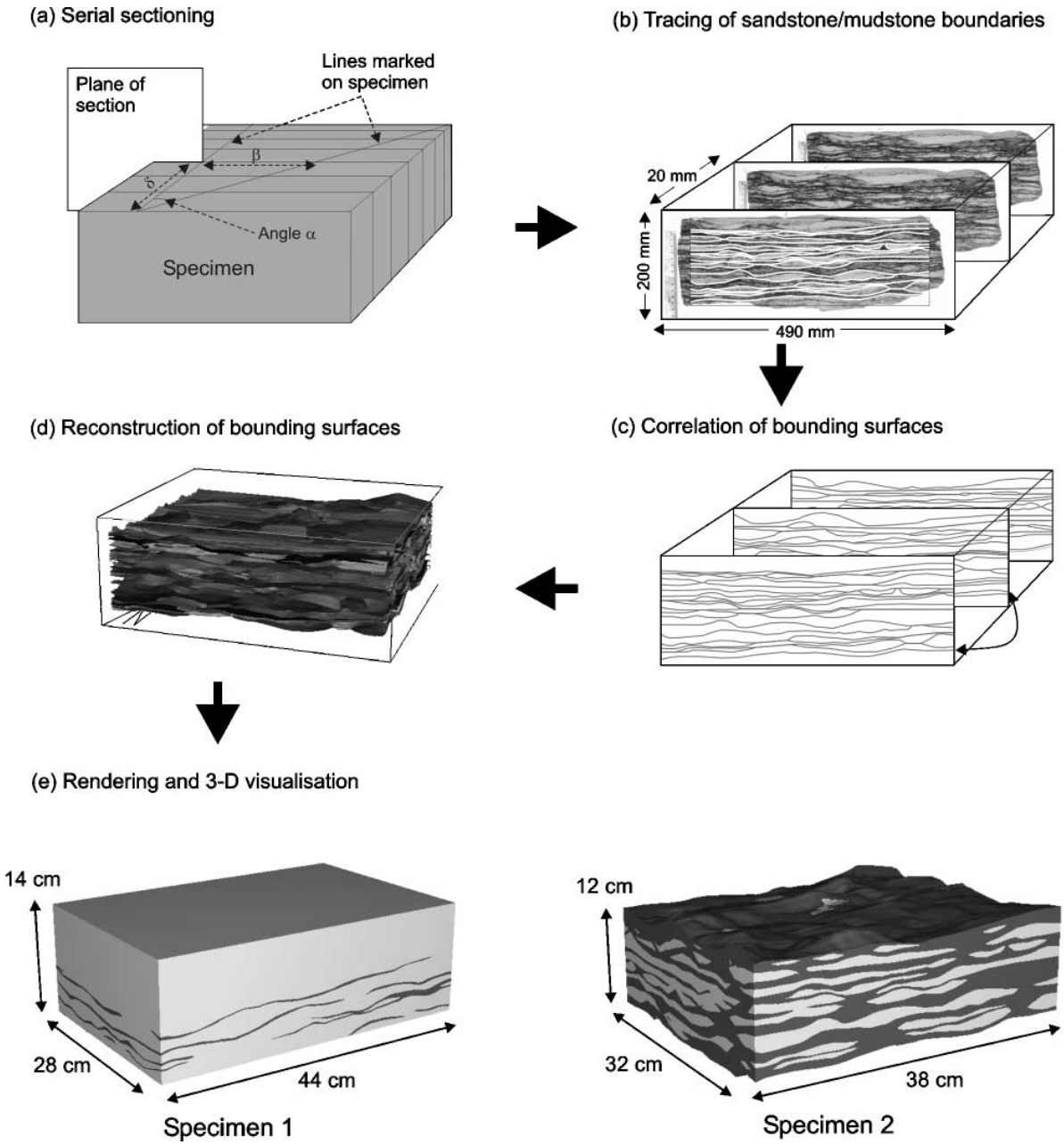


Figure 2.4: Surface-based modelling workflow for models of flaser bedded (specimen 1) and wavy bedded (specimen 2) rock specimens. (a) serial sectioning of the specimens; (b) tracing of the facies boundaries on each section, after scanning of the sections; (c) correlation of bounding surfaces from section to section; (d) 3D surface reconstruction using interpolation in geological modelling software; and (e) rendering and visualization of the two specimens. Light colours denote sandstone; dark colours denote mudstone (Jackson *et al.*, 2005).

facies boundaries or fault traces may be grossly simplified with stair-step geometries that follow the regular shape of the grid cells. When the reproduction of geometrically complex surfaces is critical - as for tidal heterolithic sandstones - alternative surface-based modelling techniques are preferred. For surface-based modelling techniques, high-resolution structural, stratigraphic and/or sedimentological surfaces are created as an initial step to reproduce heterogeneity along the surfaces. Only then is a grid honouring the geometry of the modelled surfaces built for flow simulation purposes. With a surface-based modelling workflow, the facies modelling is not subordinate to the limitations of an underlying regular grid.

Surface-based modelling workflows were developed and improved over the past ten years (Deutsch *et al.*, 2001; Jackson *et al.*, 2005; Pyrcz *et al.*, 2005; Sech *et al.*, 2009; Jackson *et al.*, 2009). All surface-based modelling workflows follow five steps, as outlined by Sech *et al.* (2009):

(1) Identify the heterogeneities in the data set and decide which will be captured in the model. Depending on the length-scale of the studied heterogeneities, a hierarchy of heterogeneities must be developed. Studies by Kjønsvik *et al.* (1994) and Sech *et al.* (2009) develop their own hierarchy for shallow-marine sandstones with four levels of heterogeneities. Small-scale heterogeneities characterized in this PhD study correspond to the smallest length-scale of both studies (Level 4 of Kjønsvik *et al.*, 1994).

(2) Decide which heterogeneities will be captured deterministically and which will incorporate a stochastic element. The choice depends on the resolution of the dataset. Stochastic modelling is much more tightly constrained with outcrop analogue data than with the subsurface data.

(3) Spatially reference the outcrop data. Digital elevation models (DEMs), global positioning systems (GPS) (Sech *et al.*, 2009), differential GPS (DGPS) data (Bryant *et al.*, 2000), laser ranging and scanning devices such as light detection and radar (LiDAR) (Bellian *et al.*, 2005), and digital photogrammetry (Sgavetti, 1992) have been used to spatially reference outcrop data in previous surface-based modelling studies.

(4) Model surfaces that capture the different levels of heterogeneity. To ensure that surfaces are suitable for later gridding, the following rules must be applied

- all surfaces and zones must be continuous across the model;
- where a zone pinches out, it is still defined but has zero thickness (i.e. the upper and lower boundaries surfaces coincide);
- surfaces cannot cross each other and should be vertically monotonic (i.e. no overhanging surfaces) (Jackson *et al.*, 2005).

(5) Gridding for flow simulation. Orthogonal Cartesian grids are generally used in flow simulation software using finite element theory assumption, because the equations of flow are easy to solve using rectangular cells. However, such grids fail to honour sediment-body geometries (White and Barton, 1999). To avoid this issue, the more computationally efficient corner-point gridding methodology is preferred. However, this methodology has its own disadvantages as it introduces numerous pinched-out cells in the reservoir model, leading to numerical artefacts in commercial flow simulator software that use 5-point flux or 9-point flux approximations to solve the flow equations.

As an example, the SBED software, developed by Wen *et al.* (1998) after generic observations on bedding styles by Rubin (1987), generates surfaces that reproduce wavy-bedding and cross-bedding structures in a surface-based modelling workflow. Unlike sedimentary process-based modelling techniques, in which approximations of the physics of grain transportation and deposition are used, SBED represents the geometrical arrangement of sedimentary bedding by migrating a set of bedding surfaces in a manner that mimics observed geometries (Wen *et al.*, 1998; Ringrose *et al.*, 2005). The input parameters to the software describe the bedform morphology in cross-section and plan-view (by a sine function), as well as the migration of the bedform surfaces in space and time with a spatial vector. The migration of bedforms, which in nature is a result of periodic avalanching and suspension fallout on the lee and stoss sides of the bedform, is simulated by displacement of successive sine curves separated by the spatial vector. The geometrical 3D-sinusoidal function together with stochastic elements introduced by 2D Gaussian functions allow the user to reproduce more accurately the form of the deposits generated by tidal currents. The SBED software has been used in numerous studies to generate reservoir models of tidally-influenced heterolithic sandstones suitable for flow simulation, in particular for wavy-bedded sandstones of the Tilje Formation (Figure 2.5) (Nordahl *et al.*, 2005, 2006; Ringrose *et al.*, 2005; Nordahl and Ringrose, 2008).

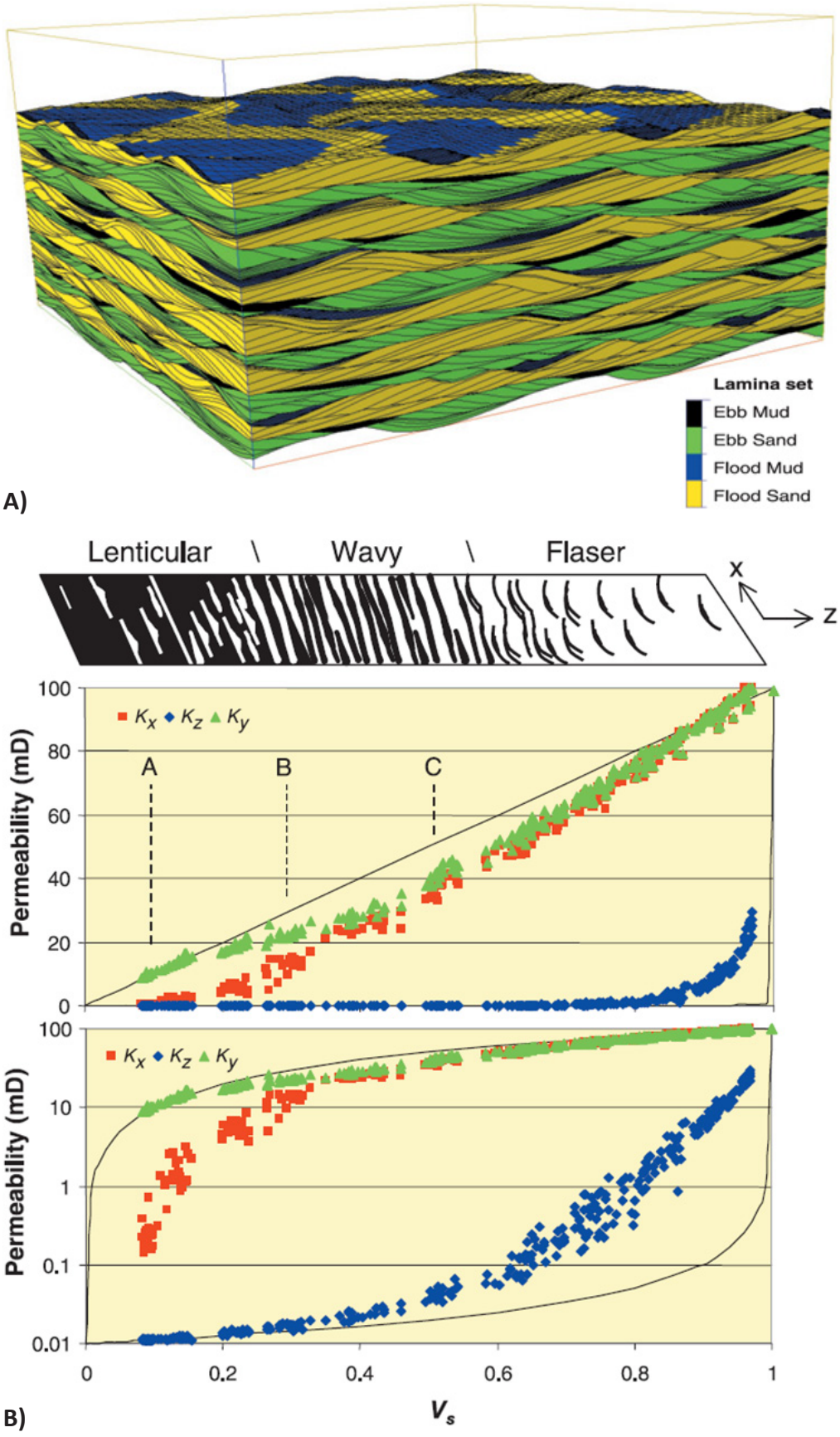


Figure 2.5: A) Surface-based model of wavy-bedded deposits generated by the software SBED. Note the bidirectional sand lamina sets (lines) and the partially preserved mudstone drapes (black and blue). The model volume is 0.5 x 0.5 x 0.1 m. B) Results of effective permeability for flow in the 3 orthogonal directions for models of the different wavy bedding structures, in both regular and logarithmic scales. For each flow orientation, a percolation threshold exists marked A, B or C, as predicted by the percolation theory (Ringrose *et al.*, 2005).

2.3. Estimation of the effects of small-scale heterogeneities on reservoir properties

Previous studies have investigated the effect of mudstone drapes on reservoir performance in tidally-influenced heterolithic sandstones. Large-scale heterogeneity surfaces have been proven to have a large impact on reservoir performances and fluid production timing at the reservoir scale. One typical example for the impact of heterogeneity surfaces in shallow-marine reservoir consists in the clinoform surfaces in deltaic systems. The facies distribution is conditioned by the clinoform surface position and geometry. In addition to the facies distribution, clinoform surfaces are typically affected by diagenetic processes, such as cementation, which happens preferentially along the heterogeneity surfaces. During waterflooding recovery, the water flow is driven preferentially along these heterogeneity surfaces, "climbing up" the surfaces, and provoking early water breakthrough compared to forecast models where deltaic deposits are modelled in a layercake setup (Jackson *et al.*, 2009, 2013; Sech *et al.*, 2009; Graham *et al.*, in review).

The impact of small-scale heterogeneities has similarly been proved important to reservoir behaviour and effective flow properties at the meter length-scale. Small-scale heterogeneities can act as flow barriers when they contribute to oil entrapment in "dead ends" where there is a significant contrast in capillary pressure between porous sandstone layers and surrounding mudstone drapes (Lasseter *et al.*, 1986). Depending on their lateral extent, small-scale heterogeneities can act as flow baffles by increasing the tortuosity of flow paths and the time required for sweep, decreasing the effective permeability (e.g. Haldorsen and Lake, 1984; Jackson and Muggeridge, 2000). However, the studies on heterogeneities impact on flow in single phase and multi-phase flow regimes are very limited, typically in 2D, limited to large-scale heterogeneities and not small-scale heterogeneities (e.g. Lasseter *et al.*, 1986; Kjonsvisk *et al.*, 1994). At the meter length-scale, studies have only focused on dune cross-bedding structures without tide influence (i.e. no mudstone drape; e.g. Kortekaas, 1985; Hartkamp-Bakker, 1991) or wavy-bedding structures (e.g. Jackson *et al.*, 2003; Nordahl *et al.*, 2005). Furthermore, reservoir performances and behaviour at the reservoir length-scale have been proved affected by small-scale heterogeneities (see all the references of this paragraph). This is

notably the case for oil entrapments due to capillary pressure effect introduced by differential permeability in heterolithic facies. Strategies of upscaling have been defined in order to integrate numerically the impact of small-scale heterogeneities at the reservoir length-scale, with the example of geopseudo functions (e.g. Ringrose *et al.*, 1993; Pickup *et al.*, 1994, 2000; Ciammetti *et al.*, 1995; Pickup and Carruthers, 1996; Pickup and Sorbie, 1996).

Despite their effect on reservoir performance, the small-scale heterogeneities of tidally-influenced heterolithic sandstones cannot be incorporated directly into reservoir models because of their small size and abundant quantity. Instead, effective reservoir properties are conventionally used to take into account the influence of the small-scale heterogeneities in reservoir models. The facies associations populating the cells of reservoir models are considered as homogeneous media. The reservoir properties assigned to these facies associations account for their reservoir performances at the length-scale of the reservoir grid cell, making them effective reservoir properties.

The estimation of effective permeabilities for heterolithic sandstone reservoirs based on subsurface data is a challenge as both individual and averaged effective permeability values vary as a function of sample volume (Jackson *et al.*, 2003; Nordahl *et al.*, 2005). The permeability data obtained from core-plug measurements will not be representative at the scale of a reservoir model grid-block, regardless of the number of measurements taken. Thus, the standard procedure of averaging or "blocking" core-plug permeability data, from the measurement scale to the model grid-block scale, will introduce an error to the resulting effective permeabilities. For models of wavy-bedded heterolithic sandstones, the error is negligible for horizontal permeability but significant for vertical permeability, especially if the contrast in permeability between lithologies is large (Jackson *et al.*, 2003). The geometric mean is the most suitable technique for averaging both horizontal and vertical core-plug measurements in most heterolithic tidal facies. However, in the case of flaser bedding, the most suitable technique for averaging horizontal permeability is the harmonic mean, and in the case of lenticular bedding, the most suitable technique for averaging vertical permeability is the arithmetic mean (Jackson *et al.*, 2003). No averaging methodology was found to predict the effective properties of tidally-influenced cross-bedded heterolithic sandstones, because of the complex architecture of the mudstone drape network.

Effective reservoir properties may instead be computed from high-resolution mini-models of the heterolithic facies. The models are fully flow simulated, reproducing the display of core-plug flow experiments, with effective permeability being back-calculated from the pressure gradient using Darcy's law. Nordahl *et al.* (2005) used a two component system (mudstone and sandstone, or siltstone and sandstone) to model small-scale heterogeneities in wavy-bedding heterolithic sandstones of the Tilje Formation. A mudstone content threshold can be observed for which the reservoir behaviour of the heterolithic rock changes from a homogeneous medium (with low mudstone content) to a heterogeneous medium (with high mudstone content). The existence of such a threshold is predicted by percolation theory, which states that, assuming two components where one is impermeable and the components are distributed randomly in space, a threshold for flow can be evaluated as a function of the conducting component (Begg and King, 1985).

These studies highlight that the behaviour of heterolithic sandstones can be understood in terms of connectivity of the sandstone and mudstone laminae. The geometry and spatial organization of the deposits are key parameters to characterize in order to estimate the effective flow properties of heterolithic sandstones (Jackson *et al.*, 2005). Inclined and intersecting discontinuous mudstone layers have a significant effect on sweep efficiency if they are continuous over large areas of bedding surfaces and are steeply inclined to the dominant flow direction (Jackson and Muggeridge, 2000). However, 3D studies show that the effect of mudstone drapes on reservoir performance is often overestimated in 2D simulations because the latter assume that mudstone layers are entirely continuous in the third dimension (Jackson and Muggeridge, 2000). Thus, the modelling techniques chosen for building models of tidally-influenced heterolithic sandstones should reproduce the 3D geometry and organization of the sandstone and mudstone deposits as accurately as possible, to obtain predictive models.

Chapter 3
Effective flow properties of heterolithic, cross-bedded tidal sandstones: part 1. Surface-based modelling

Summary

Tidal heterolithic sandstone reservoirs contain millimetre to centimetre-scale intercalations of mudstone and sandstone, and their effective flow properties are poorly predicted by data that do not sample a representative volume of rock, or models that fail to capture the complex three-dimensional architecture of sandstone and mudstone layers. We present a novel, surface-based modelling approach which honours the geometry of geologic surfaces that control such lithologic variability. The workflow uses template surfaces to represent heterogeneities classified by geometry rather than length-scale. The surface-based methodology has been applied to generate generic, 3D mini-models of cross-bedded heterolithic sandstones (volume of 9 m^3) representing trough and planar cross-bedding with differing proportions of sandstone and mudstone, using conditioning data from two outcrop analogues from a tide-dominated deltaic deposit. We show that mudstone drapes in cross-bedded heterolithic sandstones significantly reduce effective permeability and also impart permeability anisotropy in the horizontal as well as vertical flow directions. The workflow presented here can be used with subsurface data, supplemented by outcrop analogue observations, to generate effective permeability values to be derived for use in larger-scale reservoir models that better capture the impact on flow of tidal heterolithic sandstones.

3.1. Introduction

Heterolithic sandstones are generated by tidal processes in shallow marine environments such as deltaic and estuarine systems. In these tidally-influenced environments, the main current direction varies depending on the relative strength of tidal currents over cyclical time periods, and the interaction of tidal currents with waves and river currents (e.g. Dalrymple and Choi, 2007). Sand is transported as bedload by strong currents to form ripples and dunes during periods of rising (flood) and falling (ebb) tide, and mudstone drapes are deposited during intervening slack-water periods. Depending on the flow regime, the mudstone drapes are more or less continuous over the sandy bedforms (Reineck and Wunderlich, 1968; Reineck and Singh, 1980; Nio and Yang, 1991). Interstratified, millimetre- to centimetre-thick sandstone and mudstone layers are deposited as a result of such periodic variations in current velocity over multiple tidal cycles, and form the fine-scale heterogeneities that are characteristic of heterolithic tidal sandstone reservoirs. The distribution of mudstones and sandstones is delimited by a hierarchy of stratigraphic surfaces including (in order of increasing length scale): (1) lamina boundaries and reactivation surfaces that record incremental migration of bedforms, (2) the erosive bases of beds and bedsets, (3) boundaries between facies and facies associations, and (4) sequence stratigraphic surfaces. These four-level stratigraphic surfaces define the multi-scale architecture and connectivity of mudstone and sandstone layers which, in turn, exerts a key control on the flow of gas, oil and water during field production (Weber, 1986; Jackson *et al.*, 2003, 2005; Ringrose *et al.*, 2005; Nordahl *et al.*, 2005, 2006; Nordahl and Ringrose, 2008).

The presence of these multi-scale heterogeneities in heterolithic tidal sandstone reservoirs ensures that the characterisation of effective reservoir properties such as permeability, relative permeability and capillary pressure, is a recurring problem (e.g. Martinius *et al.*, 2005). Effective reservoir properties are typically derived from subsurface well data such as wireline logs and well tests, combined with laboratory measurements on cores and plugs (porosity, permeability, sandstone connectivity, porous media network, wettability). Laboratory-derived reservoir properties are measured at a length scale that is small (of order centimetres for a

typical core plug) compared to the dimensions of grid cells in reservoir simulation models (of order tens to hundreds of metres in plan-view, and tens of centimetres to metres in the vertical direction). In the case of tidal heterolithic sandstones, lateral and vertical variations in the continuity and connectivity of sandstone and mudstone laminae, are not sampled by subsurface well data or laboratory measurements. Effective reservoir properties in heterolithic units are highly dependent on the volume sampled (Norris and Lewis, 1991; Jackson *et al.*, 2003, 2005; Nordahl and Ringrose, 2008). Consequently, effective reservoir properties derived solely from subsurface and laboratory data in such heterolithic units are rarely representative of reservoir behaviour because the samples are simply too small to capture enough heterogeneities; instead, models that are required capture the continuity and connectivity of sandstone and mudstone laminae at the length-scale of interest

Two different methodologies have been used to create such models, which both use stratigraphic surfaces to reproduce multi-scale heterogeneities. The first approach mimics depositional processes by generating and translating bedforms of specific geometry, characteristic of the depositional processes (typically sinusoidal shape for cross-bedding structures or traction-related structures; planar surfaces for parallel-bedding structures or suspension-loading structures) according to user-defined inputs such as current velocity and sediment accumulation rate through time (e.g. Rubin, 1987; Wen *et al.*, 1998; Rubin and Carter, 2005). Cross-stratification is defined by the preserved remnants of the bedform-bounding surfaces, while lithologies are distributed according to the local current velocities during deposition. This process-based methodology has been used to generate highly realistic models of near-wellbore regions (with dimensions or order 0.3 x 0.3 x 2 m) (Nordahl *et al.*, 2005; Ringrose *et al.*, 2005). However, process-based methodologies suffer from two problems. First, the models cannot be conditioned directly to outcrop or subsurface data. Second, the required input parameters describing ancient depositional properties such as variations in current velocity and sediment availability are highly uncertain and have to be selected so as to produce a model that matches the preserved rock architecture observed in core or outcrop; this is a complex and non-unique inversion problem that is difficult to solve.

The second approach uses geometric and lithologic data from the subsurface in conjunction with outcrop analogues to directly condition reservoir models. For example, Jackson *et al.* (2005) generated 3D models of rock samples (with dimensions of order 0.5 x 0.5 x 0.3 m) from heterolithic tidal sandstones observed at outcrop using serial 2D sectioning, scanning and surface reconstruction techniques. Their methodology yields models that are directly conditioned to observed geologic data, but its application relies on selection of an appropriate analogue (or analogues) for the reservoir facies to be characterized. Furthermore, such a method is time-consuming, difficult to replicate, and leads to the creation of deterministic models that do not capture uncertainty in sandbody proportions, geometry, and connectivity.

In this chapter, we present a new surface-based modelling workflow to produce stochastic models of heterolithic, cross-bedded tidal sandstones conditioned to outcrop or subsurface data. A cross-bedding template surface is used in order to define and populate a rock volume. The 3D morphology of the template surface is defined by purely geometric input parameters that, in the case documented herein, were defined using measurements from an outcrop analogue (the Eocene Dir Abu Lifa Member, Western Desert, Egypt; Bown and Kraus, 1988; Legler *et al.*, 2013). The chapter has four objectives. First, we present the new surface-based modelling workflow. Second, we identify the geometric input parameters required for the modelling process and extract a range of values for these parameters from statistical analysis of the outcrop analogue dataset. Third, we describe two generic models that reproduce: (1) trough cross-bedding dominated by muddy toesets and with a relatively low sandstone content (89%), and (2) tabular cross-bedding dominated by sandy foresets and with a higher sandstone content (94%). Finally, we use flow-simulation to calculate the effective permeability of the models, in order to demonstrate the effectiveness of the surface-based modelling workflow and its application to build models suitable for flow simulation.

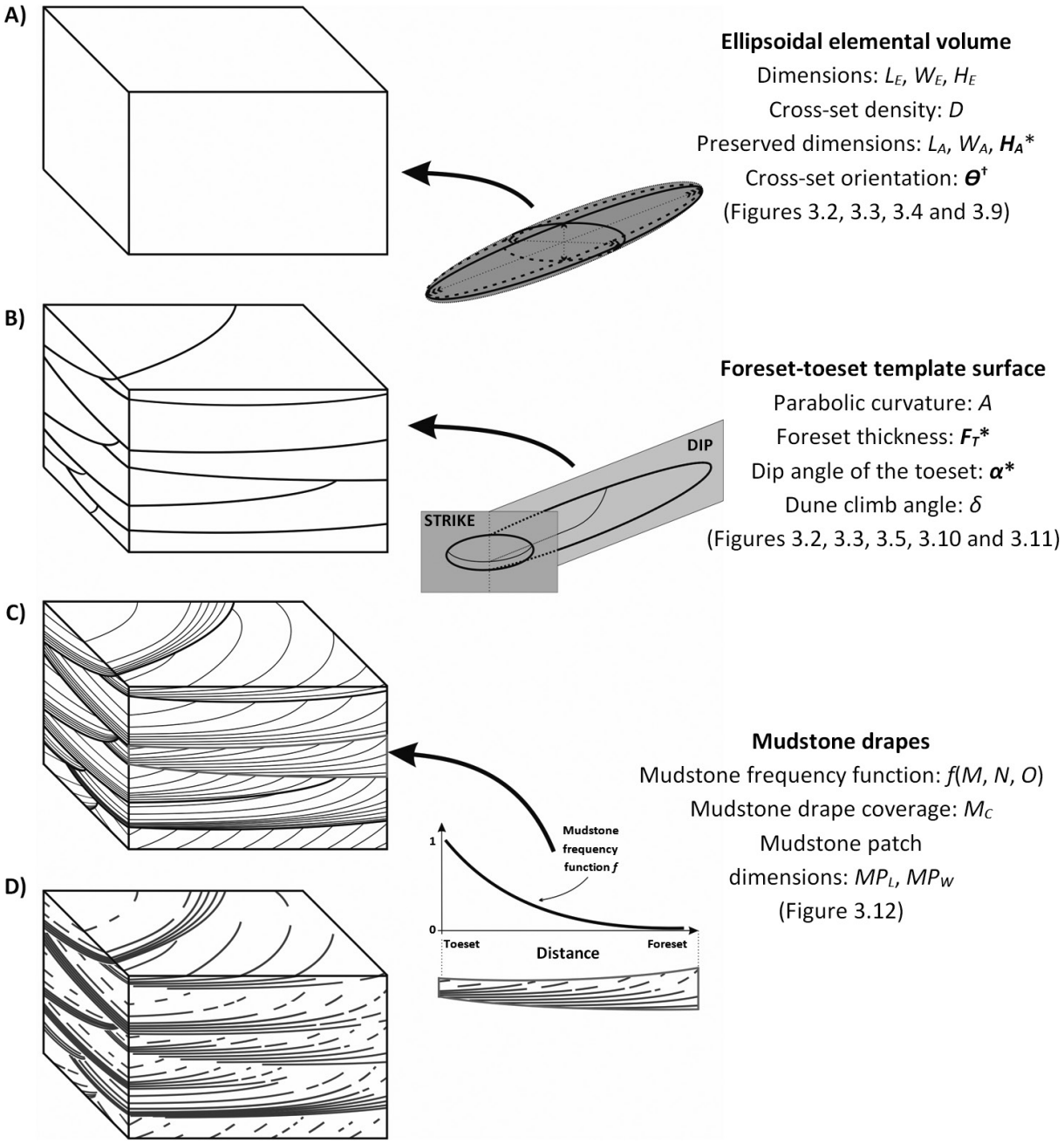
3.2. Methodology

3.2.1. Model-construction methodology

The stratigraphic surfaces that define sedimentary structures within tidal sandstone reservoirs can be categorized by their 3D geometries, irrespective of length scale: (1) planar surfaces (parallel bedding; erosive or conformable facies contacts), (2) concave-upward surfaces (sigmoidal bedding or cross bedding structures; channelized erosive contacts), or (3) wavy surfaces (wavy bedding, lenticular bedding and flaser bedding structures; irregular erosive contacts). The surface-based methodology described in this chapter makes use of these scale-independent stratigraphic surface geometries by modelling rock volumes within which surfaces share a common geometric template. Overall, the methodology comprises the following three steps (Figure 3.1).

(1) The volume of rock to be modelled is subdivided into "elemental volumes" delimited by a basal and a top surface. In each elemental volume, the heterogeneities are associated with stratigraphic surfaces that have the same 3D geometry. The elemental volumes have uniform shapes, but their dimensions can be varied. The model volume is filled with elemental volumes until an appropriate 3D-density is reached, in an approach analogous to object-based modelling (e.g. Haldorsen and Damsleth, 1990). Rules of superposition and erosion are applied to the elemental volumes to mimic their chronostratigraphic ordering. For example, if the elemental volumes represent erosively based sediment bodies, then each elemental volume is eroded by the basal surfaces of "younger" elemental volumes.

(2) Each elemental volume contains only one type of stratigraphic surface, the geometry of which is defined by a "template surface". The 3D geometry of the template surface is defined mathematically. Each elemental volume is then filled with numerous stratigraphic surfaces derived from the single template surface, following rules introduced by the user to define, for example, the vertical and horizontal surface spacing. The template surfaces within an elemental volume interact with other elemental volumes and their constituent template surfaces following the same rules of superposition and erosion as described in the previous step.



Ellipsoidal elemental volume
Dimensions: L_E, W_E, H_E
Cross-set density: D
Preserved dimensions: L_A, W_A, $\boldsymbol{H_A}$*
Cross-set orientation: $\boldsymbol{\Theta}^{\dagger}$
(Figures 3.2, 3.3, 3.4 and 3.9)

Foreset-toeset template surface
Parabolic curvature: A
Foreset thickness: $\boldsymbol{F_T}$*
Dip angle of the toeset: $\boldsymbol{\alpha}$*
Dune climb angle: δ
(Figures 3.2, 3.3, 3.5, 3.10 and 3.11)

Mudstone drapes
Mudstone frequency function: $f(M, N, O)$
Mudstone drape coverage: M_C
Mudstone patch dimensions: MP_L, MP_W
(Figure 3.12)

Figure 3.1: Three-step methodology for constructing models of heterolithic, cross-bedded tidal sandstones. A) Subdivision of the model volume into elemental volumes, in which heterogeneities have the same length scale and geometry. In the cross-bedded sandstones modelled here, the elemental volumes are cross-bed sets represented by ellipsoids with erosive bases. Ellipsoid boundaries are represented by bold black lines. B) Each ellipsoid (i.e. cross-bed set) is populated with template surfaces that represent foreset-toeset lamina boundaries. Foreset-toeset template surfaces are represented by thin black lines. C) Each foreset-toeset template surface is then lined by mudstone drapes of variable continuity, using a mudstone frequency function. Mudstone drapes are represented by bold grey lines. For each step, the required input parameters are listed on the right of the figure. Some parameters can be extracted from subsurface core data (*) or dipmeter logs (†), whereas others must be taken from sedimentological analogues.

(3) Once every elemental volume has been filled with template surfaces, a facies code is assigned to the geologic domains defined by the surfaces, or to the surfaces themselves. The facies codes constrain the modelling of fine-scale petrophysical properties such as porosity and permeability.

The surface-based model is then gridded for flow simulation. The grid is constructed around the stratigraphic surfaces, in order to retain the geometries defined by the surfaces and minimize the number of active grid cells required for flow simulation (Jackson *et al.*, 2005, 2013; Sech *et al.*, 2009). The resulting models are geometrically accurate and computationally efficient, although the complex grid architectures may introduce numerical artefacts in conventional reservoir simulators (e.g. Graham *et al.*, in review; see Chapters 3 and 4).

3.2.2. Application to heterolithic, cross-bedded tidal sandstones

The three-step methodology described above is applied herein to the modelling of heterolithic, cross-bedded tidal sandstones (Figure 3.1). Cross-bedded sandstones are common in a wide range of depositional environments, including those influenced by tides (e.g. Harms *et al.*, 1982; Rubin, 1987; Ashley, 1990). Cross-beds result from the migration of dunes (or megaripples *sensu* Allen, 1968, sand waves *sensu* Allen, 1980) in response to a unidirectional current. Dunes develop straight crests (2D dunes) under low current velocities, and sinuous or discontinuous crests (3D dunes) under high current velocities (Dalrymple *et al.*, 1978; Allen, 1980; Elliott and Gardiner, 1981; Middleton and Southard, 1984). Any dip-section (parallel to the main current direction) gives the same geometry for tabular (or planar) cross-beds resulting from the migration of 2D dunes, whereas trough cross-beds resulting from the migration of 3D dunes have a variable dip-section geometry. Each migrating dune is potentially preserved — if not completely eroded — as a cross-bed set with an erosive base, whose geometry and extent reflect the morphology and trajectory of the scoured area in front of the migrating dune. Topsets are generated from the migration of the breaking point of the dune between the lee and the stoss sides, but topsets are hardly preserved in sedimentological records as the next migrating dunes will erode them. Consequently the top surfaces of the cross-bed sets are never preserved, and consist on the connection of erosive

bases of younger and overlying dunes. In the case of 2D dunes, the unidirectional current is dispersed along a large area downstream of the dune crest, such that an extensive planar erosion surface of low scour capacity is formed (Harms *et al.* 1982). In the case of 3D dunes, the current is focused downstream of the migrating dune into scour pits, which migrate to produce a curved, concave-upwards erosion surface (Dalrymple *et al.*, 1978; Harms *et al.*, 1982). Cross-beds produced by dune migration are commonly stacked into larger sediment bodies of characteristic internal architecture. For example, the deposits of larger bedforms such as bars accumulate via the accretion of cross-beds that record the migration of smaller, superposed bedforms, such as dunes and ripples, across the bar surface. Tidal bars migrate laterally into adjacent channels due to changes in tidal flow patterns or interactions with other processes (e.g. variations in wave climate or fluvial discharge). Consequently, tidal bar deposits can be comprised entirely of stacked cross-bed sets, corresponding to the preserved remnants of repeated dune migration (Allen, 1980; Dalrymple, 1984; Ashley, 1990).

3.2.3. Modelling of elemental volumes

A volume of 9 m^3 (3 x 3 x 1 m) of cross-bedded sandstone is considered in this study; in the next chapter, we demonstrate that this volume comfortably exceeds the minimum volume (the Representative Elementary Volume) required to calculate representative values of effective permeability in these heterolithic units (see Chapter 4; see Figure 4.1). At this length scale, the elemental volumes contain tabular and trough cross-bed sets, representing the preserved parts of 2D and 3D dunes in a tidal bar succession, respectively. In each cross-bed set, the key heterogeneities captured here are mudstone drapes along foreset-toeset surfaces of consistent 3D geometry, such that each cross-bed set corresponds to an elemental volume. The model volume of 9 m^3 here samples approximately 6 cross-bed sets and 600 foreset-toeset surfaces, based on outcrop-analogue data presented in a later section.

Cross-bed set boundaries correspond to the preserved remnants of the erosive surface developed downcurrent of migrating 2D- or 3D-dunes (Figure 3.2 A). Observations of modern tidal dunes show that this erosive surface has a curved elliptical shape in the strike direction (orthogonal to the main paleocurrent direction, Figure 3.2 B). As the dunes migrate, the

resulting erosive surface is a downstream-amalgamated composite of the elliptical strike-sections that record the successive positions of the deepest part of the scour pool in front of the dune (Figure 3.2 B). In order to mimic the 3D geometry of this composite erosive surface, the corresponding elemental volumes have been modelled here as ellipsoids (Figures 3.3, 3.4). The model volume is thus subdivided into ellipsoidal elemental volumes that correspond to cross-bet sets, with tops that are truncated by the basal surfaces of overlying elemental volumes (Figure 3.1 B). The elemental volumes are modelled stochastically using the input parameters such as dimensions summarized in Table 3.1. Each elemental volume can be rotated to a specific angle which correspond to the palaeocurrent orientation ϑ for the cross-bedding surfaces modelled inside. For each parameter, the modelling algorithm can use a single value, or a distribution characterized by a mean value and a standard deviation.

3.2.4. Modelling template surfaces within elemental volumes

Each ellipsoidal elemental volume representing a cross-bed set contains multiple foreset-toeset template surfaces of uniform geometry. The spacing of foresets and toesets – and associated mudstone drapes – in cross-strata resulting from the migration of tidal dunes and bars is typically rhythmic, reflecting a hierarchy of periodic cycles in tidal current velocity (e.g. Nio and Yang, 1991). The shortest tidal cycle is semi-diurnal (c. 12 hour period), and is characterized by the alternation of flood and ebb current stages, separated by slack-water periods during which the current velocity is zero. During slack-water periods, mud particles and clay aggregates (flocks) are deposited to form mudstone drapes over sandy bedforms (Allen, 1981; Dalrymple *et al.*, 2003). In an idealized semi-diurnal tidal cycle, both the ebb and flood tides are recorded by deposition of a sand lamina on the lee face (foreset) of a dune (Visser, 1980). Slack-water periods are recorded by mudstone drapes that separate the foreset-toeset sandstone laminae representing the ebb-tidal and flood-tidal currents. The tide is typically asymmetric, such that either the ebb-tidal or flood-tidal currents are dominant (Visser, 1980). The dominant tide is represented by thicker foreset-toeset sandstone laminae and the subordinate tide by thinner laminae.

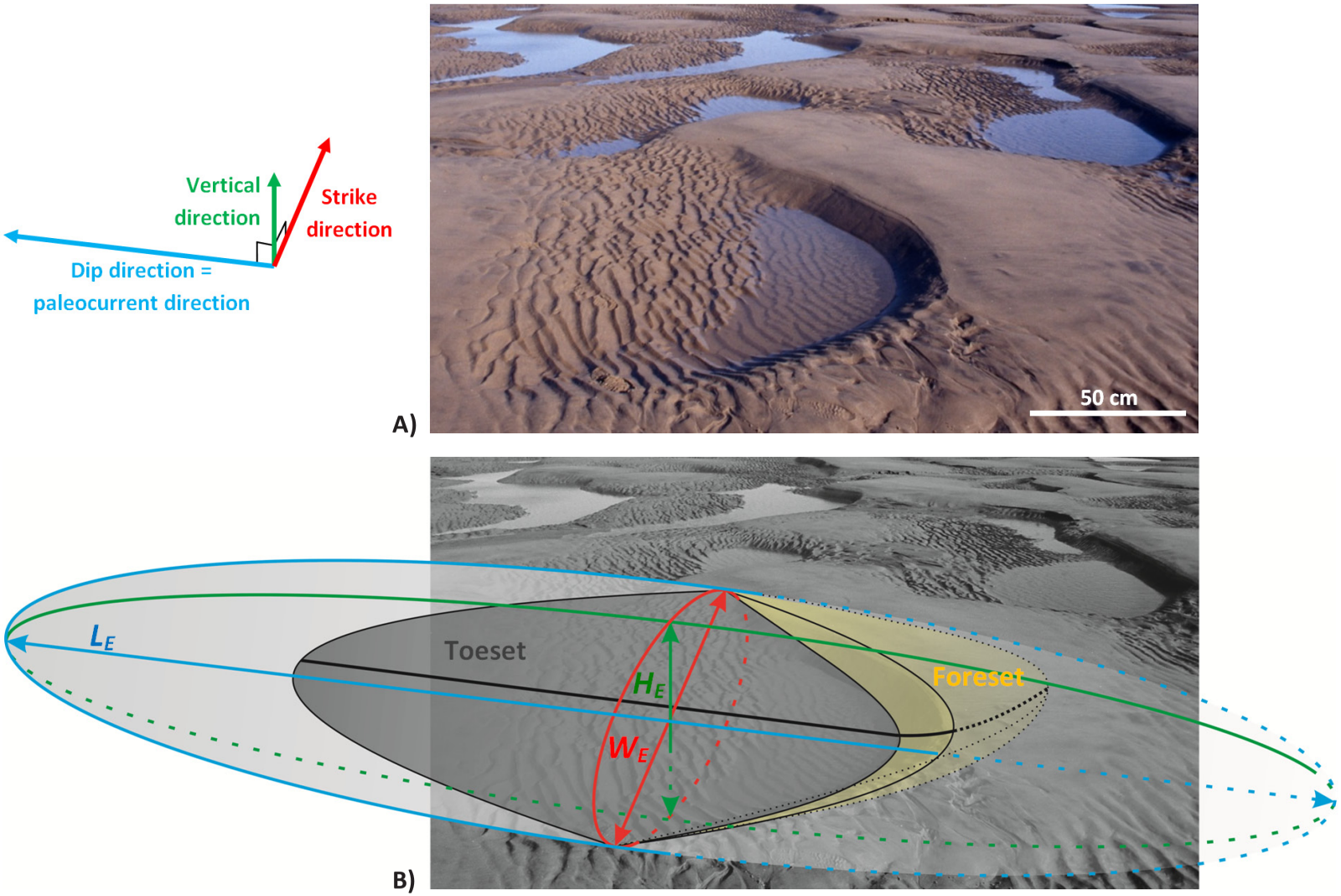


Figure 3.2: A) Modern 3D dune in an inter-tidal flat environment, the Wash Estuary, United Kingdom. B) Interpretation of the erosion surface resulting from migration of a dune and associated scour pool as the lower part of an ellipsoid of dimensions L_E (length, in blue), W_E (width, in red), and H_E (height, in green) relative to the horizontal reference plane Γ. Dotted lines correspond to parts of the ellipsoid beneath the dune in its present position. The yellow crescent corresponds to the dune foreset, and the gray truncated ellipse to the rippled dune toeset. The bold black line corresponds to the dip cross-section of one foreset-toeset surface.

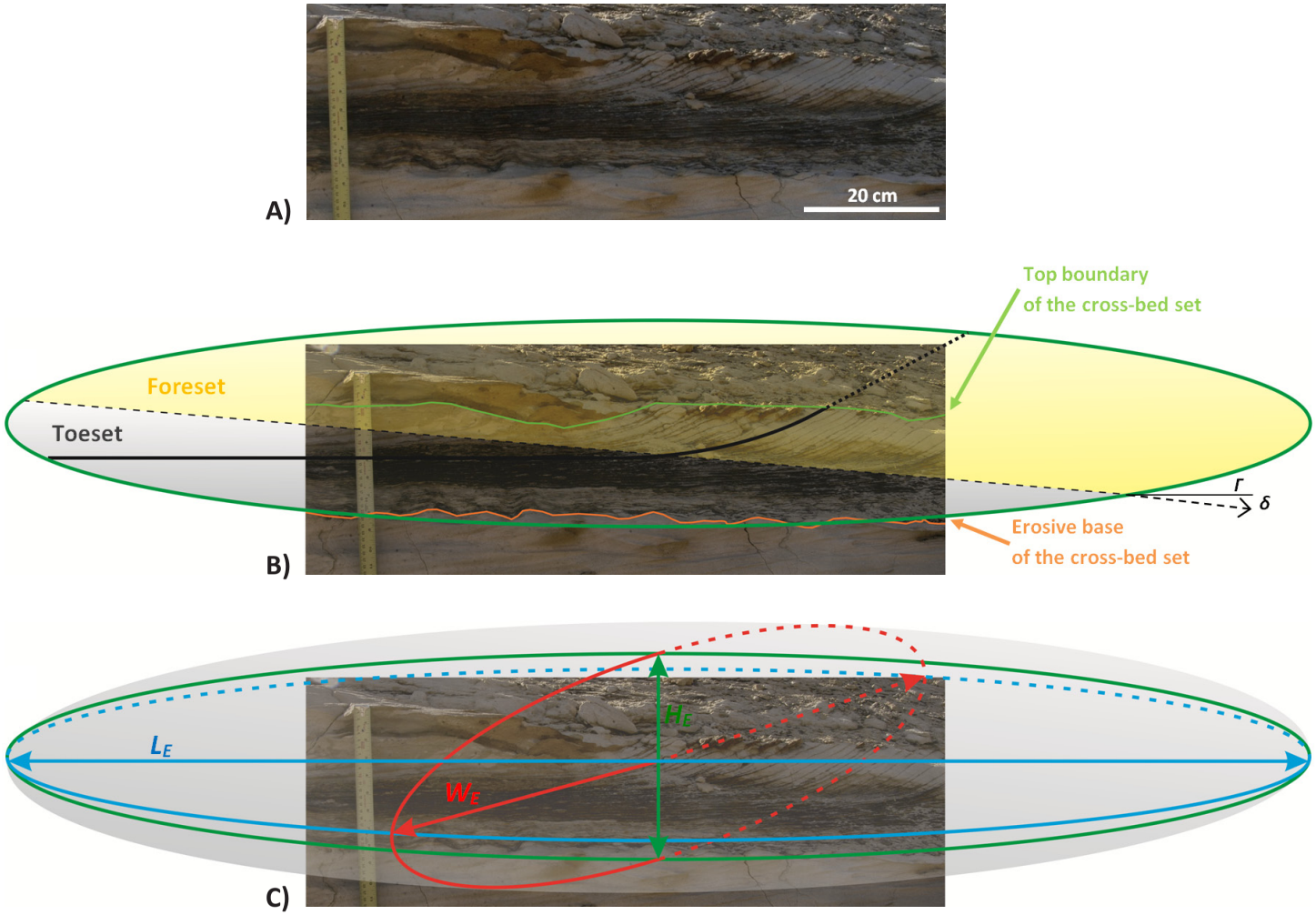


Figure 3.3: A) Ancient trough cross-bed set viewed in cross-section oriented approximately along depositional dip (parallel to the paleocurrent direction), Dir Abu Lifa Member, Gecko Nose location (NNE-SSW-oriented cliff face shown with dotted line in Figures 3.6, 3.7), Western Desert, Egypt. The cross-bed set contains tidal bundles separated by double mudstone drapes in the sandy foresets, and wavy-bedded muddy toesets. B) Interpretation of the cross-bed set as the lower part of an ellipsoidal elemental volume. The orange line shows the erosive base of the cross-bed set, and the green line shows the top surface of the preserved cross-bed set (i.e. the erosive base of an overlying cross-bed set). The thin dotted line is the boundary between foresets and toesets within the cross-bed set marking the angle of climb of the dune δ. The bold black line corresponds to an interpreted foreset-toeset template surface in dip cross-section. C) The corresponding best fit ellipsoidal elemental volume is traced in 3D (see Figure 3.2 for colours).

Input parameter	Symbol	Unit	Trough cross-bed model (Gecko Nose)	Tabular cross-bed model (Butterfly Canyon)	Definition
Volume of the model	V_T	m^3	9	9	
Elemental volume length	L_E	m	20	20	Trough cross-beds are modelled as highly elongate, oblate ellipsoids with $L_E >> W_E > H_E$. Tabular cross-beds are modelled as oblate ellipsoids with $W_E \geq L_E > H_E$, which yields laterally continuous sheets at the model scale (geometrical mean value $E[W_E]$ ± standard deviation $\sigma[W_E]$).
Elemental volume width	W_E	m	4.85 ± 1.67	20	
Elemental volume height	H_E	m	1.35 ± 0.55	1.35 ± 0.55	
Preserved length of elemental volume	L_A	m	80% of L_E	100% of L_E	These parameters define the preserved aspect of the ellipsoidal elemental volumes in the model, after erosion at the base of overlying elemental volumes (geometrical mean value $E[W_A]$ ± standard deviation $\sigma[W_A]$).
Preserved width of elemental volume	W_A	m	50% of W_E	100% of W_E	
Preserved length of elemental volume	H_A	m	30% of H_E	40% of H_E	
Elemental volume density	D	m^{-3}	6 elemental volumes in 9 m^3	4 elemental volumes in 9 m^3	Number of ellipsoidal elemental volumes present per unit volume of the model.
Elemental volume orientation	ϑ	°	0	0	The azimuthal orientation angle ϑ of the ellipsoidal elemental volumes corresponds to the paleocurrent direction indicated by the foreset-toeset surfaces within a cross-bed set.
Number of cross-bedding surfaces	N_{CB}	-	≈500	≈170	
Parabolic curvature of foreset-toeset template surfaces	A	-	5.5×10^{-3}	5.5×10^{-3}	Characteristic coefficient of the square term for a parabolic curve, $z(x) = Ax^2$ as equation (3.1)
Foreset thickness	F_T	cm	5.85 ± 3.88	10 ± 3.88	Distance between two consecutive foreset-toeset surfaces, measured between their junction points O and O' (Figure 3.5).

Toeset dip angle	α	°	8	1	Angle between the straight toeset surface and the median reference plane of the ellipsoidal elementary volume Γ (Figure 3.5)
Angle of dune climb	δ	°	5	0	Angle between the median reference plane Γ and the boundary surface Δ which separates the foreset and the toeset parts in an elementary volume (Figure 3.5)
Foreset to toeset volume ratio	$R_{F/T}$	-	6.5 : 1	24 : 1	Ratio of the volume occupied by foreset by the volume occupied by toeset in the model
Mudstone frequency function	$f(M,N,O)$	-	Function f of Figure 3.12	Function f of Figure 3.12	Defined in 2D, along the azimuth of the ellipsoidal elemental volume (i.e. dip direction), according to the distance from the top of the foreset to the junction point O with the toeset. M = -1.004, N = -4.316, and O = 1.610 for equation (3.7)
Mudstone drape coverage	M_C	-	Foreset 25% Toeset 57%	Foreset 25% Toeset 57%	Mudstone patches are added along the foreset-toeset template surfaces until a specific proportion M_C of their area is covered. $M_C = A_M / A_F$
Total area of the preserved foreset-toeset surface	A_F	cm^2	-	-	
Area of the foreset-toeset surface covered by mudstone	A_M	cm^2	-	-	
Mudstone patch length	MP_L	cm	[0-20] Uniform distribution	[0-100] Uniform distribution	After the dimension of the major axis of the elliptical patch MP_L is defined, the dimension of the minor axis MP_W is randomly set as a fraction of MP_L
Mudstone patch width	MP_W	cm	[0-20] Uniform distribution Smaller than MP_L	[0-20] Uniform distribution Smaller than MP_L	

Table 3.1: Input parameters for the Gecko Nose and Butterfly Canyon models (Figures 3.13, 3.14).

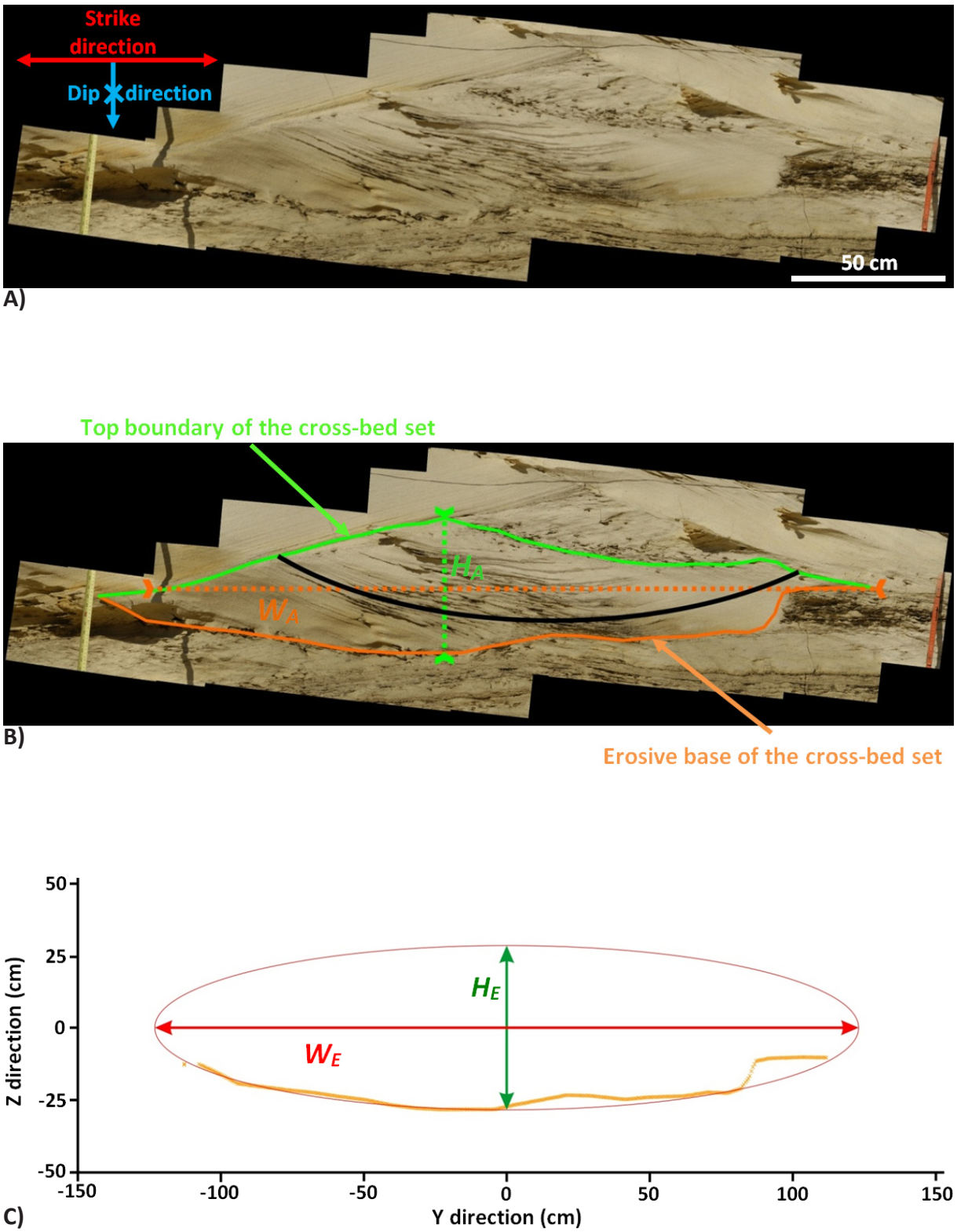


Figure 3.4: A) Ancient trough cross-bed set viewed in cross-section oriented approximately along depositional strike (perpendicular to the paleocurrent direction which corresponds to dip direction here, out of the page), Dir Abu Lifa Member, Gecko Nose location (WNW-ESE-oriented cliff face shown with bold line in Figures 3.6, 3.7; see also Figure 3.8 A), Western Desert, Egypt. B) Interpretation of the cross-bed set as the lower part of an ellipsoidal elemental volume. The orange line shows the erosive base of the cross-bed set, and the green line shows the top surface of the preserved cross-bed set. The dotted arrows indicate the preserved width W_A and height H_A of the cross-bed set. The bold black line corresponds to an interpreted foreset-toeset template surface in strike cross-section. C) The erosive base of the cross-bed set has been extracted from the photomontage and a best fit elliptical curve (in red) has been defined in order to obtain the width W_E and the height H_E of the elemental volume.

A single, fully preserved semi-diurnal tidal cycle is thus represented by two sandstone laminae and two mudstone drapes ("paired mudstone drapes" or "mud couplet"; Visser, 1980) that constitute one tidal bundle (Boersma, 1969). Longer tidal cycles, which are commonly preserved as rhythmic variations in the thickness of sandstone laminae and mudstone drapes within cross-bed sets, are diurnal (c. 24 hour period) and spring-neap (c. 14 day period) cycles. Superposition of the different tidal cycles, combined with other sediment transport processes, leads to preservation of sandy foresets and muddy toesets. A vertical profile through dune toeset deposits typically exhibits rhythmic alternation of millimetre- to centimetre-thick, wavy-bedded mudstone and sandstone laminae (Reineck and Singh, 1967). The transition between the foreset and toeset of each lamina in a cross-bed set is marked by a gradual downcurrent curvature. The resulting foreset-toeset geometry may be referred to as "shovel" shaped (Van den Berg *et al.*, 2007). In a dip-section, the shape of the foreset part is therefore approximated by a parabolic curve, and the shape of the toeset part is approximated by a straight line:

where x is the dip-direction coordinate, and z is the vertical coordinate, relative to the junction point O between the flat toeset part and the concave-upward foreset part (which is defined

$$\begin{cases} \text{Foreset}: \text{if } x > 0, z(x) = Ax^2 \\ \text{Toeset}: \text{if } x < 0, z(x) = 0 \end{cases} \tag{3.1}$$

to be the origin, $x = 0$, $z = 0$). The whole toeset-foreset surface is then rotated by an angle α, which corresponds to the dip angle of the toeset. Equation (3.1) becomes:

$$\begin{cases} \text{Foreset}: \text{ if } x > 0, z(x) = \dfrac{\cos\alpha - 2xA\cos\alpha\sin\alpha - \sqrt{\cos^2\alpha - 4Ax\sin\alpha}}{2A\sin^2\alpha} \\ \text{Toeset}: \text{if } x < 0, z(x) = x\tan\alpha \end{cases} \tag{3.2}$$

Notice that both equations have the same derivative $z'(x = 0) = \tan\alpha$ at the junction point O, so that the curve is continuous from the toeset part to the foreset part of the surface.

In a strike section with coordinate y, the foreset and toeset geometry reflects the erosive scour at the base of the migrating dune, so that the resulting cross-section in the strike direction corresponds to trough or tabular (parallel) cross-beds. Successive foreset-toeset surfaces are

parallel to each other, and parallel to the erosive base of the cross-bed set (i.e. elemental volume). Consequently, equation (3.2) is generalized for any *(x,y)* direction:

$$\begin{cases} \text{Foreset}: \text{if } x > 0, z(x,y) = \left[\dfrac{\cos\alpha - 2xA\cos\alpha\sin\alpha - \sqrt{\cos^2\alpha - 4Ax\sin\alpha}}{2A\sin^2\alpha} \right] + \left[\sum_1^i T_{Ti} + B(x,y) \right] \\ \text{Toeset}: \text{if } x < 0, z(x,y) = \left[x\tan\alpha \right] + \left[\sum_1^i T_{Ti} + B(x,y) \right] \end{cases} \quad (3.3)$$

where *B(x,y)* describes the 3D ellipsoidal shape of the basal surface of the cross-bed set (i.e. elemental volume), bold black lines in Figure 3.1 B):

$$B(x,y) = (H_E/2)\sqrt{1 - \frac{x^2}{(L_E/2)^2} - \frac{y^2}{(W_E/2)^2}} \quad (3.4)$$

The term $\sum_1^i T_{Ti}$ corresponds to the cumulative toeset thickness in the cross-bed set when considering all the *(i-1)* cross-bedding surfaces already modelled, with T_{Ti} corresponding to the individual toeset thickness. Every cross-section of one foreset-toeset surface in the strike direction is an ellipse parallel to the erosive base of the cross-bed set. In particular, for *x = O*, the strike cross-section curve links all junction points *O* of any given foreset-toeset surface, creating a junction line *Oy*, simplifying equations (3.3) and (3.4) to yield:

$$z(x=0,y) = \sum_1^i T_{Ti} + (H_E/2)\sqrt{1 - \frac{y^2}{(W_E/2)^2}} \quad (3.5)$$

The shape of the cross bedding surfaces has been approximated as a parabolic curve when in other surface-based modelling methodologies it has been approximated as a sigmoidal curve (i.e. Wen *et al.*, 1998; Ringrose *et al.*, 2005; Nordahl *et al.*, 2005). Following previous observations that topsets of cross-bed sets are hardly preserved, different shapes of curves have been tested to actual outcrop dataset, and the simplest shape, the parabolic curve, was found as a sufficient fit for such dataset (see 3.2.6 and Figure 3.10, regression factor R^2=0.98). As a result, the equations in the Cartesian coordinate system for the cross-bedding template surface were simplified compared to that of a sigmoidal surface, especially after rotation by the angle α in equation 3.2. Sigmoidal shape could have been chosen without creating significant difference in the shape of the cross-bedding as the bottom part of a sigmoidal surface approaches the shape of a parabolic curve.

In order to populate the ellipsoidal elemental volumes with foreset-toeset template surfaces, the input parameters summarized in Table 3.1 are required (Figures 3.1 C, 3.5). Toeset thicknesses T_T (Figure 3.5) are generally too small to be routinely measured directly from cores and outcrop analogues with high accuracy (< 1 cm). Therefore we calculate T_T indirectly from two other parameters: the dip angle of the toesets α and the angle of dune climb δ (Figure 3.5). α corresponds to the angle of rotation applied to the parabolic curve representing the foreset-toeset template surface. T_T is then given by:

$$T_T = F_T \sin(\alpha + \delta) \tag{3.6}$$

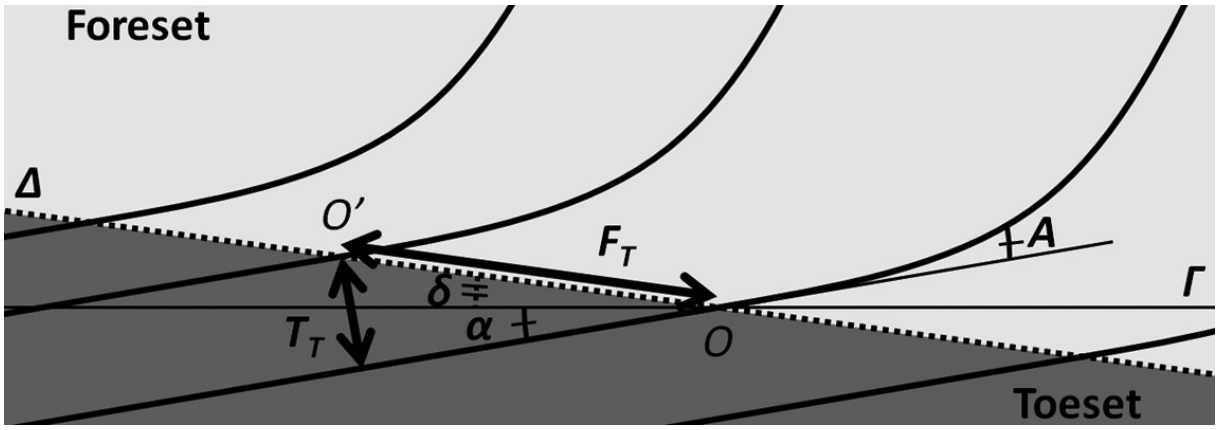


Figure 3.5: Detail of transition between foreset and toeset along template surfaces within an elemental volume. Input parameters required to describe the geometry of the foreset-toeset surfaces include foreset thickness F_T, toeset thickness T_T, the angle of climb of the dune δ, and the dip angle of the toeset α. The dotted line Δ corresponds to the limit between sandy foresets (light gray) and muddy toesets (dark gray), and links the junction points O of each foreset-toeset surface. The reference line Γ corresponds to the median plane of the ellipsoidal elemental volume that contains the foreset-toeset surfaces (blue ellipse in Figure 3.2). Once F_T is set, T_T is calculated using angles α and δ (Equation (3.6)).

3.2.5. Modelling of mudstone drapes along foreset-toeset surfaces

If the succeeding, flood-tidal or ebb-tidal current is sufficiently strong, then mudstone drapes can be partially or entirely eroded, such that only one mudstone drape and one reactivation surface may be preserved during one flood/ebb tidal cycle (de Mowbray and Visser, 1984). Thus, the foreset-toeset surfaces modelled in the previous step are not entirely covered by mudstone. The extent and continuity of mudstone drapes is defined using a function to describe mudstone frequency along the stratigraphic surfaces relative to a well-defined position on

the surfaces. Mudstone drapes are modelled as elliptical patches of mudstone that cover the stratigraphic surfaces until a user-specified proportion of their area is reached, following the methodology of Jackson and Muggeridge (2000). The mudstone drape coverage is then calculated at the transition between foreset and toeset parts (line *Δ* in Figure 3.5). The value is then used as the mudstone drape coverage for the entire toeset parts, in order to ensure mudstone drape coverage continuity between the foreset and the toeset parts. The locations of the elliptical patches are modelled stochastically, constrained by a mudstone frequency function *f*. The length and aspect ratio of each elliptical patch is also modelled stochastically and new mudstone patches superimpose with older patches to yield a complex pattern of preserved mudstone along each foreset-toeset surface. The pattern of mudstone drapes is highly dependent on the input mudstone frequency function *f*, which is determined here from outcrop analogue data. Once a centre point for an elliptical patch is chosen, the dimensions and orientation of the elliptical patch are modelled stochastically. The following equation has been used to define *f*:

$$f\left(\frac{x-x_O}{x_F-x_O}\right)=\frac{M}{1+e^{\left(N\left(\frac{x-x_O}{x_F-x_O}\right)+O\right)}} \tag{3.7}$$

where x_O corresponds to the coordinate of the junction point *O* between foreset and toeset sections, and x_F corresponds to the coordinate of the point *F* marking the preserved top of the foreset. The constants *M*, *N* and *O* are characteristic of *f* and are determined by the user. In this study, they were extracted from outcrop analogue data. The input parameters required for modelling mudstone drapes are summarized in Table 3.1 (Figure 3.1 D). Mudstone drape thickness is assumed constant at 3.5 mm; as mudstones are modelled as barriers to flow, their thickness has no impact on their flow properties; however, it does affect the total volume of the model that is occupied by mudstone. Statistics on the mudstone drape thickness was not derived from outcrop photomontages as the error margin on the measurements is high compared to the value measured. The value chosen is a typical mean value encountered in heterolithic cross-bedded tidal sandstones (Terwindt, 1971; Nio and Yang, 1991; Martinius and Van den Berg, 2011).

3.2.6. Outcrop analogue data analysis to define model input parameters

To determine values of the input parameters required to construct models of heterolithic, cross-bedded tidal sandstones, data were collected from an outcrop analogue in which such sandstones are exposed with a large degree of lateral and vertical continuity in outcrop faces that allow the 3D geometry of the elemental volumes, template surfaces and mudstone distribution to be evaluated quantitatively.

The studied outcrop analogue forms part of the Eocene Dir Abu Lifa Member, located in the Western Desert of Egypt (Figure 3.6). The Eocene to Oligocene formations were deposited in the Gindi Basin, a sub-basin from the ealier Fayoum Basin, at the northern margin of the African continent. The tectonic of the area was constrained by the opening of the Tethys Ocean. After a period of rifting initiated in the Jurassic, the central part of the Fayoum Basin was uplifted due to the collision of the African and European plates during Late Cretaceous, leading to the orogenesis of the Kattania High. The Dir Abu Lifa Member was therefore deposited in the protected shallow marine Gindi subsidising sub-basin during Eocene, preserved from wave energy and the paleo-Mediterranean Sea influence by the Kattania High, resulting in a predominance of tidal processes (Abdel-Fattah *et al.*, 2010; Legler *et al.*, 2013). The Gindi Basin surely had connection to the sea as attested by the paleoenvironment reconstructions based on ichnology, but in a limited way due to the Kattania High and the predominance of tidal indicators and lack of wave indicators. Such morphology of the basin - with an extended embayment area with limited connection to the sea - would reinforce the strength of the tidal current. This is notably the case for narrow seas with the example of the paleo-North Sea during the deposition of the Jurassic tidally-influenced deposits modelled in previous studies (Brandsaeter *et al.*, 2003; Martinius *et al.*, 2005; Ringrose *et al.*, 2005). The lower part of the Dir Abu Lifa Member consists largely of tidal bar and channel deposits that are stacked laterally and vertically (Legler *et al.*, 2013). The lower parts of tidal bar deposits typically comprise heterolithic, cross-bedded sandstones. Thus, the Dir Abu Lifa outcrops are a good analogue for tidally-dominated depositional environments.

The lower Dir Abu Lifa Member is exposed in a continuous escarpment over 20 km long, which is cut by multiple canyons that provide some three dimensional control (e.g. Legler *et al.*, 2013). The datasets used in this chapter are taken from two locations, labelled Gecko Nose and Butterfly Canyon in Figure 3.6. Gecko Nose is a small promontory which is defined by two cliff faces that trend approximately WNW-ESE and SSW-NNE, nearly perpendicular to each other (Figures 3.6, 3.7). The promontory exposes stacked trough and tabular cross-bedded sandstones, interpreted as the deposits of tidal bars in a channel belt (the "yellow channel" in the Gebel Sagha area of Legler *et al.*, 2013). The WNW-ESE-oriented cliff face (N110-N290) is 17 m long, and the SSW-NNE-oriented cliff face (N030-N210) is 12 m long. Paleocurrent measurements from the cross-beds are oriented towards N230, indicating that the WNW-ESE- and SSW-NNE-oriented cliff faces provide oblique strike and dip sections, respectively.

Butterfly Canyon contains a larger promontory than Gecko Nose, defined by two cliff faces that trend approximately N-S and W-E. The Butterfly Canyon outcrop also exposes stacked trough and tabular cross-bedded sandstones deposited in bars occupying an isolated channel in a tidal flat environment (the Wadi Ghorab area of Legler *et al.*, 2013). Paleocurrent measurements from the cross-beds are oriented towards N196, indicating that the W-E- and N-S-oriented cliff faces provide oblique strike and dip sections, respectively. Tidal bar deposits exposed at Butterfly Canyon are qualitatively sandier than those at Gecko Nose by observation of the volume fraction at the outcrops, and reproduced in our models thanks to the foreset to toeset volume ratio $R_{F/T}$ (Table 3.1). However, an important observation from outcrop is that the mudstone drape coverage at both outcrop locations is similar in nature, so that the volume fraction of mudstone compared to sandstone is only dependent on the proportion of muddy toesets over sandy foresets. After calculations, the ratio $R_{F/T}$ has been found almost 4 times higher for the Butterfly Canyon outcrop than for the Gecko Nose outcrop (Table 3.1). The two outcrop deposits are considered to be end-members of the same heterolithic, cross-bedded tidal sandstone facies.

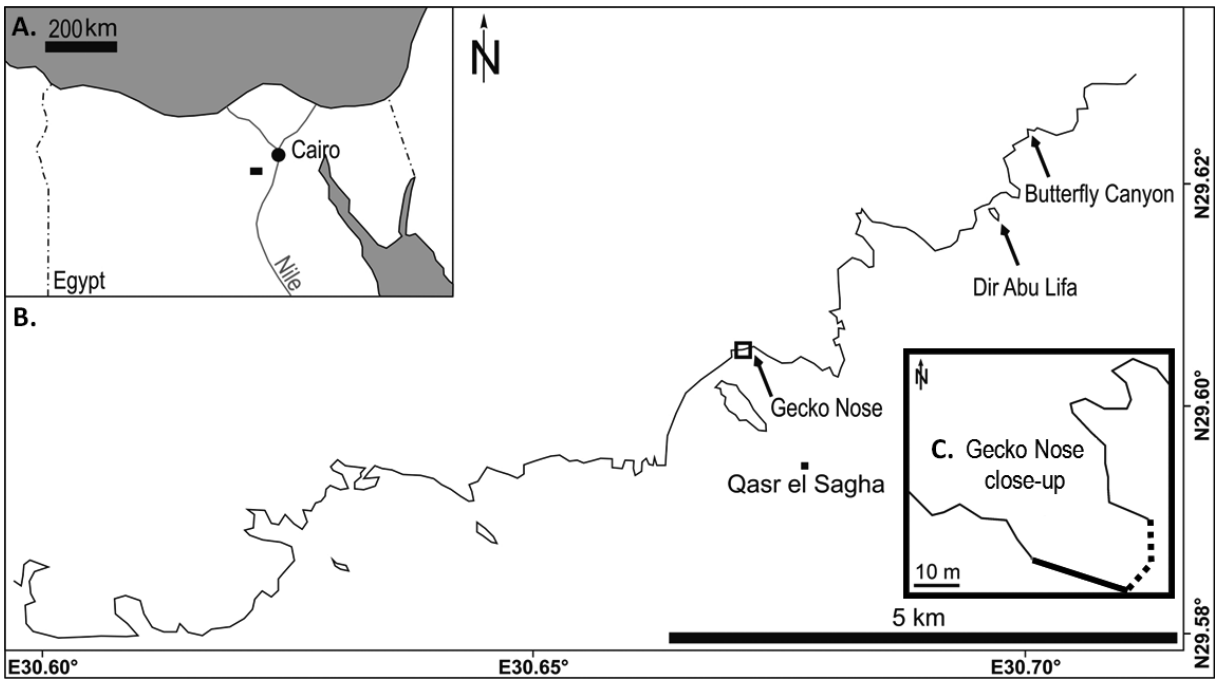


Figure 3.6: A. Map of Egypt highlighting the position of the Eocene Dir Abu Lifa outcrop belt (black rectangle, south west of Cairo) B. Map of the main outcrop belt of the Dir Abu Lifa Member, highlighting the Gecko Nose and Butterfly Canyon localities. C. Close-up of the Gecko Nose outcrop, with the two studied cliff faces shown with bold lines, the continuous line corresponding the WNW-ESE oriented section, and the dotted line to the NNE-SSW oriented cross-section (Figure 3.7).

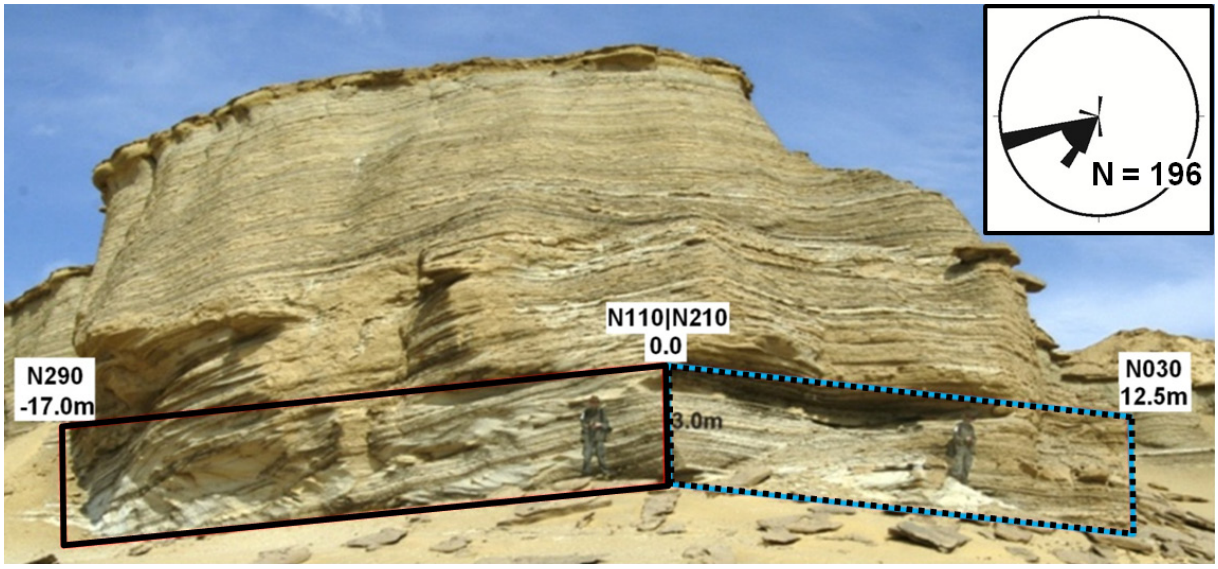


Figure 3.7: Photograph of the two nearly perpendicular cliff faces at Gecko Nose (Figure 3.6). Paleocurrents in heterolithic, trough and tabular cross-bedded sandstones are oriented towards N196 (inset rose diagram), such that the WNW-ESE-oriented (bold line) and NNE-SSW-oriented cliff faces (dotted line) approximate strike and dip sections, respectively. A person is present in front of the outcrop for scale.

High-resolution photographs and precise sketches were collected from the cliff faces of both localities, in order to capture the dimensions and geometries of cross-bed sets. Photographs were collected using lenses reducing the effect of distortion, ultimately removed by photo treatment. Each cross-bed set in the Gecko Nose outcrop has been reconstructed from the high-resolution photographs and scaled using the sketches. The boundaries of the cross-bed sets and their constituent foreset-toeset surfaces have been traced on the reconstructed pictures, enabling quantitative, statistically representative datasets to be compiled for the various input parameters of the modelling methodology described above. All values are summarized in Table 3.1.

To define the dimensions of ellipsoidal elemental volumes (L_E, W_E and H_E), the dimensions of 12 trough cross-bed set boundaries (identified in Figure 3.8 A) from the WNW-ESE-oriented face of Gecko Nose, oblique to depositional strike, have been extracted from outcrop photomontages using the method presented in Figure 3.4. A best fit elliptical curve, with dimensions corresponding to W_E and H_E, has been inferred for the erosive base of each cross-bed set (Figure 3.4 C). L_E has been estimated from cross-bed sets exposed on the SSW-NNE-oriented face of Gecko Nose, oblique to depositional dip. The basal boundaries of all of the cross-bed sets were continuous and nearly planar over the 12 m extent of this face, therefore, at the scale of our 9 m^3 model, $L_E >> W_E$. For the elemental volume density D, a total of 90 cross-bed sets have been observed at the Gecko Nose location, with 80 of them exposed on the WNW-ESE-oriented face, oblique to depositional strike. These 90 cross-bed sets are present within a volume of 12 x 17 x 3 m, such that D is equal to 0.15 elemental volumes per m^3. For the dimensions of the preserved parts of ellipsoidal elemental volumes (L_A, W_A and H_A), W_A and H_A of trough cross-bed sets have been extracted from the WNW-ESE-oriented face of Gecko Nose, oblique to depositional strike (Figure 3.8 B). Values of both W_A and H_A define log-normal distributions (Figure 3.9). All of the cross-bed sets extend across the whole of the SSW-NNE-oriented face of Gecko Nose, oblique to depositional dip, such that L_A is greater than 12 m. At Butterfly Canyon, L_A is observed in one cross-bed set to equal 25 m, which is the value used thereafter.

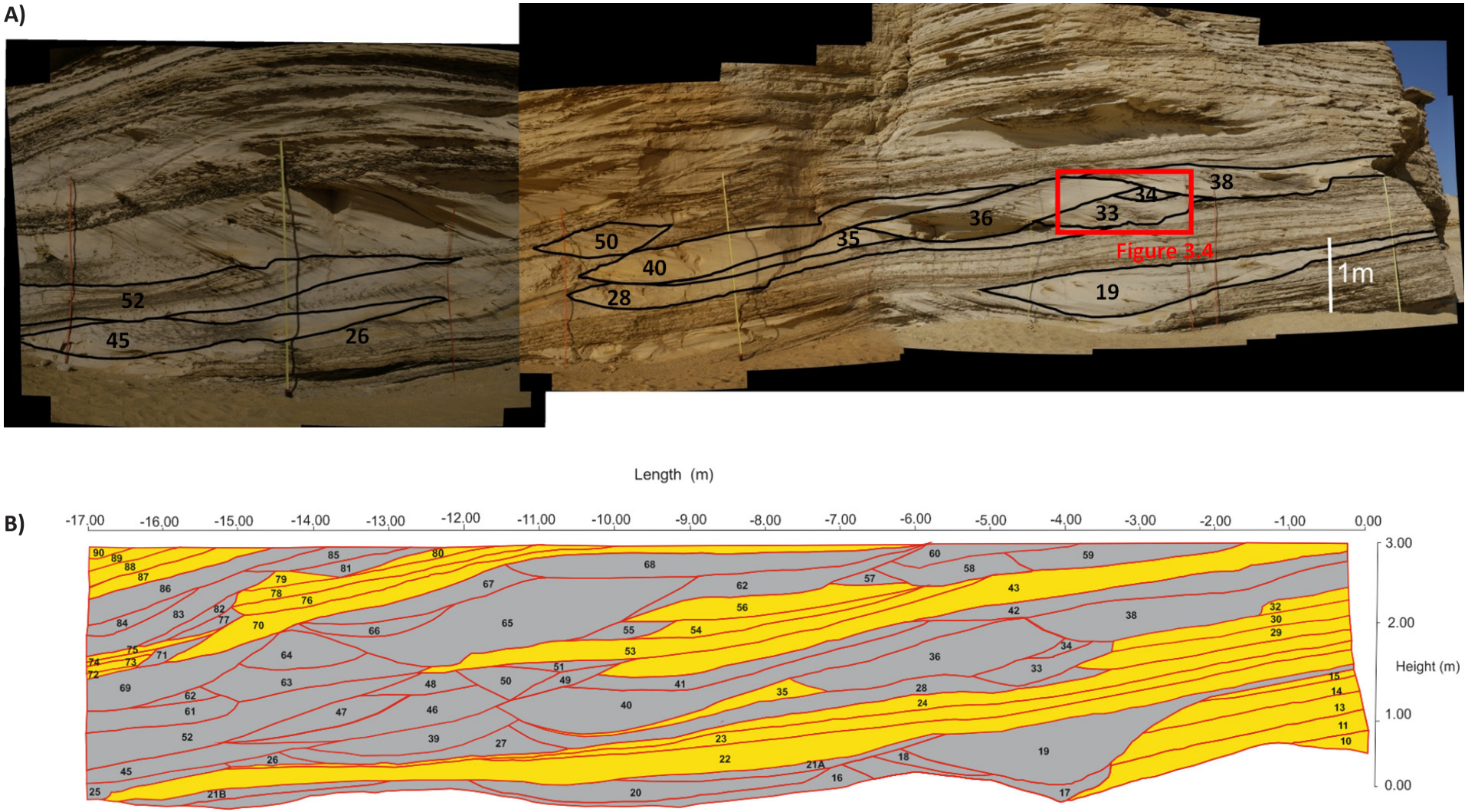


Figure 3.8: A) Photomontage of the WNW-ESE-oriented face of Gecko Nose (bold line face in Figure 3.7), oblique to depositional strike. The 12 numbered trough cross-bed sets were chosen to define best fit elliptical curves (cf. Figure 3.4). B) Interpretation of the photomontage. Trough (grey) and tabular (yellow) cross-beds are numbered sequentially and interpreted to be stacked vertically within a tidal bar deposit. Note that the numbering starts at 10, as nine underlying cross-bed sets are exposed on the adjacent SSW-NNE-oriented face (dotted line face in Figure 3.7).



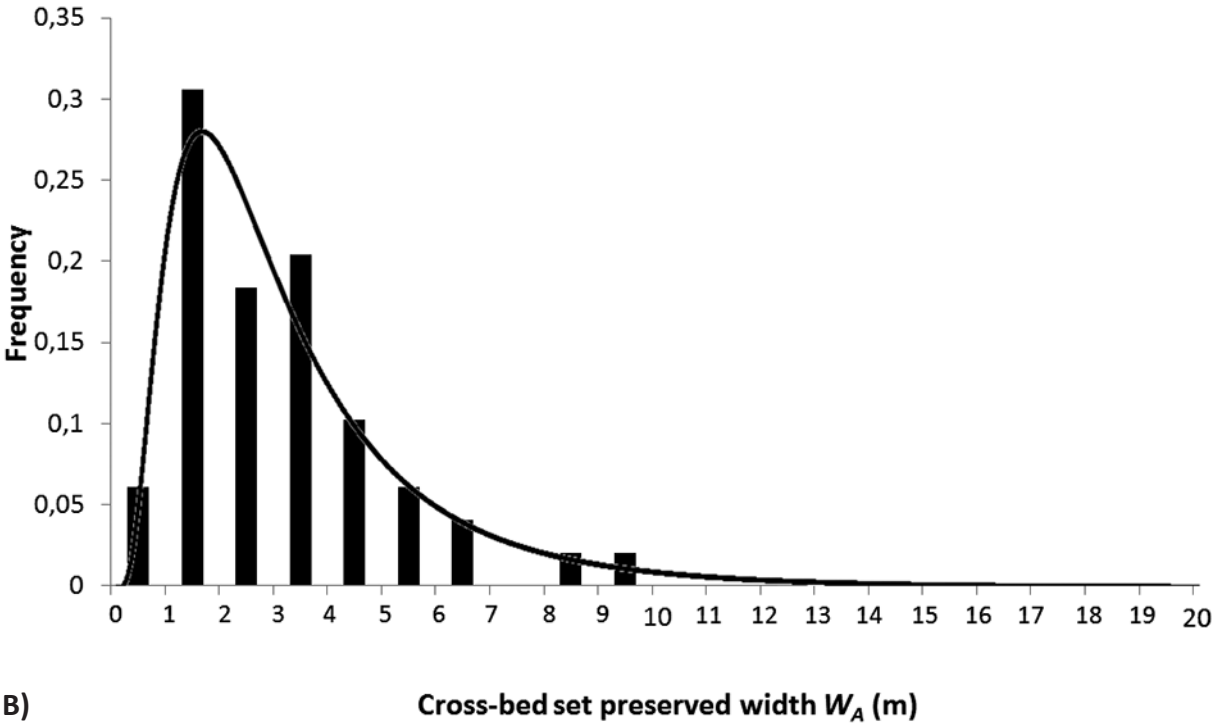


Figure 3.9: Distribution of A) the preserved height H_A and B) preserved apparent width W_A of 49 trough cross-bed sets exposed on the WNW-ESE-oriented face of Gecko Nose (red face in Figure 3.7; Figure 3.8 B), oblique to depositional strike. A log-normal distribution of the form LogN(μ,σ^2) is interpreted, with parameters μ: mean value; σ: standard deviation. p corresponds to the Kolmogorov-Smirnov test criterion: a value of 1 corresponds to a perfect fit of the data with a log-normal distribution. For the height H_A in A), μ = 0.3 cm and σ = 0.4 cm with p = 0.82; for the width W_A in B), μ = 3.1 cm and σ = 1.4 cm with p = 0.98.

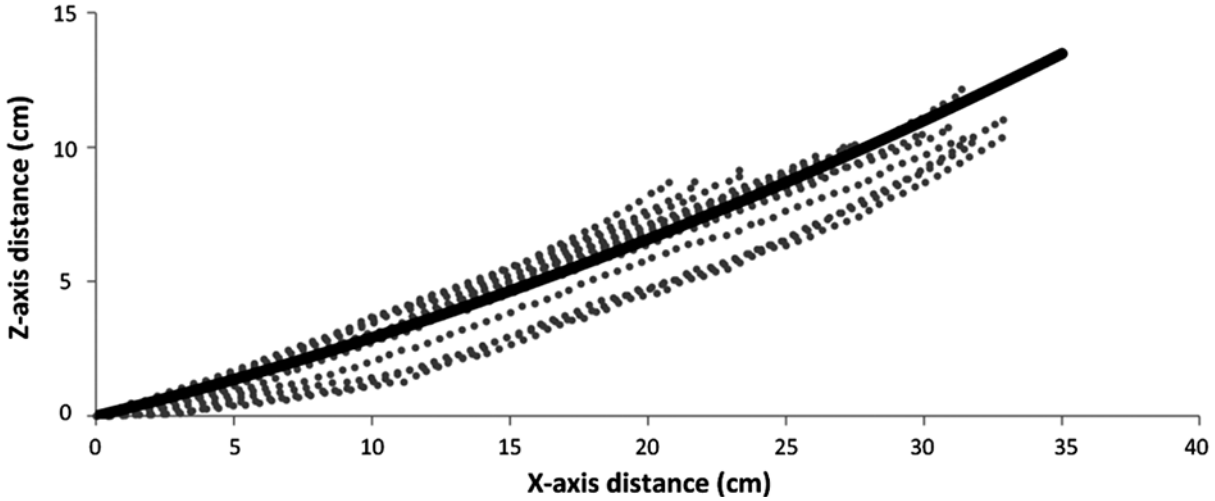


Figure 3.10: Point clouds defining the 90 foreset-toeset surfaces traced from three cross-bed sets of the WNW-ESE-oriented face of Gecko Nose (numbered 34, 50 and 52 in Figure 3.8 A). The surfaces are translated so that their foreset-to-toeset junction points (labelled *O* in Figure 3.5) are superimposed, and a best-fit line for a foreset-toeset template surface is determined (bold line). This line is described by equation (3.5) with the curvature parameter $A = 5.5 \times 10^{-3}$, and the resulting line has a very strong correlation to the data ($R^2 = 0.98$).

In order to determine the degree of curvature *A* from the Gecko Nose dataset, the 90 foreset-toeset surfaces contained in three cross-bed sets (numbered 34, 50 and 52 in Figure 3.8 A) have been extracted from photomontages. The foreset-toeset surfaces are rotated so that their toesets are horizontal. For each foreset-toeset surface, the junction point *O* is identified. All the foreset curves are then translated to the same origin and a best-fit parabolic curve is fitted to the data (Figure 3.10). To determine the foreset thickness F_T, the sandstone laminae thicknesses comprised between the 544 foreset-toeset surfaces contained in 12 studied cross-bed sets (identified in Figure 3.8 A) have been measured after extraction of the surfaces from photomontages. A log-normal distribution of F_T values is observed (Figure 3.11). The dip angle of the toesets α has been measured on photopanoramas of the NNE-SSW-oriented (oblique dip oriented) face of Gecko Nose. The angle of dune climb δ has been determined by generating a best-fit line through the foreset-to-toeset junction points *O* of laminae in each of the studied cross-bed sets.

To define the mudstone frequency function *f*, the positions of mudstone drapes along the same 90 foreset-toeset surfaces of the three cross-bed sets used to determine the parameter *A* (numbered 34, 50 and 52 in Figure 3.8 A) have been extracted from photomontages. From this dataset, a frequency distribution of mudstone drape presence relative to position along the foreset has been determined using equation (3.7) to define a best-fit curve (Figure 3.12).

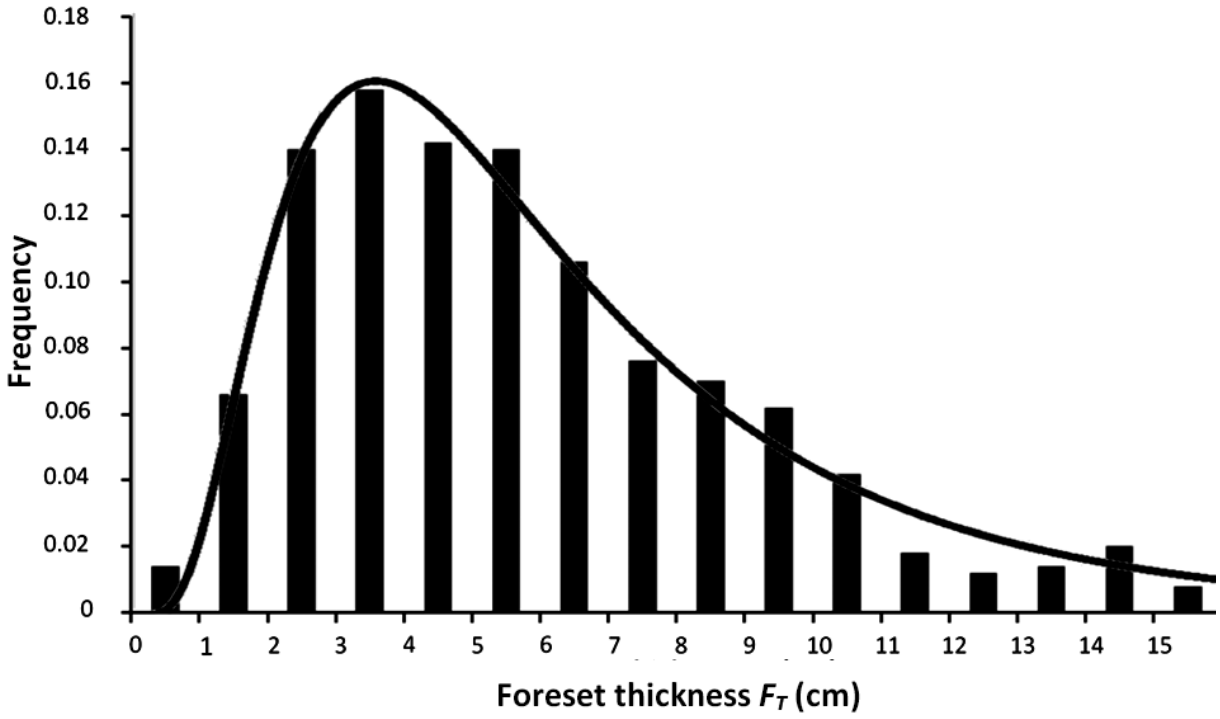


Figure 3.11: Distribution of foreset thickness F_T for the 544 foreset-toeset surfaces of 12 studied cross-bed sets (Figure 3.8 A). A log-normal distribution of the form LogN(μ,σ^2) is interpreted with parameters μ, mean value = 5.9 cm; σ, standard deviation = 2.0 cm.

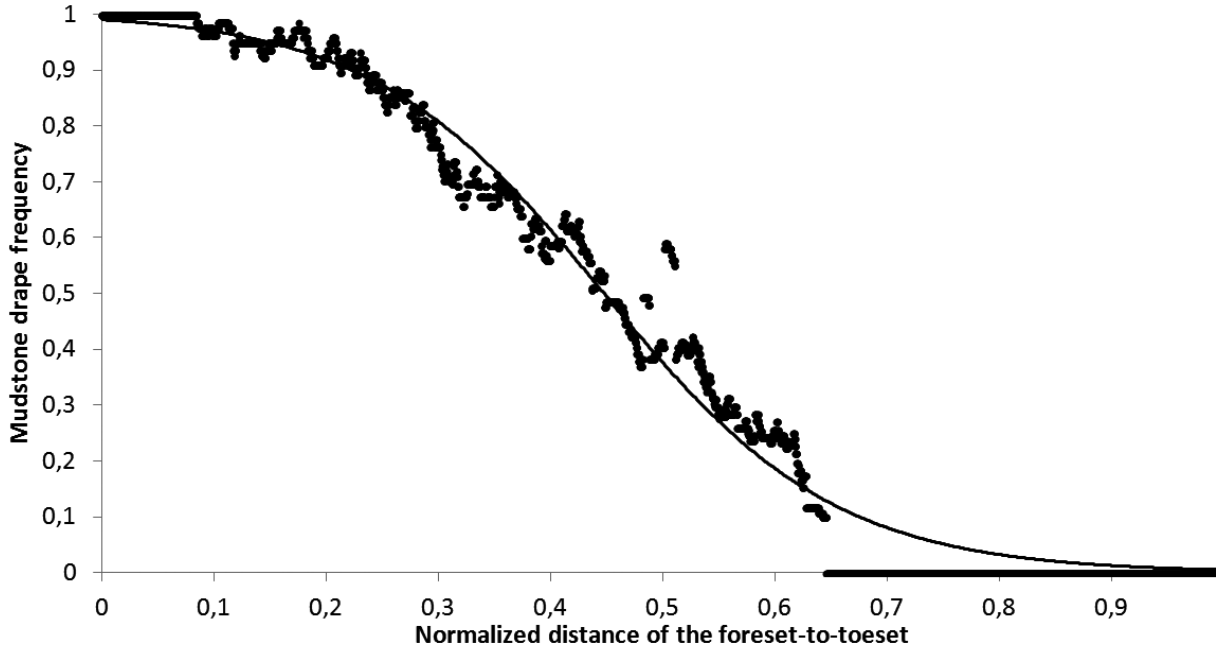


Figure 3.12: Point cloud defining the coverage of mudstone drapes along 90 foreset-toeset surfaces traced from three cross-bed sets (numbered 34, 50 and 52 in Figure 3.8 A). A best-fit line for mudstone drape coverage along a foreset-toeset surface is determined (bold line). This line is described by equation (3.4) with parameters M = -1.004, N = -4.316, and O = 1.610, and it correlates very strongly to the data (R^2 = 0.99).

3.3. Results

3.3.1. Models constructed from outcrop analogue data

The modelling methodology has been applied to create 3D models of heterolithic, cross-bedded tidal sandstones equivalent to those observed at the Gecko Nose and the Butterfly Canyon localities. Generic models have been generated using input parameters derived from both localities (Figures 3.13 and 3.14; Table 3.1). The models are stochastically generated using the data reported in the previous section, except for the elemental volumes, whose positions are extracted directly from photomontages of the two outcrop localities. Both models are 9 m^3 in volume (3 x 3 x 1 m), and contain four ellipsoidal elemental volumes in the case of the Butterfly Canyon model and six ellipsoidal elemental volumes in the case of the Gecko Nose model. The model volumes are approximately five orders of magnitude larger than the volume of a typical core plug (c. 20 cm^3). Around 500 foreset-toeset surfaces are populated in trough cross-beds in the Gecko Nose model, whereas only 170 of the same surfaces are present in the Butterfly Canyon model (parameter N_{CB} in Table 3.1). The mudstone drape coverage that was chosen for both models is equal to 25% along the foreset parts and 57% along the toeset parts of the foreset-toeset surfaces. The mudstone frequency function f defined in the previous section (Figure 3.12) was used to define the probable position of mudstone elliptical patches along foreset parts, until the specific mudstone drape coverage of 25% is reached.

A comparison between the outcrop cliff faces of Gecko Nose and Butterfly Canyon, and the corresponding generic model is presented in Figure 3.15. The model honours the geometry of the cross-bed set boundaries, in both strike and dip directions, which validates the choice of having cross-bed sets represented as ellipsoidal elemental volumes (Figures 3.2, 3.3 and 3.4). The input average foreset thickness F_T is respected as observed at the outcrop locations, with F_T being smaller for the Gecko Nose model than for the Butterfly Canyon model. The Gecko Nose model is relatively mudstone-rich (sandstone volume fraction V_S/V_T = 0.89, Table 3.1), as it comprises trough cross-beds containing a relatively high proportion of toesets (foreset to toeset volume ratio $R_{F/T}$ = 6.5 : 1, Table 3.1) due to a high dune climb angle δ = 5°; the Butterfly Canyon model is comparatively mudstone-poor (sandstone volume fraction V_S/V_T = 0.94, Table 3.1), as it comprises tabular cross-beds dominated by foresets (foreset to toeset volume ratio $R_{F/T}$ = 24 : 1, Table 3.1), with a low dune climb angle δ = 0°.

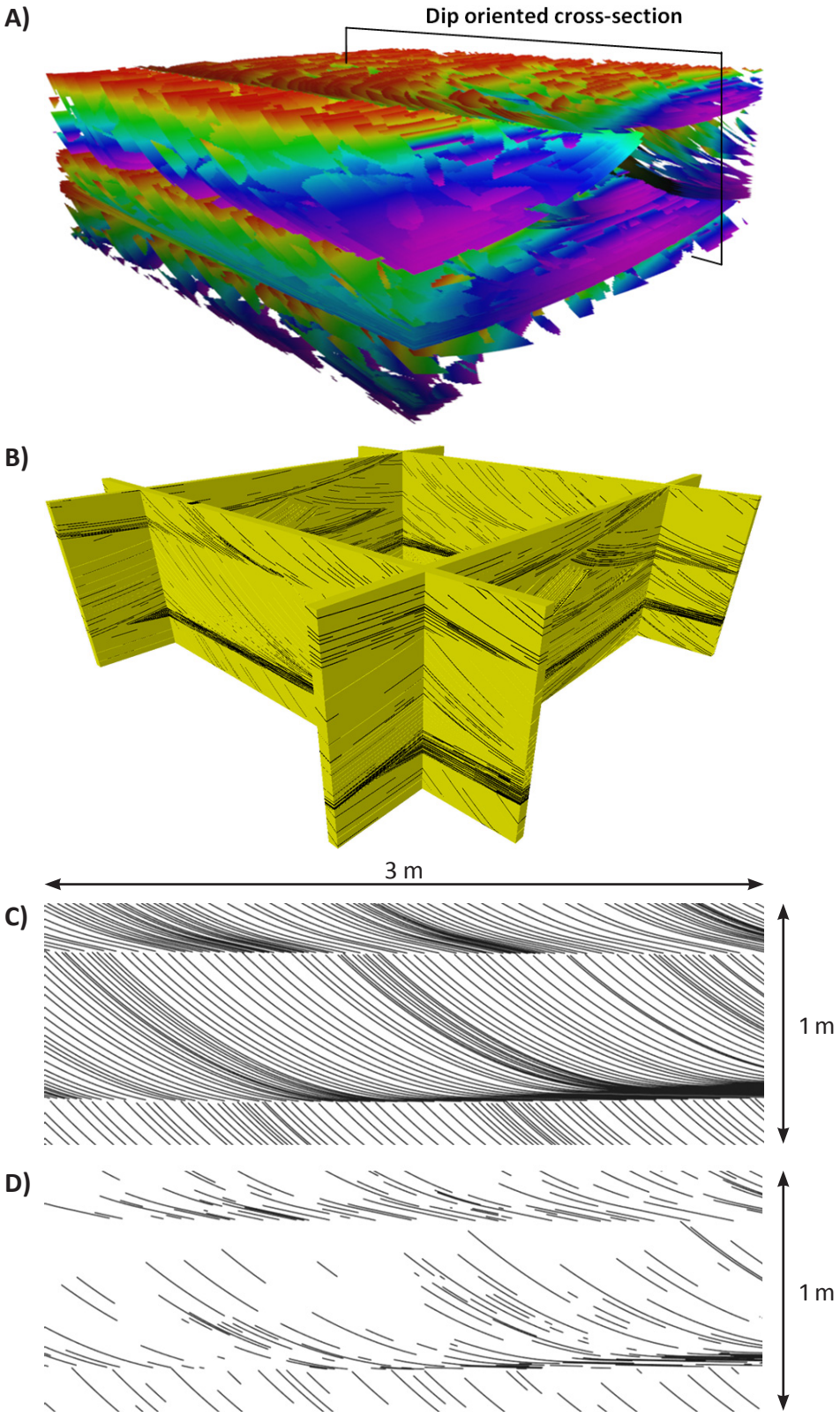


Figure 3.13 : A) 3D view of the generic trough cross-bedding model, generated with input parameters extracted from the Gecko Nose outcrop and summarized in Table 3.1. Only mudstone drapes are displayed here and sandstone is removed from the model. The model displays a mudstone drape coverage of 25% along the foreset parts, and a coverage of 57 % along the toeset parts of the foreset-toeset surfaces. The trough aspect of the cross-bedding appears in the strike direction. B) Orthogonal sections through the same model with mudstone and sandstone layers coloured in black and yellow respectively. The layers of mudstone have a constant thickness of 3.5 mm in the whole model. C) Dip oriented cross-section of the model presented in part A representing the cross-bedding surfaces. D) The same dip-oriented cross-section but with the 25% mudstone drape coverage of foresets and 57% mudstone drape coverage of toesets.

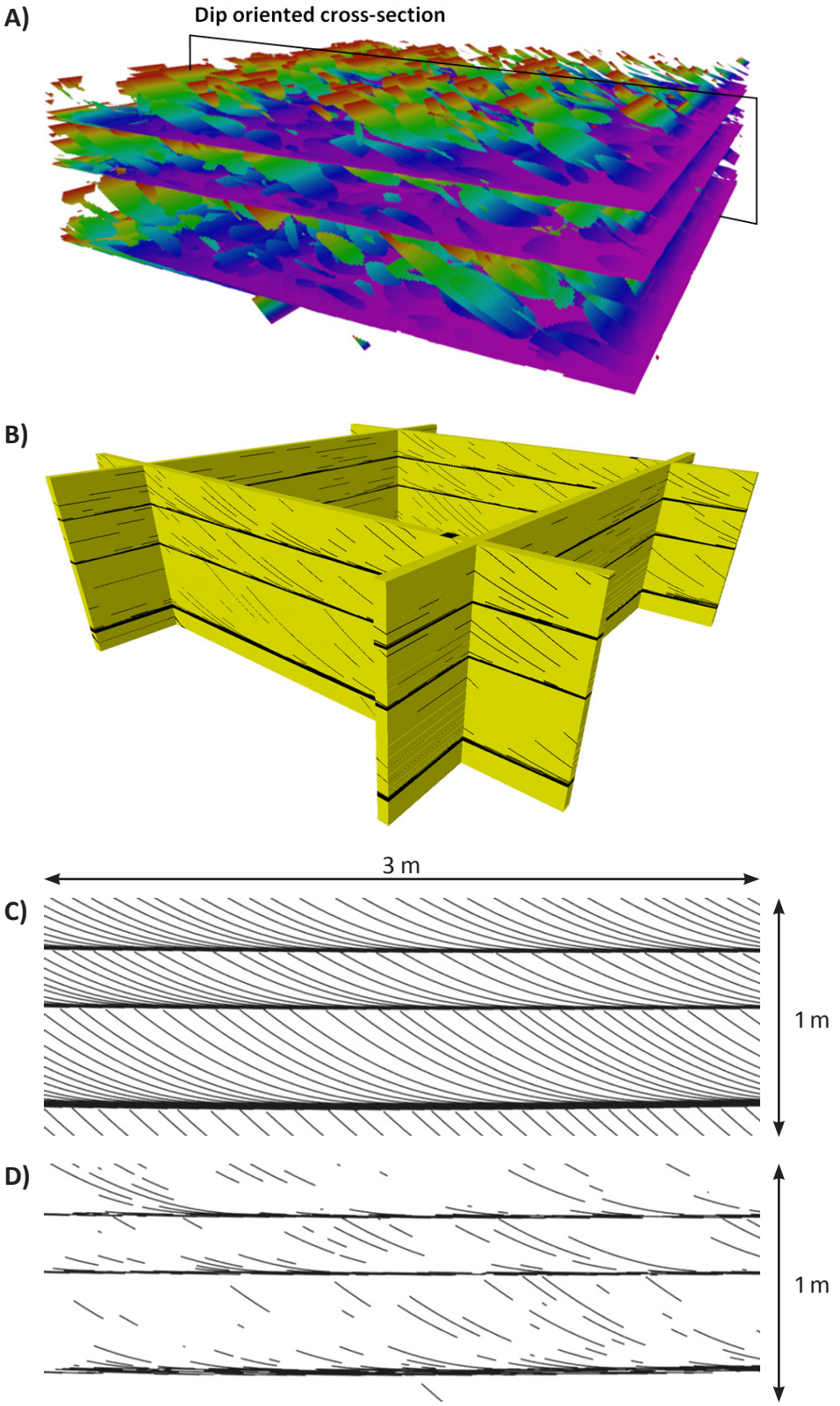


Figure 3.14 : A) 3D view of the generic tabular cross-bedding model, generated with input parameters extracted from the Butterfly canyon outcrop and summarized in Table 3.1. Only mudstone drapes are displayed here and sandstone is removed from the model. The model displays a mudstone drape coverage of 25% along the foreset parts, and a coverage of 57 % along the toeset parts of the foreset-toeset surfaces. B) Orthogonal sections through the model with mudstone and sandstone layers coloured in black and yellow respectively. The layers of mudstone have a constant thickness of 3.5 mm in the whole model. C) Dip oriented cross-section of the model presented in part A representing the cross-bedding surfaces. D) The same dip-oriented cross-section but with the 25% mudstone drape coverage of foresets and 57% mudstone drape coverage of toesets, as featured in part A.

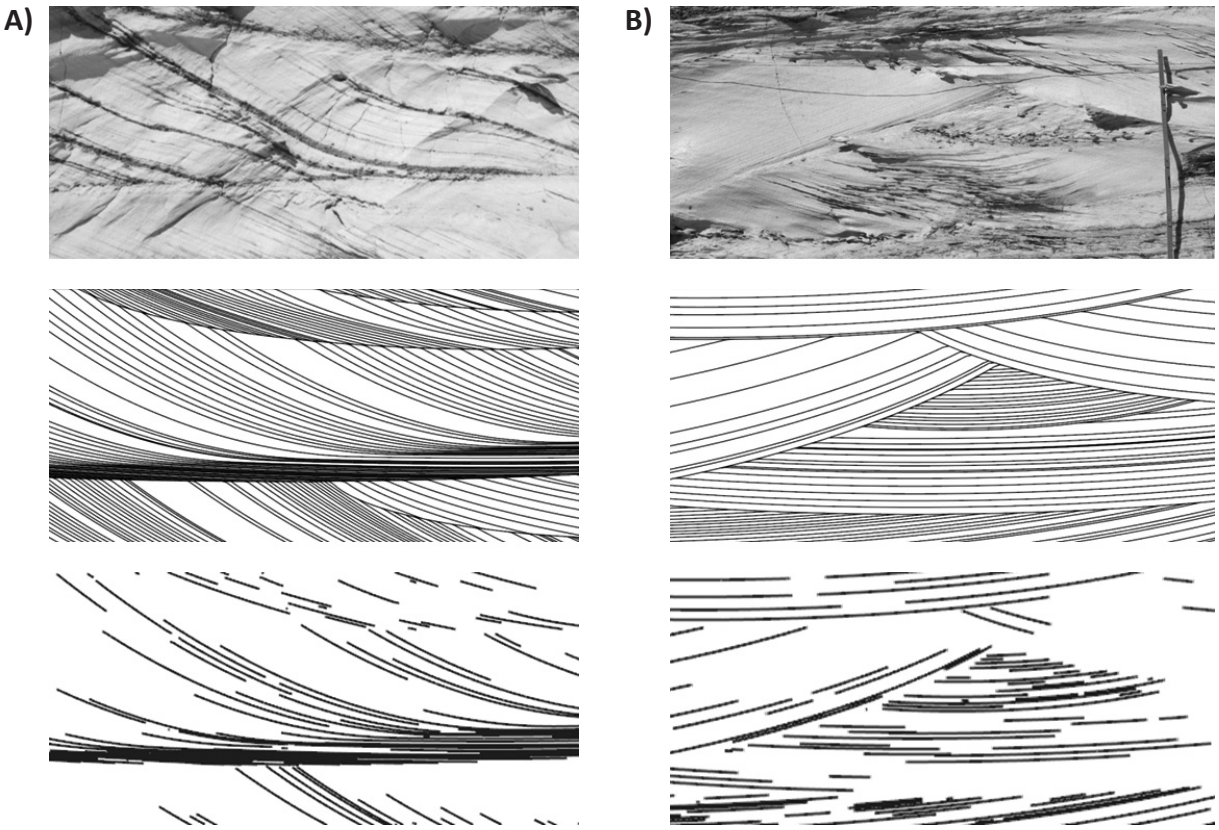


Figure 3.15: Comparison between outcrop photographs (top row), and corresponding cross-sections of the surface-based models showing foreset-toeset surfaces (central row) and mudstone drapes along these surfaces (bottom row). Column A) shows dip-oriented sections from the Butterfly Canyon outcrop and model. Column B) shows strike-oriented sections from the Gecko Nose outcrop and model (red rectangle in Figure 3.8 A).

Measured parameter	Symbol	Trough cross-bed model (Gecko Nose)	Tabular cross-bed model (Butterfly Canyon)
Mudstone volume fraction	V_M/V_T	0.11	0.06
Sandstone volume fraction	V_S/V_T	0.89	0.94
Normalized effective dip horizontal permeability	k_d^n	47.5%	70.0%
Normalized effective strike horizontal permeability	k_s^n	72.8%	90.0%
Normalized effective vertical permeability	k_v^n	2.4%	2%
Ratio of vertical permeability by horizontal permeability	k_v/k_h	0.0399	0.0025

Table 3.2: Results for the Gecko Nose and Butterfly Canyon models (Figures 3.13, 3.14) after single phase flow simulation. All measurements are dimensionless.

The distribution of mudstone drapes along the cross-bedding surfaces closely matches the distribution observed at outcrop. Both in the models and at outcrop, some mudstone drapes appear continuous along the entire cross-bedding surface, from the toeset part to the top of the foreset at the top boundary of the cross-bed set. In most cases, the mudstone drapes in the models are discontinuous over the entire length of the cross-bedding surfaces in cross-sections, but the discontinuities are limited in the third dimension, which is again a close match to outcrop observations. Discontinuities of the mudstone drapes in the models are mostly located at the top of the foreset part of the cross-bedding surfaces, following the trend of the input mudstone drape frequency function defined from the outcrop statistical analysis (Figure 3.12). For flow simulation purposes, mudstone drapes are modelled explicitly in the grid as 2mm thick layers overlying the cross-bedding surfaces, eroded (i.e. replaced by sandstone) when the mudstone drape surfaces are not present. (see Chapter 4.2.1 for further explanation on flow simulation methodology).

3.3.2. Calculation of effective permeability

Effective-permeability is calculated thanks to the Darcy's law:

$$k_e = \frac{Q\mu L}{A\Delta P} \tag{3.8}$$

where Q is the volumetric flow rate (m^3/s), μ is the viscosity (chosen arbitrarily to be 1 Pa.s), L is the model length in the direction of flow (m), A is the cross-sectional area of the model perpendicular to the direction of flow (m^2), and ΔP is the fluid potential uniform on each face drop along the model in the direction of flow (Pa). The actual methodology to calculate the input parameters for the equation 3.8 are presented in the next chapter of this thesis, consequently we only report in this chapter the results for the two models shown in Figures 3.13 and 3.14 (see Chapter 4 for further details). We report the effective permeability as a normalized value, expressed as a fraction of the sandstone permeability:

$$k_e^n = \frac{k_e}{k_{sand}} \tag{3.9}$$

The results reported in this way are independent of the value of sandstone permeability used in the models; moreover, the normalized effective permeability can be rescaled to any value of sandstone permeability obtained from core or mini-permeameter measurements.

The effective permeability of the model volume has been extracted in three orthogonal directions: the horizontal effective permeability down depositional dip k_d^n, the horizontal effective permeability along depositional strike k_s^n, and the vertical effective permeability k_v^n. The results for each model are summarized in Table 3.2. Despite the relatively low volume fraction of mudstone in the models, the presence of the mudstone drapes significantly reduces both horizontal and vertical permeability, and introduces permeability anisotropy in the horizontal as well as the vertical direction ($k_s^n \neq k_d^n$ and $k_v^n << k_h^n$ where $k_h^n = \sqrt{(k_d^n + k_s^n)}$). For the trough-cross bedded model of Gecko Nose, the dip direction horizontal permeability is only 65% of the strike direction horizontal permeability, as the flow must cross a larger number of mudstone-draped foresets when flowing down depositional dip as opposed to along depositional strike. The k_v/k_h ratio is reduced to only 0.04, reflecting that vertical flow must also cross numerous mudstone-draped foresets. The horizontal permeability anisotropy of the tabular cross-bedded Butterfly Canyon model is less pronounced than in the trough-cross-bedded model, reflecting the comparatively lower mudstone fraction: the dip direction horizontal permeability is 77% of the strike direction horizontal permeability. Despite the lower overall mudstone fraction, the k_v/k_h of the tabular cross-bedded model is one order of magnitude smaller (at 0.003) than the value of the trough-cross-bedded model. Mudstone drapes are approximately three times more numerous in the trough cross-bed model (N_{CB}≈500) than in the tabular cross-bed model (N_{CB}≈170). However, the mudstone drapes are more densely spaced and laterally continuous in the toesets of the trough cross-bed model because of the high values of the toeset dip angle α. Moreover, the sandstone volume fraction in the toesets of the tabular cross-bed model is 0.26, which is less than half of the sandstone volume fraction in the toesets of the trough cross-bed model, despite the common value of mudstone drape coverage of 57% in both models. The smaller value of k_v/k_h ratio in the tabular cross-bed model arises from the closer spacing of mudstone-draped toesets and consequent lower sandstone volume fraction in the toeset parts of cross-bed sets.

For the two models studied, the normalized effective permeability values can be rescaled to any measured sandstone permeability to yield estimates of effective permeability suitable for use on larger-scale reservoir models (Figure 3.16). For example, if the measured permeability of the sandstone was 500 mD, then the trough-cross bedded (Gecko Nose) model yields

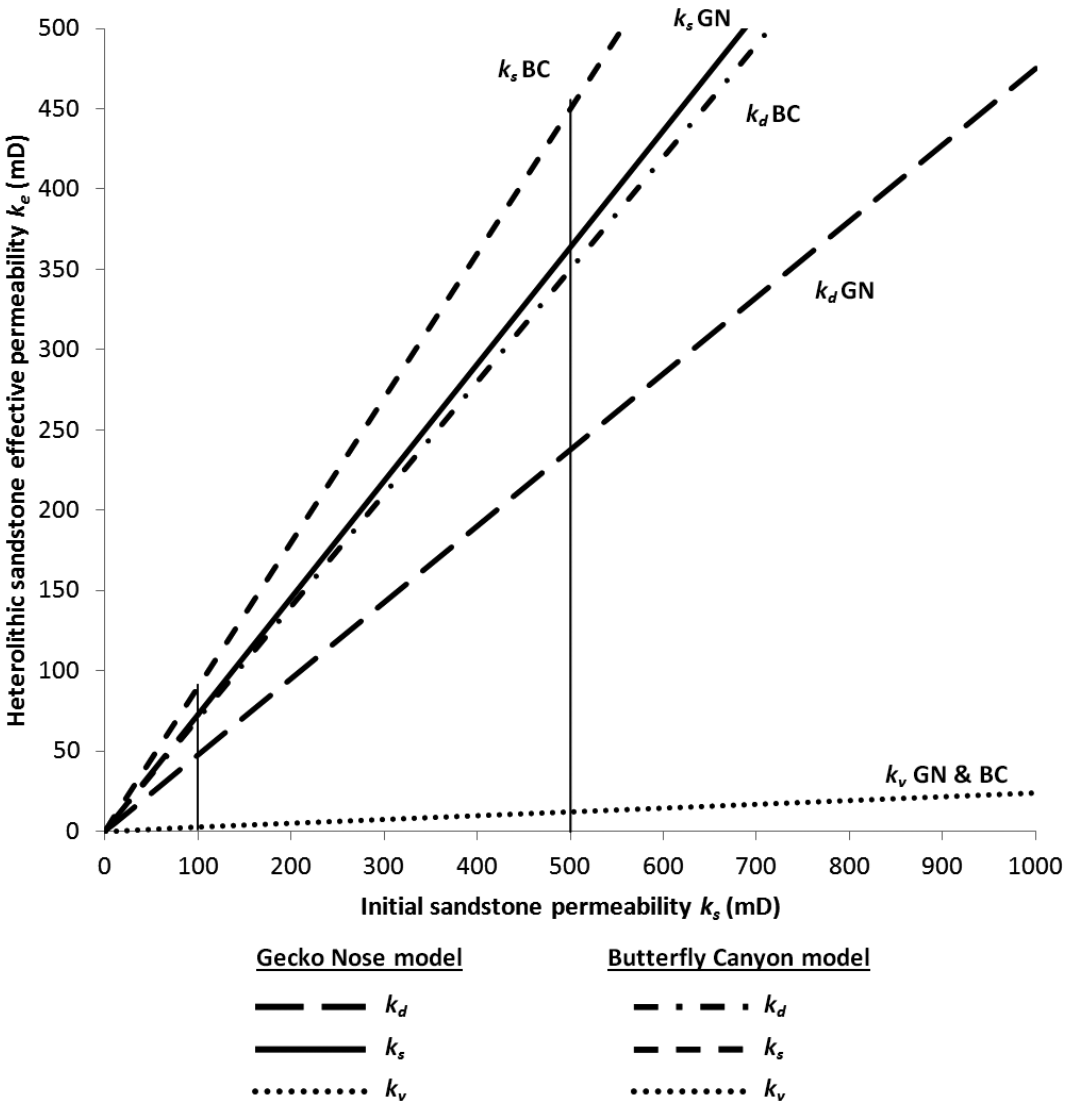


Figure 3.16: Determination of effective permeability from the flow simulation results of the two outcrop models (Figures 3.13, 3.14). If the studied heterolithic sandstone features trough cross-bedding with consequent muddy toeset regions, the Gecko Nose model has to be used for reference; if the studied heterolithic sandstone features tabular cross-bedding with a predominance of sandy foreset regions, the Butterfly Canyon model has to be used. For the reading of the effective permeability of the heterolithic sandstones, the two examples presented in the text are featured with straight vertical lines: k_{sand} = 500 mD and k_{sand} = 100 mD. The resulting effective permeability k_e can be read at the intersection of these straight lines with the different curves. Note: the vertical permeability curves for the two models are merged due to the scale of the graph.

permeability values of k_d = 238 mD, k_s = 364 mD and k_v = 12 mD, while the tabular cross-bedded (Butterfly Canyon) model yields permeability values of k_d = 350 mD, k_s = 450 mD and k_v = 10 mD. If the permeability of the sandstone was lower at 100 mD, effective permeabilities are proportionately reduced as well, yielding k_d = 48 mD, k_s = 73 mD and k_v = 3 mD for the trough-cross bedded model, and k_d = 70 mD, k_s = 90 mD and k_v = 2 mD for the tabular cross bedded model. Effective permeability values from a broader range of model geometries and mudstone fractions are reported in the next chapter.

The modelling workflow reported here can be applied to create appropriate models for the calculation of effective permeability values depending on the geometric characteristics of the heterogeneity surfaces of any tidal cross-bedded heterolithic sandstone observed at outcrop location or in subsurface. The required input parameters and the different methods of measurements for each of them are summarized in Figure 3.1. The main orientation of cross-bed sets (i.e. the paleocurrent) and its standard deviation can be deduced from dipmeter logs. The style of cross-bedding is easily recognizable from the trace of the cross-bedding plane around the core. The tracing of the cross-bedding plane on well imagery can be considered for more precision, as core observations is typically only possible on one half of the core. The foreset thickness F_T can be measured on core with a representative number of occurrences, even if the typical width of a core (8-20 cm) prevents from observing a complete neap/spring cycle of foresets with cyclical variation of the foreset thickness. Consequently, a study of one outcrop analogue example would provide more grounded and reference data for constraining F_T for the studied subsurface case. The foreset to toeset ratio $R_{F/T}$ can be appraised in a similar way from core observations, but with a limited representative display. As dune climb angle δ has typically small values, the ratio $R_{F/T}$ remains quite constant in the cross-bed set considering the dimensions of preserved cross-bed sets after stacking and erosion (Figures 3.3, 3.5). However, no lateral variation on $R_{F/T}$ can be deduced from core observations. Finally, the toeset dip angle α can be observed on core if toeset areas are sampled. All input parameters can be otherwise derived from suitable outcrop statistical analysis – when the degree of analogy with the studied subsurface case is established – in a similar way than the analysis we presented in this study using the Dir Abu Lifa Member as an outcrop analogue for the specific facies of tidally-influenced cross-bedded sandstones.

The degree of analogy with a specific subsurface field is critical to determine as results of effective permeability are very sensitive to changes in the input geometric parameters (as highlighted in the following chapter of the thesis). When it comes to tidally-influenced depositional environments, the influence of the different currents and their relative strengths should be similar (i.e. same position on the Galloway diagram, triangle with each vertex corresponding to whether marine, fluvial or tide influcences, systems are classfied on the diagram depending on the relative strengths of the currents; Galloway, 1975). The critical

parameters controlling the current ratios – especially the tide strength in shallow marine depositional environments – consist on the dimensions and morphology of the sedimentary basin. The Dir Abu Lifa Member corresponds to a restricted shallow-marine system with topographic highs protecting the area from the wave influence (Legler *et al.*, 2013). Consequently, the outcrops and the following models featured in our study are used as an example for purely tide-influenced or tide-dominated systems (*sensu* Galloway diagram, 1975; Ainsworth *et al.*, 2011). Depositional processes are similar in term of energy if the analogy in the tide influence is validated. Sedimentary structures are then of similar shapes and similar dimensions. However, the analogy in the lateral variations of the facies associations is very doubtful as lateral changes occur rather anarchically in tidally-influenced depositional environments, even when considering one single outcrop example (and the Butterfly Canyon compared to the Gecko Nose outcrop locations for the same Dir Abu Lifa Member are a good example). The effective permeability analogy is only reached at the facies length-scale discussed in this study. At this scale and in analogous depositional settings, heterogeneities feature the same geometry and the mudstone drape coverage patterns are comparable. Consequently, the sandstone connectivity and the flow tortuosity are similar and the normalized effective permeabilities are equal. Absolute values will vary depending on the clean sandstone grain sorting and permeability (Figure 3.16).

3.4. Conclusions

This chapter presents a novel reservoir modelling methodology that accurately and efficiently reproduces the geometry and connectivity of sandstone and mudstone layers in heterolithic, cross-bedded tidal sandstones by stochastically modelling stratigraphic surfaces and associated heterogeneity. The input parameters required to apply the methodology are all geometric and can be simply derived from observations of subsurface cores and outcrop analogues. The application of the modelling methodology is demonstrated via the construction of models that represent heterogeneity in significantly larger volumes (9 m^3) than those

sampled by core plugs (c. 20 cm^3), using input parameters derived from analysis of an outcrop analogue. Quantitative outcrop-analogue data are collated and used to constrain the geometry and spatial distribution of the small-scale heterogeneity surfaces (i.e. cross-bed set boundaries, cross-bedding foreset-toeset surfaces, and mudstone drapes). The resulting models are a close visual match to the outcrop data, such that the complex mudstone and sandstone connectivity of the heterolithic tidal deposits is accurately reproduced. The surface-based methodology employed here is not dependent on length scale, but on the geometric configuration and hierarchical arrangement of geologic surfaces. The methodology can therefore be generalized to a wide range of other heterolithic reservoirs in which characterisation of heterogeneity requires an accurate 3D representation of such geologic surfaces (e.g. wavy-bedded heterolithic sandstones).

Chapter 4
Effective flow properties of heterolithic, cross-bedded tidal sandstones: part 2. Single-phase flow simulation

Summary

Tidal heterolithic sandstone reservoirs are heterogeneous at the sub-metre scale, due to the ubiquitous presence of intercalated sandstone and mudstone laminae. Core-plug permeability measurements fail to sample a representative volume of this heterogeneity. Here we investigate the impact of mudstone drape distribution on the effective permeability of tidal heterolithic, cross-bedded sandstones using three-dimensional (3D) surface-based "mini-models" that capture the geometry of cross-beds at an appropriate scale. The impact of seven geometric parameters has been determined: (1) mudstone fraction, (2) sandstone laminae thickness, (3) mudstone drape continuity, (4) toeset dip, (5) climb angle of foreset-toeset surfaces, (6) proportion of foresets to toesets, and (7) trough or tabular geometry of the cross-beds.

We begin by identifying a representative elementary volume (REV) of 1 m^3, confirming that the model volume of 9 m^3 (> REV) yields representative permeability values. Effective permeability decreases as the mudstone fraction increases, and is highly anisotropic: vertical permeability falls to c. 0.5% of the sandstone permeability at a mudstone fraction of 25%, while the horizontal permeability falls to c. 5% and c. 50% of the sandstone value in the dip and strike directions, respectively. There is considerable spread around these values, because each parameter investigated can significantly impact on effective permeability, depending upon the flow direction and sandstone fraction. The results yield improved estimates of effective permeability in heterolithic, cross-bedded sandstones, which can be used to populate reservoir-scale model grid blocks using estimates of mudstone fraction and geometrical parameters obtained from wireline-log, core and outcrop-analogue data.

4.1. Introduction

Tidal influence commonly results in the rhythmic deposition of sandstone and mudstone laminae in shallow-marine depositional environments (Nio and Yang, 1991). These mudstone laminae (often termed "drapes") affect the reservoir performance of tidal heterolithic sandstone units, as they can act as baffles or barriers to flow during hydrocarbon production, depending on their lateral and vertical extent (Weber, 1982; Kjønsvik *et al.*, 1994; Martinius *et al.*, 2005; Jackson and Muggeridge, 2000). Mudstone drapes occur over a range of length-scales and with different geometric configurations, reflecting the scale of bedforms and the strength and spatial variability of tidal currents during deposition. Consequently, mudstone and sandstone laminae exhibit complex 3D architecture with highly variable lateral and vertical connectivity that is challenging to represent in geologic and flow-simulation models. Current practice is to obtain rock properties for these heterogeneous sandstones from subsurface wireline-log data or laboratory core measurements, and then to upscale these measurements to the grid-block scale in geologic models using simple averaging methods. Yet previous studies have demonstrated that averaging of core permeability measurements does not yield representative values at the grid-block scale, because these data do not sample a volume of rock that is representative of the heterogeneity (Jackson *et al.*, 2003). Values appropriate for use at larger length-scales must be derived using a Representative Elementary Volume (REV) of the rock (sensu Bear, 1972): above this minimum volume, measured or calculated properties are independent of the sample volume considered (Figure 4.1). The REV assumption is based on the effective medium theory which assumes that the correlation lengths of the different components are shorter than the model domain. At the REV, the parameter of interest is both homogeneous and statistically stationary (Nordahl and Ringrose, 2008). For example, the REV for permeability must be sufficiently large to capture the key heterogeneities dictating flow in all directions. The REV assumption is only valid if the key heterogeneities have distinct, separate length-scales which may not be the case if the REV is so large that it is not preserved in sedimentological records which rather consist of different types of facies (i.e. facies associations).

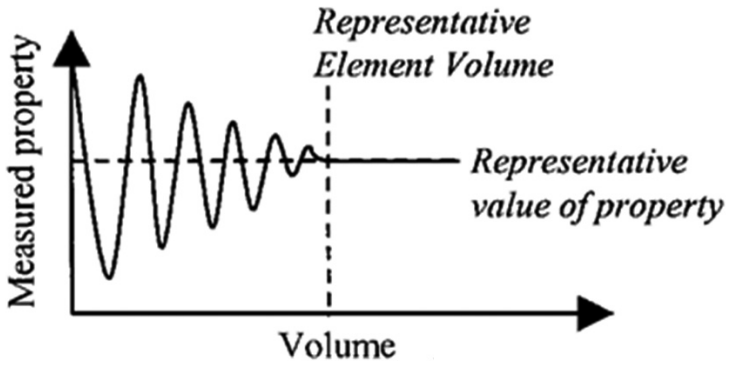


Figure 4.1: Plot illustrating the variation in a measured reservoir property for different sample volumes (Bear, 1972). Small sample volumes exhibit a wide range of values for the measured property, indicating that these volumes are unrepresentative of reservoir behaviour. A representative value of the measured property is obtained for larger sample volumes, above a threshold defined by the Representative Element Volume (REV).

In previous studies, models of small (but larger than core) volumes (27 - 180 x 10^3 cm^3) of wavy-bedded tidal sandstones have been generated using a geometric forward modelling approach that mimics the movement of bedforms during deposition (Wen *et al.*, 1998, after Rubin, 1987), in order to simulate flow and thus predict effective permeability in the near wellbore region (Ringrose *et al.*, 2003, 2005; Nordahl *et al.*, 2005). The same models were also used to determine an REV of 5 x 10^3 cm^3 for wavy-bedded tidal sandstones of varying mudstone content (Nordahl and Ringrose, 2008). A surface-based modelling technique was used by Jackson *et al.* (2005) to recreate realistic 3D models of flaser- and lenticular-bedded tidal sandstones directly from outcrop rock samples. The two 7.5 x 10^4 cm^3 samples (0.5 x 0.5 x 0.3 m; i.e. above the REV of Nordahl and Ringrose, 2008) were serially-sectioned at a spacing of 2 cm, and the surfaces bounding sandstone and mudstone lithologies traced in 2D on each section, in order to reconstruct the lithologic-boundary surfaces in 3D (Jackson *et al.*, 2005). Flow simulation of the resulting surface-based models identified the connectivity of sandstone and mudstone laminae as the main parameter controlling reservoir properties. Thus, accurate representation of sandstone- and mudstone-laminae distribution and geometry is an essential requirement for models that can predict effective permeability.

In the previous chapter, we documented a new surface-based methodology for accurate geometric representation of lithologic heterogeneity in heterolithic, cross-bedded tidal sandstones. The method requires the user to define input values for a small number of parameters that describe the geometry and spatial distribution of foreset-toeset surfaces and

the distribution of mudstone drapes along these. Values of the parameters may be derived for a given interval from a combination of wireline and/or core and outcrop-analogue data. In this chapter, we apply the surface-based methodology to construct a range of models of cross-bedded tidal sandstones, in order to investigate the impact on effective permeability of mudstone drapes along foreset-toeset surfaces within cross-beds. The chapter has four aims: (1) to identify a possible REV for heterolithic, cross-bedded tidal sandstones by investigating the impact of sample volume on permeability, (2) to quantify the impact on effective permeability of mudstone proportion, which is controlled by mudstone drape extent and continuity along foreset-toeset surfaces, (3) to determine whether effective permeability can be predicted to reasonable accuracy based only on knowledge of the sandstone fraction (the "net-to-gross"), and (4) to assess the relative sensitivity of effective permeability to six geometric parameters that are uncertain in the subsurface but control the spatial arrangement of mudstone drapes in tidal cross-bedded heterolithic sandstones, and identify which of these, if any, is key to predicting effective permeability.

4.2. Methodology

4.2.1. Surface-based model construction

Models of cross-bedded heterolithic sandstones measuring 3 x 3 x 1 m (9 m^3) were generated for this study using the surface-based methodology presented in the previous chapter, so only a brief outline of the methodology is provided here for the specific case of cross-bedded tidal sandstones, but the methodology steps related to flow simulation of the models are explained in details here. The methodology follows four key steps:

(1) Model cross-bed sets and cross-bed surfaces within sets. The volume of interest is subdivided into ellipsoidal cross-bed sets, each defined by one base and one top surface. The spatial distribution of the cross-bed sets can be modelled stochastically (i.e. cross-bed sets are placed randomly into the model volume, and the dimensions and orientations of each are drawn from an input distribution) or deterministically

(location, orientation and dimensions for each are user-specified). The base of each cross-bed set is erosive, so cross-bed sets erode into each other following the rules of stratigraphic order. Numerous cross-bed surfaces (termed here "foreset-toeset surfaces") with a common geometry are then modelled within each cross-bed set, until a specific density (number per unit volume) is reached. The geometric input parameters required to model the foreset-toeset surfaces are: (1) the foreset thickness F_T and (2) the toeset thickness T_T between two successive foreset-toeset surfaces; (3) the toeset dip angle α; (4) the dune climb angle δ; and (5) the foreset curvature, defined by the characteristic parameter A of a parabolic curve with equation $z(x) = Ax^2$ (Figure 3.5).

(2) Grid the model volume for flow simulation. The surface-based models are gridded using corner-point grids in which the grid layers are constrained by the modelled foreset-toeset surfaces, which ensures their complex geometries are preserved. In the models presented here, the grid cells measure 5 x 5 x 2 cm, except for the cells immediately above a foreset-toeset surface, which have a thickness of 0.35 cm to model the mudstone drapes (described below). The volume between two successive foreset-toeset surfaces is divided into layers of cells that are aligned parallel to the underying foreset-toeset surface. The model contains numerous zero-thickness cells, which occur where foreset-toeset surfaces downlap onto, or are truncated by, cross-bed set bounding surfaces. These zero-thickness cells are inactive and are bridged using non-neighbour connections (cf. White and Barton, 1999; Jackson *et al.*, 2005; Sech *et al.*, 2009).

(3) Model sandstone and mudstone lithologies. The lithology is assumed to be sandstone except where mudstone layers are present. More or less continuous mudstone layers are modelled stochastically along foreset-toeset surfaces to represent mudstone drapes deposited during slack-water periods on pre-existing bedforms. The thin (0.35 cm) grid layer directly above each foreset-toeset surface is used to incorporate mudstone drapes, which are documented to have a comparable thickness (Terwindt, 1971; Nio and Yang, 1991; Martinius and Van den Berg, 2011). Because mudstones are modelled as barriers to flow (see below), their thickness has no impact on their flow properties; however, it does affect the total volume of the model that is

occupied by mudstone for a given coverage of foreset-toeset surfaces (see previous chapter). Mudstone drapes are modelled as elliptical patches that cover the foreset-toeset surfaces until a user-specified proportion of their area is reached, following the methodology of Jackson and Muggeridge (2000). A mudstone frequency function, extracted from outcrop data, is used to constrain the probability that a given location on each surface is occupied by a mudstone drape (see Figure 3.12).

(4) Model petrophysical properties. The sandstone and mudstone lithologies are each modelled with uniform, isotropic permeability and the value is zero in mudstone, consistent with minipermeameter measurements that show mudstone permeability is often below instrument resolution (< 1 nD, personal measurements on Tilje cores) and at least five orders of magnitude lower than sandstone permeability in a given sample (e.g. Ringrose *et al.*, 2005). This approach yields models in which toesets contain laterally extensive sandstone laminae separated by mudstone drapes, analogous to wavy-bedded toesets. However, previous studies have shown that the lateral sandstone connectivity breaks down when the sandstone fraction falls below c. 0.29 (theoretical percolation threshold for permeability of wavy bedding structure, Nordahl *et al.*, 2005), in which case sandstones form isolated lenses comprising lenticular bedding (Jackson *et al.*, 2005). Consequently, in toeset regions, the sandstone permeability is set to zero if the volumetric sandstone fraction is less than 0.29, to mimic the lack of lateral connectivity in lenticular-bedded toesets. Note that, for the single-phase permeability calculations reported here, the sandstone porosity plays no role.

4.2.2. Identification of the REV for heterolithic, cross-bedded tidal sandstones

The impact of sample volume on effective permeability was determined in order to identify a potential REV. The model chosen for this analysis is referred as the “intermediate model”. Geometric input parameters for this model were obtained from a specific locality (termed “Gecko Nose”) within the outcrop analogue (the Eocene Dir Abu Lifa Member in the Western Desert, Egypt; Legler *et al.*, 2013) from which the modelling methodology was

derived (Figure 3.13). The input parameters correspond to the average of the ranges measured at the outcrop location (see Table 4.1). The model represents trough cross-bedding with a mudstone drape coverage of 25% along foreset surfaces and 57% along toesets (Figure 4.2). The corresponding sandstone proportion (the "net to gross") is 0.89. The largest modelled volume is 9 m^3 (3 x 3 x 1 m), which contains 6 cross-bed sets, and approximately 600 foreset-toeset surfaces. The corresponding corner-point grid has approximately 6 million cells, of which 700,000 are active for flow simulation (Figure 4.3; see also Table 4.1).

The model was subdivided into smaller samples, each sharing a common centre point, and the effective permeability was determined following the methodology presented below. The smallest sample volume investigated was 0.009 m^3 which corresponds to a typical core plug. The corner-point grid architecture remained the same in each model, so the number of cells varied with sample volume, with the smallest sample containing 1000 active cells. The cells for each sample have the same dimensions, namely 5 cm x 5 cm x 2 mm for the mudstone drape cells and 5 cm x 5 cm x 2 cm for all other cells prior to erosion by other surfaces. Because of the dimensions of the cells, and because the first and last row of cells of the models are reserved for the buffer zones, the sample model should not reach a width of cells smaller than 7 cells (35 cm) so that 5 cells are present between the buffer zones. This number of cells, 5, is empirical and derived from experimentation on flow simulation software so that the equations of flow are resolved accurately within a tolerance threshold of 1% on results (tested on 100% sandstone models for which the calculated permeability should be the same as the input permeability in the cells).

4.2.3. Impact of mudstone drape coverage on effective permeability

To determine whether effective permeability can be predicted from measurements of sandstone fraction (i.e. "net-to-gross"), the intermediate model described above was used to study the impact of mudstone drape coverage along foreset-toeset surfaces on effective permeability. The mudstone drape coverage was varied from 100% to 0%; the corresponding fraction of sandstone in the model varied from 0.74 (when all foreset-toeset surfaces are entirely covered by mudstone drapes) to 1.00 (no mudstone drape).

Input parameter	Symbol	Unit	Intermediate model	Trough cross-bed end-member model	Tabular cross-bed end-member model
Volume of the model	V_T	m^3	9	9	9
Elemental volume density	D	m^{-3}	6 elemental volumes in 9 m^3	6 elemental volumes in 9 m^3	4 elemental volumes in 9 m^3
Number of cross-bedding surfaces	N_{CB}	-	≈600	≈540	≈170
Style of cross-bedding	-	-	Trough	Trough	Tabular
Parabolic curvature of foreset-toeset template surfaces	A	-	5.5×10^{-3}	5.5×10^{-3}	5.5×10^{-3}
Foreset thickness	F_T	cm	5.9 ± 3.9	5.9 ± 3.9	10 ± 3.9
Toeset dip angle	α	°	8	8	1
Angle of dune climb	δ	°	5	5	0
Mudstone frequency function	$f(M,N,O)$	-	Function f (Figure 3.12)	Function f (Figure 3.12)	Function f (Figure 3.12)
Mudstone patch length	MP_L	cm	[10-20] Uniform distribution	[10-20] Uniform distribution	[10-100] Uniform distribution
Mudstone patch width	MP_W	cm	[10-20] Uniform distribution Smaller than MP_L	[10-20] Uniform distribution Smaller than MP_L	[10-100] Uniform distribution Smaller than MP_L
Minimum mudstone patch area	MP_S	cm^2	150	150	150
Foreset to toeset volume ratio	$R_{F/T}$	-	6.5 : 1	0.7 : 1	24 : 1

Table 4.1: Input parameters for the intermediate model used to evaluate the effect of volume sampling, and for the two end-member settings used to model and analyse the sensitivity of effective permeability to six geometric parameters (shaded in grey) that control cross-bedding style.

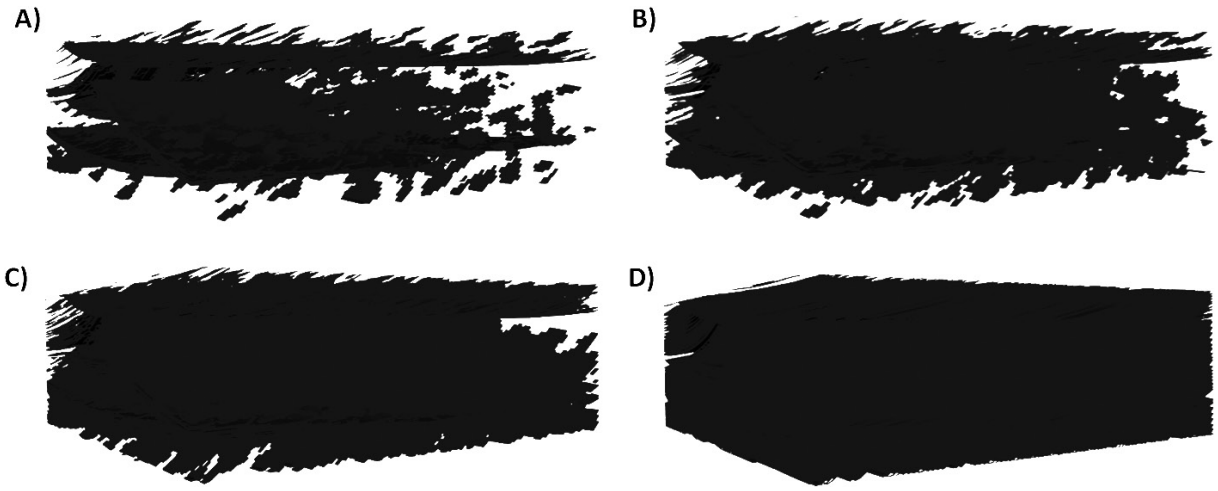


Figure 4.2: Mudstone drape coverage of the foreset components of foreset-toeset template surfaces in the intermediate model shown in Figure 4.3: A) 2.5% coverage; B) 10% coverage; C) 25% coverage; D) 100% coverage.

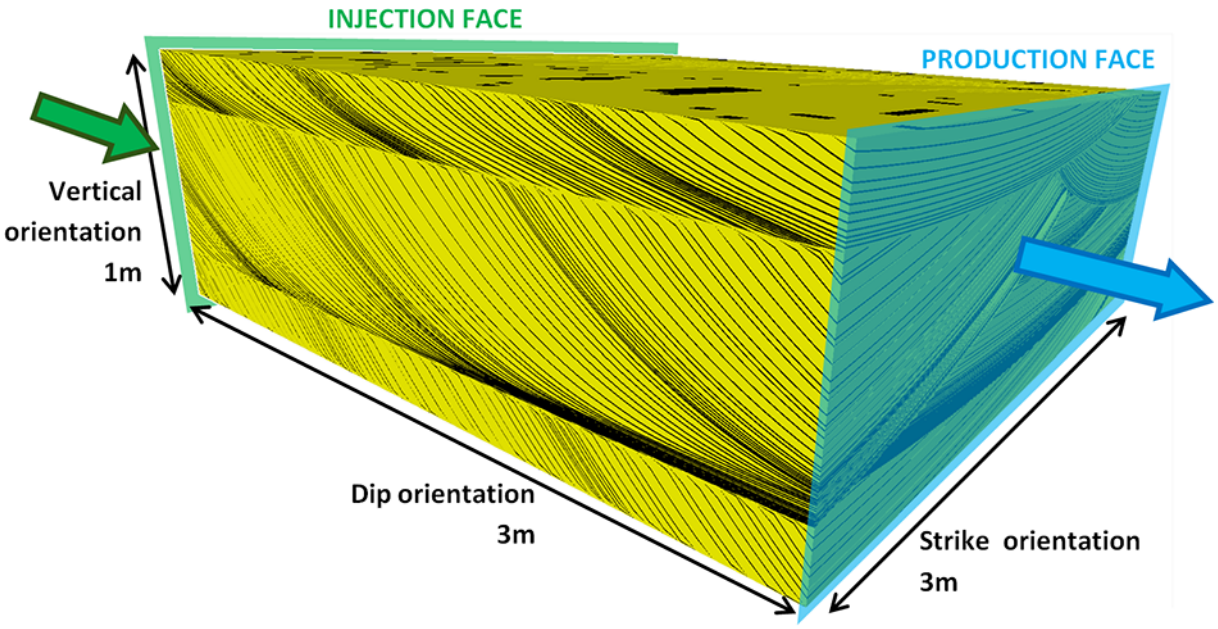


Figure 4.3: Intermediate surface-based model of trough cross-bedded tidal sandstone, generated using input parameters extracted from the Gecko Nose outcrop analogue (see Figure 3.13). The model presented here contains foreset-toeset surfaces that are entirely covered with mudstone drapes in black (i.e. 100% mudstone coverage, Figure 4.2 D). Dip, strike and vertical orientations are defined related to the orientation of the cross-bedding surfaces. The conditions of a flow simulation experiment in the dip orientation are represented on the figure: the inlet and outlet injection and production faces are reproduced with coloured rectangles, corresponding to the buffer zones of high permeability introduced for homogeneous flow injection and production.

4.2.4. Range of effective permeability from trough and tabular cross-bedded end-member models

In addition to the intermediate model described above, two "end-member" (but geologically plausible) models were created to determine the possible range of effective permeability for tidal cross-bedded sandstones, depending on the style of cross-bedding, the geometry and distribution of foreset-toeset surfaces in cross-bed sets, and the connectivity of sandstone laminae in the toeset areas. One model represents trough cross-bedded sandstone with predominant toeset areas (foreset to toeset volume ratio $R_{F/T}$ = 3 : 4) (Table 4.1; Figure 4.4); as for the intermediate model, the input data were obtained from the Gecko Nose outcrop location described in the previous chapter. The other end-member model represents tabular cross-bedded sandstone with almost non-existent toeset areas (foreset to toeset volume ratio $R_{F/T}$ = 24 : 1) (Table 4.1; Figure 4.5); input data for this model were obtained from the Butterfly Canyon locality of Legler *et al.* (2013). This model was also presented in the previous chapter (see Figure 3.14).

The settings of the six input parameters for these two end member models are summarized in Table 4.1; they were taken from the outcrop data reported in Chapter 3. The foreset thickness F_T distribution was chosen to be log-normal with a standard deviation $\sigma(F_T)$ of 1.9 cm in both trough and tabular cross-bedded models (see Figure 3.11). Mud-patch ellipse dimensions were drawn from uniform distributions that yielded mudstone drapes in the trough cross-bedded end-member model that were elongated and continuous, and mudstone drapes in the tabular cross-bedded model that were discontinuous and mostly preserved in the toesets and distal foresets. Multiple mudstone drape coverage scenarios were created for both end-member models.

4.2.5. Sensitivity analysis of geometric parameters

The models described above represent "intermediate" and "end-member" models and the final step of the work undertaken here was to investigate the sensitivity of effective permeability to uncertain parameters with a combination of settings, which represent a spread of cross-bed architectures around the intermediate case and within the range spanned by the end-member

cases. The following six parameters were varied in the sensitivity analysis, between the end-member settings reported in Table 4.1: (1) the style of cross-bedding (trough or tabular cross-bedding); (2) the volume ratio between sandy foresets and muddy toesets $R_{F/T}$; (3) foreset thickness F_T; (4) toeset dip angle α; (5) angle of dune climb δ; and (6) the length of elliptical mudstone patches placed along foreset-toeset surfaces MP_L. An experimental design approach was used, which allows the relative effects of different variables to be quantified whilst minimizing the number of simulation experiments (Box and Draper, 1987; Willis and White, 2000). A two-level fractional-factorial experimental design was selected, which yielded nine ($2^{(6-3)}$+1) different models, and allowed only the main effects of each individual parameter to be determined, but not the interaction effects (i.e. the combined effect of varying two or more parameters simultaneously, otherwise the entire 2^6+1=65 combination of models should be investigated).

4.2.6. Calculation of effective permeability

Effective permeability was calculated in all models and in all three flow directions (dip, strike and vertical) by simulating single phase flow using a conventional industry simulator (Schlumberger, 2013) and calculating the effective permeability k_e using Darcy's Law expressed as (e.g. Warren and Price, 1961):

$$k_e = \frac{Q\mu L}{A\Delta P} \tag{4.1}$$

where Q is the volumetric flow rate (m^3/s), μ is the viscosity (chosen arbitrarily to be 1 Pa.s), L is the model length in the direction of flow (m), A is the cross-sectional area of the model perpendicular to the direction of flow (m^2), and ΔP is the fluid potential drop along the model in the direction of flow (Pa).

To calculate permeability in a given direction, fluid was injected into one face of the model and the opposing face allowed fluid production; the other four model faces were sealed. Horizontal flow parallel to the main orientation of the cross-bedding surfaces is termed dip-oriented and the permeability is denoted k_d; the perpendicular, horizontal direction is termed strike-oriented, and the permeability is denoted k_s. Vertical effective permeability is denoted k_v. Injection and production faces contained a single layer of high permeability buffer cells (arbitrarily chosen to be 54 x 10^3 D) to ensure that flow was uniformly distributed

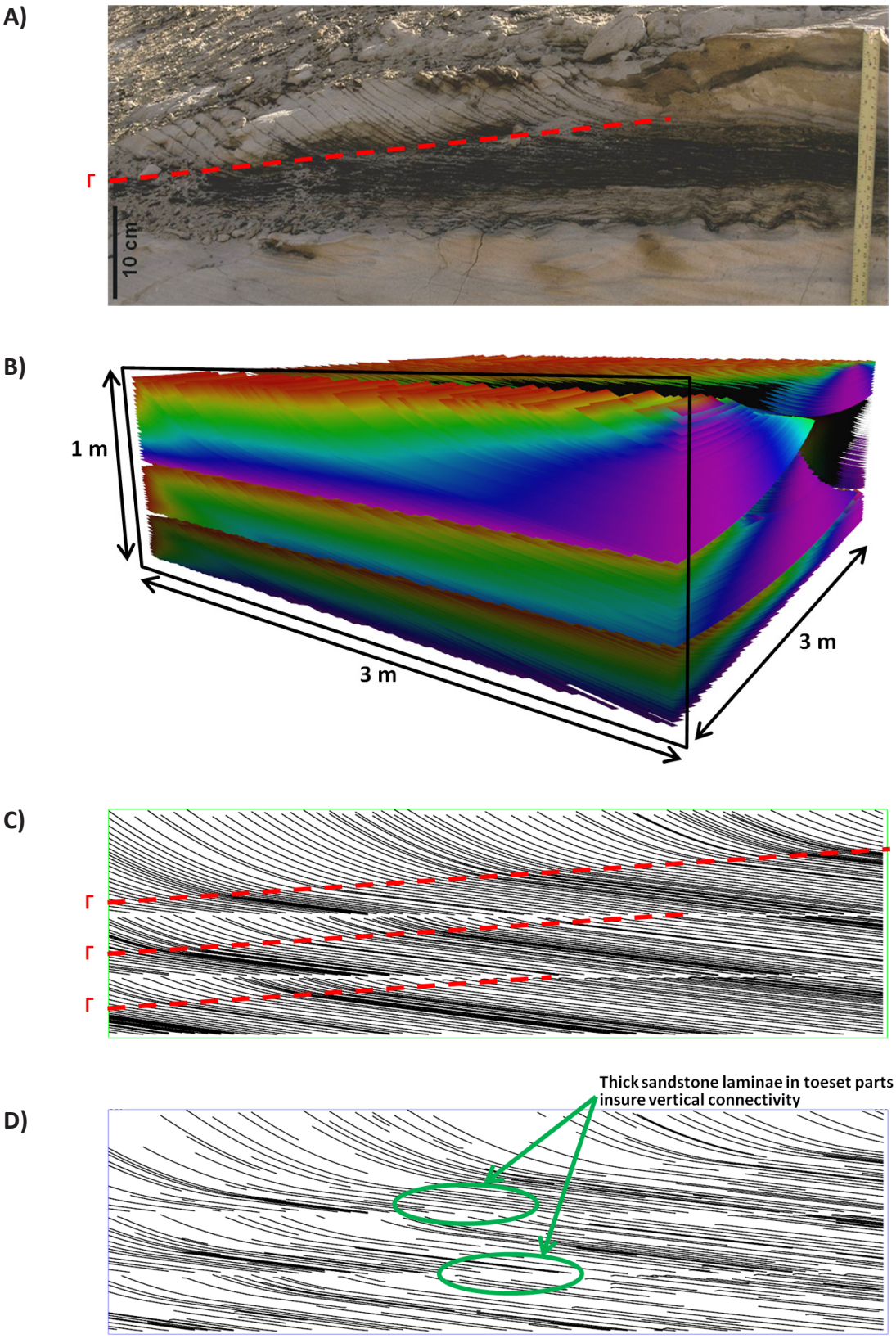


Figure 4.4: A) Outcrop photograph of one cross-bed set featuring trough cross-bedding lined up with mudstone drapes. The red dotted line Γ corresponds to the boundary between foreset and toeset parts of the cross-bed set, B) view of the trough cross-bedded end-member model of cross-bedded sandstones used to investigate the sensitivity of effective permeability to geometric input parameters (Table 4.1). Cross-bedding surfaces are coloured depending on the depth value in each cross-bed set; the rectangle indicates the position of the cross-sections C and D, C) dip-oriented cross-section illustrating foreset-toeset surfaces in the model, with the boundary between foreset and toeset parts identified in each cross-bed set, and D) dip-oriented cross-section showing 25% mudstone drape coverage along foresets in the model.

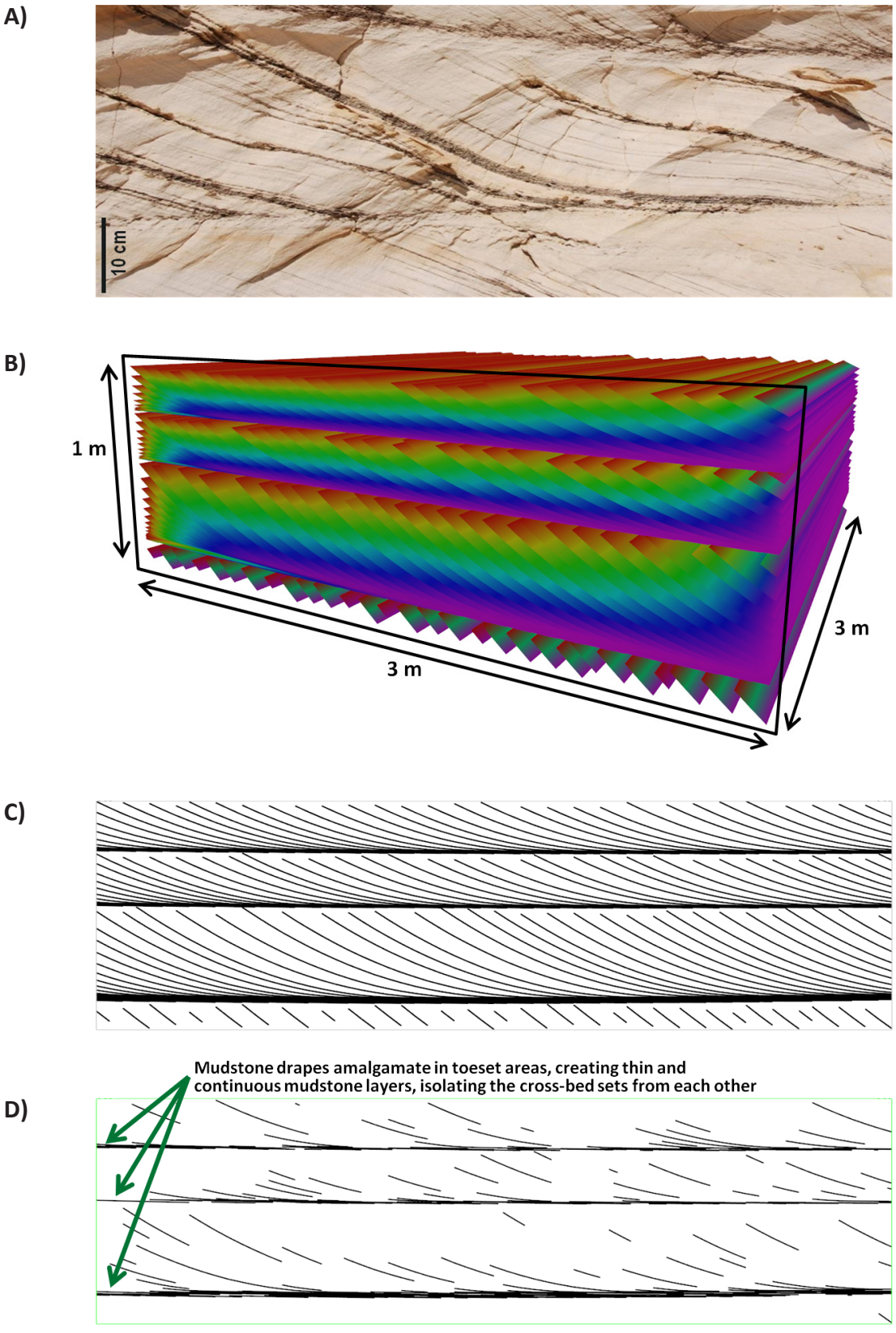


Figure 4.5: A) Outcrop photograph of tabular cross-bed sets, B) view of the tabular cross-bedded end-member model of cross-bedded sandstones used to investigate the sensitivity of effective permeability to geometric input parameters (Table 4.1). Cross-bedding surfaces are coloured following their depth value in each cross-bed set, the rectangle indicates the position of the cross-sections C and D, C) dip-oriented cross-section illustrating foreset-toeset surfaces in the model, and D) dip-oriented cross-section showing 25% mudstone drape coverage along foresets in the model.

and the fluid potential (i.e. the pressure field minus the hydrostatic pressure) was uniform. A single injection-production well pair was defined at the inlet and outlet faces respectively; the injection rate was limited by a maximum pressure, which was higher than the (atmospheric) outlet pressure, while the production rate was controlled by a fixed target. Each simulation was run until a steady-state was reached, at which injection and production rates were the same (within a tolerance of 1%) and the average fluid potential was constant (within a tolerance of 1% between timesteps). The rock and fluid had a small but non-zero compressibility, which allowed the simulator to converge to a stable solution more rapidly at each time-step whilst reaching steady-state within a short time (typically < 10^{-6} pore-volumes of fluid injected). At steady state, the flow rate Q and potential drop ΔP were determined and the effective permeability calculated using equation (4.1). Values of effective permeability k_e in a given direction are reported as a normalized value expressed as a fraction of the isotropic sandstone permeability k_{sand}:

The results reported in this way are independent of the value of sandstone permeability used in the models; moreover, the normalized effective permeability can be rescaled to any value of sandstone permeability obtained from core or mini-permeameter measurements.

The corner-point grids used to capture the complex architecture of the cross-beds contain pinched-out cells and relatively steeply inclined cells. Thus, while the grids accurately reproduce stratigraphy and heterogeneity in the models, they also cause numerical artefacts to be introduced by the flow simulator. The magnitude of these numerical errors was calculated using a reference model in which mudstone drapes are entirely absent but the corner-point grid represents the architecture of the cross-beds. The effective permeability of the reference model should be that of sandstone in the three directions of simulated flow. Differences between this and the numerically calculated value yield estimated errors in k_d of 25%, k_s of 1%, k_v of 16%, and k_v/k_h of 26%. Numerical errors in cases where the mudstone fraction is greater than zero are assumed to be the same as these determined for the reference model. Errors in normalized effective permeability are likely to be smaller than the estimates presented here because k_{sand} in equation (4.2) is the effective permeability of the reference model for the same flow direction, so the calculation artefact introduced by the corner-point grid is similar for both cases.

Multiple scenarios have been tested prior to establishing the flow simulation methodology presented here. Thus, the buffer zones of very high permeability were introduced after it was demonstrated that the pressure gradient was not uniform over the entire injection and production faces without buffer zones, preventing us from using Darcy's law to the entire model to calculate the effective permeability. This is the case for all the other parameters of the Darcy's law. Steady-state has to be reached in the model to obtain a uniform flow rate over the entire model, with constant injection and production rates. Through experiment, we have observed that the flow simulation software Eclipse was unable to converge in the solution of the flow equations when both the fluid and the rocks were given value of zero compressibility. We set the compressibility of the rock to an extremely low value. As a consequence, steady-state is not reached instantaneously but after a very short time, which enabled us to verify that the flow equations were in fact resolved accurately by tracking the "shock front" of the fluid trough time.

Thanks to the introduction of the buffer zones, the pressure gradient is uniform over the entire injection and production faces almost instantaneously which allowed us to use a couplet of only one injection and one production wells. The wells are positionned at the middle of the faces, perforated and connected to each layer of the model. Multiple wells were inserted prior to the introduction of the buffer zones in order to achieve a uniform pressure gradient but were proved unnecessary afterwards.

Mudstone drapes were physically modelled as thin layers of cells with zero permeability. Initially, the mudstone drapes were supposed to be inserted as a transmissibility multiplier so that in the modelling methodology presented in the previous chapter, mudstone drapes were created as surfaces, the same as for the cross-bedding surfaces. A transmissibility multiplier of 0 was assigned between two cells separated by a cross-bedding surface lined up with mudstone drape. Flow simulation was undertaken with this zero transmissibility multiplier instead of zero permeability cells. But, because of the corner-point structure of the grid, the underlined regular orthogonal grid of the simulation software in which flow equations are solved and the uniformity of the sandstone permeability in all cells, the results of effective permeability were always equivalent, whatever the value of mudstone drape coverage chosen.

4.3. Results

4.3.1. Visualization and qualitative analysis of cross-bedded heterolithic tidal sandstone models

The intermediate model and the two end-member models can be visualized using industry-standard geomodelling software for qualitative analysis of the heterogeneity surface geometry and mudstone distribution. The intermediate model and the tabular cross-bedded end-member model were briefly presented in Chapter 3 (Figures 3.13, 3.14); here we discuss and compare their features in more detail.

The intermediate (Figure 4.3) and the trough cross-bedded end-member (Figure 4.4) models were generated from the same outcrop location (Gecko Nose, Figure 3.8). As the foreset thickness F_T is specific to the outcrop location, its mean value is the same for both models (F_T = 5.9 ± 3.9 cm) with a progressive transition (from thin to thick sandstone laminae, and then back to thin laminae) corresponding to the neap/spring tidal cycle. The trough cross-bedded end-member model displays a higher density network of mudstone drapes (compare Figures 4.3 and 4.4) even though the foreset spacing is the same in both models; the difference arises in the volume fraction occupied by muddy toeset parts, with the toeset volume proportion of the trough cross-bedded end-member (60%, *F/T* ratio of 0.7:1) model being 4.5 times higher than the intermediate model counterpart (13%, *F/T* ratio of 6.5:1) (Table 4.1). The trough cross-bedded end-member model is directly recreated from one outcrop example of the Gecko Nose outcrop location featuring this high proportion of muddy toeset parts (Figure 4.4 A), whereas the foreset to toeset volume ratio for the intermediate model is an average of all measured trough cross-bed sets at the Gecko Nose outcrop. As mudstone drapes are more continuous in the toesets, 3D connectivity between sandstone laminae is more limited in the trough cross-bedded end-member model than in the intermediate model.

The tabular cross-bedded end-member model was generated from the Butterfly Canyon location (Figure 3.6). In this model, sandy foreset parts are predominant over the muddy toeset parts, with a toeset volume proportion of 4% reproduced directly from one example at the outcrop location (*F/T* ratio of 24:1) (Figure 4.5). The mean foreset thickness F_T is higher for this

model with F_T = 10.0 ± 3.9 cm. Consequently, mudstone content in the model only reaches a volume fraction of 0.13 when foreset-toeset surfaces are entirely covered by mudstone drapes (i.e. at 100% mudstone drape coverage).

The appearance of the muddy toesets is different between the Gecko Nose and the Butterfly Canyon outcrop locations, and is reproduced accordingly in the models reported here. Toesets at Butterfly Canyon are limited to thin but laterally continuous mudstone drapes that isolate adjacent cross-bed sets (Figure 4.5 A and D). At Gecko Nose, toesets are well expressed, comprising alternate, parallel sandstone and mudstone laminae (i.e. mudstone drapes along toeset surfaces) yielding wavy-bedding structures (Figure 4.4 and D) (Reineck and Singh, 1980; Ringrose *et al.*, 2005). This difference is reflected in the values of toeset dip angle α and dune climb angle δ (Table 4.1). The smaller these two angles are, the thinner the toeset thickness T_T (equation 3.6 in Chapter 3). As both values of α and δ are small, the toeset thickness T_T in the tabular cross-bedded end-member model is very small. In this model, mudstone drapes stack vertically with few sandstone laminae preserved in-between; moreover, as the dune climb angle δ is equal to 0, toeset surfaces merge with the erosive base of the cross-bed sets, forming the observed continuous single mudstone drape covering the erosive base, isolating overlying cross-bed sets from each other.

4.3.2. Impact of sample volume on effective permeability

We begin by presenting typical results for one flow simulation experiment, yielding a single value of effective permeability (Figure 4.6). The example is for the intermediate model with 25% mudstone drape coverage, the full sample volume of 9 m^3, and flow in the (down) dip direction. Flow rate and average fluid potential are reported as a function of pore-volumes of fluid injected (PVI). It is clear that the injection and production flow rates rapidly reach steady state, as does the average fluid pressure. At this time, the simulated flow rate and pressure drop can be used in equation (4.1), along with the model dimensions and fluid viscosity, to calculate the effective permeability.

Numerous numerical experiments of this type, with flow in different directions and using different sample volumes, yielded the values of normalized effective permeability

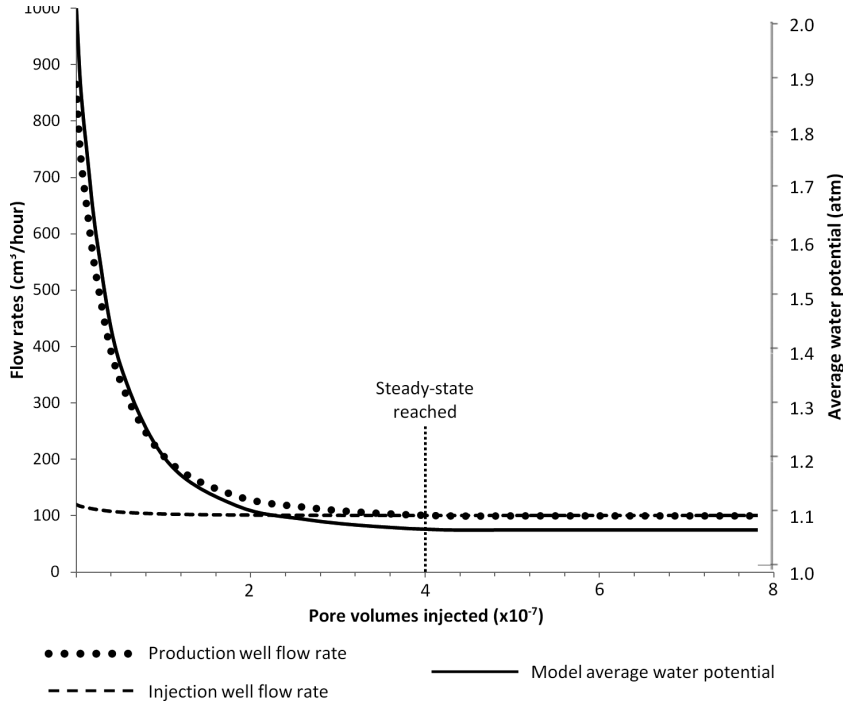


Figure 4.6: Single-phase flow simulation of the surface-based intermediate model with 25% mudstone drape coverage (Figure 4.2 C). The injection and production wells are controlled by bottom hole pressure, so flow rates are varying through time. Effective permeability of the model is calculated at steady state, when both injection and production flow rates become constant and equal, and when the average field pressure remains constant. Steady-state is achieved in a very short period (4×10^{-7} of the entire pore volume of the model is injected in 18 s), due to the incompressibility of the fluids and the very small compressibility of the rocks.

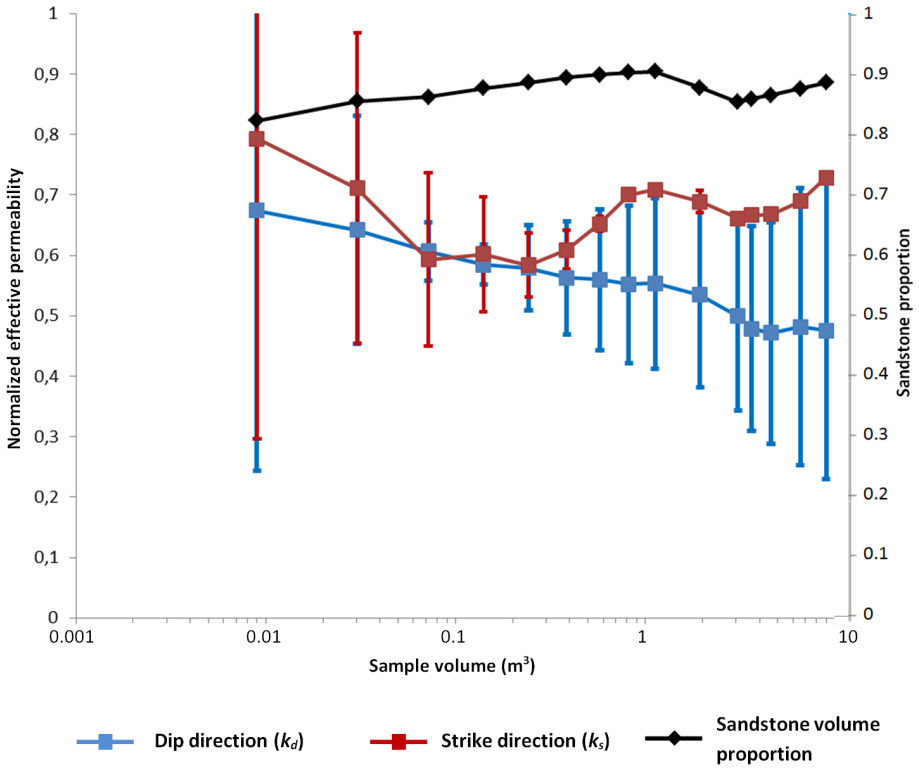


Figure 4.7: Normalized effective horizontal permeability versus sample volume. Samples are always located at the centre of the intermediate model of heterolithic, cross-bedded tidal sandstones (Figure 4.3); mudstone drape coverage along foreset-toeset surfaces is 25% (Figure 4.2 C). Error bars represent the numerical artefacts introduced by the cornerpoint grid. The values of effective permeability are normalized by the calculated permeability of the equivalent sample containing only sandstone.

for the intermediate model shown in Figure 4.7; also shown is the sandstone fraction in the corresponding model. It is clear that permeability varies as a function of sample volume, as does the fraction of sandstone. This latter variation occurs because different volumes of mudstone are included in models as the sample volume changes. Horizontal permeability in both dip and strike orientations varies with the volume of the sample, for sample volumes below 1 m^3. A sample volume of c. 1 m^3 corresponds here to the REV. The slight increase in effective permeability observed for increasing sample volumes above 1 m^3 (Figure 4.7) is attributed to the increase in sandstone proportion as more sandy foresets are sampled towards the edges of the model. The permeability variations observed for the sample models > 1 m^3 follow the same trend as the sandstone proportion variations. The trend in horizontal permeability is not clear as analytical errors are larger than the variations observed. However, the errors are only calculated in the case of 100% sandstone model, and presumed proportional for all the other cases where no measurement of the errors is possible. As for further results displaying such analytical errors, the calculated values may not correspond to the real values due to the calculation artefacts, but the trend in the results is the same. Thus the variations observed in horizontal permeability above 1 m^3 can only be explained by the change in facies proportion.

4.3.3. Impact of sandstone fraction on effective permeability

The effective permeability of the intermediate model (Figure 4.3) was calculated for 33 scenarios of mudstone drape coverage along foreset-toeset surfaces, ranging from 0% to 100% (e.g. Figure 4.2), corresponding to sandstone proportions ranging from 1.00 to 0.74 respectively. Normalized effective permeability is dependent on the proportion of sandstone, and on the direction of flow relative to the foreset-toeset surfaces (Figure 4.8). Effective permeability decreases as the sandstone fraction decreases and is highly anisotropic: the vertical permeability falls to c. 0.5% of the value for sandstone, while the horizontal permeability falls to c. 5% and c. 50% of the sandstone value in the dip and strike directions respectively.

For high proportions of sandstone (> 94%), mudstone drapes occur only along toesets, and k_d and k_s are similar. For low proportions of sandstone (< 94%), in which both foresets and toesets are lined by mudstone drapes, k_d and k_s differ such that horizontal effective

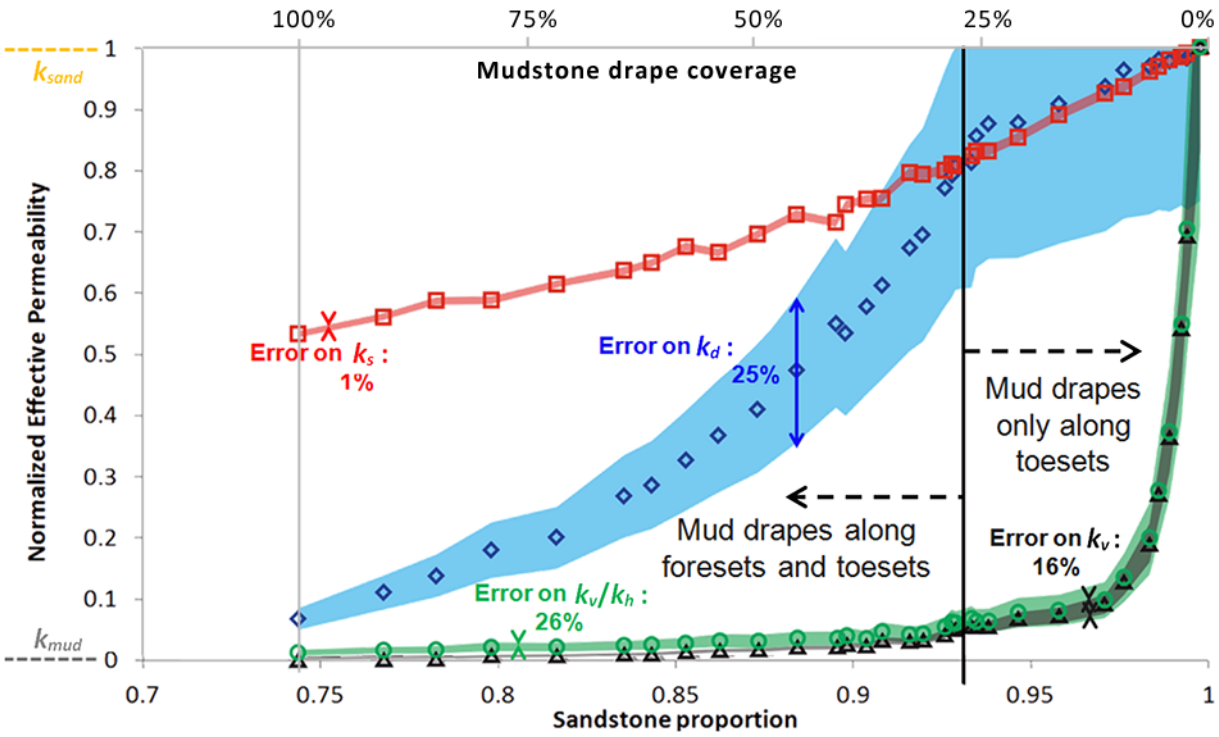


Figure 4.8: Normalized effective permeability for the intermediate model of heterolithic, cross-bedded tidal sandstones (Figure 4.3), for varying sandstone content. Effective permeability is measured in three orthogonal directions: k_d, k_s and k_v. The shaded areas correspond to the error in calculated permeability introduced by the cornerpoint grid.

permeability is anisotropic. The horizontal effective permeability along depositional strike k_s, is higher than along depositional dip k_d, because sandstone laminae are more laterally continuous along strike. Dip-oriented, horizontal flow within each cross-bed set must cross multiple foreset-toeset surfaces lined with mudstone drapes. Consequently, tortuosity of the flow is increased and interconnection of mudstone drapes may create dead-ends, especially for high mudstone contents (e.g. Figures 4.2 D, 4.4 C, 4.5 C). Dead-ends for flow in the strike direction occur where sandstone laminae of foreset areas are juxtaposed against mudstone laminae of toeset areas across an erosive cross-bed set boundary.

The vertical effective permeability k_v is generally much lower than both k_d and k_s. This effect is attributed to the presence of mudstone drapes along toesets, which are nearly horizontal and closely spaced such that they act as barriers or baffles to vertical flow, even in models with low mudstone content. As a result, the decrease in k_v with increasing mudstone content is similar to that documented for wavy-bedded sandstones, with a high decrease in the effective vertical permeability accompanying a small increase in mudstone fraction (Nordahl *et al.*, 2005; Ringrose *et al.*, 2005). Variations in the ratio between vertical and horizontal effective permeability k_v/k_h, as a function of sandstone content, are mainly controlled by the variations in k_v.

4.3.4. Range of effective permeability across end-member models of tabular and trough cross-bedding

The normalized horizontal effective permeabilities for the trough cross-bedded end-member model (Figure 4.4) and the tabular cross-bedded end-member model (Figure 4.5) are shown in Figure 4.9 for two different toeset bedding styles: in wavy-bedded toesets, the sandstone and mudstone layers are laterally continuous; in lenticular bedded toesets, the sandstones form isolated lenses encased in mudstone. Also shown for comparison are the results for the intermediate model with wavy-bedded toesets which correspond to the results of Figure 4.8.

The anisotropy in horizontal permeability observed in the intermediate model is amplified by the geometry of the cross-beds in the end-member models, especially for the dip direction k_d (Figure 4.9 A). The dip direction effective permeability decreases linearly and rapidly with increasing mudstone content for the tabular cross-bedded model regardless of the toeset bedding style, but decreases less rapidly for the trough cross-bedded model with wavy-bedded toesets (Figure 4.9 A) and is very low in this model with lenticular-bedded toesets (Figure 4.9 C). In contrast, effective permeability in the strike direction k_s is similar for all three models if they have wavy-bedded toesets (Figure 4.9 B), but differs significantly if they have lenticular-bedded toesets (Figure 4.9 D). The large range of effective permeability values between the two (realistic) end-member models confirms the strong influence of cross-bedding style on effective permeability.

Values of effective permeability are modified profoundly by the lateral continuity of sandstone and mudstone laminae in the toesets (wavy versus lenticular-bedding; compare Figure 4.9 A and B with Figure 4.9 C and D), with the exception of the tabular cross-bedded end-member model in which toesets are volumetrically subordinate. The same value of sandstone content gives very different corresponding values of effective permeability, depending on the geometry of cross-bedding, the bedding style of the toeset parts and the direction of flow. For example, a sandstone content of 90% yields dip oriented effective permeabilities k_d that are twice the value for the trough cross-bedded model (k_d = 0.72) than for the tabular cross-bedded model (k_d = 0.36) (Figure 4.9 A). For strike oriented flow, k_s is the same for the trough

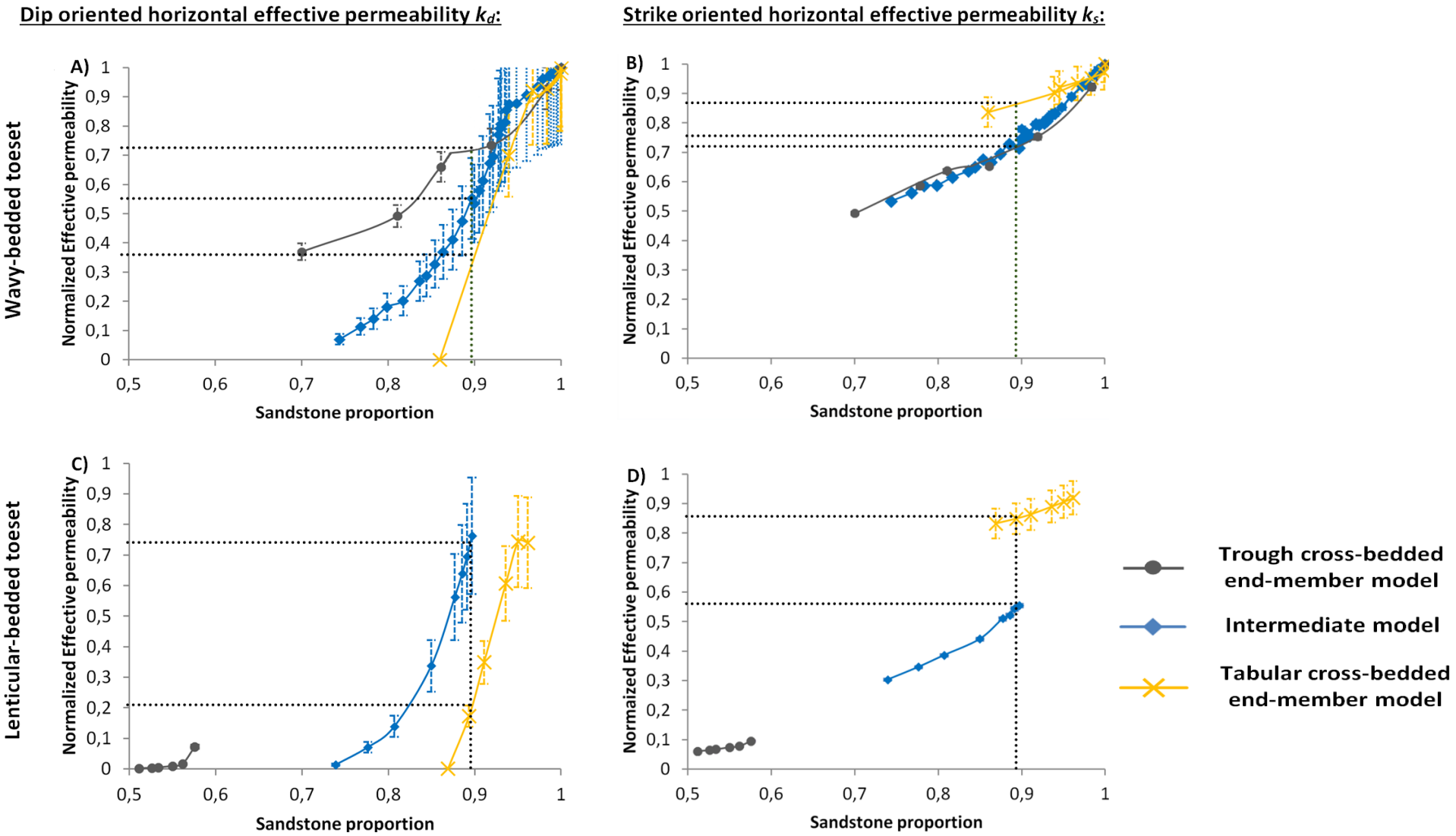


Figure 4.9: Normalized effective permeability of the intermediate, trough cross-bedded end-member, and tabular cross-bedded end-member models: A) dip-oriented effective horizontal permeability k_d for models with wavy-bedded toesets, B) strike-oriented effective horizontal permeability k_s for models with wavy-bedded toesets, C) k_d for models with lenticular-bedded toesets, and D) k_s for models with lenticular-bedded toesets. Dashed lines correspond to results discussed in the text.

cross-bedded model (k_s = 0.72) but higher for the tabular cross-bedded model (k_s = 0.87) (Figure 4.9 B). These results are extracted from models with wavy-bedded toesets; the results are different for lenticular-bedded toesets.

The spread of effective permeability values for any chosen model, independent of mudstone drape coverage, is controlled by the toeset regions of the model and their related parameters: (1) the abundance of toeset region in the model, which is controlled essentially by the foreset to toeset ratio (Table 4.1); (2) the lateral and vertical connectivity of toeset regions in different cross-bed sets, which is controlled by various parameters (3D distribution of cross-bed sets, cross-bed set density, and dune climb angle δ); (3) the wavy- or lenticular-bedded nature of the toesets, which is controlled by the mudstone drape coverage and toeset dip angle α.

4.3.5. Influence of toeset bedding style on flow and effective permeability

End-Member Models with Wavy-Bedded Toesets

The variation of the water potential at steady-state for models with wavy-bedded toesets is illustrated in Figure 4.10 (A, C and E). The water potential is influenced by the cross-bedding surfaces, with high pressures located preferentially at the bottom of the models, adjacent to the injection face; low pressures are located preferentially at the top of the models, adjacent to the production face. This aspect of the water potential is related to the concave geometry of the cross-bedding surfaces and the mudstone distribution along each surface: the lower parts of the surfaces tend to be lined with mudstone drapes, leading to locally higher pressures; in comparison, the comparatively mudstone free upper parts of the surfaces constitute pathways for flow, leading to locally lower pressures. In areas where the flow is driven down the cross-bedding surfaces, wavy-bedded layers in the toeset regions allow the flow to reach underlying cross-bed sets. As a result, all the sandstone laminae of the model are connected. Flow pathways may be highly distorted with the increase of mudstone drape coverage, but there are no dead-ends to flow.

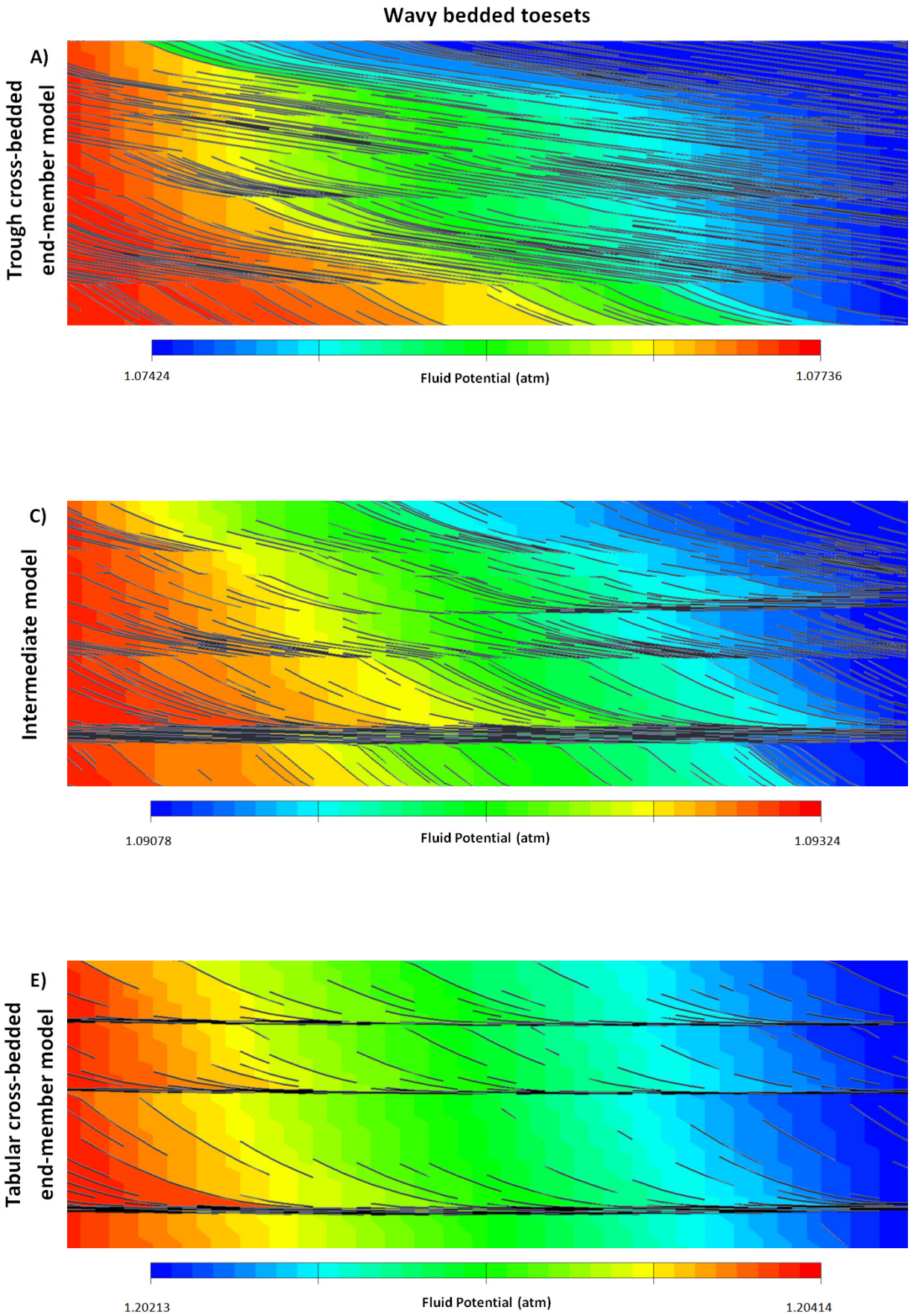
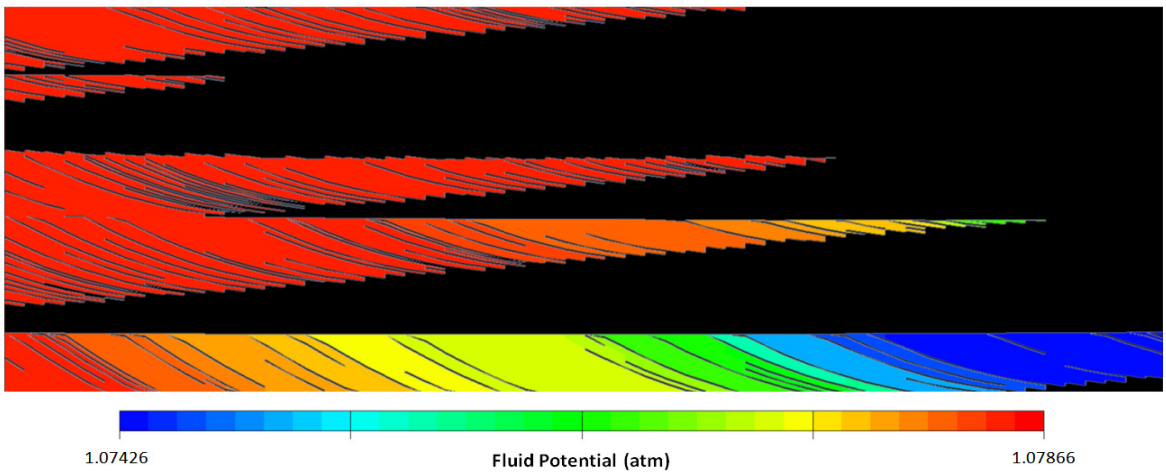


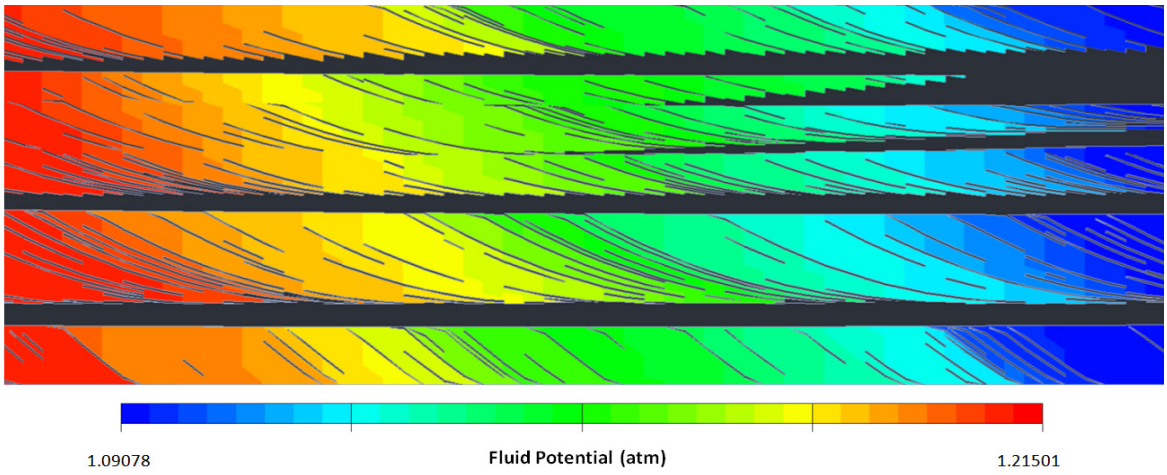
Figure 4.10: Dip-oriented cross-sections through the (A and B) trough cross-bedded end-member (Figure 4.4), (C and D) intermediate (Figures 4.2, 4.3) and (E and F) tabular cross-bedded end-member (Figure 4.5) models, showing the water potential at steady-state, with 25% mudstone drape coverage along foresets for each model. Toesets are modelled as wavy-bedded in A), C) and E), and as lenticular-bedded in B), D) and F).

Lenticular bedded toesets

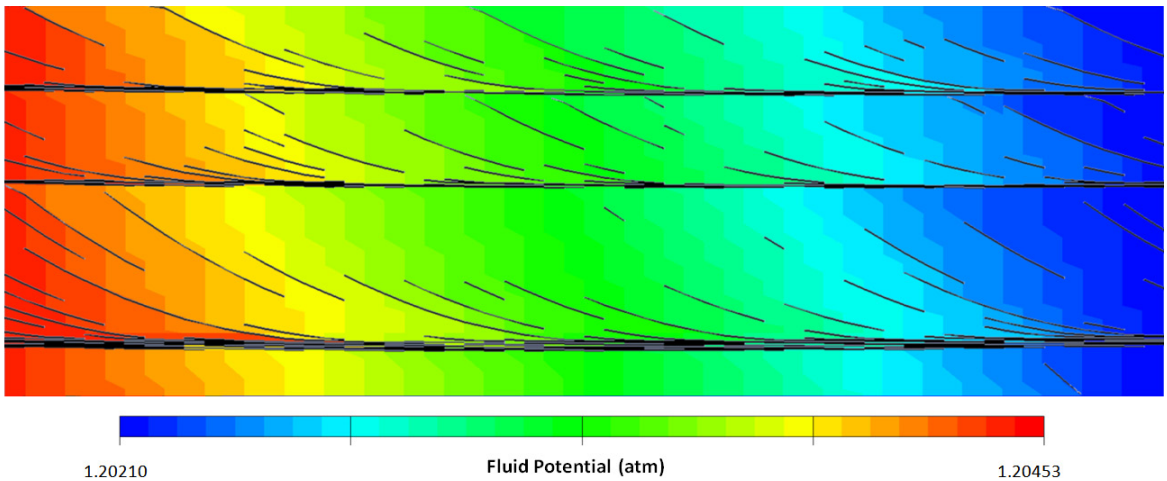
B)



D)



F)



End-Member Models with Lenticular-Bedded Toesets

The variation of the water potential at the steady state for models with lenticular-bedded toesets is illustrated in Figure 4.10 (B, D and F). In all models, the lenticular-bedded toesets stack vertically, isolating adjacent cross-bed sets and creating dead-ends to horizontal flow. Noticeably, in the trough cross-bedded model (Figure 4.10 B), only the lowermost cross-bed set is connected to both the injection and production faces; this cross-bed set constitutes the dominant flow path. The tortuosity of the flow is primarily controlled by the abundance of toesets compared to foresets; the foreset mudstone drape coverage has an impact only in cases where toesets are comparatively scarce (for example, in the tabular cross-bedded models, Figure 4.10 E and F).

4.3.6. Sensitivity analysis of effective permeability to various cross-bedding geometric parameters

The results of the experimental design to investigate the relative impact of six geometric parameters on effective permeability are presented in Figure 4.11. With increased mudstone drape coverage along foreset-toeset surfaces, it can be observed that: (1) the rank order of impact of the six parameters varies in both k_d and k_s; (2) the rank order differs for k_d and k_s; (3) the majority of the parameters induce a change of more than 10% on effective permeability; and (4) the only parameter with a consistently low impact on effective permeability is foreset thickness F_T. Each of the other parameters affects the effective permeability significantly in either the dip or strike direction. A decrease in F_T causes an increase in the number of foreset-toeset surfaces and the number of mudstone drapes that can potentially influence flow behaviour. The consistently low ranking of F_T therefore suggests that foreset regions have only limited impact on effective permeability compared to toeset regions. This inference is supported by the greater impact on effective permeability of the other five parameters, which each have a direct influence on the proportion, distribution and connectivity of toeset regions. Overall these results show that effective permeability is not controlled by just one or two key geometric parameters.

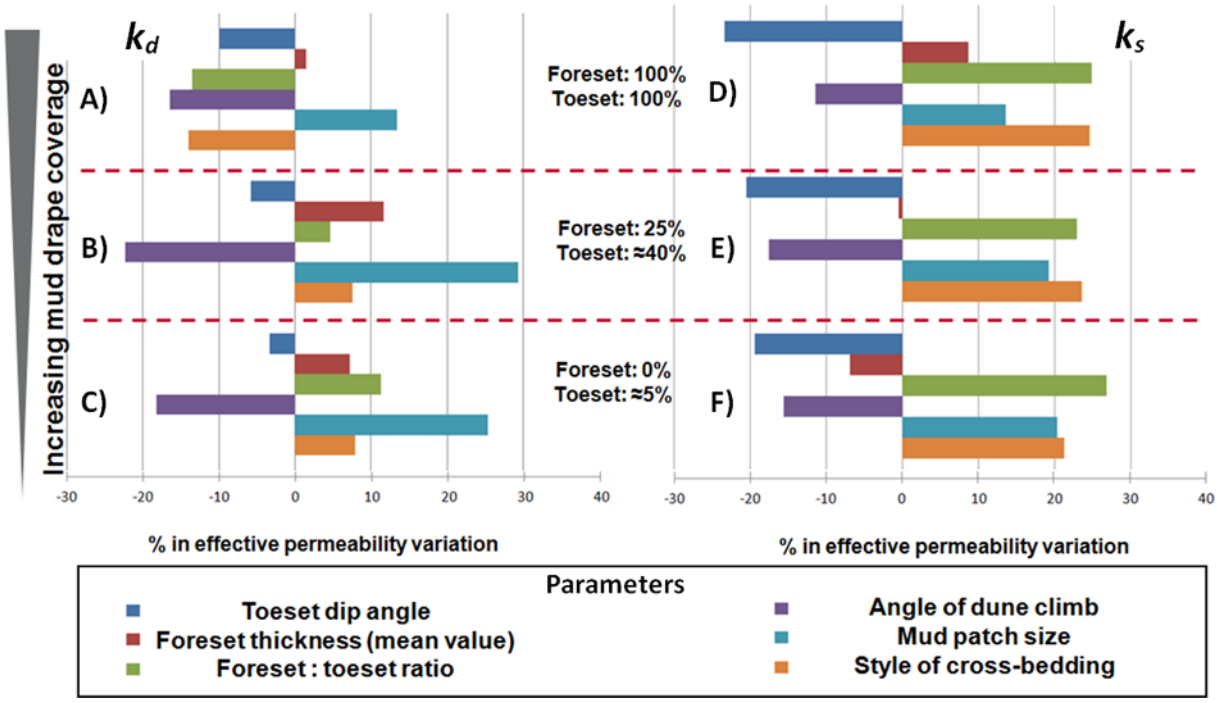


Figure 4.11: Tornado charts summarising the impact on effective permeability of variations in six geometric input parameters in the dip (A-C) and strike (D-F) directions. Three scenarios of mudstone drape coverage along foreset-toeset surfaces are presented: (A, D) have 100% coverage of foresets; (B, E) have 25% coverage of foresets; (C, F) have 0% coverage of foresets. Geometric parameters and their settings are summarized in Table 4.1.

4.4. Discussion

The results presented here demonstrate that values of effective permeability for heterolithic cross-bedded sandstones are highly sensitive to only small variations in geometry and mudstone content. Calculated values of effective permeability were highly variable in realistic models of the same interval, constructed using data extracted from different outcrop locations. Predictive relationships for effective permeability as a function of mudstone content were determined in earlier studies from mini-models of heterolithic tidal wavy-bedded sandstones, comparable in length-scale to the models presented here (Ringrose *et al.*, 2005; Jackson *et al.*, 2005). However, such relationship cannot be identified for cross-bedded tidal sandstones, because mudstone content is not an indicator of the cross-bed geometry, or the connectivity of sandstone or mudstone laminae. There is no relationship that can be used to

predict effective permeability in all heterolithic, cross-bedded tidal sandstones based only on measurements of mudstone content or a small number of geometric parameters. However, for a specific outcrop location for which tightly constrained input parameters are available, representative effective permeability can be extracted following the methodology presented in this study.

The shape of the curve of effective permeability depending on the mudstone volume fraction (or mudstone drape coverage of the cross-bedding surfaces here) displayed in Figure 4.8 is similar to those extracted by previous studies on the impact of cross-bedding with grain-size variations (but no mudstone drape) on effective permeability (Kortekaas, 1985; Ringrose *et al.*, 1993), especially the anisotropy between the horizontal and the vertical permeabilities, but also the horizontal anisotropy between dip and strike orientations. The shape of the curve is also the same than for the models of tidal wavy-bedding (see Figure 2.5, Ringrose *et al.*, 2005; Jackson *et al.*, 2005). In all cases, the shape – not the values – is similar to the predicted effective permeability based on arithmetic, geometric or harmonic average estimators. This behaviour is an indicator that the tidal cross-bedded sandstones in all the scenarios tested in our study (trough or tabular cross-bedding; wavy-bedded or lenticular bedded toesets) follow the percolation theory (Begg and King, 1985). For all examples, a mudstone fraction exists for which the system behaviour changes from a homogeneous system towards a layered system. The specific mudstone fraction corresponds to the percolation threshold: below the percolation threshold, the tidal cross-bedded sandstone is a reservoir facies. However, this study has shown that - at the difference of the tidal wavy-bedding sandstone - there is no conclusive way to determine the value of the percolation threshold (i.e. the mudstone drape coverage) for a specific mudstone fraction or for one geometric parameter controlling the shape of the cross-bedding surfaces.

For the case of a subsurface example, the problem is different, as the range in the input parameters cannot be constrained accurately using the well dataset only (log interpretation, core observations, and plug measurements). The recommended workflow to calculate effective permeability in heterolithic, cross-bedded tidal sandstones is therefore to create a number of mini-models, similar to those presented in this study, that capture the range of cross-bedding

styles, geometries and mudstone content observed in reservoir-specific subsurface and outcrop analogue data, and calculate effective single (and multiphase, where necessary) reservoir properties from these models following the "geopseudo" approach suggested in previous studies for the upscaling of the reservoir properties of heterolithic sandstone reservoirs of other depositional environments (e.g. Ringrose *et al.*, 1993; Pickup *et al.*, 1994, 2000; Ciammetti *et al.*, 1995; Pickup and Carruthers, 1996; Pickup and Sorbie, 1996). The models should capture rock volumes at, or greater than, the REV, which we find here to be of order 1000 x 10^3 cm^3 (1 m^3); for comparison, Nordahl and Ringrose (2008) identified a REV of order 5 x 10^3 cm^3 for wavy-bedded tidal sandstones of varying mudstone content. The significantly larger REV we identify here reflects the lateral extent of mudstone drapes along foreset-toeset surfaces and, in particular, the distribution and connectivity of muddy toesets that may themselves comprise wavy- or lenticular-bedded intervals. Using the geopseudo approach for permeability upscaling of tidally-influenced facies, main heterogeneity surfaces should be captured in a hierarchical way and modelled in the reservoir model, and effective permeabilities should be used to reproduce the effect of small-scale heterogeneities. For a length-scale rank higher than the length-scale of the models of this study (10s of meter compared to 1 meter), the heterogeneity surfaces correspond to facies boundaries, architectural element boundaries (tidal bar boundaries; tidal dune boundaries; tidal channel boundaries; see Legler *et al.*, 2013) and stratigraphic surfaces. Within each architectural element, effective permeabilities of the tidally influenced facies observed at outcrop should be populated in each finite element. A finite element corresponds to whether a grid cell, whether a shapeless volume bounded by one bottom and one top surface (i.e. definition of elemental volume, see Chapter 3.2 and Figure 3.1). Effective permeabilities of wavy-bedding facies, heterolithic parallel laminated facies and unstratified mudstone can be calculated based on a mudstone fraction parameter previously modelled, but this is not possible for tidal cross-bedded sandstones. We recommend that the range of permeability for tidal cross-bedded sandstones would be determined based on the reservoir behaviour of the mudstone-rich toesets: if toesets are relatively limited in term of foreset to toeset ratio (for example the tabular cross-bedding end-member model, Figure 4.5), the range of effective permeability can be constrained accurately using the mudstone fraction as observed in the sensitivity analysis of this study (yellow

curves in Figure 4.9). If mudstone-rich toesets represent a large fraction (foreset to toeset ratio $R_{F/T}$ bigger than 10:1), we recommend that foreset and toeset parts would be modelled separately and effective permeabilities of both parts could be constrained more accurately using effective permeability of toeset-free models for the sandstone-rich foreset part (yellow curves in Figure 4.9), and effective permeability of wavy-bedding calculated depending on the mudstone fraction for the mudstone-rich toeset parts (models of Ringrose *et al.*, 2005, see Figure 2.5; Jackson *et al.*, 2005).

The construction of such mini-models can be facilitated using dedicated software such as SBED (noting the limitations outlined in the introduction of this chapter: it is difficult to ensure SBED models honour geometric data obtained from the subsurface or outcrop analogues), or the software developed for this study which is presented in the appendices of this thesis. Some of the geometric parameters required to construct such models can be extracted from subsurface data; others must be estimated or obtained from outcrop analogues (see Chapter 3). A broad range of geometric parameters is expected, as heterolithic intervals vary laterally at the metre-scale in tidally influenced depositional environments. The impact of this variability on effective permeability is illustrated by the differences observed in the two end-member models constructed in this chapter using data from the same reservoir formation.

In many circumstances the creation of such mini-models will not be possible, and the results of our study provide some semi-qualitative guidance to constrain effective permeability in cross-bedded tidal sandstones when only plug measurements of permeability are available. Critically, it is likely that the effective horizontal permeability will be significantly lower than predicted from core-plug measurements (see also Jackson *et al.*, 2003, 2005), because plug-scale measurements over-estimate the lateral continuity of sandstone laminae, and fail to account for the presence of muddy toesets that reduce lateral connectivity. Even when the mudstone content is relatively low, the effective horizontal permeability may be significantly reduced; for example, in the models investigated here, a mudstone content of just 20% can reduce the effective horizontal permeability to 15 - 60% of the sandstone value (see Figures 4.8, 4.9); if the measured sandstone permeability was of order 100 mD, the effective permeability would be of order 15 – 60 mD. The decrease in vertical permeability is typically even more severe:

the same mudstone content of 20% can reduce the vertical permeability to just 2% of the sandstone value. Thus there is likely to be significant scope to reduce plug-derived values of permeability in a history match, or when comparing against permeability values interpreted from pressure transient data, even in relatively high net-to-gross intervals of cross-bedded tidal sandstone.

4.5. Conclusions

A suite of surface-based models of heterolithic, cross-bedded tidal sandstones has been investigated via flow simulation in order to calculate their effective permeability. Key findings are summarized below.

Values of effective permeability are dependent on the volume sampled, but variation is minimized for sample volumes of greater than c. 1 m^3, which then corresponds to a Representative Elementary Volume for the cross-bedded tidal sandstones.

Variation in the coverage of foreset-toeset surfaces by mudstone drapes has an impact on effective permeability, and introduces pronounced anisotropy not only between horizontal and vertical permeability, but also between dip-oriented and strike-oriented horizontal permeability. Permeability anisotropy arises from the preferential occurrence of mudstone drapes along toesets, which are closely spaced near the base of cross-bed sets to form barriers to vertical flow even for small mudstone contents, and which bound sandstone laminae of greater continuity along depositional strike compared to down depositional dip.

Variation in the continuity of sandstone laminae in the toeset regions of cross-bed sets is a critical control on effective permeability. The occurrence of discontinuous sand laminae in lenticular-bedded toesets results in flow occurring only through sandy foreset regions of cross-bed sets. The occurrence of continuous sand laminae in wavy-bedded toesets enables horizontal flow also through muddy toeset regions; furthermore, these laterally continuous sand laminae can be juxtaposed across erosive cross-bed set boundaries to enable flow between cross-bed sets.

No single parameter describing cross-bedding geometry exerts a dominant control on effective permeability. Instead, five parameters that control the distribution, extent and geometric configuration of toesets exert significant influence on effective permeability for different sandstone proportions and flow directions: (1) trough or tabular cross-bedding style; (2) the volumetric ratio between foreset and toeset regions; (3) toeset dip angle; (4) angle of dune climb; and (5) the dimensions of mudstone drapes present along foreset-toeset surfaces. Parameters that control the distribution, extent and geometric configuration of foresets are less significant. The sensitivity of effective permeability to multiple geometric parameters indicates that it is best calculated using a range of models that capture the uncertainty in cross-bedding geometry. Input parameters for these models can be extracted from core and outcrop-analogue data and the models can be constructed using the methodology and/or code described in this chapter.

Chapter 5
Effective relative permeabilities and residual oil saturation for oil/water flow in heterolithic cross-bedded tidal sandstones

Summary

Heterogeneities in cross-bedded heterolithic tidal sandstones may modify effective relative permeability at the scale of a representative elementary volume (REV). Fluid flow pathways become more tortuous as the coverage of mudstone drapes along foreset-toeset surfaces increases as illustrated in the previous chapter for single-phase flow simulation. In this chapter, we investigate the effect of heterogeneity on effective oil-water relative permeability in cross-bedded, heterolithic tidal sandstones using one three-dimensional model that samples a volume greater than the REV for single-phase flow. We conduct numerical experiments to determine the effect of flow orientation and mudstone drape coverage (i.e. mudstone content) on relative permeability and residual oil saturation.

We find that relative permeability is not affected significantly by flow orientation relative to heterogeneity surfaces, or by mudstone drape coverage ranging from 25 - 70%, except close to the residual oil saturation S_{or}. The residual oil saturation is generally higher than observed in an equivalent homogenous (sandstone-only) model, and the end-point relative permeability to water is higher. A mudstone drape coverage of 25% yields increases in S_{or} of +27% in the (down) dip direction, +51% in the strike direction and +94% in the vertical direction. A very small increase in mudstone content, from 12% to 15 % (corresponding to an increase in mudstone drape coverage from 25% to 70%) leads to a further significant increase in S_{or} of +173% in the strike direction. Bypassed oil is located primarily in the toeset areas, where dead-ends to flow are generated by locally intersecting mudstone drapes, thinning of sandstone laminae, and an increase in the tortuosity of the flow. Our results suggest that models that omit the impact on flow of mudstone drapes, even at low total mudstone fraction, may significantly underestimate residual oil saturation in cross-bedded, heterolithic tidal sandstones.

5.1. Introduction

Multi-phase flow in hydrocarbon reservoirs is a common phenomenon, as the flow of oil and gas is often associated with the flow of water. Previous studies have focused on the characterisation of effective single-phase permeability of heterolithic tidal sandstones, as discussed in the preceding chapters. A number of studies have investigated multi-phase flow, and multi-phase flow properties, in laminated and cross-bedded sandstones in which individual laminae exhibit varying grain-size and, consequent to this, varying permeability and capillary pressure (e.g. Kortekaas, 1985; Hartkamp-Bakker, 1991; Ringrose *et al.*, 1993; van Lingen *et al.*, 1996). Observed variations in relative permeability are mainly due to the action of capillary pressure: in water-wet rocks, oil tends to be trapped in high permeability laminae owing to the relatively larger capillary entry pressure of low permeability laminae.

However, heterolithic tidal cross-bedded sandstones differ from fluvial cross-bedded sandstones due to the presence of mudstone drapes along foreset-toeset surfaces. Mudstone drapes have extremely low permeability values compared to the sandstone laminae (often c. 5 orders of magnitude lower) and remain water saturated after primary drainage owing to the high capillary entry pressure associated with small pore-size; moreover, capillary entry pressures typically exceed the pressure differentials that can build up across laminae during production, so mudstone drapes act as local barriers to flow. Effective relative permeabilities of oil and water are then only dependent on the tortuosity of the flowpaths around the mudstone drapes. To date, no 3D flow simulation studies have been conducted on models of tidal cross-bedded sandstones that incorporate realistic mudstone drape geometry and distribution to investigate the effect of these small scale heterogeneities on relative permeability and oil recovery.

A number of studies have investigated two-phase flow around mudstone barriers using simple, generic models. These studies have suggested that oil located close to mudstone drapes is primarily bypassed by invading water. The oil later drains around the mudstone, due to gravitational forces (Richardson, 1978; Thomas, 1990). Bypass of oil can occur where shales intersect, creating dead-ends to the flow. Such results have been observed in some 2D simulation cases (Peilhua, 1986; Ciammetti *et al.*, 1995; White and Barton, 1999). However,

mudstone geometries are simplified in these models as parallel straight lines intersecting the flow path; moreover, length-scale and depositional environment are not similar to that of tidal cross-bedded sandstones; and then 2D models tend to overestimate the impact of dipping mudstone barriers on trapping of oil (Jackson and Muggeridge, 2000).

In the previous chapter, we have determined how the tortuosity of the flow is controlled by the 3D network of mudstone drapes, decreasing the effective permeability but as well introducing anisotropy in the horizontal direction. Prior to analysing multi-phase flow models, such anisotropy is believed to affect relative effective permeabilities as fluids would compete to cross areas with a dense mudstone drape network. Effective permeabilities were affected preferentially by the proportion of wavy-bedded or lenticular-bedded toeset parts compared to sandy-rich foreset parts. Relative permeabilities and variations in oil saturation are affected by the permeability contrast between the mudstone (mudstone drapes) and the sandstone (the bundles) lenses. Consequently, a particular attention should be given to the treatment of the toeset parts during multi-phase flow simulation, due to their high concentration in mudstone drapes.

The aim of this chapter is to determine the influence of mudstone drapes in tidal cross-bedded sandstone reservoirs on the relative permeabilities of oil and water, focussing on anisotropy in relative permeability associated with flow direction, the impacts of mudstone drape coverage along foreset-toeset surfaces and of mudstone fraction on residual oil saturation.

5.2. Methodology

5.2.1. Two-phase flow simulation

For this two-phase oil/water flow simulation study, the intermediate model of tidal cross-bedded sandstone introduced in the previous chapters has been used. The model was generated using a surface-based modelling workflow and input parameters extracted from the Dir Abu Lifa Member outcrop analogue. The model measures 3 x 3 x 1 m and corresponds

to a REV for single-phase flow. A cornerpoint grid honours the geometry of the foreset-toeset surfaces and cross-bed set boundaries. Two different scenarios of mudstone drape coverage were used in the experiments reported here: 25% mudstone drape coverage, corresponding to the value observed in outcrop (sandstone content of 88%) (Figure 5.1), and 70% mudstone drape coverage to investigate whether relative permeability is impacted by mudstone content (sandstone content of 85%).

The input parameters for models of the two mudstone drape coverage cases are summarized in Table 5.1. Single-phase effective permeabilities in each direction and for each value of mudstone content correspond to those reported in the previous chapter (Figure 4.8). Consistent with the previous chapters, the mudstone layers are modelled as impermeable to both water and oil (k_{mud} = 0); however, they are assumed to have porosity which is occupied by water and this water is included when calculating the effective water saturation in the model. Capillary pressure is also neglected: in the mudstone laminae, it is assumed the capillary entry pressure significantly exceeds the viscous pressure drop; in the sandstone laminae, it is assumed that capillary pressure is small compared to the viscous pressure drop. This also eliminates capillary end-effects. Buoyancy forces are also neglected. Thus $P_o = P_w = P$, with P_o and P_w being the pressures of oil and water respectively. Neglecting capillary pressure means that two-phase flow depends only on the tortuosity of the flowpaths, related to the lateral and vertical connectivity of sandstone laminae.

The fine-scale oil and water relative permeabilities of the sandstone are calculated using the Corey correlations (Zahoor *et al.*, 2009):

$$k_{ro}^{fs} = (k_{ro}^{e})^{fs} \left(1 - \frac{S_w^{fs} - S_{wirr}^{fs}}{1 - S_{or}^{fs} - S_{wirr}^{fs}}\right)^3 \tag{5.1}$$

$$k_{rw}^{fs} = (k_{rw}^{e})^{fs} \left(\frac{S_w^{fs} - S_{wirr}^{fs}}{1 - S_{or}^{fs} - S_{wirr}^{fs}}\right)^3 \tag{5.2}$$

where k_{ro}^{fs} and k_{rw}^{fs} are the fine scale relative permeabilities of oil and water respectively in the sandstone, and $(k_{ro}^{e})^{fs}$ and $(k_{rw}^{e})^{fs}$ are the fine scale relative permeability end point values at the irreducible water saturation and the residual oil saturation respectively. For this study, $(k_{ro}^{e})^{fs}$ and $(k_{rw}^{e})^{fs}$ were chosen equal to 0.8 and 0.3 respectively, as typical values for water-

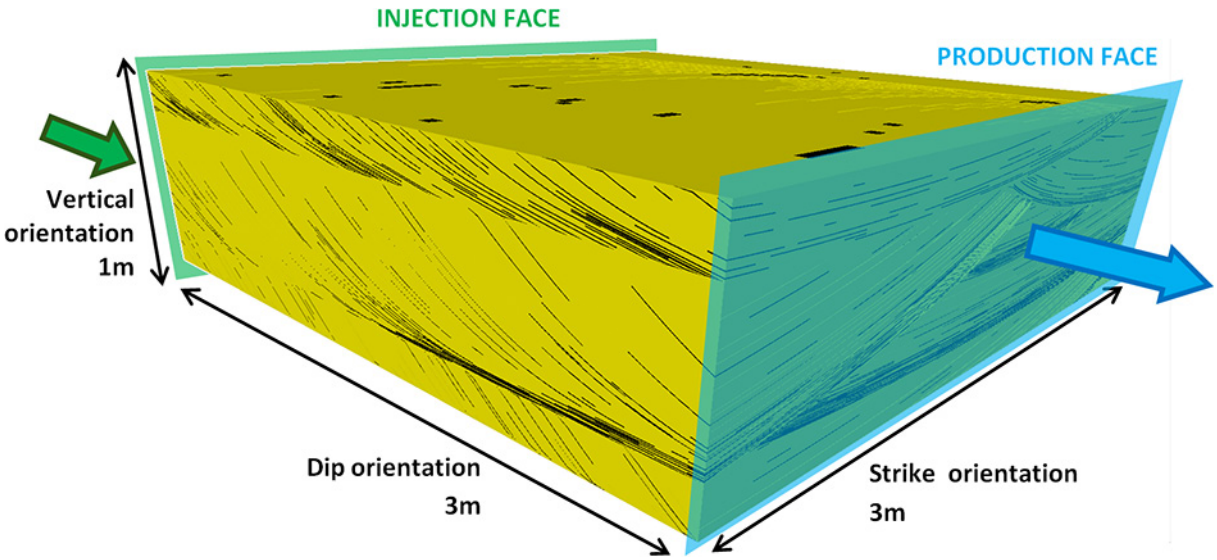


Figure 5.1: Intermediate surface-based model of trough cross-bedded tidal sandstone, generated using input parameters extracted from the Gecko Nose outcrop analogue (see Chapter 3). The model presented here contains foreset-toeset surfaces that are partially covered with mudstone drapes in black (25% mudstone coverage). Dip, strike and vertical orientations are defined related to the orientation of the cross-bedding surfaces. The conditions of a flow simulation experiment in the (down) dip orientation are represented on the figure. The inlet and outlet injection and production faces are reproduced with coloured rectangles, corresponding to the buffer zones of high permeability introduced for homogeneous injection and production flows.

Property	Value	
Rock compressibility	1.45×10^{-7} bar^{-1}	
Dip-direction horizontal effective permeability k_d	35% of k_{sand} for 25% mudstone drape coverage	12% of k_{sand} for 70% mudstone drape coverage
Strike-direction horizontal effective permeability k_s	71% of k_{sand} for 25% mudstone drape coverage	58% of k_{sand} for 70% mudstone drape coverage
Vertical effective permeability k_v	3% of k_{sand} for 25% mudstone drape coverage	1% of k_{sand} for 70% mudstone drape coverage
Oil density	1000 kg.m^{-3}	
Oil viscosity	0.31 cP	
Oil formation volume factor	1.0 rb.stb^{-1}	
Water density	1000 kg.m^{-3}	
Water viscosity	0.31 cP	
Water formation volume factor	1.0 rb.stb^{-1}	
Water compressibility	1×10^{-10} bar^{-1}	

Table 5.1: Fluid and rock properties for the oil/water flow simulation of the intermediate tidal cross-bedded sandstone model.

wet sandstones (Ringrose *et al.*, 1993). S_w^{fs} is the fine scale water saturation in the sandstone cells, while S_{or}^{fs} and S_{wirr}^{fs} correspond to the fine-scale residual oil saturation and irreducible water saturation respectively. The values of 0.1 and 0.25 that were chosen for S_{or}^{fs} and S_{wirr}^{fs} respectively are typical for water-wet sandstones (Huang *et al.*, 1996).

The flow simulations mimic steady-state core plug experiments to measure the relative permeabilities of oil and water (DeBaun *et al.*, 2005). The different steps of the simulation are as follows:

(1) The sandstone and mudstone are initially saturated with water. Oil is then injected to simulate primary drainage in the model until the irreducible water saturation value is reached (Figure 5.1).

(2) A fractional flow of oil and water is injected to simulate imbibition in the model. The total injection flow rate q_T is controlled by the pressure at the inlet. The flow rates of oil q_o and water q_w are specified depending on the target fraction *f,* with $q_T = f\, q_O + (1 - f)\, q_W$. Initially, the injecting fluid comprises solely oil, so $f = 1$. During the steady-state imbibiton process, *f* is progressively decreased (in decrements of 0.1), with steady state reached at each value of *f*, until the injecting fluid comprises solely water (i.e. $f = 0$). The value of effective water saturation S_w^{eff} in the entire model is computed at each steady state, which is reached: (i) when the injection and production flow rates of oil are equal with a tolerance of 0.1; (ii) when the injection and production flow rates of water are equal with a tolerance of 0.1; (iii) when the variation of average pressure field between two successive simulation steps is smaller than a threshold value of 0.1

(3) Effective relative permeabilities of oil and water are calculated from the Darcy's law applied to multiphase flow, where effective permeability is dependent on the composition of the fluids in place and the composition of the injected fluid (Dake, 1983):

$$k_{ro}^{eff} = \frac{q_o\, \mu_o\, L}{\Delta P\, A\, k} \tag{5.3}$$

$$k_{rw}^{eff} = \frac{q_w\, \mu_w\, L}{\Delta P\, A\, k} \tag{5.4}$$

where k_{ro}^{eff} and k_{rw}^{eff} are the effective relative permeabilities of oil and water respectively, *k* is the single phase effective permeability of the model in the same orientation (k_d for the horizontal dip direction, k_s for the horizontal strike direction, and k_v for the vertical direction)

calculated in the previous chapter, q_o and q_w are the flow rates of oil and water when steady state is reached for the given value of *f*, *A* is the cross-sectional area of the model, *L* is the length of the model, μ_o and μ_w are the viscosities of oil and water, and ΔP is the pressure difference between the opposing injection and production faces at steady-state (Figure 5.1). Relative effective permeabilities do not add up to 100% of the effective permeability of single phase fluid as the behaviour of the flow of one fluid through the rock is dependent on the fluids in place in the rock that can act as a baffle to the injected fluid. In fact, in the case of multi-phase fluids, each fluid may be divided into as many zones as the number of pores in the rock, preventing each fluid to move uniformly through the rocks. As for the single phase flow experiments, injection and production faces contain a single layer of high permeability buffer cells to ensure that flow is uniformly distributed and the fluid potential (i.e. the pressure field minus the hydrostatic pressure) is uniform at each face.

(4) The average water saturation in the model is calculated using the equation:

$$S_w^{eff} = \frac{\Sigma S_w^{fs} \emptyset_{si} V_i + \Sigma \emptyset_{mi} V_i}{\Sigma \emptyset_{si} V_i + \Sigma \emptyset_{mi} V_i} \tag{5.5}$$

where the sums are calculated over the sandstone and mudstone cells separately, ϕ_{mi} / ϕ_{si} are the porosity values of sandstone / mudstone cell *i*, and V_i is the volume of cell *i*.

Set of experiments	Mudstone drape coverage	Flow orientation	Description
	0% (only sand)	Horizontal dip; Vertical	Simulations on corner-point grid to quantify calculation artefacts introduced by the flow simulator.
1	25%	Horizontal dip and strike; Vertical; Strike reverse direction	Simulations performed in three orthogonal orientations and the reverse strike direction to study the impact of flow direction on relative permeability.
2	70%	Horizontal strike; Reverse horizontal strike	Simulation of model with higher mudstone drape coverage along stratal surfaces, to study the impact of mudstone content on relative permeability.
3	25%	Horizontal dip	Simulations using two different sets of fine-scale relative permeabilities (Corey versus linear).

Table 5.2: List of water-oil flow simulations conducted for the study. The highlighted text describes the parameter whose impact on relative permeability is investigated in each set of simulations.

5.2.2. Experimental programme

The list of experiments conducted in this study is reported in Table 5.2.

The first set of experiments was designed to quantify anisotropy in effective relative permeability by simulating flow in three different, orthogonal orientations (horizontal down-depositional dip, horizontal strike, and vertical).

Flow simulation was also performed in the reverse strike direction, to observe if the results are direction-dependent. The impact of mudstone content was investigated in the second set of experiments by varying the mudstone drape coverage.

The final set of experiments was designed to determine whether the results are strongly dependent on the fine-scale relative permeability curves, comparing the Corey-curve results with those obtained using linear fine-scale relative permeabilities.

5.2.3. Calculation artefacts introduced by corner-point grid architecture

In the previous chapter (Figure 4.8), the numerical artefacts introduced by the cornerpoint architecture of the model grid were determined for the calculation of single-phase effective permeability, due to the presence of pinched-out and steeply inclined cells. The problem is similar in the two-phase flow simulations reported here, as relative permeabilities are computed from the pressure gradient ΔP in equations (5.3) and (5.4). As the pressure gradient ΔP is dependent on the water saturation, so are the numerical artefacts introduced by the grid architecture. The error in relative permeability as a function of water saturation was determined using the same model grid geometry but in the absence of mudstone drapes (i.e. 100% sandstone).

Effective and fine-scale relative permeabilities are reported in Figure 5.2, along with the normalized difference, calculated using:

$$\delta k_{ro} = \frac{k_{ro}^{eff} - k_{ro}^{fs}}{k_{ro}^{fs}} \tag{5.6}$$

$$\delta k_{rw} = \frac{k_{rw}^{eff} - k_{ro}^{fs}}{k_{ro}^{fs}} \tag{5.7}$$

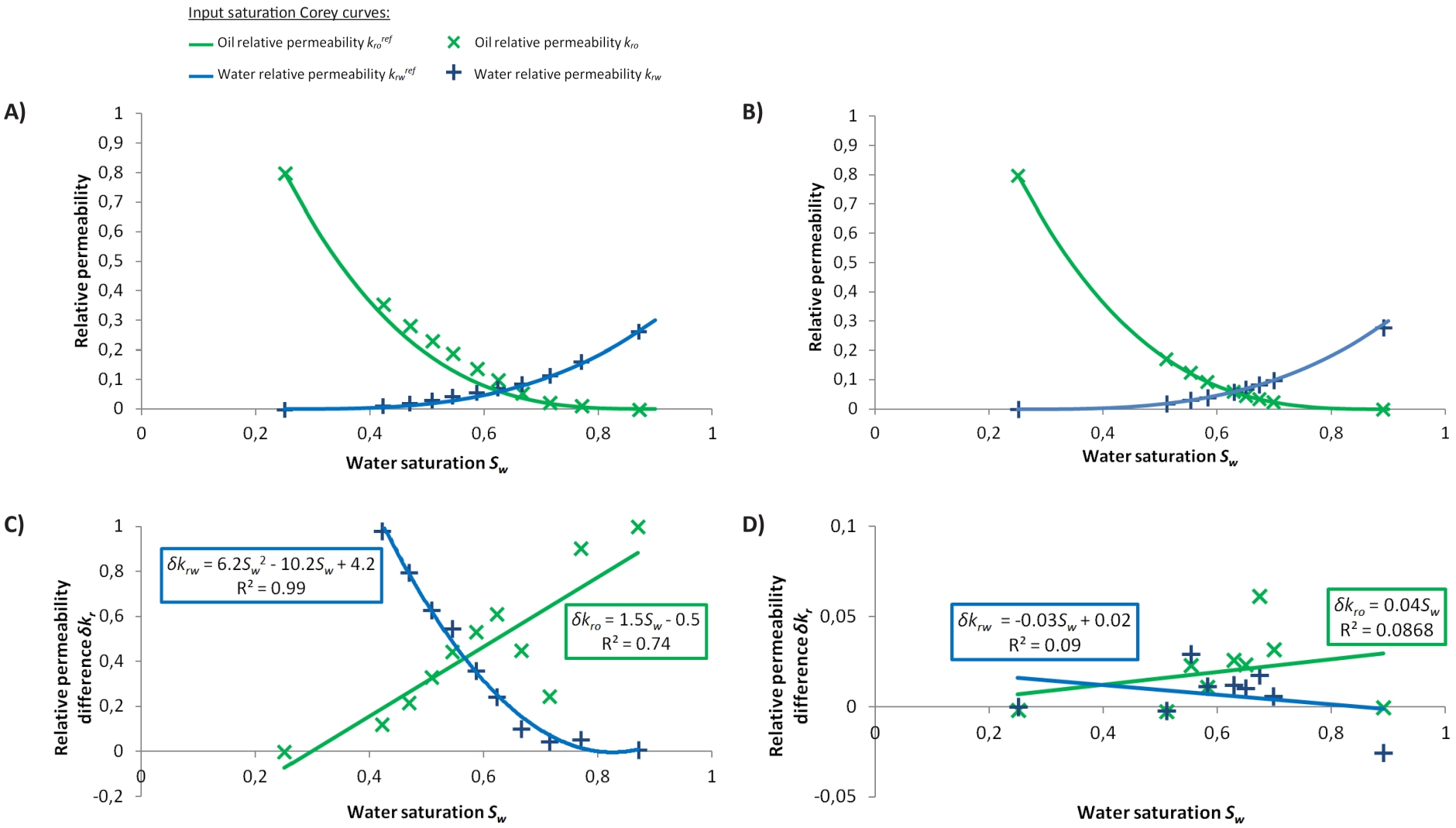


Figure 5.2: Oil/water flow simulation in the intermediate tidal cross-bedding model with only sandstone. The curves in (A) and (B) correspond to the fine-scale relative permeability curves for sandstone. The data points correspond to the calculated effective permeability in A) the horizontal, dip-oriented direction and B) the vertical direction. The difference between effective and fine-scale curves corresponds to the simulation error in C) the horizontal dip orientation and D) the vertical orientation. Linear best fit curve equations to the errors are reported for each case, as no clear trend was found.

Best fit curves for the errors are used to predict the saturation-dependent error bars reported later. In the vertical orientation, the errors are small; however, for the horizontal dip orientation, the errors are much larger. Similar results were obtained for single-phase flow. Errors for the horizontal strike orientation are assumed equal to those of the horizontal dip direction.

5.3. Results

5.3.1. Typical flow simulation results

Typical results from a single flow simulation, obtained using the intermediate model with 25% mudstone drape coverage, during the injection of water and oil with f = 0.1 and in the horizontal dip direction, are shown in Figure 5.3. Steady state is reached after c. 2500 days, when injection and production rates of oil are equal (q_o = 5.4 x 10^{-3} m^3/day, linear flow rate q_o/A = 0.18 m/day); similarly for the water injection and production rates (q_w = 1.8 x 10^{-4} m^3/day, and linear flow rate q_w/A = 0.06 m/day), and when the average field pressure P stabilizes. The pressure difference at steady state is ΔP = 240 bars. Numerous similar numerical experiments, for various values of f and in different flow directions, yield relative permeability curves such as those shown in Figure 5.4.

5.3.2. Impact of orientation of flow

Oil/water flow simulation was performed in three orthogonal orientations (Figures 5.4 and 5.5), and in both opposite directions in the horizontal strike direction (Figure 5.5). In the horizontal direction, effective and fine-scale curves are the same within experimental error, except for the final value at the residual oil saturation: the effective residual oil saturation is higher than the fine-scale residual oil saturation in all cases. Poor sweep occurs only locally, across continuous mudstone drapes near the boundaries of the model (e.g. Figure 5.6 A), or where the mudstone drapes intersect (e.g. Figure 5.6 B) These results suggest that the increase of tortuosity introduced by the presence of mudstone drapes does not significantly affect the horizontal flow of oil and water during production.

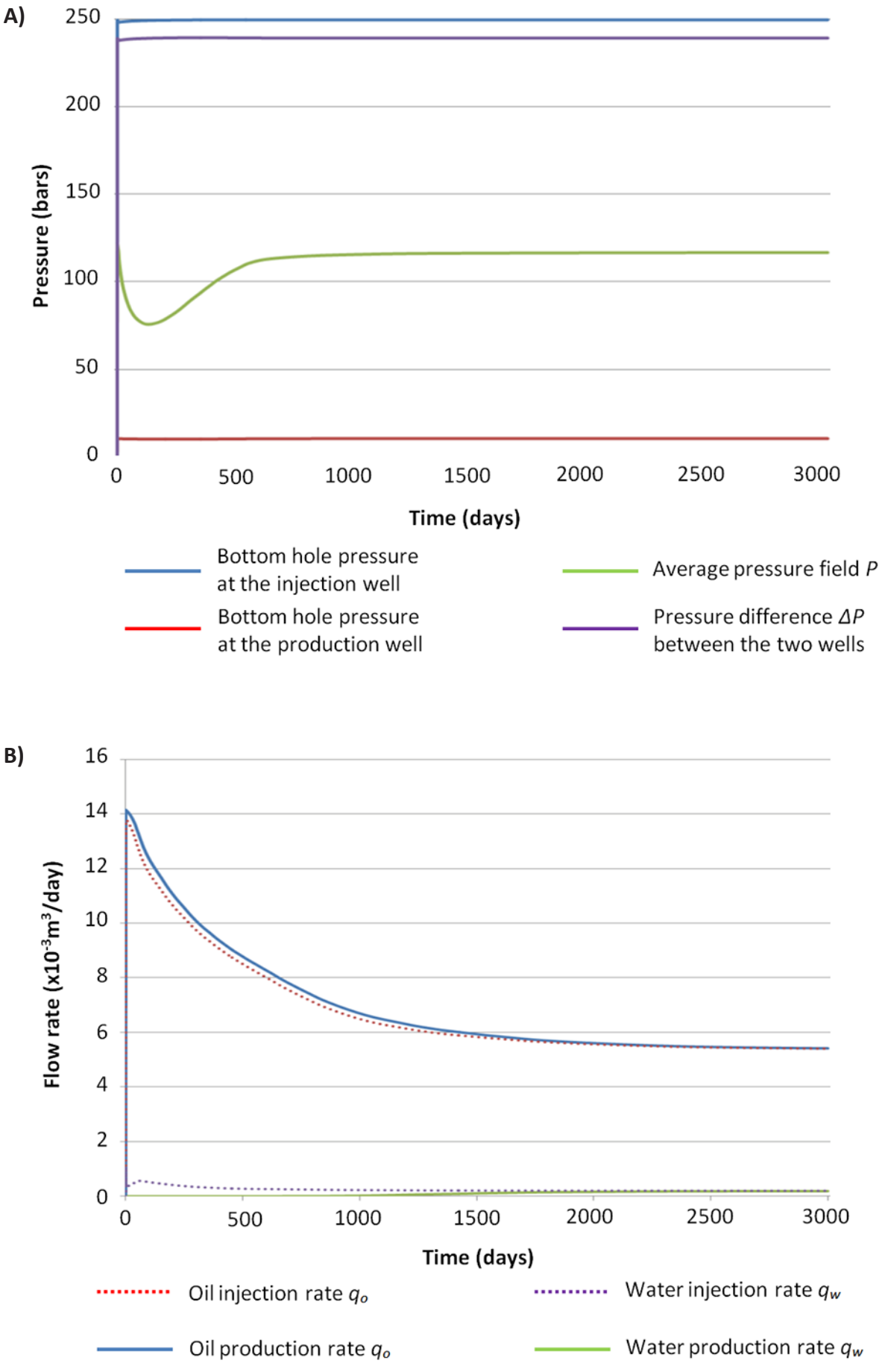


Figure 5.3: Evolution of A) pressures and B) flow rates through time in the intermediate model with 25% mudstone drape coverage for a horizontal dip oriented flow of 90% oil/10% water.

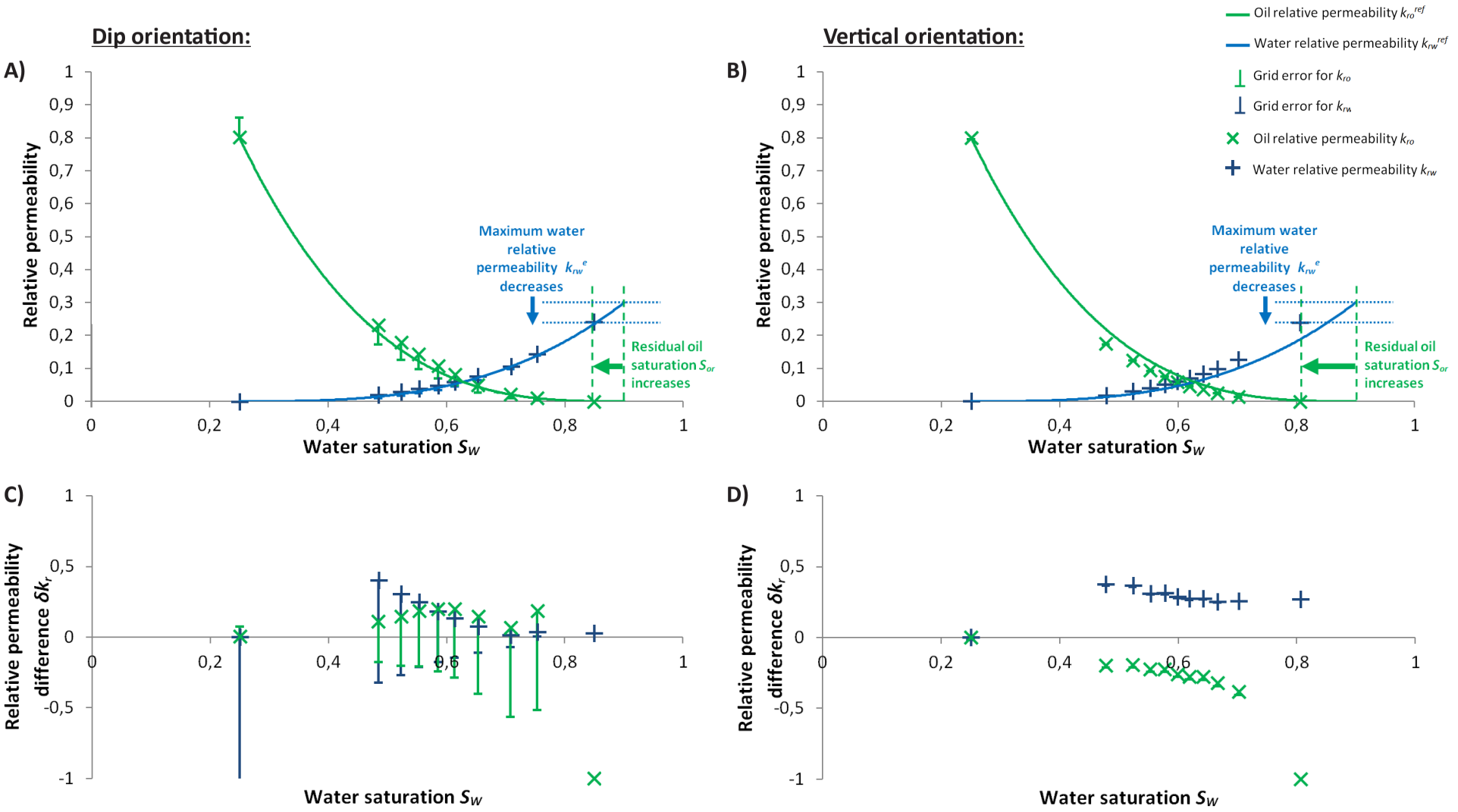


Figure 5.4: Variations in relative permeabilities for flow simulation in two perpendicular orientations of the 25% mudstone drape coverage intermediate model: A) horizontal, down depositional dip; B) vertical. The difference between the calculated relative permeabilities from the model flow simulation and the input relative permeabilities of the sandstone are represented C) in the case of the horizontal, down depositional dip flow orientation and D) in the case of the vertical flow orientation. Error bars denote the numerical errors introduced by the corner point grid, from the relationships defined in Figure 5.2.

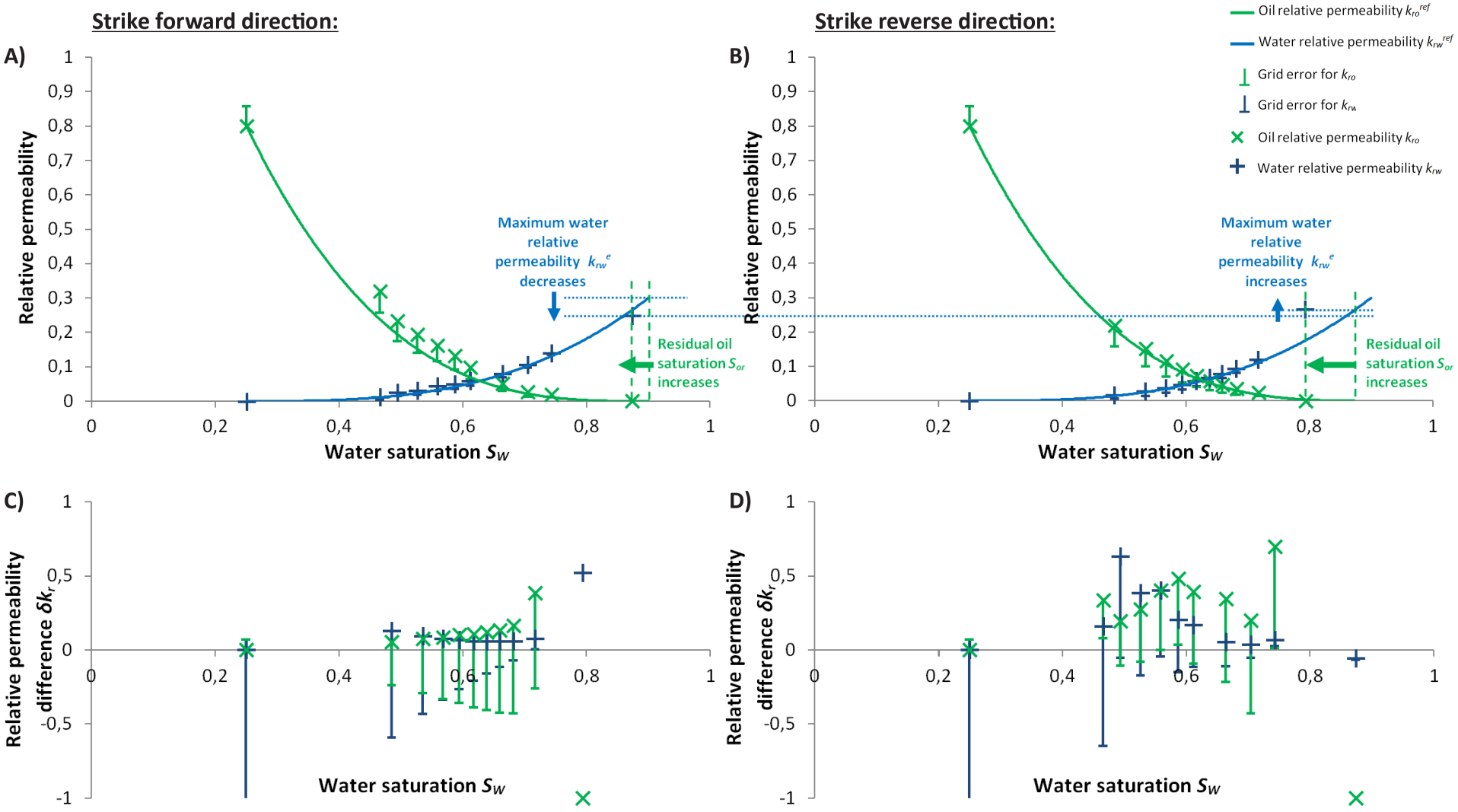


Figure 5.5: Variations in relative permeabilities for flow simulation in two opposite directions of the 25% mudstone drape coverage intermediate model: A) horizontal, forward strike direction; B) horizontal, reverse strike direction. The difference between the calculated relative permeabilities from the model flow simulation and the input relative permeabilities of the sandstone are represented C) in the case of the forward strike flow direction and D) in the case of the reverse strike flow direction. Error bars denote the numerical errors introduced by the corner point grid, from the relationships defined in Figure 5.2.

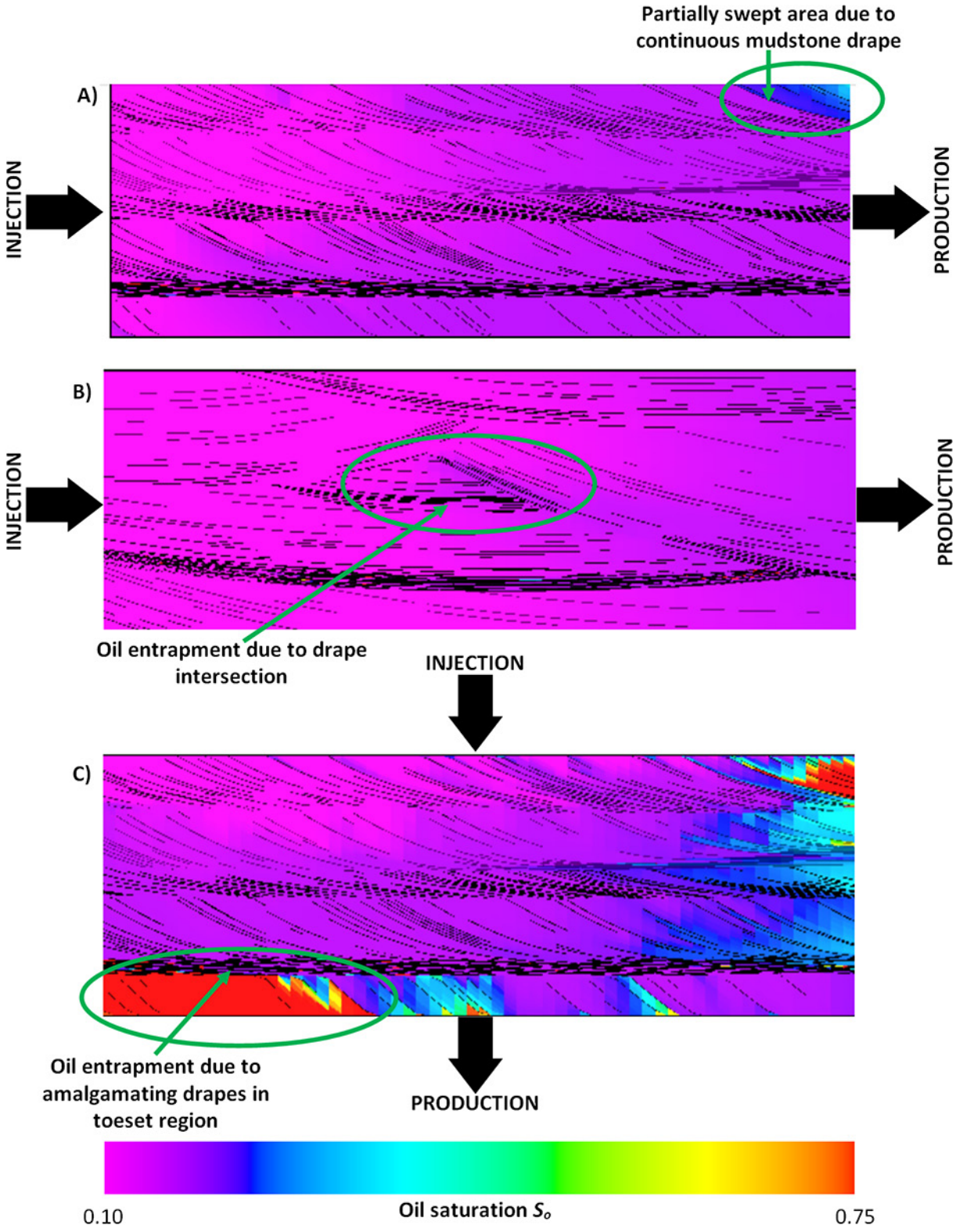


Figure 5.6: Oil saturation profiles at steady state for oil/water flow simulation in three orthogonal flow orientations: A) horizontal, down depositional dip; B) horizontal, along strike; and C) vertical. The injecting fluid is 100% water. The initial oil saturation S_{or} is equal to 0.75 (i.e. its maximum, as the irreducible water saturation S_{wirr} = 0.25).

In the vertical direction, the effective relative permeabilities of both oil and water differ from the fine-scale values; thus a modest level of anisotropy is introduced. Moreover, the residual oil saturation is significantly increased, as is the end-point relative permeability to water. Laterally continuous horizontal mudstone drapes along toesets amalgamate at the boundary between two superimposed cross-bed sets, creating barriers to flow. Consequently, oil may only flow vertically in areas where sandy foreset regions are vertically amalgamated (Figure 5.6 C). Some areas of the model are not swept by vertical flow, as they are isolated by continuous mudstone barriers formed by toeset regions.

The most significant effect of the mudstone drapes in all four flow orientations investigated is to increase the residual oil saturation relative to the fine-scale (homogenous, sandstone-only) case; for vertical flow, there is also an increase in the effective end-point relative permeability to water, consistent with injected water bypassing oil trapped behind continuous mudstone drapes.

5.3.3. Impact of mudstone drape coverage

Flow simulations were conducted along strike in both forward and reverse directions on the same model described above, but with a higher mudstone drape coverage of 70%; the increase in mudstone drape coverage (from 25% to 70%) corresponds to only a small increase in the mudstone volume content (from 12% to 15%). The resulting effective relative permeability curves are shown in Figure 5.7.

In each flow direction, the effective and fine-scale oil relative permeability curves are the same within experimental error, except at the residual oil saturation. However, the residual oil saturation is higher than the case with 25% mudstone drape coverage (Figure 5.5; S_{or} = 0.27, compared to S_{or} = 0.13); moreover, there is a significant increase in the effective relative permeability to water close to the end-point. These results are consistent with injected water bypassing oil trapped behind more continuous mudstone drapes; moreover, the increase in residual oil saturation is significant, despite the small increase in mudstone content.

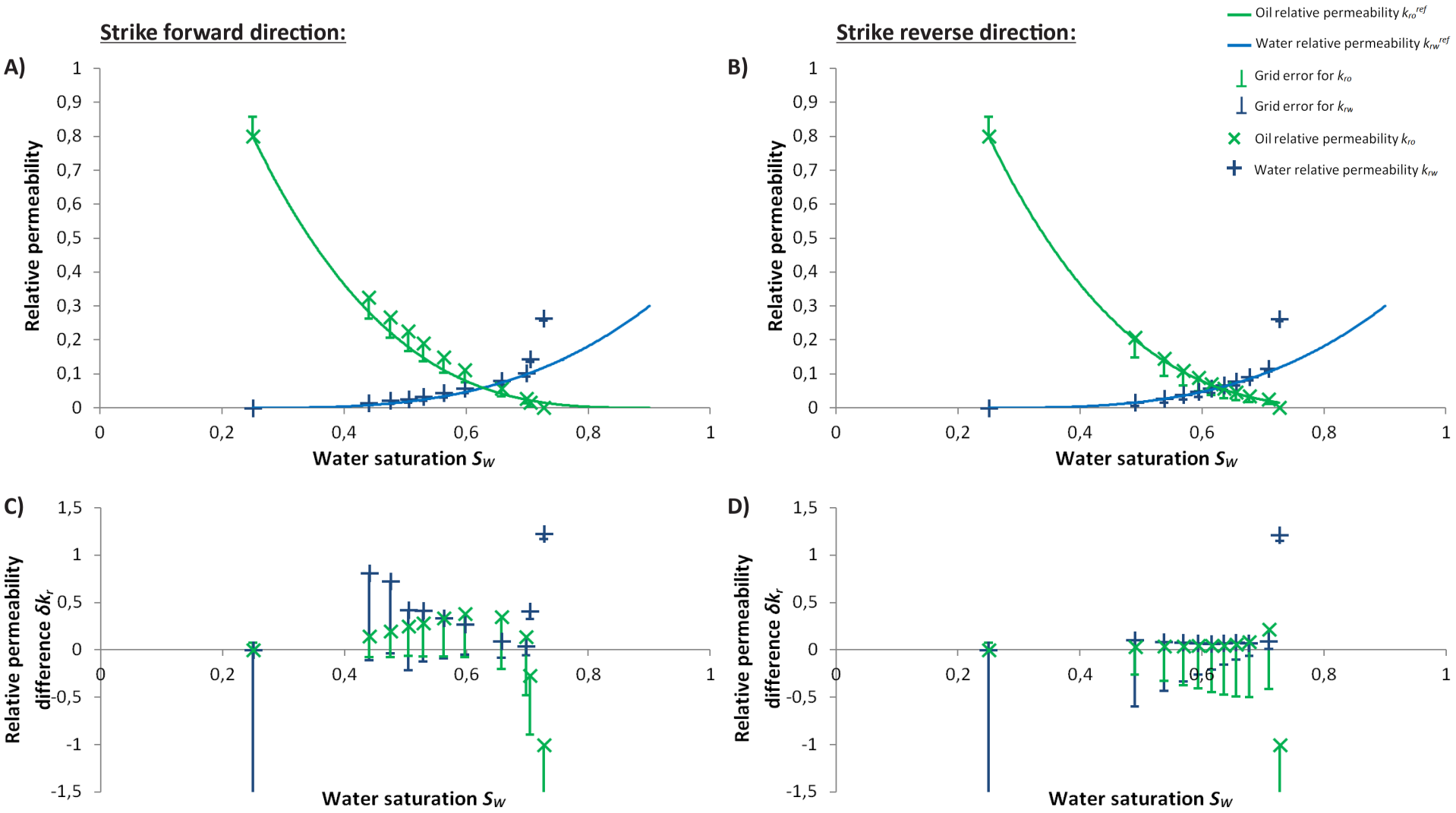


Figure 5.7: Variations in relative permeabilities for flow simulation in two opposite directions of the 70% mudstone drape coverage intermediate model: A) horizontal, forward strike direction; B) horizontal, reverse strike direction. Results The difference between the calculated relative permeabilities from the model flow simulation and the input relative permeabilities of the sandstone are represented C) in the case of the forward strike flow direction and D) in the case of the reverse strike flow direction. Error bars denote the numerical errors introduced by the corner point grid, from the relationships defined in Figure 5.2.

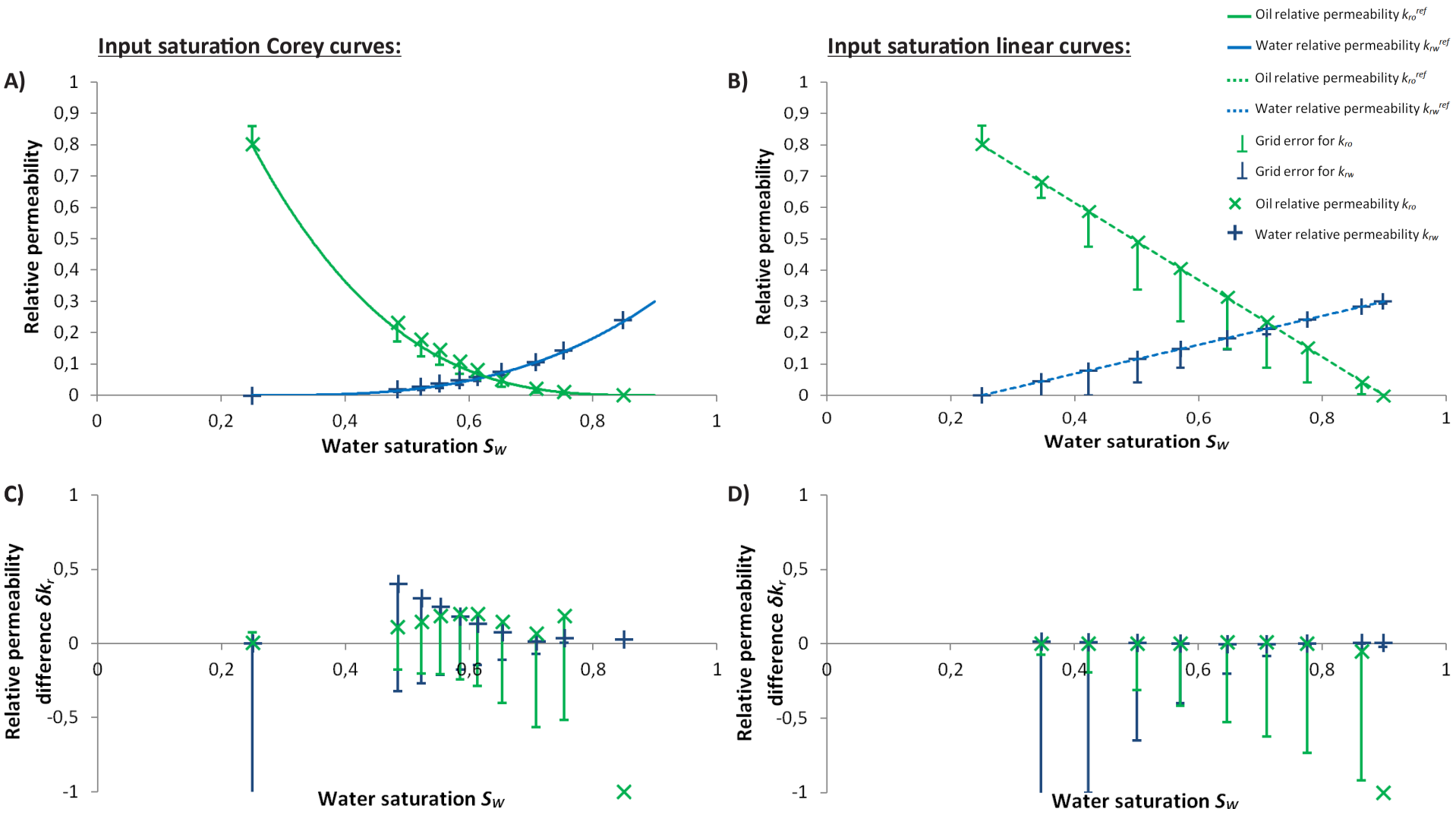


Figure 5.8: Results of relative permeabilities depending on water saturation for two different input saturation curves, A) the Corey relationships and B) linear relationships in the 25% mudstone drape coverage intermediate model. The difference between the calculated relative permeabilities from the model flow simulation and the input relative permeabilities are represented C) in the case of the Corey relationships and D) linear relationships. Error bars denote the numerical errors introduced by the corner point grid, from the relationships defined in Figure 5.2.

5.3.4. Impact of input curves of sandstone relative permeability

The results of the oil/water flow simulations using different fine-scale sandstone relative permeabilities are displayed in Figure 5.8; the results shown in Figure 5.8 A, C are the same as those shown in Figure 5.4 A, C and are included for comparison only. In both cases, the effective and fine-scale curves are identical within experimental error, except at the residual oil saturation. The results do not appear to depend significantly on the choice of fine-scale curves.

5.4. Discussion

The most significant impact of the mudstone drapes on effective relative permeability, regardless of flow direction, is to increase the residual oil saturation of the heterolithic sandstone compared to the fine-scale pure sandstone value of residual saturation (Figure 5.9). The residual oil saturation can be almost 175% higher than the input pure sandstone value of residual saturation, depending upon flow direction and mudstone drape coverage, despite the relatively high net-to-gross of the models investigated (sandstone fraction varying from 0.85 to 0.88). These results are significant because they suggest that relative permeability curves obtained from sandstone core-plugs that do not include mudstone drapes can significantly underestimate the residual oil saturation of the cross-bedded heterolithic tidal sandstones.

Previous studies conducted in generic 2D models of inclined mudstone (shale) barriers have described similar results, in which oil is bypassed in the vicinity of shales and, in particular, in dead-ends caused by intersecting shales (Peilhua, 1986; Ciammetti *et al.*, 1995; White and Barton, 1999). However, the impact of intersecting shales on oil trapping may be exaggerated in 2D flow simulation experiments (Jackson and Muggeridge, 2000); only small discontinuities in the third dimension are sufficient to facilitate efficient sweep. Jackson and Muggeridge (2000) also observed that isolated, discontinuous shales have negligible impact on sweep during water-flooding, with the noticeable exception of steeply inclined, extensive shales that are detrimental to horizontal flow. Many mudstone drapes

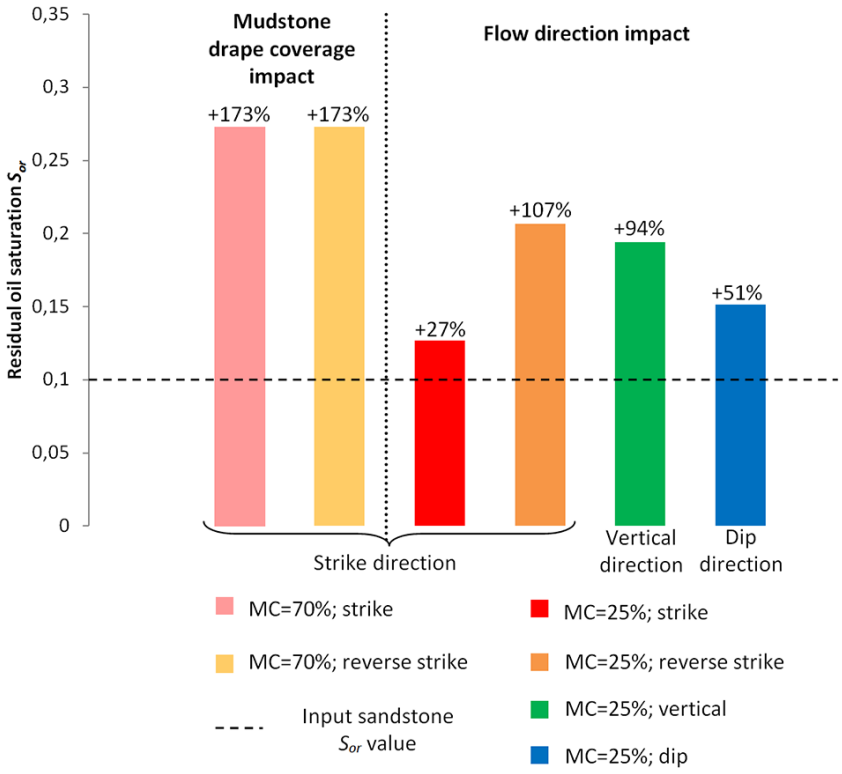


Figure 5.9: Comparison of residual oil saturation S_{or} for the different simulations presented in Figures 5.4, 5.5 and 5.7. MC = mudstone drape coverage. The percentages correspond to the difference of S_{or} of each model to the initial input value of the sandstone, based on the fine-scale sandstone curve indicated by the horizontal dashed line.

in cross-bedded tidal sandstone fall into this latter category, because they occur as near-continuous features along steeply inclined (up to 25°) foresets and their contiguous toesets (see the mudstone drape frequency function *f* in Chapter 3, Figure 3.12).

A difference in the sweep efficiency can be observed in toeset and foreset regions of cross-bed sets in our models (e.g. Figure 5.10). For example, no area of the model shown in Figure 5.10 remains unswept, as all sandstone laminae are connected from the injection face to the production face. After steady state has been reached, the quantity of extra bypassed oil is small, but sufficient to affirm that the mudstone drapes effectively act as barriers that locally trap oil (Figure 5.11). High values of oil saturation S_o are located: (1) in the toeset regions of cross-bed sets, where the close vertical stacking of near-continuous mudstone drapes in wavy bedding structures efficiently traps the oil; and (2) in foreset regions located down-flow of toeset regions that are directly connected to the production face.

Consequently, values of residual oil saturation used for reservoir simulation would be significantly underestimated if they are based on core plug measurements that do not sample the toeset parts of the tidal cross-bed sets.

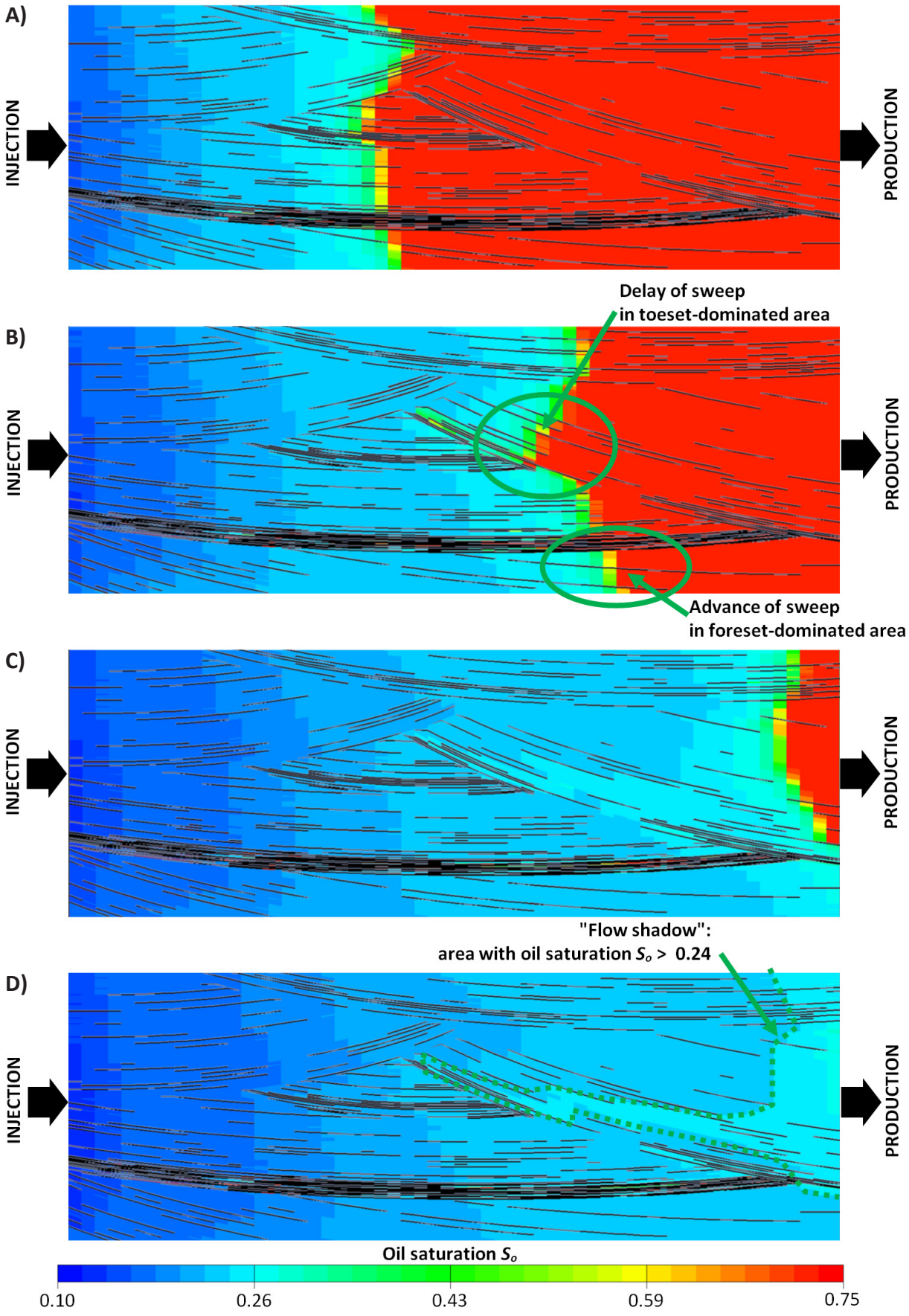


Figure 5.10: Oil saturation profile at different time steps of a simulated waterflood along depositional strike of a fully oil-saturated, tidal cross-bedded sandstone with 25% mudstone drape coverage: A) after 1 month ; B) after 2 months; C) after 4 months; D) after 5 months.

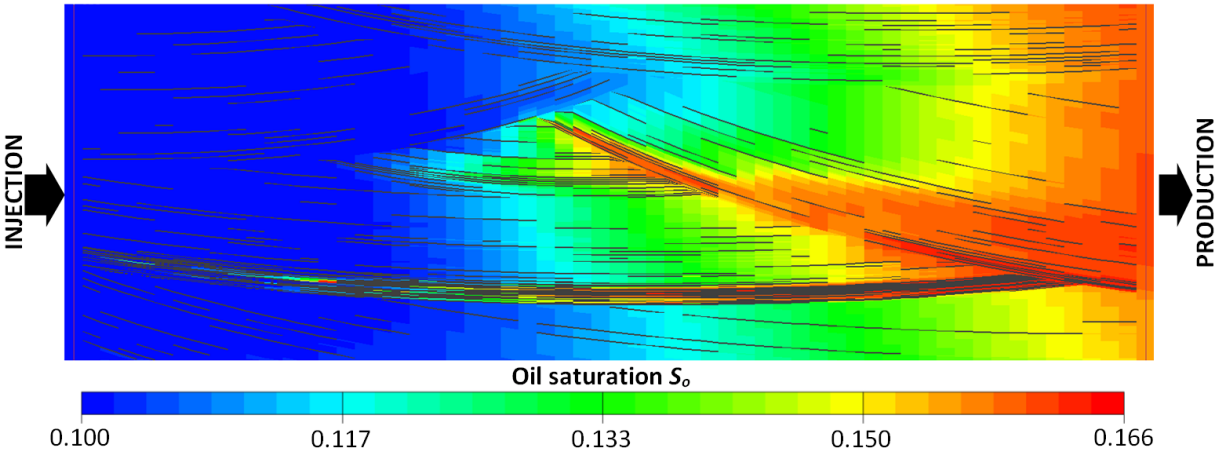


Figure 5.11: Oil saturation profile for the same water injection experiment as shown in Figure 5.10 after 30 months, when steady-state has been reached. Note the change in scale of the colour scheme used in Figures 5.10 and 5.11.

5.5. Recommendations for future work

The investigation on multi-phase flow effects on relative effective permeability presented was able to identify the key behaviour of residual saturation and hence paved the way to a more comprehensive study should additionally investigate (i) a broader range of model geometries and mudstone drape coverage, to determine whether effective relative permeability is strongly geometry or mud-fraction dependent; (ii) flow in all three orthogonal directions, and in the reverse directions, in all models, to further quantify anisotropy and directionality in effective relative permeability; (iii) a broader range of fluid properties, to determine whether effective permeability also depends strongly on viscosity contrast or buoyancy; (iv) the impact of capillary forces.

5.6. Conclusions

In this chapter, we have investigated the impact of mudstone drapes on relative permeabilities and residual oil saturation during oil/water flow simulation of tidal cross-bedded heterolithic sandstones. Anisotropy in residual oil saturation is observed depending on the flow orientation and direction. More oil is trapped in the model after drainage by vertical flow than

for drainage by horizontal flow, because laterally continuous regions of mudstone drapes along toeset laminae in cross-bed sets impede vertical flow. Close to residual oil saturation value, there is an accompanying decrease in water relative permeability, suggesting that the extra bypassed oil prevents the flow of water. An increase in mudstone drape coverage leads to a net increase in residual oil saturation despite of a very small variation in the net to gross, but has no impact on the mobility of oil as oil relative permeabilities remain unchanged. The volume of oil trapped depends on mudstone drape abundance, geometry and continuity. Together these parameters generate 3D intersections in mudstone drapes that form localised, dead-end flow paths which trap oil, but the distribution of these dead-ends is not readily predicted from the orientation and direction of flow. Bypassed oil has been tracked in the muddy rich toeset parts of the models. The results suggest that relative permeability curves obtained from sandstone core-plugs that do not sample enough foreset-toeset surfaces lined with mudstone drapes (especially bypassed oil-rich toeset areas) can significantly underestimate the residual oil saturation. The results are only preliminary, and further investigation has to be undertaken.

Chapter 6
General discussion and conclusions

6.1. Applications of outcrop-analogue based studies for reservoir modelling

One outcrop analogue study was conducted in this research project for the characterisation of the mixed tidally- and wave-influenced Tilje Formation of the Halten Terrace Linnorm field, offshore mid-Norway. The chosen outcrop analogue was the tidally-dominated Eocene Dir Abu Lifa Member, Western Desert, Egypt. This outcrop comprises shallow-marine facies typical of tide-influenced deltaic systems, positioned closely to the coastline in the associated tidal transition zone. The key findings of this study are outlined below, and can be applied to any other outcrop-analogue based study:

- On one hand, modern analogues provide a "frozen" 2D plan view of the depositional systems at a specific time, and may introduce a bias towards transgressive systems since these are prevalent today. On the other hand, ancient analogues are not biased in that way as all regimes are represented equiprobably in the sedimentological records, albeit with preservational biases that result from the combined action of erosional processes, and with geometrical and diagenetic overprints due to burial, compaction, and exhumation. Ancient outcrop analogues therefore provide a dynamic 4D view of the depositional system (including spatial and temporal dimensions) within an appropriate sequence stratigraphic context.
- The study of ancient outcrop analogues allows observation of formations as they may appear in the subsurface, with access to lateral variability at the interwell scale from laterally extensive cliff face escarpments (e.g. 50 km in the Fayoum Depression for the Dir Abu Lifa Member), and an insight to 3D facies architectures via canyons and gorges cut into the cliff face escarpments.
- The extensive exposure of facies at outcrop allowed reliable statistical analysis of the dimensions, geometry and orientation of stratal surfaces and associated heterogenetity

to be performed using a large sample size. These data allow the position and dimensions of heterogeneities to be placed within the context of a coherent interpretation of depositional environment.

- The sedimentary structures and associated heterogeneities in the tide-dominated Dir Abu Lifa Member provide a reference for the 3D geometrical characterisation of cross-bedded, heterolithic tidal sandstones deposited in the absence of reworking by waves and riverine currents. The comparison with other outcrop analogues of mixed-influence deposits would inform interpretation of the impact of wave-reworking on the development of heterogeneity in cross-bedded, heterolithic tidal sandstones.

Outcrop analogue studies give valuable information for facies modelling in subsurface reservoirs. Typically, facies modelling is performed using a combination of grid-based or pixel-based geostatistical techniques, loosely constrained by scarce data from widely spaced (c. 1 km) wells. Uncertainties in the lateral variability of facies is important in determining sandbody connectivity, sweep and hydrocarbon recovery, but can only be constrained by the appraisal of the zone surrounding the wells with wireline-log tools (c. metre-scale radius from the wellbore) and production data such as well tests and RFT data. The lateral variability of facies is commonly controlled in reservoir models by user-defined variograms for sequential indicator simulation or by training images for MPS geostatistical techniques, which respectively reproduce trends in facies dimensions and orientation, and in facies juxtapositions (e.g. Strebelle, 2002; Jung *et al.*, 2012).

The typical size of a reservoir-simulation model grid cell is 200 x 200 x 2 m. Such dimensions are compatible with outcrop analogue dimensions. From there, one can imagine a reservoir model as an assemblage of cells that correspond to an outcrop analogue code that represents an upscaled version of a finer, analogue-derived geological model on a higher resolution grid, rather than a generic facies association code. Petrophysical and effective reservoir properties for the cell would be taken from the properties of the corresponding outcrop analogue. A database of outcrop analogue models could be built, with effective reservoir properties being extracted from flow simulation of the outcrop models. In a further section, we discuss how to define the effective reservoir properties of such outcrop analogue models incorporating heterogeneities at multiple length-scales.

6.2. Advances in the potential for geological realism of reservoir models: surface-based reservoir models and gridding

Surface-based methodologies similar to that used in this thesis have been applied already with success to create reservoir models with a high degree of realism (e.g. MacDonald *et al.*, 1998; Deutsch *et al.*, 2001; Pyrcz *et al.*, 2005; Zhang *et al.*, 2009). In conventional workflows for model construction, such surfaces include the main faults and main stratigraphic horizons interpreted in seismic data, which are chosen as constraints for the building of a regular Cartesian or corner-point grid (e.g. Willis and White, 2000; Jackson *et al.*, 2013). Key stratigraphic surfaces or surfaces associated with smaller heterogeneities (i.e. facies boundaries, bed and lamina boundaries, and sub-seismic faults and fractures) are only modelled in a second step: consequently, their geometries are subsidiary to the architecture of the pre-defined grid (e.g. Bryant and Flint, 1993). When the resolution of the regular grid is high, the geometry of such surfaces can be represented with reasonable accuracy; if grid resolution is too low, the geometry of the surfaces is simplified, coarse, and geological realism may be lost. Consequently, geological reservoir model grids may include a very high number of cells, up to tens of millions, in order to incorporate as many geometrically realistic surfaces as possible. However, for flow simulation purposes, such large and computationally expensive geological model grids have to be upscaled (Haldorsen, 1986; Reading, 1986). To solve the governing flow equations, the flow simulator requires a reservoir grid which cannot contain more than a certain number of cells, depending on the computational power of the system; current reservoir simulation models do not typically include more than one million active cells. The grid upscaling step consists of decreasing the resolution of the grid. Geological realism is irredeemably lost by upscaling (e.g. Figure 6.1). After the upscaling step, the geometry of geological bodies is simplified, their continuity and connectivity may be interrupted if their orientation does not coincide with the grid orientation, and they may even disappear entirely if they are smaller than the upscaled-grid cells (Jackson *et al.*, in press).

The study of tidally-influenced cross-bedded sandstones presented in this thesis is a telling example of the necessity of building geologically realistic reservoir models. We have seen that the results of effective reservoir properties are highly dependent on the connectivity of

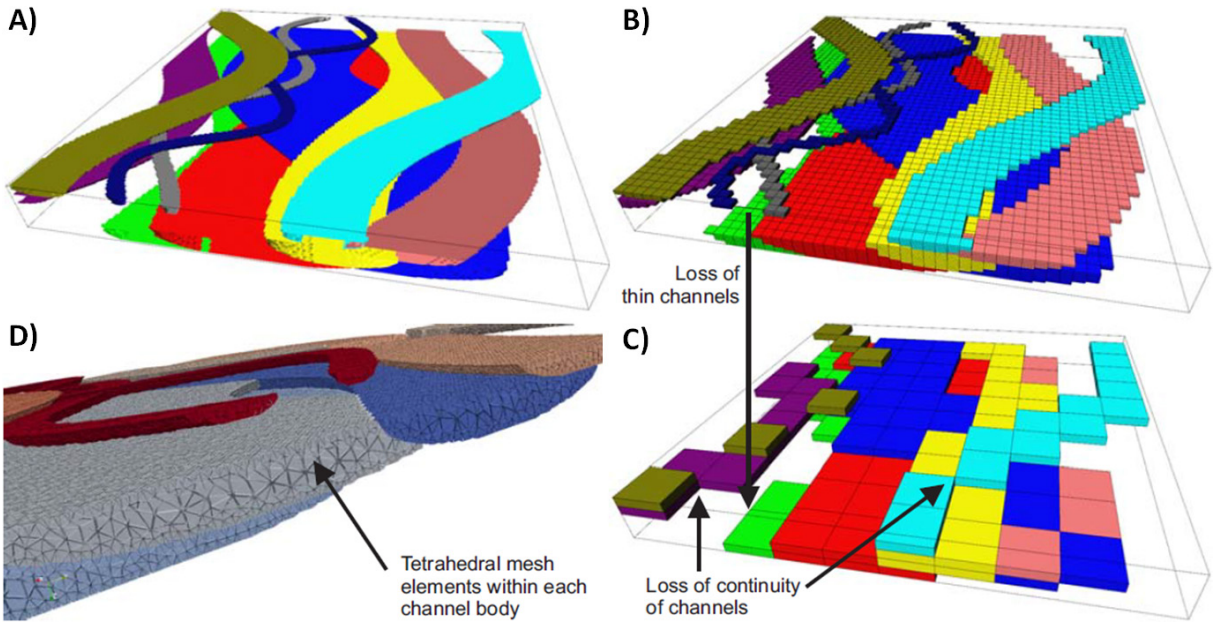


Figure 6.1: Three-dimensional models of channels created with different modelling techniques. A) Surface-based model to capture channelized sandbodies in a non-reservoir (mudstone) background. Each channelized sandbody is defined by a top and a base bounding surface. B) Object-based model of the same channelized sandbodies on a fine scale Cartesian grid. The channels have a "stair-step" geometry imposed by the grid architecture. C) Same model than in B), after the resolution of the grid is made coarser, in a similar way than after upscaling of a geological model to a reservoir simulation model. The geometry of the channels is oversimplified, such that some channels lose their continuity and other disappear entirely. D) Alternative gridding of a surface-based model with an unstructured tetrahedral mesh, honouring the geometry of top and base boundary surfaces with fine resolution, and meshing the channel volume with low resolution (Jackson *et al.*, in press).

sandstone laminae. The surface-based modelling workflow described in this thesis combined with the building of a corner-point grid ensures accurate reproduction of the connectivity of sandstone laminae at centimetre to metre length-scales in mini-models suitable for flow simulation. Such a methodology could be used for building geologically realistic reservoir models at the kilometre length-scale. In a similar way than to the mini-models of cross-bedded heterolithic sandstones, facies connectivity and heterogeneity defined by geological surfaces would be ensured, so that the predictive capabilities of reservoir models would be improved. As an example, the surface-based methodology has been implemented for the modelling of shallow-marine reservoirs to incorporate 100 metre-scale clinoform surfaces of realistic geometry in reservoir models (Sech *et al.*, 2009; Jackson *et al.*, 2009; Graham *et al.*, in review). Clinoform surfaces have an important impact on oil recovery in such reservoirs, modifying the sweep efficiency by compartmentalizing the reservoir, and leading to early water breakthrough (e.g. Ainsworth *et al.*, 1999; Howell *et al.*, 2008a, 2008b; Jackson *et al.*, 2009).

The building of a grid is necessary for flow simulation. We have observed in this thesis that the building of an irregular, non-orthogonal corner-point grid introduces pinched-out cells, resulting in numerical artefacts and errors (e.g. an error of 25% for the effective permeability in dip-oriented horizontal flow, see Figure 4.8). Distorted and irregularly shaped cells should thus be avoided in the grid building process in current commercially available software that is standard in the oil industry. Recent advances in the 3D-volume meshing of geological and reservoir models have addressed this problem via the development of unstructured tetrahedral meshes. A simplified model of cross-bed sets was gridded with such a mesh during the course of this research (Jackson *et al.*, in press) (Figure 6.2). The resolution of the mesh is increased around stratal surfaces associated with mudstone drapes, so the rendering of the surfaces is an improvement on a corner-point grid whose architecture is constrained by regularly-spaced pillars. The resolution of the unstructured tetrahedral mesh is decreased in the homogeneous parts of the models where a refinement of the grid is unnecessary.

The tetrahedral mesh would be of limited practical value if it was not coupled with a new generation of flow simulators which can solve the flow equations for irregular, non k-orthogonal, meshes. The NORMS research group at Imperial College is developing such a next-generation flow simulator by adapting the existing software Fluidity to simulate flow in porous media (Jackson *et al.*, 2013). Fluidity is a multi-phase fluid dynamics code which can numerically solve the Navier-Stokes equation using 3D unstructured, tetrahedral and adaptive meshes that evolve through time (e.g. Pain *et al.*, 2001; Davies *et al.*, 2011). Adaptive meshes increase the resolution of the grid at the flow interfaces (i.e. fluid contacts or heterogeneity surfaces), where refinement for computation efficiency and realism is required; behind the interfaces, the grid resolution is progressively decreasing through time to save computational power (Jackson *et al.*, 2013) (Figure 6.3). This new generation of flow simulators, with unstructured, adaptive meshes, would allow detailed tracking of the oil trapped in the toeset parts of tidally-influenced cross-bedded sandstones, as presented in Chapter 5. The mesh in the toeset parts would be very fine to accurately observe the fluid-rock interface effects, whereas the mesh would be coarse in the homogeneous sandstone laminae of the foreset regions (Figure 6.2). As the water front migrates during drainage, the mesh of the grid would be refined constantly at the interfaces between oil and water, before getting progressively coarser again after passage of the water front.

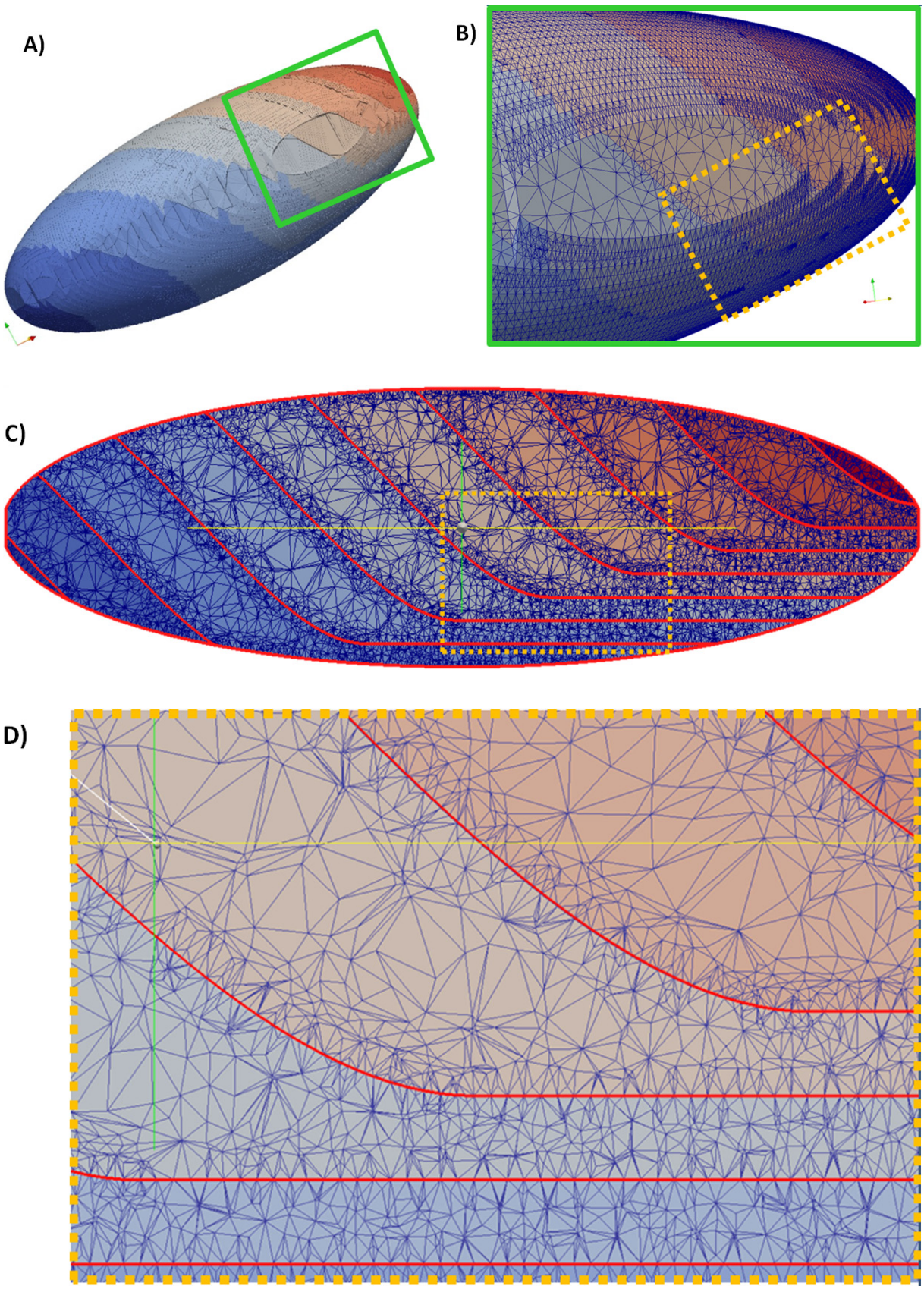


Figure 6.2: Alternative gridding for an idealized (elliptical) uneroded cross-bed set containing foreset-toeset surfaces using an unstructured tetrahedral mesh. Blue lines denote mesh elements; red lines denote foreset-toeset surfaces. A) 3D rendering of the cross-bed set; B) Close-up of A; C) Dip-oriented cross-section through the model. Note how the resolution of the grid is high around the foreset-toeset surfaces to ensure a high degree of geometrical realism. D) Close-up of C in the yellow box at the junction between the curved foreset part and linear toeset part of foreset-toeset surfaces (Jackson *et al.*, in press; after work by A. El-Sheikh and B. Y. G. Massart).

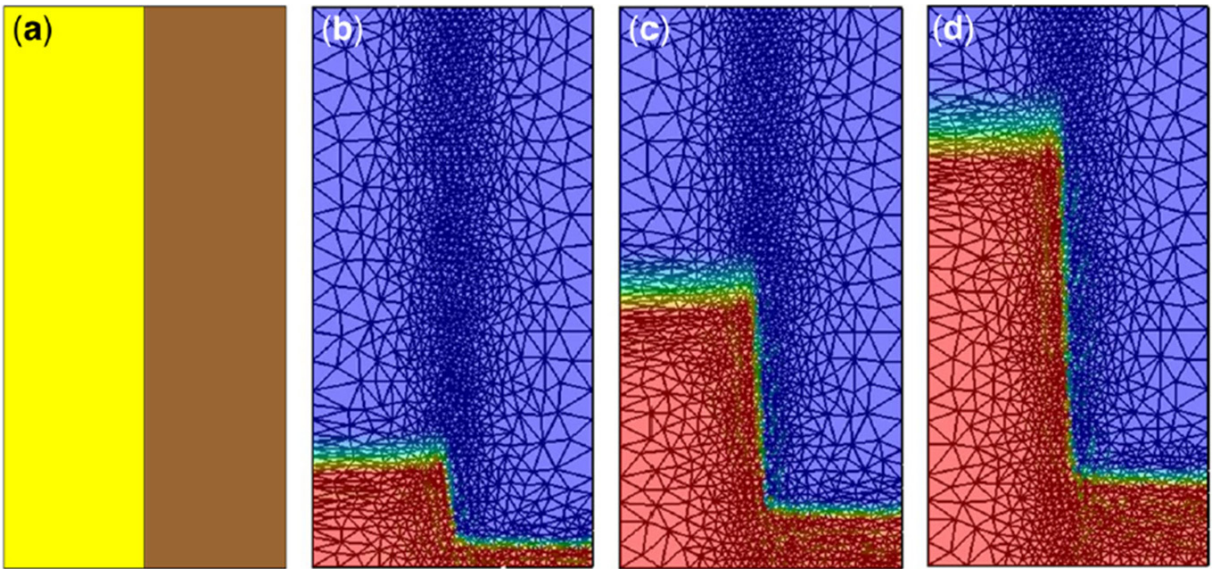


Figure 6.3: (a) Model of high (yellow) and low (brown) permeability layers. (b)–(d) Snapshots through time of the model during injection of a red tracer across the lower boundary of the model, moving upwards. The resolution of the model is higher at the flow interfaces, where computational power is required to resolve the fluid movements with realism: at the interface between the two vertical layers; at the tracer front between the tracer-saturated fluid (in red) and the initial fluid in place (blue), in each layer (Jackson *et al.*, in press).

6.3. Upscaling methodologies for heterolithic sandstones

The surface-based modelling methodology developed in this study could be adapted to other tidally-influenced heterolithic sandstones, including those featuring parallel-bedding, wavy-bedding or sigmoidal bedding. For each of these heterolithic sandstones, a template surface may be defined with specific input parameters that describe the geometry of stratal surfaces (Figure 6.4). Mini-models of the different heterolithic facies types could be built, and their effective reservoir properties extracted after flow simulation.

However, effective reservoir properties extracted from the mini-models are not directly implemented at the length-scale of an entire field in reservoir models. Reservoir properties are defined in the geological model for each cell depending on its facies code during property modelling; reservoir properties are defined by the upscaling of the values from the grid cells of the geological model to the grid cells of the simulation model. When reservoir model grid cells are populated with a combination of facies types in their precursor geological model grid cells, upscaled reservoir properties are typically averaged depending on the proportion of each facies present (e.g. Renard and de Marsily, 1997). Averaging techniques introduce an

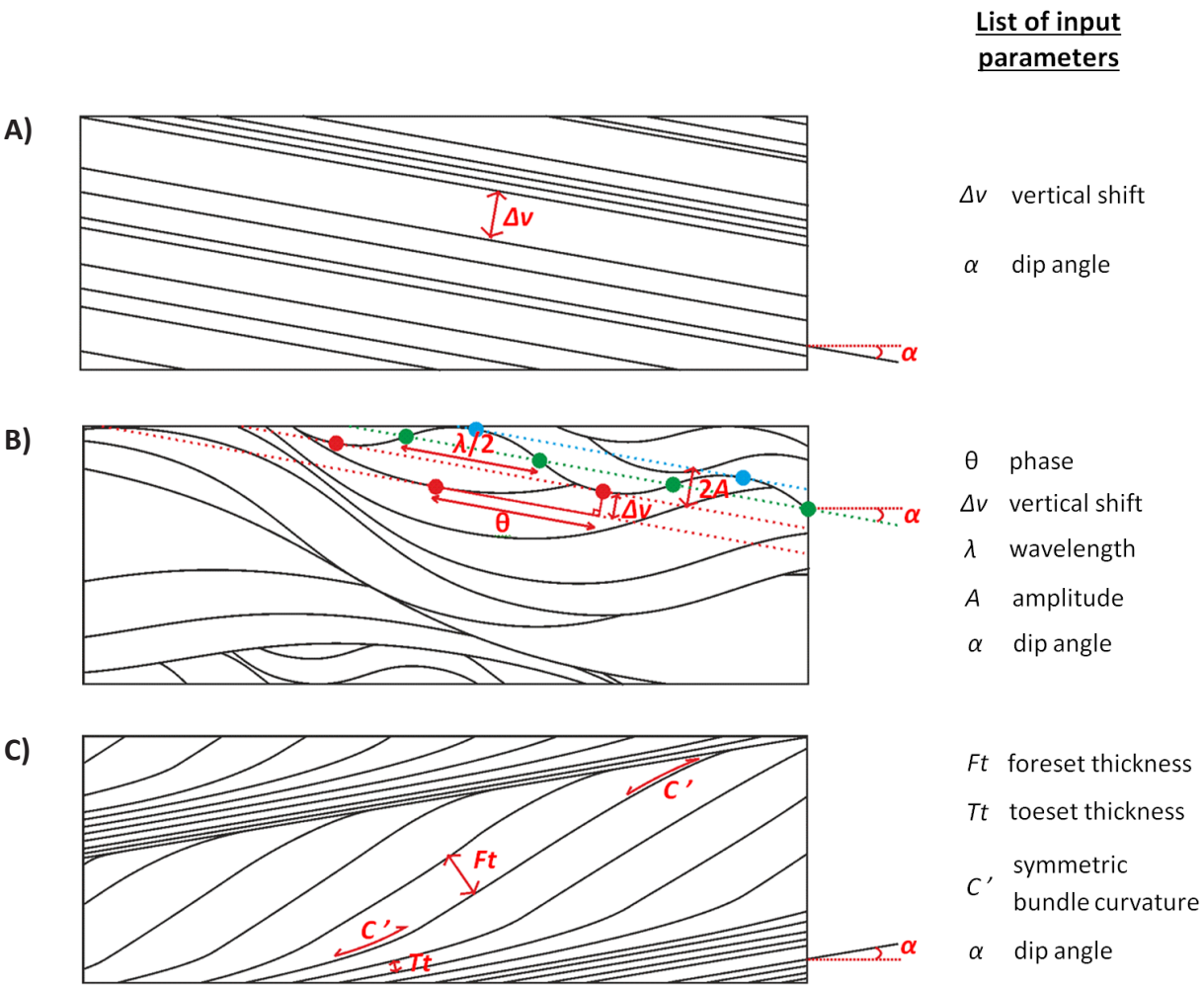


Figure 6.4: Cartoons illustrating three alternative template surfaces to capture the different bedding styles in surface-based models of tidally-influenced heterolithic sandstones, following the methodology presented in Chapter 3. The input geometrical parameters required for constraining the surface geometry and distribution are listed for each example. A) Parallel-bedding template; B) Wavy-bedding template; C) Sigmoidal-bedding template.

error in the effective properties, especially if the tortuosity of the flow is convoluted due to a complex 3D distribution and connectivity of permeable facies (Jackson *et al.*, 2003, 2005). The same problem was already raised but at a smaller length-scale when defining effective reservoir properties for heterolithic sandstones (see Chapter 4).

During upscaling, the facies model is transposed from the geological model grid to the reservoir model grid, making one reservoir model grid cell out of c. ten geological model grids, and defining one unique facies association code in the reservoir model cell. Reservoir properties are then assigned to this reservoir model grid cell by averaging the values of the geological model grid cells, depending on the facies association code. Instead of having the cells of the reservoir model being populated with one unique facies or facies association

code, facies proportions averaged by geological model cell volume could be implemented in the reservoir model cells. Thus reservoir properties which are assigned to the reservoir model cells would be derived from the specific facies proportions of the cells, not only from the single facies association code. One advantage is that upscaled reservoir properties will remain constant over a large distance if the facies proportions stay similar. As highlighted by Jackson *et al.* (2013), there is no ground for favouring spurious variations over constant values of petrophysical properties in regions of the reservoir model, as is typical after upscaling of grid-based geostatistical distributions of modelled properties, if the corresponding, realistic geological model shows no variations in facies proportions and distribution.

Facies association models should be created at an intermediate scale between the metre scale mini-models of heterolithic facies and the hundreds of metre-scale grid cell of the reservoir model. The facies association models would correspond to the deposits of typical morphological elements or genetic units in tidally-influenced depositional environments, such as tidal channels and tidal bars. Using a similar surface-based methodology to the one presented in this thesis, the key stratal surfaces at the tens-of-metre lengthscale should be identified and stochastically incorporated in the model (e.g. channel boundaries, bar and channel-margin accretion surfaces, facies boundaries, cross-bed set boundaries). The effective reservoir properties computed after flow simulation of the facies mini-models should be used to populate the facies-association models. Such methodology is similar to the approach of geopseudo functions (Ringrose *et al.*, 1993; Pickup *et al.*, 1994; Pickup and Sorbie, 1996). Functions relating effective reservoir properties to one (such as mudstone proportion in the model) or a set of parameters are used to populate reservoir properties in successive reservoir models, with higher length-scales. To be accurate though, the methodology uses the principle that the functions are defined at an REV for the length-scale considered. A problem risen by previous studies is that REV exist hypothetically, but cannot always be defined due to the stacking and erosion of successive layers, creating facies associations of variable composition. The variability featured geologically would prevent sufficient extent of the facies both laterally and vertically so that the reservoir performances of the facies would be those observed in models built at the REV.

The tidal cross-bedded sandstone facies is a good example of this problem. In Chapter 4, we have identified a REV at a length-scale similar to the cross-bed set length-scale (c. 1 m^3). The models generated for flow simulation in Chapters 4 and 5 are of similar length-scale (9 m^3) but do not capture in a sufficient representative way the variations of the cross-bed set dimensions as identified in our statistical analysis in Chapter 3 (i.e. only portions of 4 to 6 cross-bed sets in the model), and their erosive and stacking pattern as observed at outcrop location (Figure 3.8). In particular, layers made of portions of trough cross-bed sets alternate with layers made of tabular cross-bed sets, so the size of a REV for the trough cross-bed set facies or the tabular cross-bed set facies do not seem to be preserved in actual subsurface examples. An intermediate model, incorporating simplified cross-bed set geometry could be created as an intermediate between the cross-bed set REV identified in Chapter 4 and the reservoir cell length-scale. This model would capture the distribution of toeset regions in each cross-bed set with the modelling of the foreset/toeset boundary (line Γ in Figure 3.5), with effective permeability for the foreset cells being derived from 1 m^3 mini-models of foreset only regions, and effective permeability for the toeset cells depending on the mudstone content being derived from wavy-bedding mini-models studied by Ringrose *et al.* (2005).

Of course the best approach would be to have no upscaling step at all. Upscaling is only required because the flow simulator can handle a limited amount of cells for the required calculations. In a next-generation flow simulator using unstructured, adaptive meshes, an increased number of stratal surfaces at different length-scales could be included in the reservoir simulation models as the resolution of the grid is constantly optimized, minimizing the number of cells required to resolve the fine-scale details of the interfaces. In parallel, computational resources should increase, allowing direct use of the geological model with its fine resolution for flow simulation. But full representation will never be reached except if the pore structure at microscopic length-scale is captured, which means a judicious selection of the heterogeneities to be included in the models will always be required.

6.4. Recommendations for future work

The research presented in this thesis can lead to further work in the following areas:

(1) The mudstone frequency function for 3D modelling of the mudstone drapes has been found to be the predominant parameter for calculating effective permeabilities, as the tortuosity of flow is extremely sensitive to any variation in the coverage and continuity of mudstone drapes. The frequency function presented in the study has been defined from the statistical analysis of three cross-bed sets at one specific outcrop, using a total of 90 foreset-toeset surfaces. This dataset needs to be enlarged by further targeted data collection, as uncertainty associated with variations in cross-bedding geometry is not currently assessed.

(2) Surface-based algorithms should be developed for other tidal heterolithic deposits containing stratal surfaces of different geometry, such as parallel-bedding, wavy-bedding and sigmoidal-bedding, to represent the diversity of tidal reservoir facies. The cross-bedding template surfaces of this study can be replaced by other template surfaces reproducing the geometry of the different bedding styles.

(3) Combine the different facies represented in mini-models into larger reservoir models representing the stacking of facies into facies associations in tidally-influenced depositional environments. Effective flow properties of facies associations such as tidal channels, tidal bars and embayment fills could be derived in this way. Such models could allow the upscaling step from geological model grid cells to reservoir model grid cells to be bypassed. In fact, there would be no need for a precise geological model, as sedimentological objects would be introduced by surface-based modelling in the reservoir model directly, and effective properties of the facies associations should be assigned to the reservoir model cells.

(4) Heterolithic sandstones are encountered in other, non-tidal depositional environments. The surface-based modelling methodology and the effective reservoir property characterisation workflow developed in this research could be applied to

other heterolithic facies, for example in deep-marine environments within turbiditic heterolithic sandstones.

(5) Validation of the results of effective permeability, relative permeabilities to oil and water, and irreducible oil saturation should be performed by comparison with an actual example of a heterolithic sandstone reservoir. Reservoir properties should be predicted using the methodology presented in the thesis and available subsurface data, and compared with actual results using history matching against production data.

(6) The mini-models could be gridded using unstructured, adaptive, tetrahedral meshes for flow simulation, in order to reduce the numerical artefacts introduced by the simulation software. This would require use of a next-generation flow simulator capable of solving the flow equations for such complex grids. A finer mesh could be defined around the mudstone drapes in order to trace in detail the oil trapped in the models, and then to better understand the mechanisms of oil entrapment in heterolithic sandstones.

6.5. Conclusions

At the end of this study, the following conclusions can be drawn, in response to the objectives listed in Chapter 1:

(1) A new surface-based methodology for modelling heterolithic tidal sandstones with mudstone drapes has been created. The surface-based methodology is independent of the length-scale of the heterogeneities and is based on the accurate reproduction of the hierarchy of heterogeneity surface. As such it can be applied to a variety of facies, facies associations or full-field reservoir for flow simulation purposes. The methodology was implemented in independent software using outcrop analogue measurements

of heterogeneities as input parameters. A statistical analysis of the heterogeneity geometries at two outcrop locations of the Dir Abu Lifa Member has constrained input parameters for building 9 m^3 generic models of one foreset-dominated tabular cross-bedded model and one toeset-dominated trough cross-bedded model and one intermediate model of tidal cross-bedded sandstones. The two first models are used as end-member cases for the range of cross-bedded sandstones observed at outcrop. The statistical analysis on geometric parameters performed at the outcrop location is very valuable on its own as a little number of studies has reported robust statistics on centimeter and meter scale heterogeneities related to the tide influence in ancient sedimentological records (as opposed to studies on modern analogues or tank experiments).

(2) The modelling methodology allows creating realistic high resolution models fit for flow simulation, so that effective permeability of tidal cross-bedding sandstones was derived for a large range of input parameters inducing the cross-bedding surface geometry. Values of effective permeabilities computed from flow simulation of generic models of tidal cross-bedded sandstones are dependent on the volume sampled, but variation is minimized for sample volumes greater than c. 1 m^3, which approximates a Representative Elementary Volume (REV) for a cross-bed set. Mudstone drapes along foreset-toeset surfaces decrease the effective permeability of the modelled volume.

(3) The value of effective permeability is dependent on the mudstone fraction in the model. The range of realistic value of effective permeability for one mudstone fraction is high due to multiple possible distribution and preservation scenarios of the mudstone drapes along the foreset surfaces, but especially in the toeset parts. Variation in the continuity of sandstone laminae in the toeset regions of cross-bed sets has a critical control on effective permeability. The occurrence of discontinuous sandstone laminae in lenticular-bedded toesets results in flow occurring only through sandy foreset regions of cross-bed sets. The occurrence of continuous sandstone laminae in wavy-bedded toesets enables horizontal flow also through muddy toeset regions.

(4) To the question: Can the effective permeability be predicted from the single mudstone proportion parameter? The answer is no. To the question: Is there any single parameter inducing the cross-bedding surface – and then the mudstone drape – geometry that controls the effective permeability? The answer is still no. No single parameter describing cross-bedding geometry – being the mudstone proportion content, the style of cross-bedding whether tabular or trough, the foreset thickness, the toeset dip angle, the dune climb angle, the foreset to toeset volume ratio or the mudstone drape pattern – exerts a dominant control on effective permeability. Instead, parameters that control the distribution, extent and geometric configuration of toesets, which are preferentially lined by mudstone drapes and possess very variable reservoir performances depending on the connectivity of sandstone laminae, exert a significant influence on effective permeability in combination. However, for all scenarios tested, and despite a large range of values in the effective permeability, the shape of the curve of effective permeability depending on mudstone fraction is always the same, similar to the shape observed for studies on wavy-bedding structures, meaning that the tidal cross-bedded sandstones follow the percolation theory. A percolation threshold exists for each model (i.e. a specific mudstone fraction).

(5) Anisotropy in relative permeabilities and irreducible oil saturation is observed, such that more oil is trapped in the model after drainage by a vertical flow than for drainage by a horizontal flow. Increased mudstone drape coverage of foreset-toeset surfaces leads to a net increase in residual oil saturation S_{or} (+146% for a strike oriented flow, from a 25% to a 70% mudstone drape coverage scenario in the intermediate trough cross-bedded model) but has no impact on the mobility of oil, as oil relative permeabilities remain unchanged; only water mobility is affected by the increase in mudstone drape coverage but only close to oil residual saturation (decrease of 15% in maximum water permeability krw, from a 25% to a 70% mudstone drape coverage scenario in the intermediate trough cross-bedded model). The increase in bypassed oil (i.e. increase in S_{or}) is observed in toeset regions where the amalgamation of mudstone drapes combined with thinning of sandstone laminae effectively form “dead-end” flow paths in three dimensions.

Chapter 7
References

Abdel-Fattah, Z. A., Gingras, M. K., Caldwell, M. W., and Pemberton, S. G. (2010): "Sedimentary environments and depositional characteristics of the Middle to Upper Eocene whale-bearing succession in the Fayum Depression, Egypt", *Sedimentology*, Vol. 7, n°2, pp. 446-476

Ainsworth, B. R., Sanlung, M., and Duivenvoorden, S. T. C. (1999): "Correlation techniques, perforation strategies, and recovery factors: an integrated 3-D reservoir modelling study, Sirikit field, Thailand", *AAPG Bulletin*, Vol. 83, pp. 1535-1551

Allen, J. R. L. (1968): *Current ripples*, Amsterdam, North-Holland

Allen, J. R. L. (1980): "Sand waves: a model of origin and internal structure", *Sedimentary Geology*, Vol. 26, pp. 281-328

Allen, J. R. L. (1981): "Palaeotidal speeds and ranges estimated from cross-bedding sets with mud drapes", *Nature*, Vol. 293, pp. 394-396

Ashley, G. M. (1990): "Classification of large-scale subaqueous bedforms; a new look at an old problem", *Journal of Sedimentary Petrology*, Vol. 60, pp. 160-172

Bear, J. (1972): *Dynamics of fluids in porous media*, American Elsevier, New York

Begg, S. H. and King, P. R. (1985): "Modelling the effects of shales on reservoir performance: Calculation of effective vertical permeability", Society of Petroleum Engineers paper 13529, presented at the 1985 SPE Symposium on Reservoir Simulation, Dallas, TX, 10–13 February

Bellian, J. A., Kerans, C., and Jennette, D. C. (2005): "Digital outcrop models: Applications of terrestrial scanning LIDAR technology in stratigraphic modelling", *Journal of Sedimentary Research*, Vol. 72, pp. 166–176

Boersma, J. R. (1969): "Internal structure of some tidal mega-ripples on a shoal in the Westerschelde estuary, the Netherlands", *Geologie en Mijnbouw*, Vol. 48, pp. 409-414

Boersma, J. R., and Terwindt, J. H. J. (1981): "Neap-spring tide sequences of intertidal shoal deposits in a mesotidal estuary", *Sedimentology*, Vol. 28, pp. 151-170

Bown, T. M., and Kraus, M. J. (1988): "Geology and paleoenvironment of the Oligocene Jebel Qatrani Formation and adjacent rocks, Fayum depression, Egypt", *U.S. Geological Survey Professional* paper 1452, pp. 1–60

Box, G. E. P., and Draper, N. R. (1987): *Empirical model building and response surfaces*, Wiley, New York

Brandsæter, I., Wist, H. T., Næss, A., Lia, O., Arntzen, O. J., Ringrose, P. S., Martinius, A. W. and Lerdahl, T. R. (2001): "Ranking of stochastic realizations of complex tidal reservoirs using streamline simulation criteria", *Petroleum Geoscience Special Issue*, Vol. 7, pp. 53–63

Brandsæter, I., McIlroy, D., Lia, O., Ringrose, P., and Næss, A. (2005): "Reservoir modelling and simulation of Lajas Formation outcrops (Argentina) to constrain tidal reservoirs of the Halten Terrace (Norway)", *Petroleum Geoscience*, Vol. 11, pp. 37–46

Bryant, I. D., and Flint, S. S. (1993): "Quantitative clastic reservoir modelling : problems and perspectives", *In*: *The Geological Modelling of Hydrocarbon Reservoirs and Outcrop Analogues*, Flint, S. S., and Bryant, I. D. (eds), *International Association of Sedimentologists Special Publications*, Vol. 15, pp. 3-20

Bryant, I. D., Carr, D., Cirilli, P., Drinkwater, N., McCormick, D., Tilke, P., and Thurmond, J. (2000): "Use of 3D digital analogs as templates in reservoir modelling", *Petroleum Geoscience*, Vol. 6, pp. 195–201

Ciammetti, G., Ringrose, P. S., Good, T. R., Lewis, J. M. L., and Sorbie, K. S. (1995): "Waterflood recovery and fluid flow upscaling in a shallow marine and fluvial sandstone sequence", Society of Petroleum Engineers paper 79669

Dake, L. P. (1983): *Fundamentals of Reservoir Engineering*, Elsevier Science, eds., 462 pp.

Dalland, A., Worsley, D. and Ofstad, K. (1988): "A lithostratigraphic scheme for the Mesozoic and Cenozoic succession offshore mid- and northern Norway", *Norwegian Petroleum Directorate Bulletin*, Vol. 4, pp. 1-65

Dalrymple, R. W., Knight, R. J., and Lambiase, J. J. (1978): "Bedforms and their hydraulic stability relationships in a tidal environment, Bay of Fundy, Canada", *Nature*, Vol. 275, pp. 100-104

Dalrymple, R. W. (1984): “Morphology and internal structure of sand waves in the Bay of Fundy”, *Sedimentology*, Vol. 31, pp. 365-382

Dalrymple, R. W., Baker, E. K., Harris, P. T., and Hughes, M. G. (2003): “Sedimentology and stratigraphy of a tide-dominated, foreland-basin delta (Fly River, Papua New Guinea)”, *In*: *Tropical Deltas of Southeast Asia; Sedimentology, Stratigraphy, and Petroleum Geology*, Sidi, F. H., Nummedal, D., Imbert, P., Darman, H., and Posamentier, H. W., eds., *SEPM Special Publication*, Vol. 76, pp. 147-173

Dalrymple, R. W., and Choi, K. (2007): “Morphologic and Facies Trends Through the Fluvial Marine Transition in Tide Dominated Depositional Systems: a Schematic Framework for Environmental and Sequence Stratigraphic Interpretation”, *Earth Science Reviews*, Vol. 81, Issues 3-4, pp. 135-174

Davies, D. R., Wilson C. R., and Kramer, S. C. (2011): “Fluidity: A fully unstructured anisotropic adaptive mesh computational modeling framework for geodynamics”, *G^3: Geochemistry, Geophysics, Geosystems*, Vol. 12

de Mowbray, T., and Visser, M. J. (1984): “Reactivation surfaces in subtidal channel deposits, Oosterschelde, Southwest Netherlands”, *Journal of Sedimentary Petrology* Vol.54 pp.811-824

DeBaun, D., Byer, T., Childs, P., Chen, J., Wells, M., Liu, J., Cao, H., Pianelo, L., Tilakraj, V., Crumpton, P., Walsh, D., Yardumian, H., Zorzynski, R., Lim, K.-T., Schrader, M., Zapata, V., Nolen., J., and Tchelepi, H. (2005): “An extensible architecture for next generation scalable parallel reservoir simulation”, *Society of Petroleum Engineers Journal* paper 93274

Deutsch, C.V., Xie, Y., and Cullick, A.S. (2001): “Surface geometry and trend modeling for integration of stratigraphic data in reservoir models”, Society of Petroleum Engineers paper 68817

Dreyer, T. (1992): “Significance of tidal cyclicity for modelling of reservoir heterogeneities in the lower Jurassic Tilje Formation, mid-Norwegian shelf”, *Norsk Geologisk Tidsskrift*, Vol. 72, pp. 159–170

Dreyer, T. (1993): “Geometry and facies of large-scale flow units in fluvial dominated fan-delta-front sequences” *In:* Ashton, M. (ed.) *Advances in Reservoir Geology. Geological Society (London) Special Publications*, Vol. 69, pp. 135–174

Ekern, O.F. (1990): “Midgard Field – Norway, southwest Central Graben, North Sea” *In:* Beaumont, A., and Foster, N. H. (eds), *Structural Traps IV, Tectonic and Non-Tectonic Fold Traps.* American Association of Petroleum Geologists Treatise of Petroleum Geology, Atlas of Oil and Gas Fields, pp. 141–171

Elliott, T., and Gardiner, A. R. (1981): “Ripple megaripple and sandwave bedforms in the macrotidal Loughor Estuary, South Wales, U. K.”, *Special Publication International Association of Sedimentologists*, Vol. 5, pp. 51-64

Gjelberg, J., Dreyer, T., Høie, A., Tjelland, T. and Lilleng, T. (1987): “Late Triassic to Mid-Jurassic sandbody development on the Barents and mid-Norwegian shelf” *In:* Brooks, J., and Glennie, K. W. (eds) *Petroleum Geology of North West Europe,* Proceedings of the 3rd Conference, Graham and Trotman, London, pp. 1105–1129

Graham, G. H., Jackson, M. D., and Hampson, G. J., in review: “Three dimensional modeling of clinoforms within shallow-marine reservoirs”, submitted to *AAPG Bulletin*

Haldorsen, H. H., and Lake, L. W. (1984): “A new approach to shale management in field-scale models”, *Society of Petroleum Engineers Journal*, Vol. 24, pp. 447-457.

Haldorsen, H. H. (1986): “Simulator parameter assignment and the problem of scale in reservoir engineering”, *In*: *Reservoir Characterisation*, Lake L. W., and Carroll, H. B., eds., Academic Press, London, pp. 293-340

Haldorsen, H. H., and Damsleth, E. (1990): “Stochastic modeling”, *Journal of Petroleum Technology*, Vol. 42, pp. 404-412.

Harms, J. C., Southard, J. B., and Walker, R. G. (1982): “Structures and sequences in clastic rocks”, *SEPM short course*, Vol. 9, *Society of Sedimentary Geology.*

Hartkamp-Bakker, C. A. (1991): “Capillary oil entrapment in crossbedded sedimentary structures of fluvial sandstone reservoirs”, Society of Petroleum Engineers paper 22761.

Henriquez, A., and Jourdan, C. (1996): “Challenges in modelling reservoirs in the North Sea and on the Norwegian shelf”, *In:* Glennie, K., and Hurst, A. (eds) *AD1995: NW Europe’s Hydrocarbon Industry.* Geological Society, London, pp. 157–166

Howell, J. A., Vassel, Å, and Aune, T. (2008a): "Modelling of dipping clinoform barriers within deltaic outcrop analogues from the Cretaceous Western Interior Basin, U.S.A." *In*: Robinson, A., Griffiths, P., Price, S., Hegre, J. and Muggeridge, A. H., eds., *The future of geologic modelling in hydrocarbon development*, *Geological Society (London) Special Publication*, Vol. 309, pp. 99-121.

Howell, J. A., Skorstad, A., MacDonald, A., Fordham, A., Flint, S., Fjellvoll, B., and Manzocchi, T. (2008b): "Sedimentological parameterization of shallow-marine reservoirs", *Petroleum Geoscience*, Vol. 14, pp. 17-34

Huang, Y., Ringrose, P. S., and Sorbie, K. S. (1996): "The effects of heterogeneity and wettability on oil recovery from laminated structures", Society of Petroleum Engineers paper 30781.

Ichaso, A. A. and Dalrymple, R. W. (2009): "Tide- and wave-generated fluid mud deposits in the Tilje Formation (Jurassic), offshore Norway", *Geology*, vol. 37, pp. 539-542.

Jackson, M. D., and Muggeridge, A. H. (2000): "The effect of discontinuous shales on reservoir performance during immiscible flow", *Society of Petroleum Engineers Journal*, Vol. 5, pp. 446–454

Jackson, M. D., Muggeridge, A. H., Yoshida, S., and Johnson, H. D. (2003): "Upscaling permeability measurements within complex heterolithic tidal sandstones", *Mathematical Geology*, Vol. 35, pp. 499-520

Jackson, M. D., Yoshida, S., Muggeridge, A. H., and Johnson, H. D. (2005): "Three-Dimensional Reservoir Characterisation and Flow Simulation of Heterolithic Tidal Sandstones", *AAPG Bulletin*, Vol. 89, n°4, pp. 507-528

Jackson, M. D., Hampson, G. J., and Sech, R. P. (2009): "Three-Dimensional Modelling of a Shoreface-Shelf Parasequence Reservoir Analogue: Part 2. Geologic Controls on Fluid Flow and Hydrocarbon Recovery", *AAPG Bulletin*, Vol. 93, n°9, pp. 1183-1208

Jackson, M. D., Gomes, J. L. M. A., Mostaghimi, P., Percival, J. R., Tollit, B. S., Pavlidis, D., Pain, C. C., El-Sheikh, A. H., Muggeridge, A. H., and Blunt, M. J. (2013): "Reservoir modeling for flow simulation using surfaces, adaptive unstructured meshed and control-volume-finite-element methods", Society of Petroleum Engineers paper 163633

Jackson, M. D., Hampson, G. J., El-Sheikh, A., Saunders, J. H., Graham, G. H., and Massart, B. Y. G., in press: "Surface-based reservoir modelling for flow simulation", *Geological Society (London) Special Publication*, Vol. 387

Journel, A. G. and Huijbregts, C. J. (1978): *Mining Geostatistics*, Academic Press, New York.

Jung, A., Aigner, T., Palermo, D., Nardon, S. and Pontiggia, M. (2012): "A new workflow for carbonate reservoir modelling based on MPS: shoal bodies in outcrop analogues (Triassic, SW Germany)", *In*: *Advances in Carbonate Exploration and Reservoir Analysis*, Garland, J., Neilson, J. E., Laubach, S. E. and Whidden, K. J. (eds), *Geological Society (London) SpecialPublications*, Vol. 370, pp. 277-293

Karlsson, W. (1984): "Sedimentology and diagenesis of Jurassic sediments offshore mid-Norway", *In:* Spencer, A. M., Holter, E., Johnson, S. O., Mørk, A., Songstad, P., and Spinnanger, Å. (eds), *Petroleum Geology of the North European Margin,* Proceedings of the 2nd Conference, Norwegian Petroleum Society, Graham & Trotman, London, pp.389–396

Kjønsvik, D., Doyle, J., Jacobsen, T., and Jones, A. (1994): "The effects of sedimentary heterogeneities on production from a shallow marine reservoir – What really matters?", Society of Petroleum Engineers paper 28445

Klein, G. dV. (1970): "Depositional and dispersal dynamics of intertidal sand bars", *Journal of Sedimentary Petrology*, Vol. 40, pp. 1095-1127

Kortekaas, T. F. M. (1985): "Water/oil displacement characteristics in crossbedded reservoir zones", *Society of Petroleum Engineers Journal*, Vol. 25, pp. 917-926, Society of Petroleum Engineers paper 12112

Kvale, E. P., Archer, A. W., and Johnson, H. R. (1989): "Daily, monthly, and yearly tidal cycles within laminated siltstones of the Mansfield Formation (Pennsylvanian) of Indiana", *Geology (Boulder)*, Vol. 17, pp. 365-368

Lasseter, T. R., Waggoner, J. R., and Lake, L. W. (1986): "Reservoir heterogeneities and their influence on ultimate recovery", *In*: Lake, L. W. (ed.), *Reservoir characterisation*, London, Academic Press, pp. 545–559

Legler, B., Johnson, H. D., Hampson, G. J., Massart, B. Y. G., Jackson, C. A.-L., Jackson, M. D., El-Barkooky, A., and Ravnas, R. (2013): "Facies model of a fine-grained, tide-dominated delta: Lower Dir Abu Lifa Member (Eocene), Western Desert, Egypt", *Sedimentology*, Vol. 60, pp. 1313-1356

MacDonald, A. C., Fält, L.-M. and Hektoen, A.-L. (1998): "Stochastic modeling of incised valley geometries", *AAPG Bulletin*, Vol. 82, pp. 1156-1172

Martinius, A. W., Kaas, I., Næss, A., Helgesen, G., Kjærefjord, J. M. and Leith, D. A. (2001): "Sedimentology of the heterolithic and tide-dominated Tilje Formation (Early Jurassic, Halten Terrace, offshore mid-Norway)" *In:* Martinsen, O. J., and Dreyer, T. (eds) *Sedimentary Environments Offshore Norway – Paleozoic to Recent*, Norwegian Petroleum Society, *Special Publications*, Vol. 10. Elsevier, Amsterdam, pp. 103–144

Martinius, A. W., Ringrose, P. S., Brostrøm, Elfenbein, C., Næss, A., and Ringås, J. E. (2005): "Reservoir Challenges of Heterolithic Tidal Sandstone Reservoirs in Halten Terrace, mid-Norway", *Petroleum Geoscience*, EAGE/Geological Society of London, Vol. 11, n°1, pp. 3-16

Martinius, A. W., and van den Berg, J. H. (2011): *Atlas of sedimentary structures in estuarine and tidally-influenced river deposits of the Rhine-Meuse-Scheldt system*, EAGE Publications BV, Houten, 298 pp.

Middleton, G. V., and Southard, J. B. (1984): *Mechanics of sediment movement*, SEPM Short course 3, Society of Sedimentary Geology, Tulsa, USA

Nio, S.-D., and Yang, C.-S. (1991): "Diagnostic Attributes of Clastic Tidal Deposits: a Review", *Clastic Tidal Sedimentology*, Canadian Society of Petroleum Geologists, Memoir 16, pp. 3-28

Nordhal, K., Ringrose, P. S., and Wen, R. (2005): "Petrophysical Characterisation of a Heterolithic Tidal Reservoir Interval Using a Process Based Modelling Tool", *Petroleum Geoscience*, EAGE/Geological Society of London, Vol. 11, pp. 17-28

Nordahl, K., Martinius, A. W., and Kritski, A. (2006): "Time-series analysis of a heterolithic, ripple-laminated deposit (Early Jurassic, Tilje Formation) and implications for reservoir modelling", *Marine Geology*, Vol. 235, n°1-4, pp. 255-271

Nordahl, K., and Ringrose, P. S. (2008): "Identifying the Representative Elementary Volume for Permeability in Heterolithic Deposits Using Numerical Rock Models", *Math Geoscience*, Vol. 40, pp. 753-771

Norris, R. J., and Lewis, J. J. M. (1991): "The Geological Modeling of Effective Permeability in Complex Heterolithic Facies", Society of Petroleum Engineers Paper 22692, presented at the 66th annual technical conference and exhibition, Dallas, TX, USA, 6-9 October 1991

Pain, C. C., Umpleby, A. P., de Oliveira C. R. E., and Goddard A. J. H. (2001): "Tetrahedral mesh optimisation and adaptivity for steady-state and transient finite element calculations", *Comp. Meth. in Appl. Mech and Eng.*, Vol. 190, pp. 3771-3796

Pedersen, T., Harms, J. C., Harris, N. B., Mitchell, R. W., and Tooby, K. M. (1989): "The role of correlation in generating the Heidrun Field geological model", *In:* Collinson, J. D. (ed.), *Correlation in Hydrocarbon Exploration*, Graham & Trotman, London, pp. 327–338

Peihua, X. (1986): "A point bar facies reservoir model – semicommunicated sandbody", Society of Petroleum Engineers Paper 14837 presented at the 1986 SPE International Meeting on Petroleum Engineering, Beijing, 17-20 March

Pickup, G. E., Ringrose, P. S., Forrester, M. M., Jensen, J. L., Sorbie, K. S., Rezigh, A. (1994): "The Geopseudo Atlas; geologically based upscaling of multiphase flow", Society of Petroleum Engineers paper 27565.

Pickup, G. E., and Carruthers, D. (1996): "Effective flow parameters for 3D reservoir simulation", Society of Petroleum Engineers paper 35495.

Pickup, G. E., and Sorbie, K. S. (1996): "The scaleup of two-phase flow in porous media using phase permeability tensors", Society of Petroleum Engineers paper 28586.

Pickup, G. E., Ringrose, P. S., Sharif, A. (2000): "Steady-state upscaling; from lamina-scale to full-field model", *Society of Petroleum Engineers Journal*, Vol. 5, pp. 208-217

Pyrcz, M. J., Catuneanu, O., and Deutsch, C. V. (2005): "Stochastic surface-based modelling of turbidite lobes", *AAPG Bulletin*, Vol. 89, pp. 177-191

Reading, H. G. (1986): "Facies", *In*: *Sedimentary environments and facies*, Reading, H. G. (ed), Blackwell Science, Oxford, pp 4-19

Reineck, H. E., and Singh, I. B. (1967): “Primary sedimentary structures in the Recent sediments of the Jade, North Sea”, *Marine Geology*, Vol. 5, pp. 227-235

Reineck, H. E., and Wunderlich, F. (1968): “Classification and origin of flaser and lenticular bedding”, *Sedimentology*, Vol.11, n°1-2, pp. 99-104

Reineck, H. E., and Singh, I. B. (1980): *Depositional sedimentary environments with reference to terrigenous clastics*, 2nd edition, Springer-Verlag, Berlin

Renard, P., and de Marsily, G. (1997): “Calculating equivalent permeability: a review”, *Advances in Water Resources*, Vol. 20, pp. 253-278

Richardson, J. G., Harris, D. G., Rossen, R. H., van Hee, G. (1978): “The Effect of Small Discontinuous Shales on Oil Recovery”, *Journal of Petroleum Technology*, Vol. 30, pp. 1531-1537

Ringrose, P. S., Sorbie, K. S., Corbett, P. W. M. and Jensen, J. L. (1993): “Immiscible flow behaviour in laminated and cross-bedded sandstones”, *Journal of Petroleum Science and Engineering*, Vol. 9, pp. 103-124.

Ringrose, P. S., Skjetne, E., and Elfenbein, C. (2003): “Permeability Estimation Functions Based on Forward Modelling of Sedimentary Heterogeneity” Society of Petroleum Engineers paper 84275, presented at the SPE Annual Technical Conference and Exhibition held in Denver, Colorado, USA, 5–8 October

Ringrose, P. S., Nordhal, K., and Wen, R. (2005): “Vertical Permeability Estimation of Heterolithic Tidal Deltaic Sandstones”, *Petroleum Geoscience*, EAGE/Geological Society of London, Vol. 11, n°1, pp. 29-36

Rubin, D. M. (1987): *Cross-bedding, bedforms, and palaeocurrents. Concepts in Sedimentology and Paleontology*, *Society of Economic Palaeontologists and Mineralogists Special Publication*, Vol. 1

Rubin, D. M., and Carter, C. L. (2005): “Bedforms 4.0; MATLAB code for simulating bedforms and cross-bedding”, Open-File report, U. S. Geological Survey

Sech, R. P., Jackson, M. D., and Hampson, G. J. (2009): “Three-Dimensional Modelling of a Shoreface-Shelf Parasequence Reservoir Analogue: Part 1. Surface-based Modelling to Capture High Resolution Facies Architecture”, *AAPG Bulletin*, Vol. 93, n°9, pp. 1155-1181

Sgavetti, M. (1992): “Criteria for stratigraphic correlation using aerial photographs: Examples from the south-central Pyrenees”, *AAPG Bulletin*, Vol. 76, pp. 708–730

Strebelle, S. (2002): “Conditional simulation of complex geological structures using multiple-point statistics”, *Mathematical Geology*, Vol. 34, pp. 1-21

Taylor, A. M., and Gawthorpe, R. L. (1993): “Application of sequence stratigraphy and trace fossil analysis to reservoir description: Examples from the Jurassic of the North Sea”, *In:* Parker, J. R. (ed.), *Petroleum Geology of Northwest Europe: Proceedings of the 4th Conference*”, Geological Society, London, pp. 317–335

Terwindt, J. H. J. (1971): “Lithofacies of inshore estuarine and tidal inlet deposits”, *Geologie en Mijnbouw*, Vol. 50, pp. 515-526

Thomas, J. M. D. (1990): “The Movement of Oil Initially Bypassed Behind Stochastic Shale Barriers”, *In*: *North Sea Oil and Gas Reservoirs II*, Buller, A. T. *et al.*, eds., Graham and Trotman, London, pp. 437-444

Uncles, R. J., Stephens, J. A. and Law, D. J. (2006): “Turbidity maximum in the macrotidal, highly turbid Humber Estuary, UK; flocs, fluid mud, stationary suspensions and tidal bores.”, *Estuar. Coast. Shelf Sci.*, vol. 67, pp. 30-52.

van de Weerd, A. A. (1996): “Reservoir geology of the shallow-marine Early Jurassic Tilje Formation of the Njord Field, offshore Mid-Norway”, *In:* Johnson, H. D., Wonham, J. P., and Gupta, R. (eds), *Geological Characterisation of Shallow Marine Sands for Reservoir Modelling and High Resolution Stratigraphic Analysis*, Final Report European Community, Joule Program, Vol. 1

van den Berg, J. H., Boersma, J. R., and van Gelder, A. (2007): “Diagnostic sedimentary structures of the fluvial-tidal transition zone; Evidence from deposits of the Rhine and Meuse”, *Geology en Minjbouw*, Vol. 86, pp. 287-306

van Lingen, P. P., Bruining, J., and van Kruijsdijk, C. P. J. W. (1996): “Capillary entrapment caused by small-scale wettability heterogeneities”, *SPE Reservoir Engineering*, Vol. 9, pp. 93-99

Visser, M. J. (1980): “Neap-spring cycles reflected in Holocene subtidal large-scale bedform deposits: a preliminary note”, *Geology*, Vol. 8, pp. 543-546

Warren, J. E., and Price, H. S. (1961): "Flow in heterogeneous porous media", *Society of Petroleum Engineers Journal*, Vol. 1, pp. 153-169

Weber, K. J. (1982): "Influence of Common Sedimentary Structures on Fluid Flow in Reservoir Models", Society of Petroleum Engineers Paper 9247

Weber, K. J. (1986): "How heterogeneity affects oil recovery", *In*: Lake, L. W., and Carroll Jr., H. B., eds., *Reservoir characterisation*, Academic Press, New York, pp. 487-544.

Wen, R.-J., Martinius, A. W., Næss, A., and Ringrose, P. S. (1998): "Three dimensional simulation of small-scale heterogeneity in tidal deposits – A process-based stochastic method", *In:* Buccianti, A., Nardi, G., and Potenza, A. (eds), Proceedings of the 4th Annual Conference of the International Association of Mathematical Geology, Ischia, De Frede, Naples, pp. 129–134

White, C. D., and Barton, M. D. (1999): "Comparison of the recovery behavior of contrasting reservoir analogs in the Ferron Sandstone using outcrop studies and numerical simulation" Report of investigations n°249, Bureau of Economic Geology, The University of Texas at Austin, 46 p.

White, C. D., Willis, B. J., Dutton, S. P., Bhattacharya, J. P., and Narayanan, K. (2004): "Sedimentology, statistics, and flow behavior for a tide-influenced deltaic sandstone, Frontier Formation, Wyoming, United States", *In*: Grammer, G. M., Harris, P. M., and Eberli, G. P. (eds), *Integration of outcrop and modern analogs in reservoir modelling*, *AAPG Memoir*, Vol. 80, pp. 129-152

Willis, B. J., and White, C. D. (2000): "Quantitative Outcrop Data for Flow Simulation", *Journal of Sedimentary Research*, Society for Sedimentary Geology, Vol. 70, n°4, pp. 788-802

Wright, L. D., Wiseman, W. J., Bornhold, B. D., Prior, D. B., Suhayda, J. N., Keller, G. H., Yang, Z. S. and Fan, Y.B. (1988): "Marine dispersal and deposition of Yellow River silts by gravity-driven underflows.", *Nature*, vol. 332, pp. 629–632.

Zahoor, M. K., Derahman, Nawi Dearhman, M., Yunan, M. H. (2009): "Correlation for prediction and estimation of capillary pressure to account for wettability variations within reservoir - part 2", SPE/EAGE Reservoir Characterisation & Simulation Conference, United Arab Emirates.

Zhang, X., Pyrcz, M. J. and Deutsch, C. V. (2009): “Stochastic surface modeling of deepwater depositional systems for improved reservoir models”, *Journal of Petroleum Science and Engineering*, Vol. 68, pp. 118-134

Appendix
Program description

The novel surface-based modelling technique described in Chapter 3 of this thesis gave the framework for the creation of a piece of software that generates the tidal cross-bedded surface-based mini-models used in flow simulation experiments. The program can be found in the following appendices. We use the same methodology subdivisions of the surface-based workflow to explain the different parts of the program.

1) Modelling of elemental volumes

The volume of the model is specified giving the dimensions of the model in an input text file called “parameters.txt”. In the same input file, the positions of the elemental volumes subdividing the model of interest are specified. In our case, the elemental volumes created are ellipsoids to represent cross-bed sets in 3D (Figures 3.1, 3.2, 3.3 & 3.4) so the input parameters correspond to the number of ellipsoidal volumes, the positions of the centres of the volumes in 3D, the major and minor axis dimensions and the orientations (3 angles: heading, pitch, roll) . The positions of these ellipsoids were traced and extrapolated from one outcrop analogue example for the models presented in this thesis, but a randomly generated subdivision of the volume of interest could be implemented in the software to generate this list of input parameters. The subroutine “enveloppes_ellipsoid” generates the surfaces corresponding to the base and top boundaries of the elemental volumes. The surfaces are exported as zmap+ files in the subroutine “writezmapfile” that can be imported in Petrel or RMS for visualisation purposes. zmap+ format consists on a list of z-depth coordinates of regularly spaced (x,y) points in top view, with a specified number of nodes in the x direction and another specified number of nodes in the y direction. The surfaces are extended to the boundaries of the model. When a surface is eroded by another one, the initial surface takes the depth values of the eroding surface. That way, the surfaces can be extended to the boundaries of the model, with the two surfaces coinciding with similar depth values.

2) Modelling template surfaces within elemental volumes

The elemental volumes are then filled with a template surface using the subroutine "surfaces_curved_new". For the cross-bedded tidal sandstones studied in the thesis, the 3D equation of cross-bedding surface with foreset and toeset sections was used in the program (equation 3.3). The equation could be replaced to fill the elemental volumes with another bedding template (e.g. wavy-bedding template) but, because of 3D rotation of the surfaces, the equation becomes very complicated and a rotation matrix has to be used with multiple coefficient (paramA to paramZ in the subroutine). As for the cross-bed set boundaries, the zmap+ surfaces representing the cross-bedding surfaces are extended until the boundaries of the model, by attributing depth values of the cross-bed set base surface to the cross-bedding surfaces when they merge in the bottom section, and giving them the depth values of the base boundary of the eroding superimposing cross-bed set in their top section.

3) Modelling of mudstone drapes along foreset-toeset surfaces

For each of the cross-bedding surface introduced in the model, a mudstone drape is created as a zmap+ surface file similarly, with holes (i.e. undefined value) where the mudstone drapes is discontinuous due to erosion. The generation of the mudstone drape surfaces is insured by the subroutine "mudparameter". Depending on the number of mudstone drape coverage cases to be modelled indicated in the input parameter file, different mudstone drapes surfaces are created for each foreset-toeset surface.

4) Generation of grid and petrophysical parameters

A corner-point GRDECL file is created for each model generated. GRDECL grids are a format of grid used in Eclipse for flow simulation of reservoir model. The grid is built using all the zmap+ surface files generated by the subroutines "enveloppes_ellipsoids", "surfaces_curved_new" and "mudparameter" described above. The vertical pillars of the grid are regularly spaced in the x and y direction, with the same resolution that the zmap+ surface files. That way, all the nodes of the grid cell corners will correspond to depth values stored in the zmap+ files. As precaution was taken to insure that all the surfaces are extended to the boundaries of the model, a depth value is available for each grid cell corner. The stratigraphic order of the surfaces is, from top to bottom:

Surface [1]: Top boundary of uppermost cross-bed set n eroded by model flat top boundary

Surface [2]: Uppermost foreset-toeset surface mn of the cross-bed set n eroded by surface [1].

Surface [3]: Foreset-toeset surface mn-1 of the cross-bed set n eroded by surface [2].

…

Surface [mn]: Foreset-toeset surface 2 of the cross-bed set n eroded by surface [mn-1].

Surface [mn+1]: Lowermost foreset-toeset surface 1 of the cross-bed set n eroded by surface [mn].

Surface [mn+2]: Base boundary of uppermost cross-bed set n eroded by surface [mn+1].

Surface [mn+3]: Top boundary of cross-bed set n-1 eroded by surface [mn+2].

…

Surface [(m1+2) + (m2+2) + … + (mi+2) + … + (mn+2)]: Base boundary of the lowermost cross-bed set 1 merging with the model flat bottom boundary.

The volume between successive surfaces A and B is then subdivided into cell layers of uniform thicknesses, starting from the bottom surface A and parallel to the bottom surface A. Layers of cells are cut and merge with the top surface B, consequently numerous cells are “pinched-out” or have a zero volume if the top corners of the grid cells are coinciding with the bottom corners of the grid cells.

Permeability property is then populated in the cells of the grid using the zmap+ files of the mudstone drapes created by the subroutine “mudparameter”. First, all cells of the model are given the permeability value of sandstone laminae. Then, all the lowermost cell layers comprised between two successive surfaces A and B are taken into account. If surface A corresponds to a cross-bedding surface – and not a cross-bed set boundary – then a mudstone drape file is associated with the surface A. For each cell of the layer where the mudstone drape surface exists (i.e. at least 3 corners has a z-depth value in the mudstone drape zmap+ file, and not “undefined” value), the mudstone permeability value is introduced in the cell. A permeability parameter file in GRDECL format is created for each mudstone drape coverage

```
!Input parameter file
!This parameter file corresponds to the model generated in the thesis with the
name “intermediate model”

!Definition of non-value for the different files

-9999


!Number of cross-bed sets in the model

6


!Input parameter list : 20 input parameters for each cross-bed set.

!!WARNING!! the order of the cross-bed sets is of great importance! The first
line of 20 parameters will correspond to the parameters of the youngest cross-
bed set eroding all the others below. The last line correspond to the oldest
cross-bed set which is eroded by all the others.

!Parameters for defining the cross-bed set dimensions

!1) height of the ellipsoid dome/top surface representing the cross-bed set
(surface likely to be entirely) eroded by overlying cross-bed set)

!2) z’ coordinate of the base of the top dome (must be <=0)(reference is 0)

!3) depth of the ellipsoid dome/basal surface representing the cross-bed set
(erosive base of the cross-bed set)

!4) z’ coordinate of the base of the top dome (must be >=0)(reference is 0)

!Note: if 2) is bigger than 0, or if 4) is lower than 0, then there is a risk
that the two surfaces enclose a volume that does not look like an ellipsoid,
but rather a “peanut shell” (two ellipsoids on top of each other)

!Note: z’ is not set in the real coordinate of the model (x,y,z) but in an
independent coordinate system (x’,y’,z’) where each ellipsoid is created sepa-
rately, with x’ corresponding to the long horizontal axis of the ellipsoid, y’
to the short horizontal axis and z’ to the vertical axis. In this coordinate
system, the ellipsoid is NOT rotated by the rotation angle

!Note: if 2) and 4) are equal to 0 and 1) and 3) are equal (like in all mod-
els generated in for the thesis, and for this case in particular) then the
two basal and top surfaces correspond to the boundaries of the same ellipsoid

!5) x’ dimension of the ellipsoid (dip direction of cross-bedding surfaces)

!6) y’ dimension of the ellipsoid (strike direction of cross-bedding surfaces)

!Note: 5) and 6) correspond to the dimensions of the horizontal ellipse that
marks the junction between the top and the basal surfaces


!Parameters for defining the cross-bedding surfaces orientation within the
cross-bed set

!7) theta, angle of rotation of the cross-bed set around the z’ axis (for sim-
plifying the problem, the angles of rotation phi and psi, respectively around
```

the x’ and y’ axis, are set to 0 in the software)

!8) alpha, angle of rotation of the cross-bedding surfaces (or toeset dip angle) inside the cross-bet set (rotation around the y’ axis)

!9) <nothing> not used in the software

!Parameters for the positioning of the cross-bed set in the model

!10) 11) and 12) are the X,Y,Z coordinates of the center of the cross-bed set in the final model (x,y,z) coordinate system

!Parameters for the density of cross-bedding surfaces within the cross-bed set

!13) hspacemean is the average horizontal space between two successive cross-bedding surfaces within the cross-bed set (see Figure 3.5 of the thesis, hspacemean = F_T * cos(delta) with F_T = Foreset thickness and delta = dune climb angle)

!14) hspacestdevor is the standard deviation for the horizontal space between two successive cross-bedding surfaces 13). This paramater is introduced to reproduce the trend of cyclical foreset thickness observed during 28 successive tidal bundles (neap/spring tide cycle)

!15) vspacemean is the average vertical space between two successive cross-bedding surfaces within the cross-bed set (see Figure 3.5 of the thesis, vspacemean = F_T * sin(delta) with F_T = Foreset thickness and delta = dune climb angle)

!16) vspacestdevor is the standard deviation for the vertical space between two successive cross-bedding surfaces 15). This paramater is introduced to reproduce the trend of cyclical foreset thickness observed during 28 successive tidal bundles (neap/spring tide cycle)

!Note: when the value of hspace is big, the value of vspace should be small, and conversely. It is made that way in order to reproduce trends observed at outcrops that neap tides produce thin foresets and thick toesets, while spring tidels produce thick foreset and thin toeset

!17) delta, dune climb angle (Delta line is the boundary between foreset and toeset parts of the cross-bed set, joining all O junction points, see Figure 3.5 of the thesis)

!18) limitTF origin correspond to the z’ coordinate at which point the Delta line crosses the z’ axis for x’=0 in the independent (x’,y’,z’) coordinate system of the cross-bed set.

!Parameters for mudstone drape size

!19) maximum horizontal extent (along the x’ axis of the cross-bed set) of a mudstone drape being preserved along the cross-bedding surfaces

!20) maximum size for the major axis of the elliptical patches of mudstone being distributed along the cross-bedding surfaces to generate mudstone drapes.

56.0 0 56.0 0 1000 235.1 0 12.3 0 63.1 85.3 82.9 3.57 1.9 0.96 0.16 0.5 -50 100 30

```
52.8 0   52.8 0 1000  166.8 0 10 0 42.6  -136.1 56 3.57 1.9 0.96 0.16 4.5 -50 100 30
116  0   116  0 1000  327.7 0 1.9 0 -9.1 262.4 77.4 3.57 1.9 0.96 0.16 2.3 -116 100 30
45.2 0   45.2 0 1000  132.3 0 8 0 79.8  -3.8 40.1 3.57 1.9 0.96 0.16 0 -40  100 30
51.1 0   51.1 0 1000  252.5 0 2 0 -11.6  9.9  16.3 3.57 1.9 0.96 0.16 0 -45 100 30
83.8 0   83.8 0 1000  341   0 8 0 0 141.5 -13  3.57 1.9 0.96 0.16 2.3 -75 100 30

!Dimensions of the model in the x, y and z directions, in centimeters
300 300 100

!Definition of the center point of the model, origin of the coordinate system
(x,y,z)
0 0 0

!Grid resolution of the model in the x, y and z directions (here, there are
60 grid cells in the x direction, meaning that each cell is 5 cm long)
!Note: surfaces are generated as zmap+ files. For convenience, the coordinates
of the points stored in the zmap+ files correspond to the corner of the cells
of the corner-point grid.
60 60 2

!Number of mudstone drape coverage scenario built for the model
22

!Mudstone drape coverage for each of the cases specified in the previous pa-
rameter
0 1.25 2.5 3.75 5 7.5 10 12.5 15 17.5 20 25 30 35 40 45 50 60 70 80 90 100

!-------------------------------------------------------------------------
!-------------------------------------------------------------------------
!-------------------------------------------------------------------------
```

```
program principal

implicit none


!Declaration of subroutines

interface
     subroutine enveloppes _ ellipsoid(Nonvalue,SURF,resolx,resoly,parameters,N
umElement,limitesCUBE)
    real:: Nonvalue,resolx,resoly,limitesCUBE(6)
    integer:: NumElement
    real, allocatable:: SURF(:,:,:)
    real, allocatable:: parameters(:,:)
    end subroutine
end interface


interface
    subroutine surfaces _ curved _ new(Nonvalue,parameters,SURF,MUD,resolx,reso
ly,NumElement,Numsurf,limitesCUBE,nbmudcases,mudcases)
    real:: Nonvalue,resolx,resoly,limitesCUBE(6)
    real, allocatable:: parameters(:,:)
    real, allocatable:: SURF(:,:,:)
    real, allocatable:: MUD(:,:,:)
    real,allocatable:: mudcases(:)
    integer:: NumElement,nbmudcases
    integer, allocatable:: Numsurf(:)
    end subroutine
end interface



interface
    subroutine mudparameter(nbmudcases,mudcases)
    real, allocatable:: mudcases(:)
    integer:: nbmudcases
    end subroutine
end interface


interface
    subroutine writezmapfile(name,m,n,xmin,xmax,ymin,ymax,Nonvalue,TOWRITE)
    character:: name*50
    integer:: m,n
    real:: xmin,xmax,ymin,ymax,Nonvalue
    real, allocatable :: TOWRITE(:,:)
    end subroutine
end interface


interface
    subroutine writegridfile(limitesCUBE,resolx,resoly,Nbcellsx,Nbcellsy,numlay
ers,nbzones,nblayers,SPACE,n,m,resolz)
    real:: limitesCUBE(6)
    real:: resolx,resoly,resolz
    integer:: Nbcellsx,Nbcellsy,nbzones,nblayers,SPACE,n,m
    integer:: numlayers(5000)
```

```
    end subroutine
end interface
!Declaration of variables of the main program

real:: Nonvalue,Lx,Ly,Lz,PointO(3),resolx,resoly,resolz,limitesCUBE(6),xmin,xmax,
ymin,ymax,heightlayer,heightlayermax
integer:: Element,i,Nbcellsx,Nbcellsy,n,m,NumElement,j,SPACE,comptk,kter,k,comp
t,ibis,comptElement,kbis,rank,nbmudcases,kmudcase
integer:: numlayer,nbzones,l,numlayers(5000),nblayers,comptpoints,comptpointsb
is,nbpointstotal
integer, allocatable:: Numsurf(:)
real, allocatable:: parameters(:,:)
real, allocatable:: SURF(:,:,:)
real, allocatable:: MUD(:,:,:)
real, allocatable:: TOWRITESURF(:,:)
real, allocatable:: TOWRITEMUD(:,:)
real, allocatable:: SURFLIMIT(:,:)
real, allocatable:: mudcases(:)
character:: namesurf*50,namemud*50,id*3,ig*3,ih*3,ii*3,nameSURFb*50


!listing is a small program that generates a text file with the list of the
positive integers from 1 to the specified number as input variable, here 2000.
Instead of using ASCII codes of the numbers for creating file names, numbers
are read as characters from the listing text file.

    call listing(2000)


!parameters for the model and for each of the cross-bed set of the model are
read from a parameters.txt text file. See above for a description of the input
parameters of the text file, especially the meaning of the 20 parameters per
cross-bed set.

    open(unit=50,file="parameters.txt")
    read(50,*) Nonvalue
    read(50,*) Element
    allocate(parameters(Element,20))
    do i=1,Element
        read(50,*) parameters(i,1:20)
    end do
    read(50,*) Lx,Ly,Lz
    read(50,*) PointO(1:3)
    read(50,*) Nbcellsx,Nbcellsy,resolz
    read(50,*) nbmudcases
    allocate(mudcases(nbmudcases))

    read(50,*) mudcases(1:nbmudcases)
    close(unit=50)

      allocate(Numsurf(Element))

!resolx and resoly are the dimensions of the cells of the future grid of the
model, and now the spacing between two successive nodes of the zmap+ surfaces
in the x and y directions

      resolx=Lx/Nbcellsx
      resoly=Ly/Nbcellsy
```

```
      do i=1,5000
      numlayers(i)=0
      end do

!limitesCUBE(1:6) correspond to the (x,y,z) coordinates of the boundaries of
the model (a rectangle parallellepiped)

      limitesCUBE(1)=PointO(1)-Lx/2
      limitesCUBE(2)=PointO(1)+Lx/2
      limitesCUBE(3)=PointO(2)-Ly/2
      limitesCUBE(4)=PointO(2)+Ly/2
      limitesCUBE(5)=PointO(3)-Lz/2
      limitesCUBE(6)=PointO(3)+Lz/2


!n and m are the number of nodes in the x and y directions respectively for
the zmap+ files (future corners of the grid cells of the model)

      n=(limitesCUBE(2)-limitesCUBE(1))/resolx+1
      m=(limitesCUBE(4)-limitesCUBE(3))/resoly+1
      xmin=limitesCUBE(1)
      xmax=limitesCUBE(2)
      ymin=limitesCUBE(3)
      ymax=limitesCUBE(4)


!SURFLIMIT is a surface that correspond during the process of populating the
volume of the desired model to the association of all the cross-bed sets or
the volume top boundary (the rectangle top face) overlying the cross-bed set
being modelled at each step. The cross-bed sets are modelled from the top to
the base, from the youngest to the oldest so that the erosive bottom surface
of each cross-bed set can kept into memory.

!Note: SURFLIMIT corresponds to the top face / boundary of the model initially
which will cut the uppermost cross-bed set which will be the first one to be
modelled.

    if(allocated(SURFLIMIT)) then;
      deallocate(SURFLIMIT)
      end if
      allocate(SURFLIMIT(n,m))
      do i=1,n
      do j=1,m
      SURFLIMIT(i,j)=limitesCUBE(6)
      end do
      end do

open(unit=100,file="listfiles.txt")

nbzones=0
nblayers=0
nbpointstotal=0
ComptElement=1


!Main steps of the main program start here

!Note: the succession of steps of the main program are described here, but
for a more exhaustive description, see the introduction to the program at the
```

```
beginning of the appendices

!The following "do loop" will take into account the modelling of each cross-
bed set one after the other, the first cross-bed set to be modelled being the
first one whose parameters are described in the parameter file, which is the
youngest one, eroding all the others located below

do NumElement=1,Element


!Memory allocation for the arrays of the different surfaces. The surfaces will
be stored as zmap+ files. SURF will contain the z coordinates of all the nodes
of the zmap+ surfaces corresponding to the erosive bottom boundary of the
cross-bed set and the top boundary, as well as all the cross-bedding surfaces
of the cross-bed set.

SPACE=1500
if (allocated(SURF)) then;
deallocate (SURF)
end if
allocate (SURF(SPACE,n,m))


!Memory allocation for all the mudstone drape surfaces being modelled for each
cross-bedding surface in the cross-bed set, with the number of surfaces being
stored being nbmudcases time more numerous than the cross-bedding surfaces
as for each cross-bedding surface, the different scenarios of mudstone drape
coverage informed in the parameter text file are created.

if (allocated(MUD)) then;
deallocate (MUD)
end if
allocate (MUD(nbmudcases*SPACE,n,m))


!For each cross-bed set, the bottom and top boundary surfaces are created with
the subroutine enveloppes _ ellipsoid depending on the required dimensions of
the cross-bed set stored in the parameter file

call enveloppes _ ellipsoid(Nonvalue,SURF,resolx,resoly,parameters,NumElement,l
imitesCUBE)


!Then the cross-bedding surfaces are created within each cross-bed set using
the subroutine surfaces _ curved _ new. Mudstone drapes are generated within
the same subroutine

call  surfaces _ curved _ new(Nonvalue,parameters,SURF,MUD,resolx,resoly,NumElem
ent,Numsurf,limitesCUBE,nbmudcases,mudcases)


!In the next loop, all the surfaces stored in the SURF and MUD arrays are
compared to the SURFLIMIT surface which erode all of them. If one zdepth coor-
dinate of one of the nodes of the surfaces is found higher than the SURFLIMIT
reference, then the zdepth is made equal to SURFLIMIT.

!Note: The surfaces always span over the entire volume of the model, from one
face to the parallel one facing it. It will allow to build a corner-point grid
later with raw of pinch-out cells or no-volume cells.
```

```
comptpoints=0
comptpointsbis=0

do i=1,n
      do j=1,m

      do kbis=1,Numsurf(NumElement)
      k=Numsurf(NumElement)-kbis+1


          if (SURF(k,i,j)-1<Nonvalue) then;
            SURF(k,i,j)=SURFLIMIT(i,j)

          else;

              if(SURF(k,i,j)<SURFLIMIT(i,j)) then;
                  comptpoints=comptpoints+1
                  if (SURF(k,i,j)<=limitesCUBE(5)) then;
                  comptpointsbis=comptpointsbis+1
                  SURF(k,i,j)=limitesCUBE(5)
                  end if
              else;
                  SURF(k,i,j)=SURFLIMIT(i,j)
              end if
          end if


!The bottom surface (k=1) and the top surface (k=2) of the cross-bed sets are
not lined up with mudstone drapes. So MUD of these surfaces is set to Nonvalue

         if (k==1.or.k==2) then;
         MUD(k,i,j)=Nonvalue
         end if


!Here SURFLIMIT is updated to be given the values of the bottom surface of
the cross-bed set for the erosion of the next cross-bed sets to be modelled

         if(k==1) then;
           SURFLIMIT(i,j)=SURF(k,i,j)
           end if

      end do
      end do
end do


!The mudstone drapes are eroded as well if the cross-bedding surfaces they
are lying on were eroded by SURFLIMIT in the previous step

do i=1,n
      do j=1,m
      do k=3,nbmudcases*(Numsurf(NumElement)-2)+2

              if(MUD(k,i,j)<=SURF(1,i,j).or.MUD(k,i,j)>=SURF(2,i,j)) then;
              MUD(k,i,j)=Nonvalue
              end if

      end do
      end do
```

```
end do

!comptk and compt are introduced to check that at least one node of the zmap+
surface is not eroded by SURFLIMIT. comptk corresponds to the number of cross-
bedding surfaces originally modelled that are preserved in parts at least in
the final model. compt is the number of zdepth nodes of each cross-bedding
that are present inside the model. If compt stays equal to 0, then the sur-
face is not modelled


comptk=1
      do kter=3,numsurf(NumElement)
      k=numsurf(NumElement)-kter+3
      compt=0
      do i=1,n
        do j=1,m
                    if  (SURF(k,i,j)-1>Nonvalue.and.SURF(k,i,j)>SURF(1,i,j).and.
SURF(k,i,j)<SURF(2,i,j)) then;
            compt=compt+1
            end if
        end do
    end do

if(compt>0) then;
      comptk=comptk+1


!The following structure calculates the maximum height along the vertical
axis z that exists between two successive surfaces inside the cross-bed set.
The maximum height is then divided by the vertical resolution of the grid
(maximum height of a cell prior to pinch-out) to determine in how many layers
of cells (nblayers) each zone is divided. One zone corresponds to the volume
between two successive surfaces in the model.

      heightlayermax=0
      do i=1,n
      do j=1,m
          if(kter==3) then;
          l=2
          else;
          l=k+1
          end if
          heightlayer=SURF(l,i,m-j+1)-SURF(k,i,m-j+1)-0.35
          if ((SURF(l,i,m-j+1)-SURF(k,i,m-j+1))<0.35) then;
          heightlayer=0
          end if
        if(heightlayer>heightlayermax) then;
        heightlayermax=heightlayer
        end if
    end do
    end do
    nbzones=nbzones+2
    if (heightlayermax>0) then;
    numlayers(nbzones-1)=ceiling(heightlayermax/resolz)
    else;
    numlayers(nbzones-1)=1
    end if
    nblayers=nblayers+numlayers(nbzones-1)+1
```

```
!All the following steps allow creating a name for the zmap+ file of each
cross-bedding surface of the cross-bed set

    open(unit=15,file="listing.txt")
        do ibis=1,comptElement
            read(15,*) id
        end do
    close(unit=15)




    open(unit=17,file="listing.txt")
        do ibis=1,comptk-1
            read(17,*) ii

        end do
        read(17,*) ig
    close(unit=17)

    if (comptk-1==1) then;
    nameSURF=»SURF _ Element _ »//trim(id)//» _ Zone _ 1 _ st.zmap+»
    write(100,*) nameSURF
    end if

    nameSURF="SURF _ Element _ "//trim(id)//" _ Zone _ "//trim(ig)//" _ st.zmap+"
    nameSURFb=»SURF _ Element _ »//trim(id)//» _ Zone _ »//trim(ii)//» _ tm.zmap+»

    write(100,*) nameSURFb
    write(100,*) nameSURF


    if (allocated(TOWRITESURF)) then;
    deallocate(TOWRITESURF)
    end if
    allocate(TOWRITESURF(n,m))


!Each cross-bedding surface to be modelled is transmitted to the subroutine
writezmapfile to create the corresponding zmap+ file, once stored in the TWOW-
RITESURF array

    do i=1,n
    do j=1,m
        TOWRITESURF(i,j)=SURF(k,i,m-j+1)
        nbpointstotal=nbpointstotal+1
    end do
    end do

    call writezmapfile(nameSURF,m,n,xmin,xmax,ymin,ymax,Nonvalue,TOWRITESURF)


!An exact replica of each cross-bedding surface, but located 0.35 cm above, is
created at the same time, with the name stored in SURFb, that will correspond
to the one layer of cells in which mudstone will be potentially distributed
in the grid to represent the mudstone drape.

    do i=1,n
    do j=1,m
```

```
        TOWRITESURF(i,j)=SURF(k,i,m-j+1)+0.35
        nbpointstotal=nbpointstotal+1
        if (TOWRITESURF(i,j)>SURF(k+1,i,m-j+1)) then;
        TOWRITESURF(i,j)=SURF(k+1,i,m-j+1)
        end if
        if (SURF(k,i,m-j+1)-SURF(1,i,m-j+1)==0) then;
        TOWRITESURF(i,j)=SURF(1,i,m-j+1)
        end if
    end do
    end do

    call writezmapfile(nameSURFb,m,n,xmin,xmax,ymin,ymax,Nonvalue,TOWRITESURF)


!Mudstone drape surfaces corresponding to all the mudstone drape coverage
scenario are stored in zmap+ files in the same way than cross-bedding surfaces,
using the writezmapfile subroutine

do kmudcase=1,nbmudcases

    open(unit=19,file="listing.txt")
        do ibis=1,kmudcase
            read(19,*) ih
        end do
    close(unit=19)

         nameMUD="MUD _ case _ "//trim(ih)//" _ Element _ "//trim(id)//" _ Zone _ "//
trim(ii)//".zmap+"


    if (allocated(TOWRITEMUD)) then;
    deallocate(TOWRITEMUD)
    end if
    allocate(TOWRITEMUD(n,m))

    do i=1,n
    do j=1,m
            TOWRITEMUD(i,j)=MUD(((numsurf(NumElement)-2)*nbmudcases+2)-(kter-
2)*nbmudcases+kmudcase,i,m-j+1)
    end do
    end do

    call writezmapfile(nameMUD,m,n,xmin,xmax,ymin,ymax,Nonvalue,TOWRITEMUD)

end do

end if

end do


!Once all cross-bedding surfaces and their associated mudstone drape surfaces
have been created as zmap+ files, the same method is applied to the bottom and
top boundaries / surfaces of the cross-bed set

if(comptk>2) then;


!The number of layers between the boundary surface and the closest cross-
bedding surface is calculated in a similar way than between two successive
```

```
cross-bedding surfaces. Only this time there is no mudstone drape being mod-
elled along the erosive boundary surfaces so there is no need for a duplicate
of the boundary surfaces being created 0.35 cm above, as it was the case for
each cross-bedding surface before.

    heightlayermax=0
      do i=1,n
      do j=1,m
          heightlayer=TOWRITESURF(i,j)-SURF(1,i,m-j+1)
        if(heightlayer>heightlayermax) then;
        heightlayermax=heightlayer
        end if
    end do
    end do


    nbzones=nbzones+2
    if (heightlayermax>0) then;
    numlayers(nbzones-1)=ceiling(heightlayermax/resolz)
    else;
    numlayers(nbzones-1)=1
    end if
    nblayers=nblayers+numlayers(nbzones-1)+1


!Note: in the following, k=1 refers to the bottom surface / boundary of the
cross-bed set and k=2 to the top surface / boundary

    do kbis=1,2
    open(unit=15,file="listing.txt")
        do ibis=1,comptElement
            read(15,*) id
        end do
    close(unit=15)

    open(unit=17,file="listing.txt")
        if (kbis==2) then;
        rank=1
        else
        rank=comptk
        end if
        do ibis=1,rank
            read(17,*) ig
        end do
    close(unit=17)

    if (rank==1) then;
    nameSURF=»SURF _ Element _ »//trim(id)//» _ Zone _ 1 _ st.zmap+»
    else;
    nameSURF="SURF _ Element _ "//trim(id)//" _ Zone _ "//trim(ig)//" _ tm.zmap+"
    write(100,*) nameSURF
    end if


    if (allocated(TOWRITESURF)) then;
    deallocate(TOWRITESURF)
    end if
    allocate(TOWRITESURF(n,m))

    do i=1,n
```

```
    do j=1,m
        TOWRITESURF(i,j)=SURF(kbis,i,m-j+1)
        nbpointstotal=nbpointstotal+1
    end do
    end do

    call writezmapfile(nameSURF,m,n,xmin,xmax,ymin,ymax,Nonvalue,TOWRITESURF)

    end do

!Note: below, the parameter corresponding to the number of the cross-bed set
in the final model, comptElement, is increased. As it is part of the if condi-
tion that there is at least one cross-bedding surface being introduced in the
model, the parameter will not increase in this specific case. That way, the
next cross-bed set to be introduced will "take the place" (take the number)
of this too small elemental volume. This is to insure that the cross-bed set
introduced in the model are big enough for the size of the model.


    numsurf(comptElement)=comptk
    comptElement=comptElement+1
end if


!Note: the "end do" below marks the end of the long loop of each cross-bed set
being modelled one after the other

end do


!Files are created where results of the modelling process are stored. This
data is required for the grid creation and property modelling below.

!In the results.txt file, only the cross-bed sets finally introduced in the
model are liste, with the number of cross-bedding surfaces being created for
each of these cross-bed sets.

open(unit=60,file="results.txt")
      write(60,*)Nonvalue
      write(60,*)comptElement-1
      write(60,*)limitesCUBE(1),limitesCUBE(2),limitesCUBE(3),limitesCUBE(4),limi
tesCUBE(5),limitesCUBE(6)
      write(60,*)n,m
      do i=1,comptElement-1
      write(60,*) i,numsurf(i)
      end do
      do i=comptElement+1,Element
      numsurf(i)=0
      end do
close(unit=60)


!In particular, the number of layers per zone to be created is stored in the
layers.txt file

nbzones=nbzones-1
nblayers=nblayers-1
numlayer=0
print*,nbpointstotal
```

```
open(unit=70,file="layers.txt")
write(70,*) nbzones
write(70,*) nblayers
print*, nbzones,nblayers
do i=1,nbzones

if (numlayers(i)>0) then;
numlayer=numlayer+numlayers(i)
else;
numlayer=numlayer+1
write(70,*) numlayer
end if

end do

write(70,*) "     "
do i=1,nbzones
write(70,*) numlayers(i)
end do
close(unit=70)
close(unit=100)
!writegridfile subroutine is called to generate the corner-point grid based
on the zmap+ files created and the number of layers per zone as documented in
the nblayers.txt file

call writegridfile(limitesCUBE,resolx,resoly,Nbcellsx,Nbcellsy,numlayers,nbzone
s,nblayers,SPACE,n,m,resolz)


!The permeability parameter for the grid (or any other parameter)is created
using the corner-point grid and the mudstone drape zmap+ surfaces. Mutliple
parameter files are created for one model corresponding to the different mud-
stone drape coverage scenarios specified in the input parameter text file.

call mudparameter(nbmudcases,mudcases)

stop
end program


!-------------------------------------------------------------------------
!-------------------------------------------------------------------------
!-------------------------------------------------------------------------

subroutine listing(SPACE)

integer :: SPACE, i

open(unit=40, file="listing.txt")
do i=1,SPACE
write(40,*) i
end do
close(unit=40)

return
end subroutine listing

!-------------------------------------------------------------------------
!-------------------------------------------------------------------------
```

```
!-----------------------------------------------------------------------

subroutine  enveloppes _ ellipsoid(Nonvalue,SURF,resolx,resoly,parameters,NumEl
ement,limitesCUBE)
      implicit none
     real:: Xorigin,Yorigin,Zorigin,Htop,Ctop,Hbot,Cbot,Lengthmax,Lengthmin,Abo
t,Atop,Bbot,Btop,Rbot,Rtop
     real:: Abotaxis,Bbotaxis,Atopaxis,Btopaxis,Nonvalue,resolx,resoly,xp,yp
     real,allocatable:: SURF(:,:,:)
     real,allocatable:: parameters(:,:)
     integer:: n,m,i,j,Numelement
     real:: limitesCUBE(6)
     real:: theta,psi,phi,paramA,paramB,paramC,paramD,paramE,paramF,paramG,par
amH,paramI,paramJ
     real:: paramM,paramN,paramO,paramP,paramQ,paramR,paramS,paramT,paramU,par
amV,paramW,paramX,paramY
     real:: DELTA,sol1,sol2,pi
    parameter(pi=3.14159265)

!Define the center of the cartesian grid
     Xorigin=0
     Yorigin=0
     Zorigin=0

!Define the dimensions of the two enveloppes, boudary surfaces of the cross-
bed set
       Htop=parameters(NumElement,1)
       Ctop=parameters(NumElement,2)
       Hbot=parameters(NumElement,3)
       Cbot=parameters(NumElement,4)
       Lengthmax=parameters(NumElement,5)
       Lengthmin=parameters(NumElement,6)

!Calculation of the two others axis of the two ellipsoids
       Abot=Xorigin
       Bbot=Yorigin
       Atop=Xorigin
       Btop=Yorigin
       Rbot=SQRT((Cbot-Zorigin)**2)+Hbot
       Rtop=SQRT((Ctop-Zorigin)**2)+Htop
       Abotaxis=SQRT((Lengthmax**2)*(1/(1-((Zorigin-Cbot)**2/Rbot**2))))
       Bbotaxis=SQRT((Lengthmin**2)*(1/(1-((Zorigin-Cbot)**2/Rbot**2))))
       Atopaxis=SQRT((Lengthmax**2)*(1/(1-((Zorigin-Ctop)**2/Rtop**2))))
       Btopaxis=SQRT((Lengthmin**2)*(1/(1-((Zorigin-Ctop)**2/Rtop**2))))

!Dimension of the grid:
n=(limitesCUBE(2)-limitesCUBE(1))/resolx+1
     m=(limitesCUBE(4)-limitesCUBE(3))/resoly+1

!Creation of the two matrix (n,m) with the z coordinates of the enveloppes for
each point of the grid
     theta=parameters(NumElement,7)*pi/180
     phi=0
     psi=0

!Note: the list of parameters defined below of the form param? correspond to
the different terms of the rotation matrix required to rotate the surfaces in
a cartesian coordinate system. These parameters have been checked mutliple
times and are correct as it is. DO NOT CHANGE THEM!
```

```
!Note: some of these parameters are only calculated for convenience in order
to simplify very long calculations... see paramJ for example. Again, do not
change them...

    paramA=cos(theta)*cos(phi)
    paramB=cos(phi)*sin(theta)
    paramC=-sin(phi)
    paramD=cos(theta)*sin(phi)*sin(psi)-sin(theta)*cos(psi)
    paramE=sin(phi)*sin(psi)*sin(theta)+cos(theta)*cos(psi)
    paramF=cos(phi)*sin(psi)
    paramG=sin(phi)*cos(psi)*cos(theta)+sin(theta)*sin(psi)
    paramH=sin(phi)*cos(psi)*sin(theta)-cos(theta)*sin(psi)
    paramI=cos(phi)*cos(psi)
                          paramJ=(paramA*paramI-paramC*paramG)*(paramA*paramE-
paramB*paramD)+(paramA*paramF-paramC*paramD)*(paramB*paramG-paramA*paramH)
    paramS=(paramA*paramF*paramB-paramA*paramC*paramE)/paramJ
    paramT=(paramA*paramC*paramD-paramA*paramA*paramF)/paramJ
    paramU=(paramA*paramA*paramE-paramA*paramB*paramD)/paramJ
   paramP=(paramB*paramG*paramS-paramA*paramH*paramS-paramB)/(paramA*paramE-
paramB*paramD)
   paramQ=(paramB*paramG*paramT-paramA*paramH*paramT+paramA)/(paramA*paramE-
paramB*paramD)
          paramR=(paramB*paramG*paramU-paramA*paramH*paramU)/(paramA*paramE-
paramB*paramD)
    paramM=(1-paramD*paramP-paramG*paramS)/paramA
    paramN=(-paramD*paramQ-paramG*paramT)/paramA
    paramO=(-paramD*paramR-paramG*paramU)/paramA
paramV=(paramO**2)/(Abotaxis**2)+(paramR**2)/(Bbotaxis**2)+(paramU**2)/(Rbot**2)


!For each point of the zmap+ grid regularly spaced depending on the resolution
in the x direction and the resolution in the y direction, corresponds a zdepth
value for the base surface SURF(1,:,:) and the top surface SURF(2,:,:). But this
point is the result of the rotation of the elemental volume / cross-bed set,
which was initially located in the (x',y',z') coordinate system. The rotation
matrix parameters corresponding to the angle theta calculated above are used
to go back to the "initial" position of the point prior to the rotation. Once
we know the position of the point initially, we determine its zdepth using the
3D equation of an ellipsoid.

      do i=1,n
            do j=1,m

            xp=(i-1)*resolx+limitesCUBE(1)-parameters(NumElement,10)
        yp=(j-1)*resoly+limitesCUBE(3)-parameters(NumElement,11)
      paramW=2*paramM*paramO*xp/(Abotaxis**2)+2*paramN*paramO*yp/(Abotaxis**2)
paramW=paramW+2*paramP*paramR*xp/(Bbotaxis**2)+2*paramQ*paramR*yp/(Bbotax-
is**2)
paramW=paramW+2*paramS*paramU*xp/(Rbot**2)+2*paramT*paramU*Yp/(Rbot**2)
            paramX=(paramM**2)*(xp**2)/(Abotaxis**2)+(paramN**2)*(yp**2)/(Abotax
is**2)+2*paramM*paramN*xp*yp/(Abotaxis**2)
      paramX=paramX+(paramP**2)*(xp**2)/(Bbotaxis**2)+(paramQ**2)*(yp**2)/(Bbota
xis**2)+2*paramP*paramQ*xp*yp/(Bbotaxis**2)
      paramX=paramX+(paramS**2)*(xp**2)/(Rbot**2)+(paramT**2)*(yp**2)/
(Rbot**2)+2*paramS*paramT*xp*yp/(Rbot**2)-1
      paramY=(paramS*xp+paramT*yp)/(-paramU)
      DELTA=paramW**2-4*paramV*paramX

            if (DELTA>=0) then;
            sol1=(-paramW-SQRT(DELTA))/(2*paramV)
```

```
            sol2=(-paramW+SQRT(DELTA))/(2*paramV)
            if(sol1>paramY.and.sol2>paramY) then;
            SURF(1,i,j)=Nonvalue
            SURF(2,i,j)=Nonvalue
            else;
                if (sol1>sol2) then;
                SURF(1,i,j)=sol2+parameters(NumElement,12)
                SURF(2,i,j)=sol1+parameters(NumElement,12)
                else;
                SURF(1,i,j)=sol1+parameters(NumElement,12)
                SURF(2,i,j)=sol2+parameters(NumElement,12)
                end if
            end if
        else;
        SURF(1,i,j)=Nonvalue
        SURF(2,i,j)=Nonvalue
        end if

        end do
    end do
         paramV=(paramO**2)/(Atopaxis**2)+(paramR**2)/(Btopaxis**2)+(paramU**2)/
(Rtop**2)
      do i=1,n
            do j=1,m

            xp=(i-1)*resolx+limitesCUBE(1)-parameters(NumElement,10)
        yp=(j-1)*resoly+limitesCUBE(3)-parameters(NumElement,11)

          paramW=2*paramM*paramO*xp/(Atopaxis**2)+2*paramN*paramO*yp/(Atopax-
is**2)
            paramW=paramW+2*paramP*paramR*xp/(Btopaxis**2)+2*paramQ*paramR*
yp/(Btopaxis**2)
            paramW=paramW+2*paramS*paramU*xp/(Rtop**2)+2*paramT*paramU*Yp/
(Rtop**2)

            paramX=(paramM**2)*(xp**2)/(Atopaxis**2)+(paramN**2)*(yp**2)/(Atopax
is**2)+2*paramM*paramN*xp*yp/(Atopaxis**2)
            paramX=paramX+(paramP**2)*(xp**2)/(Btopaxis**2)+(paramQ**2)*(yp**2)/
(Btopaxis**2)+2*paramP*paramQ*xp*yp/(Btopaxis**2)
            paramX=paramX+(paramS**2)*(xp**2)/(Rtop**2)+(paramT**2)*(yp**2)/
(Rtop**2)+2*paramS*paramT*xp*yp/(Rtop**2)-1

            paramY=(paramS*xp+paramT*yp)/(-paramU)

            DELTA=paramW**2-4*paramV*paramX

            if (DELTA>=0) then;
            sol1=(-paramW-SQRT(DELTA))/(2*paramV)
            sol2=(-paramW+SQRT(DELTA))/(2*paramV)
            if(sol1>paramY.or.sol2>paramY) then;
                if (sol1<sol2) then;
                SURF(2,i,j)=sol2+parameters(NumElement,12)
                if(SURF(1,i,j)-1<Nonvalue) then;
                SURF(1,i,j)=sol1+parameters(NumElement,12)
                end if
                else;
                SURF(2,i,j)=sol1+parameters(NumElement,12)
                if(SURF(1,i,j)-1<Nonvalue) then;
                SURF(1,i,j)=sol2+parameters(NumElement,12)
                end if
```

```
                end if
            end if
        else;
        SURF(2,i,j)=Nonvalue
        end if

        end do
    end do


      end subroutine enveloppes _ ellipsoid


!-------------------------------------------------------------------------
!-------------------------------------------------------------------------
!-------------------------------------------------------------------------


subroutine  surfaces _ curved _ new(Nonvalue,parameters,SURF,MUD,resolx,resoly,N
umElement,Numsurf,limitesCUBE,nbmudcases,mudcases)

    interface
    subroutine muddrapesref(Nonvalue,NumElement,limitesCUBE,SURFref,resolx,re
soly,nbpointsline,nbpointsround,nbpointsroundpreserved,parameters,coordicente
r,coordjcenter,dimi,dimj,Xcenter,idistancemax,jdistancemax,routa,routb,routc,l
engthpreserved,prop)
    real:: Nonvalue,resolx,resoly,Xcenter,routa,routb,routc,idistancemax,jdista
ncemax,lengthpreserved,prop
    integer:: NumElement,coordicenter,coordjcenter,dimi,dimj,nbpointsline,nbp
ointsround,nbpointsroundpreserved
    real, allocatable:: SURFref(:,:,:)
    real, allocatable:: parameters(:,:)
    real:: limitesCUBE(6)
    end subroutine
    end interface

    real:: Nonvalue,resolx,resoly,limitesCUBE(6)
    real, allocatable:: parameters(:,:)
    real, allocatable:: SURF(:,:,:)
    real, allocatable:: MUD(:,:,:)
    real, allocatable:: TOWRITE(:,:)
    character :: name*50
    integer:: NumElement,nbmudcases,kcase,mudcase,periode
    integer, allocatable:: Numsurf(:)
    real:: hspace, vspace,temp,htop,Ctop,Hbot,Cbot,Lengthmax,Lengthmin,hspace
mean,hspacestdev,vspacemean,vspacestdev,Abot,Bbot,Atop,Btop,xmin,xmax,ymin,ym
ax,prop
       real::  Rbot,Rtop,Abotaxis,Bbotaxis,Atopaxis,Btopaxis,theta,phi,depth _
max,depth _ min,Xcenter,vspacecum,hspacecum,Xcenterellipsoid,Yceterellipsoid,Z
centerellipsoid,routa,routb,routc
    integer:: n,m,k,i,j,coordiinf,coordjinf,nbcontrol,compt,coordicenter,coordj
center,dimi,dimj,nbpointsroundpreserved
    real::xfinal,yfinal,xorigin,yorigin,zfinal,thetaorigin,thetafinal,pi,xp,yp,xcen
terfinal,ycenterfinal,delta,x,y,z,psi,zfinal1,zfinal2,phi0
    real:: paramA,paramB,paramC,paramD,paramE,paramF,paramG,paramH,paramI,par
amJ,paramK,paramM,paramN,paramO,paramP,paramQ,paramR,paramS,paramT,paramU
    real:: paramAbis,paramBbis,paramCbis,paramDbis,paramEbis,paramFbis,paramG
bis,paramHbis,paramIbis,paramJbis,paramKbis
    real:: paramMbis,paramNbis,paramObis,paramPbis,paramQbis,paramRbis,paramS
```

```
bis,paramTbis,paramUbis,paramXbis,paramVbis,paramWbis,theta0
    real:: idistancemax,jdistancemax,idist,jdist,lengthpreserved,period,hspace
stdevor,vspacestdevor,anglelimitTF,limitTForigin
     real,allocatable::SURFref(:,:,:)
     real,allocatable::MUDref(:,:,:)
     real,allocatable:: mudcases(:)

     parameter(pi=3.14159265)


!All parameters below were already described previously

       Htop=parameters(NumElement,1)
       Ctop=parameters(NumElement,2)
       Hbot=parameters(NumElement,3)
       Cbot=parameters(NumElement,4)
       Lengthmax=parameters(NumElement,5)
       Lengthmin=parameters(NumElement,6)
       hspacemean=parameters(NumElement,13)
       hspacestdevor=parameters(NumElement,14)
       vspacemean=parameters(NumElement,15)
       vspacestdevor=parameters(NumElement,16)
       paramK=0.00375
       paramKbis=paramK
       Xcenterellipsoid=parameters(NumElement,10)
     Ycenterellipsoid=parameters(NumElement,11)
     Zcenterellipsoid=parameters(NumElement,12)
     anglelimitTF=parameters(NumElement,17)
     limitTForigin=parameters(NumElement,18)

     CALL RANDOM_SEED()
     call random_number(lengthpreserved)
     lengthpreserved=parameters(NumElement,19)
       Abot=0
       Bbot=0
       Atop=0
       Btop=0

       Rbot=SQRT((Cbot)**2)+Hbot
       Rtop=SQRT((Ctop)**2)+Htop

       Abotaxis=SQRT((Lengthmax**2)*(1/(1-((-Cbot)**2/Rbot**2))))
       Bbotaxis=SQRT((Lengthmin**2)*(1/(1-((-Cbot)**2/Rbot**2))))

       Atopaxis=SQRT((Lengthmax**2)*(1/(1-((-Ctop)**2/Rtop**2))))
       Btopaxis=SQRT((Lengthmin**2)*(1/(1-((-Ctop)**2/Rtop**2))))

     theta=parameters(NumElement,7)*pi/180
     phi=parameters(NumElement,8)*pi/180
     theta0=0
     phi0=0
     psi=0
     paramA=cos(theta)*cos(phi)
     paramB=cos(phi)*sin(theta)
     paramC=-sin(phi)
     paramD=cos(theta)*sin(phi)*sin(psi)-sin(theta)*cos(psi)
     paramE=sin(phi)*sin(psi)*sin(theta)+cos(theta)*cos(psi)
     paramF=cos(phi)*sin(psi)
     paramG=sin(phi)*cos(psi)*cos(theta)+sin(theta)*sin(psi)
     paramH=sin(phi)*cos(psi)*sin(theta)-cos(theta)*sin(psi)
```

```
    paramI=cos(phi)*cos(psi)
                        paramJ=(paramA*paramI-paramC*paramG)*(paramA*paramE-
paramB*paramD)+(paramA*paramF-paramC*paramD)*(paramB*paramG-paramA*paramH)
    paramS=(paramA*paramF*paramB-paramA*paramC*paramE)/paramJ
    paramT=(paramA*paramC*paramD-paramA*paramA*paramF)/paramJ
    paramU=(paramA*paramA*paramE-paramA*paramB*paramD)/paramJ
   paramP=(paramB*paramG*paramS-paramA*paramH*paramS-paramB)/(paramA*paramE-
paramB*paramD)
   paramQ=(paramB*paramG*paramT-paramA*paramH*paramT+paramA)/(paramA*paramE-
paramB*paramD)
          paramR=(paramB*paramG*paramU-paramA*paramH*paramU)/(paramA*paramE-
paramB*paramD)
    paramM=(1-paramD*paramP-paramG*paramS)/paramA
    paramN=(-paramD*paramQ-paramG*paramT)/paramA
    paramO=(-paramD*paramR-paramG*paramU)/paramA
    paramAbis=cos(theta0)*cos(phi)
    paramBbis=cos(phi)*sin(theta0)
    paramCbis=-sin(phi)
    paramDbis=cos(theta0)*sin(phi)*sin(psi)-sin(theta0)*cos(psi)
    paramEbis=sin(phi)*sin(psi)*sin(theta0)+cos(theta0)*cos(psi)
    paramFbis=cos(phi)*sin(psi)
    paramGbis=sin(phi)*cos(psi)*cos(theta0)+sin(theta0)*sin(psi)
    paramHbis=sin(phi)*cos(psi)*sin(theta0)-cos(theta0)*sin(psi)
    paramIbis=cos(phi)*cos(psi)
      paramJbis=(paramAbis*paramIbis-paramCbis*paramGbis)*(paramAbis*paramEb
is-paramBbis*paramDbis)+(paramAbis*paramFbis-paramCbis*paramDbis)*(paramBbis-
*paramGbis-paramAbis*paramHbis)
    paramSbis=(paramAbis*paramFbis*paramBbis-paramAbis*paramCbis*paramEbis)/
paramJbis
    paramTbis=(paramAbis*paramCbis*paramDbis-paramAbis*paramAbis*paramFbis)/
paramJbis
    paramUbis=(paramAbis*paramAbis*paramEbis-paramAbis*paramBbis*paramDbis)/
paramJbis
     paramPbis=(paramBbis*paramGbis*paramSbis-paramAbis*paramHbis*paramSbis-
paramBbis)/(paramAbis*paramEbis-paramBbis*paramDbis)
    paramQbis=(paramBbis*paramGbis*paramTbis-paramAbis*paramHbis*paramTbis+p
aramAbis)/(paramAbis*paramEbis-paramBbis*paramDbis)
    paramRbis=(paramBbis*paramGbis*paramUbis-paramAbis*paramHbis*paramUbis)/
(paramAbis*paramEbis-paramBbis*paramDbis)
    paramMbis=(1-paramDbis*paramPbis-paramGbis*paramSbis)/paramAbis
    paramNbis=(-paramDbis*paramQbis-paramGbis*paramTbis)/paramAbis
    paramObis=(-paramDbis*paramRbis-paramGbis*paramUbis)/paramAbis

    periode=0
      hspace=0
    vspace=0
    hspacestdev=hspacestdevor
    vspacestdev=0
    do while (hspace<0.6.or.hspace>16)
    call RANDOM_NUMBER(temp)
      temp = log(SQRT(hspacestdev)) * SQRT(-2.0*LOG(temp)) * COS(2*pi*temp) +
log(hspacemean)
    hspace=exp(temp)
    end do
    vspace=hspace*tan(anglelimitTF*pi/180)



    n=(limitesCUBE(2)-limitesCUBE(1))/resolx+1
```

```
    m=(limitesCUBE(4)-limitesCUBE(3))/resoly+1


    k=3

!Each cross-bedding surface is created in the cross-bed set, with the first
one having its junction line between foreset and toeset part (junction of O
points in the y direction, see Figure 3.5) having its lowest point at a depth
equal to depth _ min. The position of the lowermost O point corresponds to the
coordinates Xcenter, Ycenter and Zcenter in the (x',y',z') coordinate system of
the cross-bed set, that is prior to the rotation theta of the cross-bed set.

!Note: Ycenter is always equal to 0 in this coordinate system, and Zcenter
is equal to depth _ min. The junction line of the O points in the y' direc-
tion corresponds to an ellipse which is parallel to the ellipsoidal erosive
base surface of the cross-bed set (i.e. the junction line of O points in an
ellipse with the same dimensions than the cross-section of the ellipsoid for
y'=Ycenter which is an ellipse)

!Note: Xcenter is chosen arbitrarly in the software but this is the optimal
solution in order to get the cross-bed set populated with a 1:1 foreset to
toeset volume ratio in the final cross-bed set, whatever the dune climb angle.

    depth _ min=Zcenterellipsoid+limitTForigin-2*Lengthmax*tan(anglelimitTF*pi
/180)+vspace
    depth _ max=depth _ min+2*Rbot+vspace
    Xcenter=-2*Lengthmax+Xcenterellipsoid+hspace
    vspacecum=0

    routa=Abotaxis
    routb=Bbotaxis
    routc=Rbot
    dimi=(routa+1)/(resolx)+1
    dimi=dimi*2-1
    dimj=(routb+1)/(resoly)+1
    dimj=dimj*2-1


!Cross-bedding surfaces are created until the cross-bed set is entirely filled
with them, that is to say while the uppermost tip of the cross-bedding is
contained inside the cross-bed set. This correponds to the condition of the
"while loop" with checking the position of Xcenter. Xcenter is increased by
hspace at the end of the loop which corresponds to the horizontal space be-
tween two cross-bedding surfaces (see explanations on input parameters 13) to
16) in parameter text file)

!Note: for simplification, cross-bedding surfaces are in fact entirely filling
a rectangle parallelepiped of the same dimensions than the ellipsoid of the
cross-bed set. Consequently some cross-bedding surfaces that are created by
the software will be entirely located outside the cross-bed set. These sur-
faces are ultimately not inserted in the final model as in the main program we
check that final model surfaces are inside the cross-bed set and that at least
one part of it is preserved from erosion from other younger cross-bed sets.

    do while (Xcenter<Xcenterellipsoid+Lengthmax)

    if (allocated(SURFref)) then;
    deallocate(SURFref)
    end if
    allocate(SURFref(2,dimi,dimj))
```

```
    if (allocated(MUDref)) then;
    deallocate(MUDref)
    end if
    allocate(MUDref(2,dimi,dimj))

    compt=0
    nbpointsround=0
    nbpointsline=0
    nbpointsroundpreserved=0
    idistancemax=0
    jdistancemax=0
    open(unit=30,file='report.txt')
!The same way than for the boundary surfaces of the cross-bed set, each point
of the final zmap+ file (i,j) has a xfinal and yfinal position in the (x,y,z) co-
ordinate system of the model. But these coordinates are after the cross-bed
set have been rotated by an angle theta. So first, the coordinates (xorigin,
yorigin) of the point in the (x',y',z') coordinate sytem of the cross-bed set
prior to rotation are calculated using the rotation matrix parameters param?,
and then the zorigin of the point is calculated using the equation of the
cross-bedding surface template (see equation 3.3 in the thesis). The zfinal is
calculated after positionning the cross-bed set in the z direction so that
zfinal = zorigin + Zcenterellipsoid

!1) Creation of the foreset curved part

    do i=1,n
    do j=1,m

        xfinal=(i-1)*resolx+limitesCUBE(1)
        yfinal=(j-1)*resoly+limitesCUBE(3)
        dist=SQRT((xfinal-Xcenterellipsoid)**2+(yfinal-Ycenterellipsoid)**2)

        if (xfinal==Xcenterellipsoid.or.yfinal==Ycenterellipsoid) then;
            if(xfinal==Xcenterellipsoid.and.yfinal==Ycenterellipsoid) then;
            thetafinal=0
            elseif(xfinal==Xcenterellipsoid) then;
                if (yfinal<Ycenterellipsoid) then;
                thetafinal=-pi/2
                else;
                thetafinal=pi/2
                end if
            else;
                if (xfinal<Xcenterellipsoid) then;
                thetafinal=-pi
                else;
                thetafinal=0
                end if
            end if
        else;

                if ((yfinal-Ycenterellipsoid)/(xfinal-Xcenterellipsoid)<0) then;
                    if (yfinal-Ycenterellipsoid<0) then;
                     thetafinal=atan((yfinal-Ycenterellipsoid)/(xfinal-Xcenterel-
lipsoid))
                    else;
                                thetafinal=atan((yfinal-Ycenterellipsoid)/(xfinal-
Xcenterellipsoid))+pi
                    end if
                else;
```

```
                    if (yfinal-Ycenterellipsoid<0) then;
                              thetafinal=atan((yfinal-Ycenterellipsoid)/(xfinal-
Xcenterellipsoid))+pi
                    else;
                     thetafinal=atan((yfinal-Ycenterellipsoid)/(xfinal-Xcenterel-
lipsoid))
                    end if
                end if

        end if



        if (thetafinal<0) then;
        thetafinal=thetafinal+2*pi
        elseif (thetafinal>=2*pi) then;
        thetafinal=thetafinal-2*pi
        end if

        if(xfinal==Xcenterellipsoid.and.yfinal==Ycenterellipsoid) then;
        xorigin=xfinal
        yorigin=yfinal
        else;
        thetaorigin=thetafinal-theta

        xorigin=dist*cos(thetaorigin)+Xcenterellipsoid
        yorigin=dist*sin(thetaorigin)+Ycenterellipsoid


            if (SURF(1,i,j)-1>Nonvalue) then;
                if (xorigin>=Xcenter) then;
                            zfinal=depth _ min-tan(phi)*(xorigin-Xcenter)+(Rbot-
Zcenterellipsoid+SURF(1,i,j))
                else;
                    if(Xcenter<Xcenterellipsoid) then;
                     xcenterfinal=SQRT((Xcenterellipsoid-Xcenter)**2)*cos(theta+
pi)+Xcenterellipsoid
                     ycenterfinal=SQRT((Xcenterellipsoid-Xcenter)**2)*sin(theta+
pi)+Ycenterellipsoid
                    else;
                     xcenterfinal=SQRT((Xcenterellipsoid-Xcenter)**2)*cos(theta)
+Xcenterellipsoid
                     ycenterfinal=SQRT((Xcenterellipsoid-Xcenter)**2)*sin(theta)
+Ycenterellipsoid
                    end if
                  xp=xfinal-xcenterfinal
                  yp=yfinal-ycenterfinal
               Delta=(2*paramM*paramO*xp+2*paramN*paramO*yp-paramU/paramK)**2-
4*(paramO**2)*((paramM*xp)**2+(paramN*yp)**2+2*paramM*paramN*xp*yp-paramS*xp/
paramK-paramT*yp/paramK)
                  if (Delta>=0) then;
                zfinal1=(-(2*paramM*paramO*xp+2*paramN*paramO*yp-paramU/paramK)-
SQRT(Delta))/(2*(paramO**2))
                     zfinal2=(-(2*paramM*paramO*xp+2*paramN*paramO*yp-paramU/
paramK)+SQRT(Delta))/(2*(paramO**2))
                    if (zfinal1<zfinal2) then;
                    zfinal=zfinal1
                    else;
                    zfinal=zfinal2
```

```
                    end if
                x=paramM*xp+paramN*yp+paramO*zfinal
                y=paramP*xp+paramQ*yp+paramR*zfinal
                z=paramS*xp+paramT*yp+paramU*zfinal
                zfinal=zfinal+depth _ min+(Rbot-Zcenterellipsoid+SURF(1,i,j))
                else;
                zfinal=Nonvalue
                end if

                end if
            else;
            zfinal=Nonvalue
            end if
        end if

             if (zfinal<=SURF(2,i,j).and.zfinal-1>Nonvalue.and.zfinal>=SURF(1,i,j))
then;
            SURF(k,i,j)=zfinal
            compt=compt+1
            else;
                    if(zfinal-1>Nonvalue.and.zfinal<SURF(1,i,j).and.SURF(1,i,j)-
1>Nonvalue) then;
                SURF(k,i,j)=SURF(1,i,j)
                  elseif(zfinal-1>Nonvalue.and.zfinal>SURF(2,i,j).and.SURF(1,i,j)-
1>Nonvalue) then;
                SURF(k,i,j)=SURF(2,i,j)
                else;
                SURF(k,i,j)=Nonvalue
                end if
            end if

    end do
    end do


!A parameter compt has been introduced to calculate how many nodes of the
zmap+ file are preserved within the cross-bed set and in the boundaries of
the final model. If any part of the curved foreset part is preserved, then the
modelling process continue by creating the "flat" toeset part (always parallel
to the erosive base though)

!2) Creation of the flat toeset part

if (compt>0) then;

    do i=1,dimi
    do j=1,dimj

        xfinal=Xcenterellipsoid-((dimi-1)/2)*resolx+(i-1)*resolx
        yfinal=Ycenterellipsoid-((dimj-1)/2)*resoly+(j-1)*resoly
        dist=SQRT((xfinal-Xcenterellipsoid)**2+(yfinal-Ycenterellipsoid)**2)

        if (xfinal==Xcenterellipsoid.or.yfinal==Ycenterellipsoid) then;
            if(xfinal==Xcenterellipsoid.and.yfinal==Ycenterellipsoid) then;
            thetafinal=0
            elseif(xfinal==Xcenterellipsoid) then;
                if (yfinal<Ycenterellipsoid) then;
                thetafinal=-pi/2
                else;
```

```
                thetafinal=pi/2
                end if
            else;
                if (xfinal<Xcenterellipsoid) then;
                thetafinal=-pi
                else;
                thetafinal=0
                end if
            end if
        else;

                if ((yfinal-Ycenterellipsoid)/(xfinal-Xcenterellipsoid)<0) then;
                    if (yfinal-Ycenterellipsoid<0) then;
                     thetafinal=atan((yfinal-Ycenterellipsoid)/(xfinal-Xcenterel-
lipsoid))


                else;
                                thetafinal=atan((yfinal-Ycenterellipsoid)/(xfinal-
Xcenterellipsoid))+pi
                    end if
                else;
                    if (yfinal-Ycenterellipsoid<0) then;
                                thetafinal=atan((yfinal-Ycenterellipsoid)/(xfinal-
Xcenterellipsoid))+pi
                    else;
                     thetafinal=atan((yfinal-Ycenterellipsoid)/(xfinal-Xcenterel-
lipsoid))
                    end if
                end if

        end if

        if (thetafinal<0) then;
        thetafinal=thetafinal+2*pi
        elseif (thetafinal>=2*pi) then;
        thetafinal=thetafinal-2*pi
        end if

        if(xfinal==Xcenterellipsoid.and.yfinal==Ycenterellipsoid) then;
        xorigin=xfinal
        yorigin=yfinal
        else;
        thetaorigin=thetafinal-theta0

        xorigin=dist*cos(thetaorigin)+Xcenterellipsoid
        yorigin=dist*sin(thetaorigin)+Ycenterellipsoid

           DELTA=1-((xorigin-Xcenterellipsoid)/routa)**2-((yorigin-Ycenterellip-
soid)/routb)**2

        if (DELTA<0) then;
        surfreftop=Nonvalue
        surfrefbottom=Nonvalue
        else;
        surfreftop=SQRT(routc**2*DELTA)+Zcenterellipsoid
        surfrefbottom=Zcenterellipsoid-SQRT(routc**2*DELTA)
        end if
```

```
            if (surfrefbottom-1>Nonvalue) then;
                if (xorigin>=Xcenter) then;
                                zfinal=depth _ min-tan(phi)*(xorigin-Xcenter)+(Rbot-
Zcenterellipsoid+surfrefbottom)
                else;
                    if(Xcenter<Xcenterellipsoid) then;
                    xcenterfinal=SQRT((Xcenterellipsoid-Xcenter)**2)*cos(theta0
+pi)+Xcenterellipsoid
                    ycenterfinal=SQRT((Xcenterellipsoid-Xcenter)**2)*sin(theta0
+pi)+Ycenterellipsoid
                   else;
                    xcenterfinal=SQRT((Xcenterellipsoid-Xcenter)**2)*cos(theta0
)+Xcenterellipsoid
                    ycenterfinal=SQRT((Xcenterellipsoid-Xcenter)**2)*sin(theta0
)+Ycenterellipsoid
                   end if



                xp=xfinal-xcenterfinal
                yp=yfinal-ycenterfinal
               Delta=(2*paramMbis*paramObis*xp+2*paramNbis*paramObis*yp-par-
amUbis/paramKbis)**2-4*(paramObis**2)*((paramMbis*xp)**2+(paramNbis*yp)**2+2*pa
ramMbis*paramNbis*xp*yp-paramSbis*xp/paramKbis-paramTbis*yp/paramKbis)
                if (Delta>=0) then;
                 zfinal1=(-(2*paramMbis*paramObis*xp+2*paramNbis*paramObis*yp-
paramUbis/paramKbis)-SQRT(Delta))/(2*(paramObis**2))
                 zfinal2=(-(2*paramMbis*paramObis*xp+2*paramNbis*paramObis*yp-
paramUbis/paramKbis)+SQRT(Delta))/(2*(paramObis**2))
                   if (zfinal1<zfinal2) then;
                   zfinal=zfinal1
                   else;
                   zfinal=zfinal2
                   end if
                x=paramMbis*xp+paramNbis*yp+paramObis*zfinal
                y=paramPbis*xp+paramQbis*yp+paramRbis*zfinal
                z=paramSbis*xp+paramTbis*yp+paramUbis*zfinal
                zfinal=zfinal+depth _ min+(Rbot-Zcenterellipsoid+surfrefbottom)
                else;
                zfinal=Nonvalue
                end if

                end if
            else;
            zfinal=Nonvalue
            end if
        end if
```

```
!In order to simplify the latter mudstone drape modelling process, we intro-
duce a SURFref array for storage of two values: in SURFref(1,:,:) the surface z
depth for the zmap+ file, and in SURFref(2,:,:) a code associated to each point,
whether 1, 2 or 3. If a point is part of the toeset area, the code is 1; if
it is part of the foreset area, then it is 2, except if it is located too far
away from the junction point O (i.e. too high along the foreset surface), then
it is given code 3. Zone 2 corresponds to the part of the foreset area where
mudstone drape can be potentially preserved.
```

```
          if (zfinal<=surfreftop.and.zfinal-1>Nonvalue.and.zfinal>=surfrefbottom)
then;
             SURFref(1,i,j)= zfinal


                 if (xorigin>=Xcenter)then;
                 nbpointsline=nbpointsline+1
                 SURFref(2,i,j)=1
                 else;
                 nbpointsround=nbpointsround+1
                 SURFref(2,i,j)=3
                 idist=SQRT((xorigin-Xcenter)**2)
                 if (idist<=lengthpreserved) then;
                 nbpointsroundpreserved=nbpointsroundpreserved+1
                 SURFref(2,i,j)=2
                 end if
                 if (idist>idistancemax) then;
                 idistancemax=idist
                 end if
                 jdist=SQRT((yorigin-Ycenterellipsoid)**2)
                 if (jdist>jdistancemax) then;
                 jdistancemax=jdist
                 end if
                 end if

             else;
             SURFref(1,i,j)=Nonvalue
             SURFref(2,i,j)=Nonvalue
             end if

    end do
    end do

    do i=1,dimi
    do j=1,dimj
    MUDref(1,i,j)=SURFref(1,i,j)
    MUDref(2,i,j)=SURFref(2,i,j)
    end do
    end do

    do mudcase=1,nbmudcases

    do i=1,dimi
    do j=1,dimj
    SURFref(1,i,j)=MUDref(1,i,j)
    SURFref(2,i,j)=MUDref(2,i,j)
    end do
    end do

   prop=mudcases(mudcase)


!For each cross-bedding surface, mutliple mudstone drape surfaces are created
depending on the number of mudstone drape coverage scenarios required in the
input parameter text file ("do loop" mudcase=1,nbmudcases above) by using the
subroutine muddrapesref

call  muddrapesref(Nonvalue,NumElement,limitesCUBE,SURFref,resolx,resoly,nbpoi
ntsline,nbpointsround,nbpointsroundpreserved,parameters,coordicenter,coordjc
```

```
enter,dimi,dimj,Xcenter,idistancemax,jdistancemax,routa,routb,routc,lengthpres
erved,prop)


!After the mudstone drape modelling, SURFref(2,:,:) is modified so that if there
is mudstone, SURFref(2,:,:) is made equal to 1; in the other case (mudstone
free cross-bedding surface, SURFref(2,:,:) is made equal to 0.
    do i=1,dimi
    do j=1,dimj
        if(SURFref(2,i,j)-1<Nonvalue) then;
        SURFref(2,i,j)=Nonvalue
        else;
            if (SURFref(2,i,j)<0.5) then;
            SURFref(2,i,j)=1
            else;
            SURFref(2,i,j)=0
            end if
        end if
    end do
    end do


!This final step is to ensure that the point of the cross-bedding surface is
located inside the cross-bed set ellipsoid (remember that the surfaces were
created initially in a rectangle parallelepiped)

    do i=1,n
    do j=1,m

        xfinal=(i-1)*resolx+limitesCUBE(1)
        yfinal=(j-1)*resoly+limitesCUBE(3)
        dist=SQRT((xfinal-Xcenterellipsoid)**2+(yfinal-Ycenterellipsoid)**2)
        if (xfinal==Xcenterellipsoid) then;
            if (yfinal==Ycenterellipsoid) then;
            thetafinal=0
            elseif (yfinal>Ycenterellipsoid) then;
            thetafinal=pi/2
            else;
            thetafinal=-pi/2
            end if
        elseif (xfinal>Xcenterellipsoid) then;
        thetafinal=atan((yfinal-Ycenterellipsoid)/(xfinal-Xcenterellipsoid))
        else;
        thetafinal=atan((yfinal-Ycenterellipsoid)/(xfinal-Xcenterellipsoid))+pi
        end if
        thetaorigin=thetafinal-theta
        xorigin=dist*cos(thetaorigin)+Xcenterellipsoid
        yorigin=dist*sin(thetaorigin)+Ycenterellipsoid
        coordiinf=coordicenter-(Xcenter-xorigin)/resolx
        coordjinf=coordjcenter-(Ycenterellipsoid-yorigin)/resoly
            kcase=(k-3)*nbmudcases+2+mudcase
        if (coordiinf<1.or.coordjinf<1.or.coordiinf+1>dimi.or.coordjinf+1>dimj)
then;
            MUD(kcase,i,j)=Nonvalue
            else;


!nbcontrol is a binary parameter of 4 digits corresponding to the 4 corners
of one cell. If mudstone is located only at 1 corner, or 2 diagonally opposite
corners, then there is no mudstone being modelled in the grid cell lately when
```

```
we create the grid parameter based on the mudstone drape zmap+ surface. In
all other cases (nbcontrol= 11, 101, 111, 1010, 1011, 1100, 1101, 1110 and 1111)
the mudstone drape will be created inside the cell grid.

nbcontrol=SURFref(2,coordiinf,coordjinf)*100+SURFref(2,coordiinf,coordjinf+1)*1
000+SURFref(2,coordiinf+1,coordjinf)*1+SURFref(2,coordiinf+1,coordjinf+1)*10
          if(nbcontrol==1001.or.nbcontrol==110.or.nbcontrol==1.or.nbcontrol==10.
or.nbcontrol==100.or.nbcontrol==1000.or.nbcontrol==0.or.nbcontrol<0) then;
                    MUD(kcase,i,j)=Nonvalue
                    else;
                    MUD(kcase,i,j)=SURF(k,i,j)
                    end if
                end if

    end do
    end do
    end do

    end if
!hspace and vspace are calculated based on the previous value and the sta-
tistics on standard deviation located in the parameter text file. That is to
ensure that foreset thickness follows a cycle to mimic the neap/spring tide
cyclicity. Xcenter and depth _ min are then recalculated for the next cross-
bedding surface to be created, starting from the beginning of the long “while
loop”.

    periode=periode+1
    hspace=0
    vspace=10
    hspacestdev=((cos((periode*1./28)*2*PI)/2)+0.5)*hspacestdevor
    vspacestdev=((cos((periode*1./28-0.5)*2*PI)/2)+0.5)*vspacestdevor
    do while (hspace<0.6.or.hspace>16)
    if (MOD(periode,28)==14) then;
    hspace=hspacemean
    else;
    call RANDOM _ NUMBER(temp)
      temp = log(SQRT(hspacestdev)) * SQRT(-2.0*LOG(temp)) * COS(2*pi*temp) +
log(hspacemean)
    hspace=exp(temp)
    end if
    end do

    vspace=hspace*tan(anglelimitTF*pi/180)

    depth _ min=depth _ min+vspace
    depth _ max=depth _ max+vspace
    Xcenter=Xcenter+hspace
    vspacecum=vspacecum+vspace

    if (compt>1) then;
    k=k+1
    end if

    end do

    Numsurf(NumElement)=k-1

    close (unit=30)

    end subroutine surfaces _ curved _ new
```

```
!-----------------------------------------------------------------------
!-----------------------------------------------------------------------
!-----------------------------------------------------------------------

subroutine muddrapesref(Nonvalue,NumElement,limitesCUBE,SURFref,resolx,resoly
,nbpointsline,nbpointsround,nbpointsroundpreserved,parameters,coordicenter,c
oordjcenter,dimi,dimj,Xcenter,idistancemax,jdistancemax,routa,routb,routc,leng
thpreserved,proportion)

    real::Nonvalue,limitesCUBE(6),resolx,resoly,routa,routb,routc,pi,proportion,
ell,paramG,paramH,paramK,coordireal,coordjreal
    integer::NumElement,n,m,dimi,dimj,nbpointsround,nbpointsline,i,j,nbpointsd
oneline,nbpointsdoneround,ismall,nbpointsroundpreserved
    real::radius,radiusmax,angle,pos,major,minor,ipole1,ipole2,jpole1,jpole2,imi
n,imax,jmin,jmax,ref,mud,Xcenter,idistancemax,jdistancemax,slope,length,length
preserved,paramtoeset,paramforeset
    integer::nbpointsell,coordiinf,coordjinf,coordicenter,coordjcenter,ismalle
st,nbpointsroundtrunc,k,nbpointscoordicenterdone,comptbreak
    real, allocatable:: parameters(:,:)
    real, allocatable:: TOWRITE(:,:)
    real, allocatable:: SURFref(:,:,:)
    character:: name*50

    parameter(pi=3.14159265)

    ell=parameters(NumElement,20)

    theta=0

    Xcenterellipsoid=parameters(NumElement,10)
    Ycenterellipsoid=parameters(NumElement,11)
    Zcenterellipsoid=parameters(NumElement,12)

    n=dimi
    m=dimj


!paramG, paramH and paramK are the three parameters of the mudstone frequency
function determined from outcrop analogue (see Figure 3.12)

    paramG=1.00354
    paramH=-9.65442/(2*lengthpreserved*0.00375)
    paramK=-4.3162



    coordicenter=((Xcenter-Xcenterellipsoid)/resolx)+n/2.
    ismallest=coordicenter

    coordjcenter=m/2.

    nbpointsdoneround=0
    nbpointsdoneline=0

    if (proportion==100) then;
    do i=1,dimi
    do j=1,dimj
        if (SURFref(1,i,j)-1>Nonvalue) then;
        SURFref(2,i,j)=0
```

```
        end if
    end do
    end do
    else;


    if (idistancemax>=2*resolx) then;

    if (coordicenter>0) then;


!First, mudstone drape ellitpical patches are added at the beginning along the
foreset part using the mudstone drape coverage of the scenario.

    do while(nbpointsdoneround<nbpointsroundpreserved*proportion/100)
        pos=2
        ref=0
        mud=1

        do while(ref<mud)
        coordiinf=1
        coordjinf=1


!Randomly choosing the location of the center of the elliptical patches.

        do while (SURFref(1,coordiinf,coordjinf)-1<Nonvalue)
        call random _ number(length)
        call random _ number(pos)
        coordireal=coordicenter*1.-(lengthpreserved/resolx)*pos
        call random _ number(length)
        call random _ number(pos)
            if(length>=0.5) then;
            coordjreal=coordjcenter*1.+(jdistancemax*1./resoly)*pos
            else;
            coordjreal=coordjcenter*1.-(jdistancemax*1./resoly)*pos
            end if

                coordiinf=coordireal+1
                coordjinf=coordjreal
                 if (coordiinf>n.or.coordjinf>m.or.coordiinf<2.or.coordjinf<2)
then;
                coordiinf=2
                coordjinf=2
                end if
                if (coordiinf>coordicenter) then;
                coordiinf=coordicenter
                end if

            end do

!Checking at the randomly chosen point of the elliptical mud patch what is
the condition to get mudstone being preserved from erosion using the mudstone
frequency function. The number is called ref, and is calculated between 0 and
1. Then a random number mud is picked between 0 and 1. If ref is bigger than
mud, then there can be an elliptical mud patch being located at this loca-
tion. If not, then we start again at the beginning of the "while loop" to find
another location that would satisfy the condition.

                slope=(ABS(SURFref(1,coordiinf,coordjinf)-SURFref(1,coordiinf-
1,coordjinf)))/resolx
```

```
        slope=slope+(ABS(SURFref(1,coordiinf+1,coordjinf)-SURFref(1,coordiinf,c
oordjinf)))/resolx
        slope=slope/2
        ref=paramG/(1+exp(paramH*slope+paramK))
        call random _ number(mud)
        mud=mud
        end do

        nbpointsell=0
```

!Now that the location of the elliptical mud patch has been approved, the dimensions of the elliptical patch are chosen randomly and the number of nodes of the grid covered by the ellipse are calculated. If there are less than 10 nodes, then dimensions are picked again randomly until 10 points of mud are at least generated.

```
              do while (nbpointsell<10)

                  nbpointsell=0
                        call random _ number(major)
                  major=ell*(major)*lengthpreserved/100
                  call random _ number(minor)
                  minor=minor*major

                        ipole1=(SQRT(major**2-minor**2))/resolx
                jpole1=0
                ipole2=-ipole1
                jpole2=-jpole1
                imin=-(major/resolx)-1
                imax=(major/resolx)+1
                jmin=-(minor/resoly)-1
                jmax=(minor/resoly)+1

                        do i=imin,imax
                  do j=jmin,jmax
                    dist=SQRT(((ipole1*1.-i*1.)*resolx)**2+((jpole1*1.-j*1.)*resoly
)**2)+SQRT(((ipole2*1.-i*1.)*resolx)**2+((jpole2*1.-j*1.)*resoly)**2)
                     if (dist<2*major) then;
                     nbpointsell=nbpointsell+1
                     end if
                     end do
                end do

        end do
```

!The angle of rotation of the mud patch is chosen randomly and positions of the two poles of the ellipse are calculated accordingly.

```
        call random _ number(anglemud)
        anglemud=anglemud*pi
        jpole1=coordjreal+(ipole1*resolx)*sin(anglemud)/resoly
        jpole2=coordjreal+(ipole2*resolx)*sin(anglemud)/resoly
        ipole1=coordireal+(ipole1*resolx)*cos(anglemud)/resolx
        ipole2=coordireal+(ipole2*resolx)*cos(anglemud)/resolx
```

```
        imin=floor(coordireal-(major/resolx))
        if(imin<1) then;
        imin=1
        end if
        imax=ceiling(coordireal+(major/resolx))
        if(imax>dimi) then;
        imax=dimi
        end if
        jmin=floor(coordjreal-(major/resoly))
        if(jmin<1) then;
        jmin=1
        end if
        jmax=ceiling(coordjreal+(major/resoly))
        if(jmax>dimj) then;
        jmax=dimj
        end if
```

!Checking if the points are well inside the mudstone patch and if there was mudstone being already modelled at the position. If not, then a new mudstone point is added, and that until we reach the proportion of the surface being covered by mudstone drape specified in the input parameter file. We count the points being modelled along the foreset part or the toeset part of the cross-bedding surface.

```
        do i=imin,imax
            do j=jmin,jmax
                        if (SURFref(2,i,j)>0.5) then;
                                    dist=SQRT(((ipole1-i)*resolx)**2+((jpole1-
j)*resoly)**2)+SQRT(((ipole2-i)*resolx)**2+((jpole2-j)*resoly)**2)

                    if (dist<2*major) then;
                        if (SURFref(2,i,j)==1) then;
                        SURFref(2,i,j)=0
                        nbpointsdoneline=nbpointsdoneline+1
                        else if (SURFref(2,i,j)==2.or.SURFref(2,i,j)==3) then;
                        SURFref(2,i,j)=0
                        nbpointsdoneround=nbpointsdoneround+1
                            if(i<ismallest) then;
                            ismallest=i
end if
end if
end if
end if
end do
end do
end do
end if

    else;
```

!This one is a repeat of the previous section for the case when the preserved cross-bedding surface is very small (only covering a distance of 1 resolx in the x direction, meaning only two raw of nodes: the raw of nodes corresponding to the junction line of the 0 points between foreset and toeset parts, and one additional raw of points). This is too small for the previous conditions

```
to be used. Mudstone can only be populated four nodes by four nodes to in-
sure that, ulitmately, when creating the mudstone parameter from the mudstone
drape zmap surface (see section on the binary codes 0,1,10,11,100,101...1111 and
so on, at least two diagonally opposite nodes with mudstone drape for mudstone
being populated in the cell), the proportion of cells with mudstone will be
respected.

        if (coordicenter>0) then;

    do while(nbpointsdoneround<nbpointsroundpreserved*proportion/100)

        pos=2
        ref=0
        mud=1
        coordiinf=1
        coordjinf=1

                    do   while   (SURFref(1,coordiinf,coordjinf)-1<Nonvalue.
and.SURFref(1,coordiinf+1,coordjinf)-1<Nonvalue.and.
SURFref(1,coordiinf,coordjinf+1)-1<Nonvalue.and.SURFref(1,coordiinf+1,coordji
nf+1)-1<Nonvalue)
        call random_number(length)
        call random_number(pos)
        coordireal=coordicenter*1.-(idistancemax/resolx)*pos
        call random_number(length)
        call random_number(pos)
            if(length>=0.5) then;
            coordjreal=coordjcenter*1.+(jdistancemax*1./resoly)*pos
            else;
            coordjreal=coordjcenter*1.-(jdistancemax*1./resoly)*pos
            end if

                coordiinf=coordireal
                coordjinf=coordjreal
                 if (coordiinf>n.or.coordjinf>m.or.coordiinf<1.or.coordjinf<1)
then;
                coordiinf=1
                coordjinf=1
                end if
                if (coordiinf>coordicenter) then;
                coordiinf=coordicenter
                end if

            end do

        nbpointsell=0

        do while (nbpointsell<10)

                  nbpointsell=0
                        call random_number(major)
                  major=ell*(major)*lengthpreserved/100
                  call random_number(minor)
                  minor=minor*major

                        ipole1=(SQRT(major**2-minor**2))/resolx
                jpole1=0
                ipole2=-ipole1
                jpole2=-jpole1
                imin=-(major/resolx)-1
```

```
                imax=(major/resolx)+1
                jmin=-(minor/resoly)-1
                jmax=(minor/resoly)+1

                        do i=imin,imax
                  do j=jmin,jmax
                    dist=SQRT(((ipole1*1.-i*1.)*resolx)**2+((jpole1*1.-j*1.)*resoly
)**2)+SQRT(((ipole2*1.-i*1.)*resolx)**2+((jpole2*1.-j*1.)*resoly)**2)
                     if (dist<2*major) then;
                     nbpointsell=nbpointsell+1
                     end if
                     end do
                end do

        end do

        call random _ number(anglemud)
        anglemud=anglemud*pi
        jpole1=coordjreal+(ipole1*resolx)*sin(anglemud)/resoly
        jpole2=coordjreal+(ipole2*resolx)*sin(anglemud)/resoly
        ipole1=coordireal+(ipole1*resolx)*cos(anglemud)/resolx
        ipole2=coordireal+(ipole2*resolx)*cos(anglemud)/resolx

        imin=floor(coordireal-(major/resolx))
        if(imin<1) then;
        imin=1
        end if
        imax=ceiling(coordireal+(major/resolx))
        if(imax>dimi) then;
        imax=dimi
        end if
        jmin=floor(coordjreal-(major/resoly))
        if(jmin<1) then;
        jmin=1
        end if
        jmax=ceiling(coordjreal+(major/resoly))
        if(jmax>dimj) then;
        jmax=dimj
        end if

        do i=imin,imax
            do j=jmin,jmax
                        if (SURFref(2,i,j)>0.5) then;
                                    dist=SQRT(((ipole1-i)*resolx)**2+((jpole1-
j)*resoly)**2)+SQRT(((ipole2-i)*resolx)**2+((jpole2-j)*resoly)**2)

                     if (dist<2*major) then;
                         if (SURFref(2,i,j)==1) then;
                         SURFref(2,i,j)=0
                         nbpointsdoneline=nbpointsdoneline+1
                         else if (SURFref(2,i,j)==2.or.SURFref(2,i,j)==3) then;
                         SURFref(2,i,j)=0
                         nbpointsdoneround=nbpointsdoneround+1
                         end if

                     end if

                         end if
            end do
        end do
```

```
    end do
    end if
    end if


!Secondly, the mudstone patches are being modelled along the linear toeset
part of the cross-bedding surface, using the proportion of mudstone at the
junction line as a reference for the proportion of mudstone along the toeset,
in order to insure continuity between the toeset and the foreset in the mud-
stone drape proportion (proportion is varying from bottom to top due to the
mudstone frequency function).


!Here we count the number of points at the junction line where mudstone was
modelled during the first part of the subroutine along the foreset part of the
cross-bedding surface.

    nbpointsroundtrunc=0
    nbpointscoordicenterdone=0
    if (coordicenter>0) then;
    do j=1,m
        if (SURFref(1,coordicenter,j)-1>Nonvalue) then;
        nbpointsroundtrunc=nbpointsroundtrunc+1
        end if
     if (SURFref(2,coordicenter,j)<0.5.and.SURFref(2,coordicenter,j)-2>Nonvalue)
then;
        nbpointscoordicenterdone=nbpointscoordicenterdone+1
        end if
    end do
    end if

    if (nbpointsroundtrunc>0.5) then;
    paramtoeset=(paramG/(1+exp(paramH*(tan(-parameters(NumElement,8)*pi/180))+p
aramK)))*100
    paramforeset=nbpointscoordicenterdone*100/nbpointsroundtrunc
        if (paramforeset<paramtoeset) then;
        proportion=(paramforeset+paramtoeset)/2.
        else;
        proportion=paramforeset
        end if
    else;
     paramtoeset=paramG/(1+exp(paramH*(tan(-parameters(NumElement,8)*pi/180))+p
aramK))
    proportion=paramtoeset*100
    end if



!The modelling of mudstone patches along the toeset part starts here, in a
very similar fashion than for the foreset part.

if (nbpointsline>0) then;

    if (proportion==100) then;
    do i=coordicenter+1,dimi
    do j=1,dimj
        if (SURFref(1,i,j)-1>Nonvalue) then;
```

```
        SURFref(2,i,j)=0
        end if
    end do
    end do

    else;

    do while(nbpointsdoneline<nbpointsline*proportion/100)

        pos=2
        ref=0
        mud=1

        do while(ref<mud)
        coordiinf=1
        coordjinf=1

            do while (SURFref(1,coordiinf,coordjinf)-1<Nonvalue)
            call random _ number(pos)
            call random _ number(length)
            call random _ number(angle)
            coordireal=(n*1.-coordicenter*1.)*length+coordicenter*1.
            if (angle>=0.5) then;
            coordjreal=(m*pos/2)+coordjcenter*1.
            else;
            coordjreal=-(m*pos/2)+coordjcenter*1.
            end if
            coordiinf=coordireal
            coordjinf=coordjreal
                 if (coordiinf>n.or.coordjinf>m.or.coordiinf<1.or.coordjinf<1)
then;
                coordiinf=1
                coordjinf=1
                end if
            end do

        if (coordiinf>1) then;
                slope=(ABS(SURFref(1,coordiinf,coordjinf)-SURFref(1,coordiinf-
1,coordjinf)))/resolx
        slope=slope+(ABS(SURFref(1,coordiinf+1,coordjinf)-SURFref(1,coordiinf,c
oordjinf)))/resolx
        slope=slope/2
        else;
        slope=-Nonvalue
        end if

        ref=paramG/(1+exp(paramH*slope+paramK))
        call random _ number(mud)
        end do

        nbpointsell=0

        do while (nbpointsell<10)

                nbpointsell=0
                    call random _ number(major)
                major=ell*(major)*lengthpreserved/100
                call random _ number(minor)
                minor=minor*major
```

```
                        ipole1=(SQRT(major**2-minor**2))/resolx
                jpole1=0
                ipole2=-ipole1
                jpole2=-jpole1
                imin=-(major/resolx)-1
                imax=(major/resolx)+1
                jmin=-(minor/resoly)-1
                jmax=(minor/resoly)+1

                        do i=imin,imax
                  do j=jmin,jmax
                    dist=SQRT(((ipole1*1.-i*1.)*resolx)**2+((jpole1*1.-j*1.)*resoly
)**2)+SQRT(((ipole2*1.-i*1.)*resolx)**2+((jpole2*1.-j*1.)*resoly)**2)
                     if (dist<2*major) then;
                     nbpointsell=nbpointsell+1
                     end if
                     end do
                end do
        end do

call random _ number(anglemud)
        anglemud=anglemud*pi
        jpole1=coordjreal+(ipole1*resolx)*sin(anglemud)/resoly
        jpole2=coordjreal+(ipole2*resolx)*sin(anglemud)/resoly
        ipole1=coordireal+(ipole1*resolx)*cos(anglemud)/resolx
        ipole2=coordireal+(ipole2*resolx)*cos(anglemud)/resolx

        imin=floor(coordireal-(major/resolx))
        if(imin<1) then;
        imin=1
        end if
        imax=ceiling(coordireal+(major/resolx))
        if(imax>dimi) then;
        imax=dimi
        end if
        jmin=floor(coordjreal-(major/resoly))
        if(jmin<1) then;
        jmin=1
        end if
        jmax=ceiling(coordjreal+(major/resoly))
        if(jmax>dimj) then;
        jmax=dimj
        end if

        do i=imin,imax
            do j=jmin,jmax
                        if (SURFref(2,i,j)>0.5) then;
                                    dist=SQRT(((ipole1-i)*resolx)**2+((jpole1-
j)*resoly)**2)+SQRT(((ipole2-i)*resolx)**2+((jpole2-j)*resoly)**2)
                     if (dist<2*major) then;
                        if (SURFref(2,i,j)==1) then;
                        SURFref(2,i,j)=0
                        nbpointsdoneline=nbpointsdoneline+1
                        else if (SURFref(2,i,j)==2.or.SURFref(2,i,j)==3) then;
                        SURFref(2,i,j)=0
                        nbpointsdoneround=nbpointsdoneround+1
                        end if
                     end if
                        end if
            end do
```

```
        end do


    end do
    end if
    end if
    end if


!Final creation of the mudstone drape parameter in SURFref(1,:,:)

    do i=1,n
    do j=1,m
        if(SURFref(2,i,j)==0) then;
        SURFref(1,i,j)=SURFref(1,i,j)
        else;
        SURFref(1,i,j)=Nonvalue
        end if
    end do
    end do

end subroutine muddrapesref

!-------------------------------------------------------------------------
!-------------------------------------------------------------------------
!-------------------------------------------------------------------------

!This subroutine was never implemented but is supposed to create the input
parameter text file containing all the informations in an automated process.

subroutine create _ parameters(Nonvalue)

real:: Nonvalue
integer:: Nbelements
real:: parametersfile(50,20)
real:: PointO(3)
integer:: Nbcellsx,Nbcellsy,nbmudcases
real::resolz,Lx,Ly,Lz,pi,propell,angleprograd,hspacemean,hspacestdev,vspacemea
n,vspacestdev,routa,routb,routc,hspace,vspace,routamean,routbmean,routcmean,ro
utastdev,routbstdev,routcstdev
real::anglerot,anglerotstdev,anglerotmean,temp,deltax,deltay,deltaz,deltazm
ean,deltazstdev,deltaymean,deltaystdev,xcenter,ycenter,zcenter,xp,yp,zp,xor-
igin,yorigin
real:: angledip,angledipmean,angledipstdev,anglelimitTF
real, allocatable:: mudcases(:)
real:: limitesCUBE(6)
parameter(pi=3.14159265)

Nonvalue=-9999
PointO(1)=0
PointO(2)=0
PointO(3)=0


print*,'Size of the model in the x,y and z direction (in cm):'
read*,Lx,Ly,Lz
print*,'Number of cells in the x and y direction:'
read*,Nbcellsx,Nbcellsy
print*,'Thickness of cell layers:'
```

```
read*,resolz
print*,'Number of muddrape cases:'
read*,nbmudcases
if(allocated(mudcases)) then;
deallocate(mudcases)
end if
allocate(mudcases(nbmudcases))
do i=1,nbmudcases
print*,'Mud case',i,':'
read*,mudcases(i)
end do
print*,'Proportion (0-100) of the length of mud patches compared to surface:'
read*,propell
print*,'Angle of progradation:'
read*,angleprograd
print*,'Mean dip angle toesets:'
read*,angledip

hspacemean=3.57
hspacestdev=1.9
vspacemean=0.96
vspacestdev=0.16
routamean=1250
routastdev=100
routbmean=239.5
routbstdev=131
routcmean=72.5
routcstdev=63.4
deltaymean=-41.3
deltaystdev=411.8
deltazmean=-3.1
deltazstdev=103.7
anglerotstdev=25*PI/180

CALL RANDOM_SEED()
routa=-Nonvalue
do while (routa>2*routamean.or.routa<routamean/2)
call RANDOM_NUMBER(temp)
temp = log(SQRT(routastdev)) * SQRT(-2.0*LOG(temp)) * COS(2*pi*temp) +
log(routamean)
routa=exp(temp)
end do
routb=routa+1
do while(routb>routa.or.routb<50)
call RANDOM_NUMBER(temp)
temp = log(SQRT(routbstdev)) * SQRT(-2.0*LOG(temp)) * COS(2*pi*temp) +
log(routbmean)
routb=exp(temp)
end do
routc=routb+1
do while (routc>routb.or.routc<15)
call RANDOM_NUMBER(temp)
temp = log(SQRT(routcstdev)) * SQRT(-2.0*LOG(temp)) * COS(2*pi*temp) +
log(routcmean)
routc=exp(temp)
end do
call RANDOM_NUMBER(temp)
temp = log(SQRT(anglerotstdev)) * SQRT(-2.0*LOG(temp)) * COS(2*pi*temp) + log(PI)
anglerot=exp(temp)-PI
```

```
call RANDOM _ NUMBER(temp)
anglelimitTF=temp*10
xcenter=PointO(1)-Lx/2
ycenter=PointO(2)+Ly/2
zcenter=PointO(3)-Lz/2-routc
limitesCUBE(1)=PointO(1)-Lx/2
limitesCUBE(2)=PointO(1)+Lx/2
limitesCUBE(3)=PointO(2)-Ly/2
limitesCUBE(4)=PointO(2)+Ly/2
limitesCUBE(5)=PointO(3)-Lz/2
limitesCUBE(6)=PointO(3)+Lz/2
n=(limitesCUBE(2)-limitesCUBE(1))/resolx+1
m=(limitesCUBE(4)-limitesCUBE(3))/resoly+1
Nbelements=0

do while (zcenter-routc<=PointO(3)+Lz/2)
Nbelements=Nbelements+1
parametersfile(Nbelements,1)=routc
parametersfile(Nbelements,2)=0
parametersfile(Nbelements,3)=routc
parametersfile(Nbelements,4)=0
parametersfile(Nbelements,5)=routa
parametersfile(Nbelements,6)=routb
parametersfile(Nbelements,7)=anglerot*180/PI
parametersfile(Nbelements,8)=angledip
parametersfile(Nbelements,9)=0
parametersfile(Nbelements,10)=xcenter
parametersfile(Nbelements,11)=ycenter
parametersfile(Nbelements,12)=zcenter
parametersfile(Nbelements,13)=hspacemean
parametersfile(Nbelements,14)=hspacestdev
parametersfile(Nbelements,15)=0
parametersfile(Nbelements,16)=0
parametersfile(Nbelements,17)=anglelimitTF
parametersfile(Nbelements,18)=0
parametersfile(Nbelements,19)=0
parametersfile(Nbelements,20)=propell

routa=-Nonvalue
do while (routa>2*routamean.or.routa<routamean/2)
call RANDOM _ NUMBER(temp)
temp   =   log(SQRT(routastdev))   *   SQRT(-2.0*LOG(temp))   *   COS(2*pi*temp)   +
log(routamean)
routa=exp(temp)
end do
routb=routa+1
do while(routb>routa.or.routb<50)
call RANDOM _ NUMBER(temp)
temp   =   log(SQRT(routbstdev))   *   SQRT(-2.0*LOG(temp))   *   COS(2*pi*temp)   +
log(routbmean)
routb=exp(temp)
end do
routc=routb+1
do while (routc>routb.or.routc<15)
call RANDOM _ NUMBER(temp)
temp   =   log(SQRT(routcstdev))   *   SQRT(-2.0*LOG(temp))   *   COS(2*pi*temp)   +
log(routcmean)
routc=exp(temp)
end do
```

```
call RANDOM _ NUMBER(temp)
temp = log(SQRT(anglerotstdev)) * SQRT(-2.0*LOG(temp)) * COS(2*pi*temp) + log(PI)
anglerot=exp(temp)-PI
call RANDOM _ NUMBER(temp)
temp = log(SQRT(Deltazstdev)) * SQRT(-2.0*LOG(temp)) * COS(2*pi*temp) + log(ABS(
Deltazmean))*(ABS(Deltazmean)/Deltazmean)
Deltaz=exp(temp)
call RANDOM _ NUMBER(temp)
temp = log(SQRT(Deltaystdev)) * SQRT(-2.0*LOG(temp)) * COS(2*pi*temp) + log(ABS(
Deltaymean))*(ABS(Deltaymean)/Deltaymean)
Deltay=exp(temp)
Deltax=Deltaz/tan(angleprograd*PI/180)
call RANDOM _ NUMBER(temp)
anglelimitTF=temp*10
xcenter=xcenter+Deltax
ycenter=ycenter+Deltay
zcenter=zcenter+Deltaz
end do

open(unit=10,file="parameters.txt")
write(10,*) Nonvalue
write(10,*) Nbelements
do i=1,Nbelements
write(10,*) parametersfile(Nbelements-i+1,1:20)
end do
write(10,*) Lx,Ly,Lz
write(10,*) PointO(1:3)
write(10,*) Nbcellsx,Nbcellsy,resolz
write(10,*) nbmudcases
write(10,*) mudcases(1:nbmudcases)
close(unit=10)

end subroutine create _ parameters


!---------------------------------------------------------------------------
!---------------------------------------------------------------------------
!---------------------------------------------------------------------------
subroutine mudparameter(nbmudcases,mudcases)
    interface
        subroutine readzmapfilesbis(NumElement,Numsurf,MUDDRAPE,SPACE,name)
            real, allocatable :: MUDDRAPE(:,:)
            integer :: NumElement,Numsurf,SPACE
            character:: name*50
        end subroutine
    end interface

    interface
        subroutine writegridfaciesfile(GRIDFACIES,nblayers,n,m,nameBIS)
            integer :: m,n,nblayers
            real, allocatable :: GRIDFACIES(:,:,:)
            character:: nameBIS*50
        end subroutine
    end interface

integer, allocatable :: Nbsurf(:)
real, allocatable:: mudcases(:)
real, allocatable :: MUDDRAPE(:,:)
real, allocatable :: GRIDFACIES(:,:,:)
```

```
real, allocatable :: GRIDFACIES2(:,:,:)
integer::Element,n,m,i,nbzones,j,k,nblayers,numlayer,nbcontrol,NumElement,Nums
urf,nbmudcases,mudcase,ibis,l
real::Nonvalue,limitesCUBE(6)
character:: name*50,id*5,ie*5,ig*5,nameBIS*50


!This subroutine will create all permeability parameters corresponding to the
different mudstone drape scenarios for the grid as well as the grid file. All
files are grdecl files that can be imported into Eclipse for flow simulation.

open(unit=50,file="results.txt")
    read(50,*) Nonvalue
    Nonvalue=-Nonvalue
    read(50,*) Element
    read(50,*) limitesCUBE(1:6)
    read(50,*) n,m
    allocate (Nbsurf(Element))
    do i=1,Element
    read(50,*) Nbsurf(i),Nbsurf(i)
    end do
close(unit=50)

do mudcase=1,nbmudcases
nbpointstotal=0
open(unit=60, file="layers.txt")
    read(60,*) nbzones
    read(60,*) nblayers

    if(allocated(GRIDFACIES)) then;
      deallocate(GRIDFACIES)
      end if
    allocate(GRIDFACIES(nblayers,n-1,m-1))


!The permeability for the sandstone which is used in the parameter file is 77
mD. Mudstone is set with 0 mD.

do k=1,nblayers
    do i=1,n-1
    do j=1,m-1
        GRIDFACIES(k,i,j)=77
    end do
    end do
end do


!All the cross-bedding surfaces are opened one after the other from the bot-
tom of the model to the top in order to recover the zdepth of the nodes of
the zmap+ surfaces that will correspond to the corners of the grid cells of
the grid created.

do l=1,Element
do k=1,Nbsurf(l)
if (l==Element.and.k==Nbsurf(l)) then;
else;
read(60,*) numlayer
if(k/=Nbsurf(l)) then;
   open(unit=15,file="listing.txt")
```

```
        do ibis=1,mudcase
            read(15,*) ig
        end do
   close(unit=15)
   open(unit=15,file="listing.txt")
        do ibis=1,l
            read(15,*) id
        end do
    close(unit=15)
    open(unit=15,file="listing.txt")
        do ibis=1,k
            read(15,*) ie
        end do
    close(unit=15)
  name="MUD _ case _ "//trim(ig)//" _ Element _ "//trim(id)//" _ Zone _ "//trim(ie)//".
zmap+"

    if (allocated(MUDDRAPE)) then;
    deallocate(MUDDRAPE)
    end if
    allocate(MUDDRAPE(n,m))
    call readzmapfilesbis(l,k,MUDDRAPE,n,name)

    do i=1,n-1
    do j=1,m-1
nbcontrol=MUDDRAPE(i,j)*100+MUDDRAPE(i,j+1)*1000+MUDDRAPE(i+1,j)*1+MUDDRAPE(i+1
,j+1)*10


!Mudstone permeability (0mD) is set in the grid only if there is mudstone lo-
cated at two diagonally opposite corners of the grid cell.
          if(nbcontrol==1001.or.nbcontrol==110.or.nbcontrol==1.or.nbcontrol==10.
or.nbcontrol==100.or.nbcontrol==1000.or.nbcontrol==0) then;
        GRIDFACIES(numlayer,m-j,i)=77
        nbpointstotal=nbpointstotal+1
        else;
        GRIDFACIES(numlayer,m-j,i)=0
        nbpointstotal=nbpointstotal+1
        end if
    end do
    end do
    end if
    end if
end do
end do
close(unit=60)


!The grid files and the parameter files are generated by the subroutine write-
gridfaciesfile

print*,nbpointstotal
nameBIS="HorizontalPermeabilityMuddcase"//trim(ig)//".GRDECL"
call writegridfaciesfile(GRIDFACIES,nblayers,n,m,nameBIS)


!The vertical permeability case corresponds to the same parameter than the
horizontal permeability but for flow simulation experiments where the flow is
vertical. Because we introduce buffer zones at two opposite faces of the mod-
el, we need to create two extra layers of cells in the case of the vertical
```

flow simulation, as the first and last layer of cells are not continuous over the entire model and not uniform in thickness. So, two extra layers are created for the vertical flow simulation. The permeability file is the same than the for the horizontal flow simulation except that we add two layers of cells with the permeability of sandstone in the first layer and in the last layer of cells, so the permeability parameter is shifted from GRIDFACIES(k-1,:,:) to GRIDFACIES2(k,:,:). The grid file and parameter files are generated by the writegridfaciesfile subroutine.

```
nameBIS="VerticalPermeabilityMuddcase"//trim(ig)//".GRDECL"
    if(allocated(GRIDFACIES2)) then;
      deallocate(GRIDFACIES2)
      end if
    allocate(GRIDFACIES2(nblayers+2,n-1,m-1))

do k=1,nblayers+2
do i=1,n-1
do j=1,m-1
if (k==1.or.k==nblayers+2) then;
GRIDFACIES2(k,i,j)=77
else;
GRIDFACIES2(k,i,j)=GRIDFACIES(k-1,i,j)
end if
end do
end do
end do

call writegridfaciesfile(GRIDFACIES2,nblayers+2,n,m,nameBIS)

end do

end subroutine mudparameter

!-------------------------------------------------------------------------
!-------------------------------------------------------------------------
!-------------------------------------------------------------------------

subroutine readzmapfiles(name,MUDDRAPE,SPACE)

integer:: n,m,NumElement,Numsurf,ibis,nfile,mfile,i,j,k,SPACE
real, allocatable:: MUDDRAPE(:,:)
integer:: dummy1,lines,rest,h,raw,mode, numsurfCUBEmax
character:: name*100,ie*5,id*5
character:: dummy2*10
real :: numb,xminfile,xmaxfile,yminfile,ymaxfile,Nonvaluefile
real :: passagefive(5),passagefour(4),passagethree(3),passagetwo(2)
real :: passageone
real:: passage(SPACE,5)


call listing(1000)

    open(unit=15,file="listing.txt")
        do ibis=1,NumElement
            read(15,*) id
        end do
    close(unit=15)
    open(unit=15,file="listing.txt")
        do ibis=1,Numsurf
            read(15,*) ie
```

```
        end do
    close(unit=15)


!The subroutine is for reading any zmap+ file as exported from Petrel or RMS.
The data is stored in different parameters. Parameters on the number of nodes
and spacing between the nodes - the x and y resolution - can be deduced from
the header of the file. Then the zdepth values of the nodes of the surface are
read and stored in the array MUDDRAPE that is transmitted to the subroutine
and handed back to the main program with the values for the surface.

open(unit=20,file=name)
    read(20,*) dummy2
      read(20,*) dummy2
      read(20,*) dummy2
      read(20,*) dummy2
      read(20,*) dummy2
      read(20,*) dummy2
      read(20,*) numb, Nonvaluefile
      read(20,*) mfile, nfile, xminfile, xmaxfile, yminfile, ymaxfile
      read(20,*) dummy2
    read(20,*) dummy2

    lines=mfile/5+1
    rest=mfile-(lines-1)*5
      if (rest==0) then;
      lines=lines-1
    end if

      do i=1,nfile
      h=1
        do j=1,(lines-1)
        read(20,*) passagefive
        passage(h,1:5)=passagefive
        h=h+1
      end do

            if (rest==1) then;
          read (20,*) passageone
          passage(h,1)=passageone
        else if (rest==2) then;
          read (20,*) passagetwo
          passage(h,1:2)=passagetwo
        else if (rest==3) then;
          read (20,*) passagethree
          passage(h,1:3)=passagethree
        else if (rest==4) then;
          read (20,*) passagefour
          passage(h,1:4)=passagefour
        else;
          read (20,*) passagefive
          passage(h,1:5)=passagefive
            end if

            do k=1,mfile
          raw=k/5
          mode=k-raw*5
          if (mode==0) then;
            mode=5
            raw=raw-1
```

```
          end if
          MUDDRAPE(i,k)=passage(raw+1,mode)
        end do
     end do
 close(unit=20)

 end subroutine readzmapfiles

!-------------------------------------------------------------------------
!-------------------------------------------------------------------------
!-------------------------------------------------------------------------

subroutine readzmapfilesbis(NumElement,Numsurf,MUDDRAPE,SPACE,name)

integer:: n,m,NumElement,Numsurf,ibis,nfile,mfile,i,j,k,SPACE
real, allocatable:: MUDDRAPE(:,:)
integer:: dummy1,lines,rest,h,raw,mode, numsurfCUBEmax
character:: name*50,ie*5,id*5
character:: dummy2*10
real :: numb,xminfile,xmaxfile,yminfile,ymaxfile,Nonvaluefile
real :: passagefive(5),passagefour(4),passagethree(3),passagetwo(2)
real :: passageone
real:: passage(SPACE,5)


call listing(1000)


!At the difference of the previous subroutine, this subroutine is used to read
the zmap+ files (cross-bedding surfaces and mudstone drapes) that have been
created during the modelling process of the program. The header is different
than for a file exported from Petrel and RMS. There is room for improvement in
order to combine the two subroutines into a single one...

open(unit=20,file=trim(name))
    read(20,*) dummy2
      read(20,*) dummy2
      read(20,*) dummy2
      read(20,*) dummy2
      read(20,*) dummy2
      read(20,*) dummy2
      read(20,*) numb, Nonvaluefile
      read(20,*) mfile, nfile, xminfile, xmaxfile, yminfile, ymaxfile
      read(20,*) dummy2
    read(20,*) dummy2

    lines=mfile/5+1
    rest=mfile-(lines-1)*5
      if (rest==0) then;
      lines=lines-1
    end if

      do i=1,nfile
      h=1
        do j=1,(lines-1)
        read(20,*) passagefive
        passage(h,1:5)=passagefive
        h=h+1
      end do
```

```
            if (rest==1) then;
          read (20,*) passageone
          passage(h,1)=passageone
        else if (rest==2) then;
          read (20,*) passagetwo
          passage(h,1:2)=passagetwo
        else if (rest==3) then;
          read (20,*) passagethree
          passage(h,1:3)=passagethree
        else if (rest==4) then;
          read (20,*) passagefour
          passage(h,1:4)=passagefour
        else;
          read (20,*) passagefive
          passage(h,1:5)=passagefive
            end if

            do k=1,mfile
          raw=k/5
          mode=k-raw*5
          if (mode==0) then;
            mode=5
            raw=raw-1
          end if
          MUDDRAPE(i,k)=passage(raw+1,mode)
        end do
    end do
 close(unit=20)

 do i=1,nfile
 do j=1,mfile
     if (MUDDRAPE(i,j)+1>Nonvaluefile) then;
     MUDDRAPE(i,j)=0
     else;
     MUDDRAPE(i,j)=1
     end if
 end do
 end do

 end subroutine readzmapfilesbis

!---------------------------------------------------------------------------
!---------------------------------------------------------------------------
!---------------------------------------------------------------------------

subroutine writegridfaciesfile(GRIDFACIES,nblayers,n,m,nameBIS)

character :: nameBIS*50
integer :: m,n,i,j,k,nblayers
real, allocatable :: GRIDFACIES(:,:,:)

!The paramater file for permeability is only a list of numbers, corresponding
to the value of permeability in all the cells of the grid, after the keyword
PERMX is introduced.

      open(unit=30,file=nameBIS)
      write(30,"(A5)") "PERMX"
    do k=1,nblayers
    do i=1,n-1
          write(30,"(1F10.4,1X,1F10.4,1X,1F10.4,1X,1F10.4,1X,1F10.4)")
```

```
GRIDFACIES(k,i,1:m-1)
    end do
    end do
    write(30,"(A1)") "/"
    close(unit=30)


end subroutine writegridfaciesfile

!---------------------------------------------------------------------------
!---------------------------------------------------------------------------
!---------------------------------------------------------------------------

subroutine writegridfile(limitesCUBE,resolx,resoly,Nbcellsx,Nbcellsy,numlayers,
nbzones,nblayers,SPACE,n,m,resolz)

interface
    subroutine readzmapfiles(name,MUDDRAPE,SPACE)
    character:: name*100
    real, allocatable:: MUDDRAPE(:,:)
    integer:: SPACE
    end subroutine
end interface

real:: limitesCUBE(6)
real:: resolx,resoly,coordy,coordx,refbottom,resolz
integer:: Nbcellsx,Nbcellsy,nbzones,nblayers,i,j,ibis,jbis,kbis,SPACE,layer,n,m,
nbzonesmade,compt,nbtotallayers,nbpointstotal,iter,jter,kter
integer:: numlayers(5000)
character:: nameSURFtop*100, nameSURFbottom*100
real, allocatable:: SURFTOP(:,:)
real, allocatable:: SURFBOTTOM(:,:)
real, allocatable:: ACTNUM(:,:,:)


!This is maybe the most complicated part of the code, not in term of the sci-
ence, but because of the orientation convetions of Petrel and Eclipse for the
grid. The subroutine generates the grdecl GRID file for flow simulation. The
grid is a corner-point grid.

nbpointstotal=0
if (allocated(ACTNUM)) then;
deallocate (ACTNUM)
end if
allocate (ACTNUM(nblayers+1,n,m))
do k=1,nblayers+1
do i=1,n
do j=1,m
ACTNUM(k,i,j)=9999
end do
end do
end do


!For the same reasons explained in the mudparameter subroutine, two grids are
created simultaneously: the GridmodelVertical grid is created for flow simula-
tion experiments with a vertical flow orientation in order because of the two
extra layers of cells required for introducing a uniformly thick buffer zone
at the two opposite bottom and top faces.
```

```
open(unit=10,file="GridmodelHorizontal.grdecl")
open(unit=30,file="GridmodelVertical.grdecl")


!The keyword SPECGRID is transparent: after that, the number of cells in the
x direction, then in the y direction, then the number of layers in the z di-
rection is introduced.

write(10,"(A8,/,I5,1X,I5,1X,I5,A2)") "SPECGRID",Nbcellsx, Nbcellsy,nblayers," /"
write(30,"(A8,/,I5,1X,I5,1X,I5,A2)") "SPECGRID",Nbcellsx, Nbcellsy,nblayers+2," /"


!The keyword COORD is introduced afterwards. It is followed by the list of
the (x,y) coordinates of the regularly spaced vertical pillars of the corner-
point grid.

write(10,"(A5)") "COORD"
write(30,"(A5)") "COORD"
coordy=limitesCUBE(4)-limitesCUBE(3)
do j=1,Nbcellsy+1
coordx=0
    do i=1,Nbcellsx+1
    write(10,"(1F10.4,1X,1F10.4,1X,1F10.4,1X,1F10.4,1X,1F10.4,1X,1F10.4)") coordx,coo
rdy,limitesCUBE(5),coordx,coordy,limitesCUBE(6)
               write(30,"(1F10.4,1X,1F10.4,1X,1F10.4,1X,1F10.4,1X,1F10.4,1X,1F10.4)")
coordx,coordy,limitesCUBE(5)-resolz,coordx,coordy,limitesCUBE(6)+resolz
    coordx=coordx+resolx
    nbpointstotal=nbpointstotal+1
    end do
coordy=coordy-resoly
end do
write(10,*) "/"
write(30,*) "/"


!Then comes the main bit of the subroutine... The ZCORN keyword. Here, the
depths or zcoordinates of the 8 corners of each grid cells are indicated. They
would correspond to coordinates in the z direction along the vertical pillars
of the grids listed in the COORD keyword.

print*,nbpointstotal
compt=0
nbzonesmade=0
nbtotallayers=0
nbpointstotal=0
write(10,"(A5)") "ZCORN"
write(30,"(A5)") "ZCORN"
!Bottom faces

do kter=1,4
do jter=1,m-1
do iter=1,n-1
write(30,"(1F10.4)") limitesCUBE(5)-resolz
end do
end do
end do
do kter=1,4
do jter=1,m-1
do iter=1,n-1
```

```
write(30,"(1F10.4)") limitesCUBE(5)
end do
end do
end do


!For each zone, two surfaces are selected, the surface corresponding to the
top of the cell layer, the surface corresponding to the bottom of the cell
layer. Then the number of layers per zone is read in numlayers(:). Afterwards,
each cell of the zone is created from base to top, each time giving the zdepth
of the corners of the cell, first the 4 corners of the bottom, for all corners
of the bottom surface, and only then the 4 corners of the top for all the top
surface.

do ibis=1,nbzones

open(unit=20,file="listfiles.txt")
do jbis=1,nbzonesmade+1
read(20,*) nameSURFtop
end do
read(20,*) nameSURFbottom
close(unit=20)

if (allocated(SURFTOP)) then;
deallocate (SURFTOP)
end if
allocate (SURFTOP(n,m))

if (allocated(SURFBOTTOM)) then;
deallocate (SURFBOTTOM)
end if
allocate (SURFBOTTOM(n,m))
call readzmapfiles(nameSURFtop,SURFTOP,SPACE)
call readzmapfiles(nameSURFbottom,SURFBOTTOM,SPACE)

if (numlayers(ibis)>0) then;
    if (ibis==nbzones) then;
    print*,"last zone"
    end if
    do kbis=1,numlayers(ibis)
    nbtotallayers=nbtotallayers+1
    layer=numlayers(ibis)-kbis+1


!The first part here is for zones with one layer only, corresponding to the
mudstone drape layer. In ACTNUM, we store a number whether 0 or 1 for the grid
cell. If the cell has zero thickness, i.e. if all the bottom and top nodes of
the cell are located at the same depth, then the cell will be inactivated in
Eclipse, so in the following ACTNUM keyword, a 0 has to be indicated.

  if(numlayers(ibis)==1) then;

       do jter=1,m-1
            j=m-jter

            do i=1,n-1
            write(10,"(1F10.4)") SURFTOP(i,j+1)
            write(30,"(1F10.4)") SURFTOP(i,j+1)
            nbpointstotal=nbpointstotal+1
```

```
        ACTNUM(nbtotallayers,i,j+1)=SURFTOP(i,j+1)
        write(10,"(1F10.4)") SURFTOP(i+1,j+1)
        write(30,"(1F10.4)") SURFTOP(i+1,j+1)
        nbpointstotal=nbpointstotal+1

        ACTNUM(nbtotallayers,i+1,j+1)=SURFTOP(i+1,j+1)
        compt=compt+2
        end do

        do i=1,n-1
        write(10,"(1F10.4)") SURFTOP(i,j)
        write(30,"(1F10.4)") SURFTOP(i,j)
        nbpointstotal=nbpointstotal+1

        ACTNUM(nbtotallayers,i,j)=SURFTOP(i,j)
        write(10,"(1F10.4)") SURFTOP(i+1,j)
        write(30,"(1F10.4)") SURFTOP(i+1,j)
        nbpointstotal=nbpointstotal+1

        ACTNUM(nbtotallayers,i+1,j)=SURFTOP(i+1,j)
        compt=compt+2
        end do

    end do

    do jter=1,m-1
        j=m-jter

        do i=1,n-1
        write(10,"(1F10.4)") SURFBOTTOM(i,j+1)
        write(30,"(1F10.4)") SURFBOTTOM(i,j+1)
        nbpointstotal=nbpointstotal+1
        ACTNUM(nbtotallayers+1,i,j+1)=SURFBOTTOM(i,j+1)
        write(10,"(1F10.4)") SURFBOTTOM(i+1,j+1)
        write(30,"(1F10.4)") SURFBOTTOM(i+1,j+1)
        nbpointstotal=nbpointstotal+1
        ACTNUM(nbtotallayers+1,i+1,j+1)=SURFBOTTOM(i+1,j+1)
        compt=compt+2
        end do

        do i=1,n-1
        write(10,"(1F10.4)") SURFBOTTOM(i,j)
        write(30,"(1F10.4)") SURFBOTTOM(i,j)
        nbpointstotal=nbpointstotal+1
        ACTNUM(nbtotallayers+1,i,j)=SURFBOTTOM(i,j)
        write(10,"(1F10.4)") SURFBOTTOM(i+1,j)
        write(30,"(1F10.4)") SURFBOTTOM(i+1,j)
        nbpointstotal=nbpointstotal+1
        ACTNUM(nbtotallayers+1,i+1,j)=SURFBOTTOM(i+1,j)
        compt=compt+2
        end do

    end do

!The part after correspond to zones with more than one layer, for which there
is no intermediate surface between the top and bottom surface of the zone.
So, after one cell of layers have been created, the next layer should be lo-
cated 2 cm above the previous one (resolz=2) until it is as high as the top
surface; if it is higher than the top surface, the node is given the value of
the top surface.
```

```
else;

        do jter=1,m-1
            j=m-jter

            do i=1,n-1
            refbottom=SURFBOTTOM(i,j+1)-layer*resolz

            if (refbottom<SURFTOP(i,j+1)) then;
                write(10,"(1F10.4)") SURFTOP(i,j+1)
                write(30,"(1F10.4)") SURFTOP(i,j+1)
                nbpointstotal=nbpointstotal+1
                ACTNUM(nbtotallayers,i,j+1)=SURFTOP(i,j+1)
                compt=compt+1
            else;
                write(10,"(1F10.4)") refbottom
                write(30,"(1F10.4)") refbottom
                nbpointstotal=nbpointstotal+1
                ACTNUM(nbtotallayers,i,j+1)=refbottom
                compt=compt+1
            end if

            refbottom=SURFBOTTOM(i+1,j+1)-layer*resolz

            if (refbottom<SURFTOP(i+1,j+1)) then;
                write(10,"(1F10.4)") SURFTOP(i+1,j+1)
                write(30,"(1F10.4)") SURFTOP(i+1,j+1)
                nbpointstotal=nbpointstotal+1
                ACTNUM(nbtotallayers,i+1,j+1)=SURFTOP(i+1,j+1)
                compt=compt+1
            else;
                write(10,"(1F10.4)") refbottom
                write(30,"(1F10.4)") refbottom
                nbpointstotal=nbpointstotal+1
                ACTNUM(nbtotallayers,i+1,j+1)=refbottom
                compt=compt+1
            end if
            end do

            do i=1,n-1
            refbottom=SURFBOTTOM(i,j)-layer*resolz
            if (refbottom<SURFTOP(i,j)) then;
                write(10,"(1F10.4)") SURFTOP(i,j)
                write(30,"(1F10.4)") SURFTOP(i,j)
                nbpointstotal=nbpointstotal+1
                ACTNUM(nbtotallayers,i,j)=SURFTOP(i,j)
                compt=compt+1
            else;
                write(10,"(1F10.4)") refbottom
                write(30,"(1F10.4)") refbottom
                nbpointstotal=nbpointstotal+1
                ACTNUM(nbtotallayers,i,j)=refbottom
                compt=compt+1
            end if

            refbottom=SURFBOTTOM(i+1,j)-layer*resolz

            if (refbottom<SURFTOP(i+1,j)) then;
                write(10,"(1F10.4)") SURFTOP(i+1,j)
```

```
            write(30,"(1F10.4)") SURFTOP(i+1,j)
            nbpointstotal=nbpointstotal+1

            ACTNUM(nbtotallayers,i+1,j)=SURFTOP(i+1,j)
            compt=compt+1
        else;
            write(10,"(1F10.4)") refbottom
            write(30,"(1F10.4)") refbottom
            nbpointstotal=nbpointstotal+1
            ACTNUM(nbtotallayers,i+1,j)=refbottom
            compt=compt+1
        end if
        end do
        end do

    do jter=1,m-1
        j=m-jter

        do i=1,n-1
        refbottom=SURFBOTTOM(i,j+1)-(layer-1)*resolz
        if (refbottom<SURFTOP(i,j+1)) then;
            write(10,"(1F10.4)") SURFTOP(i,j+1)
            write(30,"(1F10.4)") SURFTOP(i,j+1)
            nbpointstotal=nbpointstotal+1
            ACTNUM(nbtotallayers+1,i,j+1)=SURFTOP(i,j+1)
            compt=compt+1
        else;
            write(10,"(1F10.4)") refbottom
            write(30,"(1F10.4)") refbottom
            nbpointstotal=nbpointstotal+1
            ACTNUM(nbtotallayers+1,i,j+1)=refbottom
            compt=compt+1
        end if

        refbottom=SURFBOTTOM(i+1,j+1)-(layer-1)*resolz
        if (refbottom<SURFTOP(i+1,j+1)) then;
            write(10,"(1F10.4)") SURFTOP(i+1,j+1)
            write(30,"(1F10.4)") SURFTOP(i+1,j+1)
            nbpointstotal=nbpointstotal+1
            ACTNUM(nbtotallayers+1,i+1,j+1)=SURFTOP(i+1,j+1)
            compt=compt+1
        else;
            write(10,"(1F10.4)") refbottom
            write(30,"(1F10.4)") refbottom
            nbpointstotal=nbpointstotal+1
            ACTNUM(nbtotallayers+1,i+1,j+1)=refbottom
            compt=compt+1
        end if
        end do

        do i=1,n-1
        refbottom=SURFBOTTOM(i,j)-(layer-1)*resolz
        if (refbottom<SURFTOP(i,j)) then;
            write(10,"(1F10.4)") SURFTOP(i,j)
            write(30,"(1F10.4)") SURFTOP(i,j)
            nbpointstotal=nbpointstotal+1
            ACTNUM(nbtotallayers+1,i,j)=SURFTOP(i,j)
            compt=compt+1
        else;
            write(10,"(1F10.4)") refbottom
```

```
                write(30,"(1F10.4)") refbottom
                nbpointstotal=nbpointstotal+1
                ACTNUM(nbtotallayers+1,i,j)=refbottom
                compt=compt+1
            end if

            refbottom=SURFBOTTOM(i+1,j)-(layer-1)*resolz
            if (refbottom<SURFTOP(i+1,j)) then;
                write(10,"(1F10.4)") SURFTOP(i+1,j)
                write(30,"(1F10.4)") SURFTOP(i+1,j)
                nbpointstotal=nbpointstotal+1
                ACTNUM(nbtotallayers+1,i+1,j)=SURFTOP(i+1,j)
                compt=compt+1
            else;
                write(10,"(1F10.4)") refbottom
                write(30,"(1F10.4)") refbottom
                nbpointstotal=nbpointstotal+1
                ACTNUM(nbtotallayers+1,i+1,j)=refbottom
                compt=compt+1
            end if
            end do
            end do
    end if
    end do


!Security of doing it again for zones with no layers. Adding one layer that
will be entirely filled with zero thickness cells. ACTNUM will be the same than
the layer above to insure communication.

else;

    nbtotallayers=nbtotallayers+1
     do jter=1,m-1
            j=m-jter

        do i=1,n-1
        write(10,"(1F10.4)") SURFTOP(i,j+1)
        write(30,"(1F10.4)") SURFTOP(i,j+1)
        nbpointstotal=nbpointstotal+1
        ACTNUM(nbtotallayers,i,j+1)=SURFTOP(i,j+1)
        write(10,"(1F10.4)") SURFTOP(i+1,j+1)
        write(30,"(1F10.4)") SURFTOP(i+1,j+1)
        nbpointstotal=nbpointstotal+1
        ACTNUM(nbtotallayers,i+1,j+1)=SURFTOP(i+1,j+1)
        compt=compt+2
        end do

        do i=1,n-1
        write(10,"(1F10.4)") SURFTOP(i,j)
        write(30,"(1F10.4)") SURFTOP(i,j)
        nbpointstotal=nbpointstotal+1
        ACTNUM(nbtotallayers,i,j)=SURFTOP(i,j)
        write(10,"(1F10.4)") SURFTOP(i+1,j)
        write(30,"(1F10.4)") SURFTOP(i+1,j)
        nbpointstotal=nbpointstotal+1
        ACTNUM(nbtotallayers,i+1,j)=SURFTOP(i+1,j)
        compt=compt+2
        end do
    end do
```

```
    do jter=1,m-1
          j=m-jter

        do i=1,n-1
        write(10,"(1F10.4)") SURFBOTTOM(i,j+1)
        write(30,"(1F10.4)") SURFBOTTOM(i,j+1)
        nbpointstotal=nbpointstotal+1
        ACTNUM(nbtotallayers+1,i,j+1)=SURFBOTTOM(i,j+1)
        write(10,"(1F10.4)") SURFBOTTOM(i+1,j+1)
        write(30,"(1F10.4)") SURFBOTTOM(i+1,j+1)
        nbpointstotal=nbpointstotal+1
        ACTNUM(nbtotallayers+1,i+1,j+1)=SURFBOTTOM(i+1,j+1)
        compt=compt+2
        end do

        do i=1,n-1
        write(10,"(1F10.4)") SURFBOTTOM(i,j)
        write(30,"(1F10.4)") SURFBOTTOM(i,j)
        nbpointstotal=nbpointstotal+1
        ACTNUM(nbtotallayers+1,i,j)=SURFBOTTOM(i,j)
        write(10,"(1F10.4)") SURFBOTTOM(i+1,j)
        write(30,"(1F10.4)") SURFBOTTOM(i+1,j)
        nbpointstotal=nbpointstotal+1
        ACTNUM(nbtotallayers+1,i+1,j)=SURFBOTTOM(i+1,j)
        compt=compt+2
        end do

    end do
end if

nbzonesmade=nbzonesmade+1
end do

!At the end, the last layer of cells is created for the grid for vertical flow
simulation by adding up resolz to the top surface of the model.

do kter=1,4
do jter=1,m-1
do iter=1,n-1
write(30,"(1F10.4)") limitesCUBE(6)
end do
end do
end do
do kter=1,4
do jter=1,m-1
do iter=1,n-1
write(30,"(1F10.4)") limitesCUBE(6)+resolz
end do
end do
end do

write(10,*) "/"
write(30,*) "/"

print*,nbpointstotal
nbpointstotal=0


!Finally, the keyword ACTNUM is inserted, with 0 corresponding to inactive
```

```
cells in the model (zero thickness cells) and 1 to the cells activated for the
flow simulation (all other cells). ACTNUM has been created during the precious
keyword creation ZCORN.

write(10,"(A6)") "ACTNUM"
write(30,"(A6)") "ACTNUM"
!This is the first bottom layer for the grid for vertical flow simulation

do jter=1,m-1
do iter=1,n-1
write(30,*) "1"
end do
end do


!The value of ACTNUM in the file will correspond to the value stored in our
previously built ACTNUM(k,i,j) array, depending on the thickness of the cell
at each pillar.

do k=1,nblayers
do jter=1,m-1
j=m-jter
    do i=1,n-1
    if ( (ACTNUM(k,i,j)+ACTNUM(k,i+1,j)+ACTNUM(k,i,j+1)+ACTNUM(k,i+1,j+1)) - (ACTNU
M(k+1,i,j)+ACTNUM(k+1,i+1,j)+ACTNUM(k+1,i,j+1)+ACTNUM(k+1,i+1,j+1))<0) then;
    write(10,*) "1"
    write(30,*) "1"
    nbpointstotal=nbpointstotal+1
    else;
    write(10,*) "0"
    write(30,*) "0"
    nbpointstotal=nbpointstotal+1
    end if
    end do
end do
end do

!This is the last layer for the grid for vertical flow simulation

do jter=1,m-1
do iter=1,n-1
write(30,*) "1"
end do
end do

write(10,*) "/"
write(30,*) "/"
print*,nbpointstotal

close(unit=10)
close(unit=30)

end subroutine writegridfile

!-------------------------------------------------------------------------
!-------------------------------------------------------------------------
!-------------------------------------------------------------------------

subroutine writezmapfile(name,m,n,xmin,xmax,ymin,ymax,Nonvalue,TOWRITE)
```

```
character :: name*50
integer :: m,n,Numb,numsurf,i,j
real :: xmin, xmax, ymin,ymax,Nonvalue
real, allocatable :: TOWRITE(:,:)

      open(unit=30,file=trim(name))
    write(30,*)'!'
    write(30,*)'!      ZIMS FILE NAME :  Envtopsphere.txt'
    write(30,*)'!      FORMATTED FILE CREATION DATE: ??/??/2010'
    write(30,*)'!      FORMATTED FILE CREATION TIME: ??:??'
    write(30,*)'!'
    write(30,10)'@Grid HEADER, GRID, 5'
10  format(A21)
    write(30,*)'15,',-Nonvalue,',   ,    4 ,1.0000'
    write(30,"(I6,A,I5,A,1F12.4,A,1X,1F12.4,A,1F12.4,A,1F12.4)") m,',',n,',',xmin,',',x
max,',',ymin,',',ymax
    write(30,*)'0.0000      0.0000      0.0000'
      write(30,20)'@'
20    format(A1)
    do i=1,n
           write(30,"(1F10.4,1X,1F10.4,1X,1F10.4,1X,1F10.4,1X,1F10.4)")
-TOWRITE(i,1:m)
    end do
    close(unit=30)

end subroutine writezmapfile
```